THE DIFFRACTIVE PHOTOPRODUCTION OF VECTOR MESONS

THE UNIVERSITY of MANCHESTER

A thesis submitted to the University of Manchester
for the degree of Doctor of Philosophy
in the Faculty of Science and Engineering

By
Gavin Poludniowski
Department of Physics and Astronomy

2003

Contents

List of Figures **7**

List of Tables **14**

Abstract **15**

Copyright and Ownership of Intellectual Property Rights **16**

Declaration **17**

Acknowledgements **18**

Autobiographical Note **19**

Publications **20**

Dedication **21**

1 Introduction **22**

1.1 Particle physics and the strong force 22

1.2 S-matrix theory 24

1.3 Regge theory 28

1.4 QCD in the Regge region 32

1.5 Vector meson photoproduction 42

1.6 From hadrons to partons and back again 46

2 Two gluon exchange **54**

2.1 Factorisation formulae . . . 55

2.1.1 The $\gamma q \to V q$ amplitude . . . 55

2.1.2 Diffractive factorisation . . . 59

2.1.3 Fierz factorising . . . 60

2.2 The hard scattering amplitude . . . 61

2.2.1 $qq \to qq$: one gluon exchange . . . 62

2.2.2 $qq \to qq$: two gluon exchange . . . 63

2.2.3 Generalised Processes . . . 70

2.2.4 The hard subprocess Fierz trace . . . 83

2.3 From partons to mesons . . . 85

2.3.1 The soft subprocess Fierz traces: The light-cone matrix elements . . . 85

2.3.2 Inputting the polarisation vector . . . 86

2.3.3 Transform to Fourier space . . . 87

2.3.4 Lorentz contraction of the hard subprocess with the light-cone matrix elements . . . 88

2.4 Vector meson photoproduction: the story so far . . . 92

2.5 Summary . . . 95

3 BFKL calculation 1: heavy and collinear quarks **96**

3.1 Two gluon exchange . . . 97

3.1.1 Collinear quark and anti-quark . . . 97

3.1.2 The $\tilde{\mathbf{P}}(\tilde{\mathbf{r}}, u)$ and $\tilde{R}(\tilde{\mathbf{r}}, u)$ functions . . . 98

3.1.3 The impact factors . . . 99

3.1.4 The two-gluon exchange amplitudes . . . 100

3.1.5 The heavy meson approximation . . . 101

3.2 Beyond two-gluon exchange . . . 102

3.2.1 The BFKL solution . . . 102

3.2.2 The projection of the $q \to q$ impact factor 103
3.2.3 The projection of the $\gamma \to V$ impact factor 107
3.2.4 Result: the BFKL amplitude 111
3.2.5 The two-gluon exchange limit 112
3.3 Summary 113

4 BFKL calculation 2: generic non-collinear quarks 114

4.1 Two gluon exchange 115
4.1.1 Collinear quark and anti-quark 115
4.1.2 The $\tilde{\mathbf{P}}(\tilde{\mathbf{r}}, u)$ and $\tilde{R}(\tilde{\mathbf{r}}, u)$ functions 116
4.1.3 The impact factors 118
4.1.4 The two-gluon exchange amplitudes 119
4.2 Beyond two-gluon exchange 121
4.2.1 The BFKL solution 121
4.2.2 The projection of the $q \to q$ impact factor 121
4.2.3 The projection of the $\gamma \to V$ impact factor 122
4.2.4 Results: the BFKL amplitudes 130
4.2.5 The massless quark limit 133
4.3 Summary 137

5 Phenomenology 138

5.1 The experiments 138
5.2 The observables 140
5.3 Parameters and prescriptions 143
5.4 Phenomenology for the ρ meson. 148
5.4.1 The collinear and δ-function approximations 148
5.4.2 Collinear approximation and asymptotic distribution amplitudes 152
5.4.3 Higher twist effects 156
5.4.4 The sensitivity of predictions to parameters 163
5.4.5 Sensitivity to distribution amplitudes 177

5.5 Phenomenology for the ρ, ϕ and J/ψ 183
5.6 Summary 192

6 Conclusion 193

A The polarisation vectors of a vector meson 195

B The electronic decay width of a meson 198

C The angular distribution of the $\mu^+\mu^-$ decay from a vector meson produced by diffractive photoproduction 202

D Vector meson distribution amplitudes 207
D.1 Twist-2 distribution amplitudes 209
D.2 Twist-3 distribution amplitudes 209
D.3 Twist-4 distribution amplitudes 210
D.4 Distribution amplitude schemes 211
D.4.1 Prescription 1: leading twist (collinear) approximation with δ-function distributions 211
D.4.2 Prescription 2: leading twist (collinear) approximation with asymptotic distribution amplitudes 212
D.4.3 Prescription 3: higher twist approximation with asymptotic distribution amplitudes 212
D.4.4 Prescription 4: higher twist approximation with BBKT distribution amplitudes 213

E The (++) even amplitude: a study of the end-point contributions 214
E.1 The light-quark limit 214
E.2 Born level 215
E.3 Resummation of the BFKL Equation 216
E.4 Resummation: the (++) even amplitude 219

E.5 The BFKL calculation in the small u limit. 221
E.6 The single-parton coupling correspondence 225
E.7 Conclusions 227

List of Figures

1.1 A picture of the process $ab \to cd$, in terms of an unspecified interaction represented by a 'blob'. Crossing symmetry allows us to related this to the process $a\bar{c} \to \bar{b}d$ by the substitution of momenta corresponding to the change $s \leftrightarrow t$. 27

1.2 The total $p\bar{p}$ cross-section and the fit of [8]. The data only show statistical errors and are taken from [7]. 31

1.3 The QCD and QED Feynman rules in the Feynman gauge. The boson-boson couplings do not occur in QED because it is an abelian theory. . 34

1.4 The lowest order impact factor representation of QCD colour singlet amplitude; two gluon exchange. 36

1.5 The impact factor representation of QCD colour singlet amplitude; leading log QCD pomeron exchange. 37

1.6 The gluon ladder consisting of gluons and the effective three-gluon vertex Γ. The sum over all possible gluon exchanges and all possible Γ couplings results in the reggeisation of the gluon. 39

1.7 Diffractive vector meson photoproduction at large momentum transfer. 43

1.8 The experimental arrangement for the ZEUS detector at HERA for observation of the process $e^+p \to e^+VX$. The mesons are tagged by the decays $\rho \to \pi\pi$, $\phi \to KK$ and $J/\psi \to ll$. The components indicated are the proton remnant tagger (PRT), the forward, rear and back calorimeter (FCAL, RCAL, BCAL) and the central tracking detector (CTD). The plot is taken from [28]. 45

1.9 Deeply inelastic scattering (DIS) of an electron from a proton. 46

1.10 Deeply inelastic scattering (DIS) of an electron from a proton. Q^2 is of sufficient magnitude that it probes distances $r \sim 1/|Q| \ll r_p$, where r_p is the size of a proton and $r_p \sim 1/m_p$ where m_p is the mass of a proton. The photon therefore resolves the internal structure of the proton. . . 49

1.11 The $q\bar{q} \to V$ transition. Γ_t is the possible Dirac structure of the coupling of the meson to the $q\bar{q}$ pair; $\Gamma_t \in \{1, -i\gamma_5, \gamma_\mu, -\gamma_\mu\gamma_5, \sigma_{\mu\nu}\}$. 51

2.1 The process $\gamma q \to Vq$. This process is depicted as factorised into the convolution of the hard subprocess $\gamma q \to q'\bar{q}'q$ with the soft transition $q'\bar{q}' \to V$. The soft transition is assumed to occur at a time $t' \gg t$ where t is the time of the hard interaction, allowing factorisation. The zig-zag object is the colour singlet exchange mediator; the pomeron. . . 56

2.2 One gluon exchange. 62

2.3 Two gluon exchange. (a) is the s-channel diagram. (b) is the $s \leftrightarrow u$ crossed diagram with respect to (a). 63

2.4 The s-channel two gluon exchange diagram. The dashed line is the Cutkosky cut. 64

2.5 A generalised process $ab \to cd$, mediated by two-gluon colour singlet exchange. The dashed-line is the cut of the Cutkosky rules. $\{i\}$ and $\{j\}$ are the daughter particles of a and b respectively. 71

2.6 The two-gluon exchange impact factor representation of QCD colour singlet amplitude. 75

2.7 The amplitude for $q \to q$ via gluon Compton scattering, amputated in the final state gluon polarisations. 76

2.8 The amplitude for the $\gamma \to q\bar{q}$ transition via gluon emission/absorption, amputated in the final state gluon polarisations. 77

3.1 The types of diagram that contribute to the colour dipole impact factor: (a) the pomeron couples to two separate partons ($2p$); (b) the pomeron couples to one parton ($1p$). The BFKL eigenfunction takes on a non-zero value for diagrams of type (a), but is forced to zero for type (b). . 103
3.2 The $\gamma(+)q \rightarrow V(+)q$ heavy meson amplitude for $z = 0$. The dots correspond to two-gluon exchange. The sum over conformal spins builds up the two-gluon in the $z \rightarrow 0$ limit. The constant, $C_q = s\alpha_s^2(N^2 - 1/N^2)f_V m_V e e_q$. 112

4.1 The quark and anti-quark coordinate systems in momentum space. The quark and anti-quark have 4-momenta q_1 and q_2 respectively and these need not lie in the $x - z$ plane. The primed coordinate system is that where the initial state photon and proton define the z-axis. The 'tilde' coordinate system is that where the outgoing meson direction defines the z-axis. We have defined the momentum given to the meson, q, to be in the x direction; therefore $\sin\theta \simeq \frac{2|q|}{\sqrt{s}} \rightarrow \cos\theta \sim 1 + \frac{2t}{s}$. This result corresponds to (1.23), quoted in Chapter 1. 115
4.2 The $\mathcal{M}_{++}^{even}$ amplitude differential in u plotted against u. The thick solid line shows the leading pole approximation. The other curves show the full amplitude for different m. The fixed parameter values are $(z, m_V, |t|) = (1.0, m_\rho, 10\,\mathrm{GeV}^2)$. The constant, $C_q = s\alpha_s^2(N^2 - 1/N^2)f_V m_V e e_q$. The asymptotic distribution amplitudes were used. . . 135
4.3 The $\mathcal{M}_{++}^{even}$ amplitude against m, the quark mass parameter. The circles are numerical results using the formulae (4.70, 4.75). The fixed parameter values are $(z, m_V, |t|) = (1.0, m_\rho, 10\,\mathrm{GeV}^2)$. The constant, $C_q = s\alpha_s^2(N^2 - 1/N^2)f_V m_V e e_q$. The asymptotic distribution amplitudes were used. 136

5.1 The coordinate systems defined by the initial (γp) and final (VX) states. 139
5.2 Diffractive vector meson photoproduction at large momentum transfer. 141

5.3 Collinear and δ-function approximation: $d\sigma/dt$ for parameter values, $(\alpha_s^{BFKL},\, m) = (0.2,\, m_\rho/2)$. 150

5.4 Collinear and δ-function approximation: r-matrix elements. The predictions are parameter independent. 151

5.5 Collinear approximation: $d\sigma/dt$ for parameter values, $(\alpha_s^{BFKL},\, m) = (0.2,\, m_\rho/2)$. 154

5.6 Collinear approximation: r-matrix elements for parameter values, $(\alpha_s^{BFKL},\, m) = (0.2,\, m_\rho/2)$. 155

5.7 Higher twist effects: $d\sigma/dt$ for parameter values, $(\alpha_s^{IF}, \alpha_s^{BFKL},\, \Lambda^2,\, m) = (0.17,\, 0.2,\, m_V^2,\, m_\rho/2)$. 160

5.8 Higher twist effects: r-matrix elements for parameter values, $(\alpha_s^{BFKL},\, \Lambda^2,\, m) = (0.2,\, m_V^2,\, m_\rho/2)$. 161

5.9 Higher twist effects: even to odd amplitude ratios for parameter values, $(\alpha_s^{BFKL},\, \Lambda^2,\, m) = (0.2,\, m_V^2,\, m_\rho/2)$. 162

5.10 The sensitivity to varying α_s^{BFKL}: $d\sigma/dt$ for parameter values, $(\alpha_s^{IF},\, \Lambda^2,\, m) = (0.17,\, m_\rho^2 - t,\, m_\rho/2)$. 165

5.11 The sensitivity to varying α_s^{BFKL}: r-matrix elements for parameter values, $(\Lambda^2,\, m) = (m_\rho^2 - t,\, m_\rho/2)$. 166

5.12 The sensitivity to varying γ: $d\sigma/dt$ for parameter values, $(\alpha_s^{IF},\, \alpha_s^{BFKL},\, m) = (0.17,\, 0.2,\, m_\rho/2)$. 167

5.13 The sensitivity to varying γ: r-matrix elements for parameter values, $(\alpha_s^{BFKL},\, m) = (0.2,\, m_\rho/2)$. 168

5.14 The sensitivity to varying z: the six helicity amplitudes differential in u. The y-axis is $\frac{1}{C_\rho}\frac{d\mathcal{M}_{+i}^{odd/even}}{du}$, where $C_\rho = i\hat{s}\alpha_s^{IF^2}(N^2 - 1/N^2)eQ_\rho f_\rho$ and $(m,\, |\mathbf{q}|) = (m_\rho/2,\, \sqrt{10}\,\mathrm{GeV})$. 169

5.15 An improved fit: $d\sigma/dt$ for parameter values, $(\alpha_s^{IF},\, \alpha_s^{BFKL},\, \Lambda^2,\, m) = (0.17,\, 0.25,\, m_\rho^2 - t,\, m_\rho/2)$ 170

5.16 An improved fit: r-matrix elements for parameter values, $(\alpha_s^{BFKL},\, \Lambda^2,\, m) = (0.25,\, m_\rho^2 - t,\, m_\rho/2)$. 171

5.17 The sensitivity to varying m: $d\sigma/dt$ for parameter values, $(\alpha_s^{IF},\ \alpha_s^{BFKL}, \Lambda^2)$ $= (0.17,\ 0.2,\ m_\rho^2)$. 174

5.18 The sensitivity to varying m: r-matrix elements for parameter values, $(\alpha_s^{BFKL}, \Lambda^2) = (0.2,\ m_\rho^2)$. 175

5.19 The sensitivity to varying m: the six helicity amplitudes differential in u. The y-axis is $\frac{1}{C_\rho}\frac{d\mathcal{M}_{+i}^{odd/even}}{du}$, where $C_\rho = i\hat{s}\alpha_s^{IF^2}(N^2-1/N^2)eQ_\rho f_\rho$ and $(z,\ |\mathbf{q}|) = (0.75,\ \sqrt{10}\,\mathrm{GeV})$. 176

5.20 The effect BBKT DA: $d\sigma/dt$ for parameter values, $(\alpha_s^{IF},\ \alpha_s^{BFKL},\ \Lambda^2,\ m)$ $= (0.17,\ 0.25,\ m_\rho^2 - t,\ m_\rho/2)$ 180

5.21 The effect of BBKT DA: r-matrix elements for parameter values, $(\alpha_s^{BFKL},\ \Lambda^2,\ m)$ $= (0.25,\ m_\rho^2 - t,\ m_\rho/2)$ 181

5.22 The effect of BBKT DA: the six helicity amplitudes differential in u. The y-axis is $\frac{1}{C_\rho}\frac{d\mathcal{M}_{+i}^{odd/even}}{du}$, where $C_\rho = i\hat{s}\alpha_s^{IF^2}(N^2-1/N^2)eQ_\rho f_\rho$ and $(z,\ m,\ |\mathbf{q}|) = (0.75,\ m_\rho/2,\ \sqrt{10}\,\mathrm{GeV})$. 182

5.23 ρ photoproduction: $d\sigma/dt$. The fixed two-gluon curve was calculated with the parameter values $(\alpha_s^{IF},\ f_\rho,\ f_\rho^T,\ m) = (0.27,\ 0.216\,\mathrm{GeV},\ 0.160\,\mathrm{GeV},\ m_\rho/2)$. The run two-gluon curve was calculated with the parameter values $(\alpha_s^{IF}(1\,\mathrm{GeV}),\ f_\rho,\ f_\rho^T,\ m)$ =$(0.30,\ 0.216\,\mathrm{GeV},\ 0.160\,\mathrm{GeV},\ m_\rho/2)$. The BFKL calculated for the parameter values $(\alpha_s^{IF},\ \alpha_s^{BFKL},\ \Lambda^2,\ f_\rho,\ f_\rho^T,\ m) = (0.17,\ 0.25,\ m_\rho^2 - t,\ 0.216\,\mathrm{GeV},\ 0.160\,\mathrm{GeV},\ m_\rho/2)$. 186

5.24 ρ photoproduction: r-matrix elements. The two-gluon curve was calculated with the parameter values $(f_\rho,\ f_\rho^T,\ m) = (0.216\,\mathrm{GeV},\ 0.160\,\mathrm{GeV},\ m_\rho/2)$. The BFKL curve was calculated for the parameter values $(\alpha_s^{BFKL},\ \Lambda^2,\ f_\rho,\ f_\rho^T,\ m)$ $= (0.25,\ m_\rho^2 - t,\ 0.216\,\mathrm{GeV},\ 0.160\,\mathrm{GeV},\ m_\rho/2)$. 187

5.25 ϕ photoproduction: $d\sigma/dt$ for parameter values. The fixed two-gluon curve was calculated with the parameter values $(\alpha_s^{IF},\ f_\phi,\ f_\phi^T,\ m) = (0.25,\ 0.231\,\mathrm{GeV},\ 0.215\,\mathrm{GeV},\ m_\phi/2)$. The run two-gluon curve was calculated with the parameter values $(\alpha_s^{IF}(1\,\mathrm{GeV}),\ f_\phi,\ f_\phi^T,\ m) = (0.28,\ 0.231\,\mathrm{GeV},\ 0.215\,\mathrm{GeV},\ m_\phi/2)$. BFKL prediction (1) is for the parameter values $(\alpha_s^{IF},\ \alpha_s^{BFKL},\ \Lambda^2,\ f_\phi,\ f_\phi^T,\ m) = (0.17,\ 0.25,\ m_\phi^2 - t,\ 0.231\,\mathrm{GeV},\ 0.215\,\mathrm{GeV},\ m_\phi/2)$. BFKL prediction (2) is for the parameter values $(\alpha_s^{IF},\ \alpha_s^{BFKL},\ \Lambda^2,\ f_\phi,\ f_\phi^T,\ m) = (0.17,\ 0.25,\ m_\phi^2 - t,\ 0.231\,\mathrm{GeV},\ 0.171\,\mathrm{GeV},\ m_\phi/2)$. 188

5.26 ϕ photoproduction: r-matrix element. The fixed two-gluon curve was calculated with the parameter values $(f_\phi,\ f_\phi^T,\ m) = (0.231\,\mathrm{GeV},\ 0.215\,\mathrm{GeV},\ m_\phi/2)$. The BFKL prediction ((2)) is for the parameter values $(\alpha_s^{BFKL},\ \Lambda^2,\ f_\phi,\ f_\phi^T,\ m) = (0.25,\ m_\phi^2 - t,\ 0.231\,\mathrm{GeV},\ 0.171\,\mathrm{GeV},\ m_\phi/2)$. 189

5.27 J/ψ photoproduction: $d\sigma/dt$. The fixed two-gluon curve was calculated with the parameter values $(\alpha_s^{IF},\ f_{J/\psi},\ f_{J/\psi}^T,\ m) = (0.23,\ 0.405\,\mathrm{GeV},\ 0.405\,\mathrm{GeV},\ m_{J/\psi}/2)$. The run two-gluon curve was calculated with the parameter values $(\alpha_s^{IF}(1\,\mathrm{GeV})\ \ f_{J/\psi},\ f_{J/\psi}^T,\ m) = (0.29,\ 0.405\,\mathrm{GeV},\ 0.405\,\mathrm{GeV},\ m_{J/\psi}/2)$. BFKL prediction (1) is for the parameter values $(\alpha_s^{IF},\ \alpha_s^{BFKL},\ \Lambda^2,\ f_{J/\psi},\ f_{J/\psi}^T,\ m) = (0.17,\ 0.25,\ m_{J/\psi}^2 - t,\ 0.405\,\mathrm{GeV},\ 0.405\,\mathrm{GeV},\ m_{J/\psi}/2)$. BFKL prediction (2) is for the parameter values $(\alpha_s^{IF},\ \alpha_s^{BFKL},\ \Lambda^2,\ f_{J/\psi},\ f_{J/\psi}^T,\ m) = (0.17,\ 0.25,\ m_{J/\psi}^2 - t,\ 0.405\,\mathrm{GeV},\ 0.300\,\mathrm{GeV},\ m_{J/\psi}/2)$. 190

5.28 J/ψ photoproduction: r-matrix elements. The two-gluon curve was calculated with the parameter values $(f_{J/\psi},\ f_{J/\psi}^T,\ m) = (0.405\,\mathrm{GeV},\ 0.405\,\mathrm{GeV},\ m_{J/\psi}/2)$. The BFKL prediction ((2)) is for the parameter values $(\alpha_s^{BFKL},\ \Lambda^2,\ f_{J/\psi},\ f_{J/\psi}^T,\ m) = (0.25,\ m_{J/\psi}^2 - t,\ 0.405\,\mathrm{GeV},\ 0.300\,\mathrm{GeV},\ m_{J/\psi}/2)$. 191

B.1 The lowest order contribution to the decay $V \to e^+e^-$. 198

C.1 The coordinate systems defined by the initial (γq) and final (Vq) states. For the calculation of the helicity amplitudes we work in the γq CM frame. The meson 3-momentum defines the $\tilde{z}$-axis. Helicity amplitudes are Lorentz invariant. For the decay of the vector meson we work in the vector meson rest-frame. Note that the muon pair decay vectors will not in general lie in the $x - z$ plane. 204

List of Tables

1.1 The initial and final state Feynman rules for external states. The symbol linking the fields and states indicates that they are contracted together. See for example [11]. 33

5.1 Classification of helicity amplitudes in twist. 143

5.2 The meson strong couplings [33]. 147

5.3 The meson charge couplings. 147

D.1 Classification of distribution amplitudes up to twist-4. 207

D.2 Chiral even parameters: $\mu^2 = 1\,\mathrm{GeV}^2$. 208

D.3 Chiral odd parameters: $\mu^2 = 1\,\mathrm{GeV}^2$. 208

Abstract

UNIVERSITY OF MANCHESTER

ABSTRACT OF THESIS submitted by **Gavin Poludniowski** for the Degree of Doctor of Philosophy and entitled **The diffractive photoproduction of vector mesons**

Month and Year of Submission: 2003

We study the diffractive photoproduction of vector mesons: $\gamma p \to VX$. We calculate the relevant set of impact factors and obtain the Born level helicity amplitudes for the process. We then generalise to all orders in the strong coupling, within the leading logarithm approximation, and find these helicity amplitudes using the solution to the Balitsky, Fadin, Kuraev and Lipatov (BFKL) equation. We compare to data recently obtained by the ZEUS and H1 collaborations at DESY for the ρ, ϕ and J/ψ mesons and show that although our calculation cannot give a complete description of all the observables, it remains a marked improvement on the Born level results.

Copyright and Ownership of Intellectual Property Rights

Declaration

No portion of the work referred to in this thesis has been submitted in support of an application for another degree or qualification of this or any other university or other institution of learning.

Acknowledgements

Thanks to a lot of people. Thanks to PPARC for funding me and providing the money for a trip to America. Thanks, also, to my parents (and other relatives) for funding me, though I don't see them as a Research Council. My parents provided support for me whenever I needed with no questions asked, PPARC, however nice, always required me to fill in a form. Thanks to friends who I shan't name in case I forget anyone. Thanks to my supervisor Jeff Forshaw for an apt choice of project and his continued support. Thanks to Leszek Motyka and Rikard Enberg for being perfect collaborators, on a personal, as well a professional level. In particular, thanks to Leszek for his appreciation of the mathematics and Rikard for not only proofreading part of this thesis, but actually suggesting he enjoyed it. Thanks also to Rikard for cross-checking numerics, without which I doubt any of my numbers would have been right. Thanks to my office mates Tom and Rob, who without having had a chance to get to know, I would have been less of a person. Especially thanks to Zoe, without who's love and support, I wouldn't have been able to get out of bed, let alone write a thesis.

Autobiographical Note

The author was born in Norfolk and Norwich Hospital at slightly after 6pm on the evening of the 28th December 1977. In 1996 he ended up at university in Manchester. He graduated in 2000 with a 1st class degree and the Platt Prize. He stayed at Manchester. He started a Ph.D.. He was awarded the John Birks Prize in the 1st year assessment and won the poster competition in the 2nd. He is leaving theoretical particle physics to work for the NHS.

Publications

"VECTOR MESON PHOTOPRODUCTION FROM THE BFKL EQUATION. II. PHENOMENOLOGY"

R. Enberg, J.R. Forshaw, G. Poludniowski and L. Motyka, hep-ph/0311017.

"VECTOR MESON PHOTOPRODUCTION FROM THE BFKL EQUATION. I. THEORY"

R. Enberg, J.R. Forshaw, G. Poludniowski and L. Motyka, JHEP 09(2003)008.

"DIFFRACTIVE VECTOR MESONS AT LARGE MOMENTUM TRANSFER FROM THE BFKL EQUATION"

R. Enberg, L. Motyka and G. Poludniowski, Acta Phys. Polon. **B33** (2002) 3511.

"DIFFRACTIVE HEAVY VECTOR MESON PRODUCTION FROM THE BFKL EQUATION"

R. Enberg, L. Motyka and G. Poludniowski, Eur. Phys. J.**C26** (2002) 219.

"VECTOR MESON PHOTOPRODUCTION AT HIGH T AND COMPARISON TO HERA DATA"

J.R. Forshaw and G. Poludniowski, Eur. Phys. J. **C26** (2003) 411.

Dedication

For my brother.

Chapter 1

Introduction

1.1 Particle physics and the strong force

Particle physics is mostly about hitting fast moving particles together and measuring what happens. These particles are very small. Our common sense relates to bigger particles. Being hit by a fast moving football hurts. It hurts because the football has a lot of momentum; it is travelling fast and has mass. That mass consists of electrons, protons and neutrons bound into atoms. Although the number of protons and neutrons, generically called hadrons, is comparable to that of electrons, they make up over 99.95% of the mass. Despite this fact, for a long time we have understood the 0.05% much better. There are reasons why this is so. Electrons are easier to remove from atoms and they are the essence of chemistry and chemical interactions. Interaction is easier to investigate than inaction. The common sense observation that a football remains a football instead of its hadrons wandering off, has been a difficult fact to explain ever since these hadrons were discovered.

In 1897, JJ Thompson and co-workers discovered the electron. In 1911, in Manchester, Rutherford discovered the nucleus of the atom in his famous experiment with Geiger and Marsden, paving the way for the discovery of the proton and neutron. The revolutions in particle physics during the early decades of the twentieth century produced non-relativistic quantum theory, through the work of such people as Heisenberg, Schrödinger and Dirac. A fully relativistic field theory of quantum particles had a more difficult birth, but by 1965 the quantum dynamics of the electron, or Quantum Electrodynamics (QED), was well understood; Feynman, Schwinger and Tomanga shared the Nobel Prize for it in that year. The force that binds the protons and neutrons into the nucleus of atoms was still largely a mystery. A perturbative field theory seemed far away. Despite this fact, progress was made through considering the general properties of the scattering matrix, or S-matrix. Then at the end of the sixties, experiment revealed the composite nature of the hadrons. In the early seventies a candidate for a perturbative theory of the strong force between these hadronic contents emerged, quantum chromodynamics (QCD). Now, thirty years later, QCD has had many successes and few would doubt its validity.

However, QCD is a difficult theory. The perturbative coupling is large (strong) and rises as the scale in a problem falls. Although this is essential, if we hope to reproduce in predictions the fact that the contents of the hadrons and nucleus are confined, it makes perturbative calculations problematic. In fact many of the successful predictions of QCD have been qualitative, or in ratios of physical quantities predicted from the colour algebra. If we wish to do quantitative analysis we need all the help we can get and that means looking in the right places. We will argue that diffractive vector meson photoproduction at high momentum exchange is an example of such a good place to look. This thesis is an attempt to make a contribution to an understanding of the strong force through an investigation of this process and the confrontation of QCD with data. The insights from S-matrix theory prove general enough to aid us in this. Because of the involved nature of some of the calculations in later chapters, Chapter 1 serves not only as an introduction but also presents many of the important results used later, that if presented then, would obscure the line of reasoning. Chapter 2 is the lowest order calculation for the process. The next two chapters generalise the lowest order result to higher orders. Chapter 5 is the phenomenology of our calculations and Chapter 6 concludes the thesis. Key results throughout are sandwiched between pairs of horizontal lines.

1.2 S-matrix theory

The S-matrix consists of elements corresponding to the overlap between free-particle *in*-states and *out*-states. The analysis regarding it in this section and that on Regge theory in the next are inspired by, if not always following that of [1]. We also refer the reader to the alternative sources [2, 3].

We can write the S-matrix for a transition $a \to b$,

$$S_{ab} = \langle b(t \to \infty) | a(t \to -\infty) \rangle. \tag{1.1}$$

We will assume that the S-matrix is Lorentz invariant. So, even though the lifetime of a decay may take a different value in different observation frames, the branching ratio remains invariant. A consequence of the Lorentz invariance of the S-matrix is that it can be expressed in terms of Lorentz invariants, these depending on the momenta of incoming and outgoing states. For two-particle scattering

$$a + b \to c + d, \tag{1.2}$$

the most natural variables are defined

$$\begin{aligned} s &= (p_a + p_b)^2, \\ t &= (p_a - p_c)^2 \end{aligned} \tag{1.3}$$

and

$$u = (p_a - p_d)^2, \tag{1.4}$$

in addition to the four masses, m_a, m_b, m_c and m_d. $\sqrt{s}$ is the centre-of-mass energy and $-t$ the centre-of-mass three-momentum exchange squared. u is fully constrained by s and t,

$$s + t + u = m_a^2 + m_b^2 + m_c^2 + m_d^2. \tag{1.5}$$

We will also assume conservation of probability, giving us a unitary S-matrix

$$SS^\dagger = S^\dagger S = 1. \tag{1.6}$$

The S-matrix holds the probability of incoming particles evolving into out states with or without interaction. We are interested only in interactions, so it is convenient to introduce the T-matrix

$$S = 1 + iT. \tag{1.7}$$

Further, we understand that we must have conservation of momenta, which allows us to define the scattering amplitude

$$T_{if} = (2\pi)^4 \delta^{(4)} \left(\sum_i p_i - \sum_f p_f \right) \mathcal{A}_{if}. \tag{1.8}$$

The scattering amplitude is the quantity we are interested in calculating; it allows us to find the cross-section for interaction by squaring it. For the scattering of an initial state of two particles $a + b \to f$ where f are the final state particles, we can write

$$d\sigma_{if} = \frac{1}{2E_a 2E_b |v_a - v_b|} d(P.S.^f)(2\pi)^4 \delta^{(4)} \left(\sum_i p_i - \sum_f p_f \right) |\mathcal{A}_{if}|^2, \tag{1.9}$$

where $d(P.S.^f)$ is the f body phase space. Note that at s high enough we can neglect masses, giving $2E_a 2E_b |v_a - v_b| \simeq 2s$. The unitarity of the S-matrix enforces

$$i(T_{if} - T_{if}^\dagger) = -T_{in} T_{nf}^\dagger, \tag{1.10}$$

with a summation over n implied, leading to

$$2\mathrm{Im}\mathcal{A}_{if} = (2\pi)^4 \sum_n \int d(P.S.^n) \delta^{(4)} \left(\sum_n p_n - \sum_f p_f \right) \mathcal{A}_{in} \mathcal{A}_{nf}^\dagger. \tag{1.11}$$

This formula proves to be important, as in perturbation theory it leads to the Cutkosky rules that we shall make use of later.

A further assumption that we will now make is that the scattering amplitude is an analytic function of the Lorentz invariants s and t considered as complex variables, with only the singularities required by unitarity. That we require singularities becomes obvious when we put $i = f$ in equation (1.11) with $t = 0$. This gives us the optical theorem, that relates the imaginary part of a forward elastic amplitude to the total cross-section;

$$\frac{\mathrm{Im}\mathcal{A}_{ii}(s, t = 0)}{s} = \sigma_{tot} \tag{1.12}$$

We see that for a cross-section to be non-zero we require a non-zero imaginary component of the scattering amplitude. We also observe that physical values of s lie on the positive real axis. Any cross-section has a physical threshold below which the production of the final state particles is kinematically impossible. Below that threshold on the real axis, we have a real scattering amplitude. This means that the scattering amplitude obeys the Schwarz reflection principle. It is analytic and real on part of the real axis, therefore it can be expressed as a power series with real coefficients and can be analytically continued into the complex plane with real coefficients. Therefore everywhere within its domain of analyticity the amplitude satisfies

$$\mathcal{A}(s,t)^* = \mathcal{A}(s^*,t). \tag{1.13}$$

In order to have a non-zero imaginary part above threshold we therefore require branch singularities. Therefore for our amplitude

$$\begin{aligned} \mathrm{Im}\mathcal{A}(s,t) &= \frac{\mathcal{A}(s,t) - \mathcal{A}(s,t)^*}{2i} \\ &= \frac{\mathcal{A}(s,t) - \mathcal{A}(s^*,t)}{2i} \end{aligned} \tag{1.14}$$

and hence for real s,

$$\mathrm{Im}\mathcal{A}(s,t) = \frac{1}{2i}\lim_{\epsilon\to 0}[\mathcal{A}(s+i\epsilon,t) - \mathcal{A}(s-i\epsilon,t)] \equiv \Delta_s\mathcal{A}(s,t). \tag{1.15}$$

Another consequence of analyticity is crossing symmetry. A 'blob' representing an undefined interaction of two particles to two particles can be orientated in space-time a number of ways. For example, consider $a+b\to c+d$. This is depicted in figure[1] 1.1, where we take time as moving from left to right. The definitions of the Lorentz invariants s, t and u have the physical values, $s>0$ and t and $u<0$. Reorienting the 'blob' gives us $a+\bar{c}\to\bar{b}+d$ and a new scattering amplitude with physical region $t>0$ and s and $u<0$. These two scattering amplitudes are related via analytic continuation between the regions. This can be expressed as

$$\mathcal{A}_{a+\bar{c}\to\bar{b}+d}(s,t,u) = \mathcal{A}_{a+b\to c+d}(t,s,u) \tag{1.16}$$

[1]This and many other diagrams in this thesis were constructed using Axodraw [4].

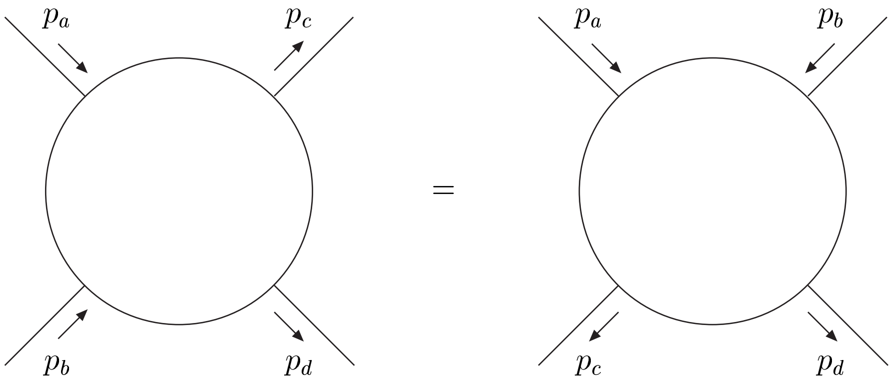

Figure 1.1: A picture of the process $ab \to cd$, in terms of an unspecified interaction represented by a 'blob'. Crossing symmetry allows us to related this to the process $a\bar{c} \to \bar{b}d$ by the substitution of momenta corresponding to the change $s \leftrightarrow t$.

and for the process $a + \bar{d} \to \bar{b} + c$,

$$\mathcal{A}_{a+\bar{d}\to\bar{b}+c}(s,t,u) = \mathcal{A}_{a+b\to c+d}(u,t,s). \tag{1.17}$$

Physical processes for the u and t channels necessitate cuts along the real u and t axis. For $t < 0$ and $-t \ll s$ for example, the u threshold, u_0^+, translates to a cut on the negative real axis, $s_0^- = \sum_i m_i^2 - t - u_0^+$. The import of this discussion about the analytical behaviour of the scattering amplitude becomes clear when we now make use of the Cauchy residue theorem. We can write

$$\mathcal{A}(s,t) = \frac{1}{2\pi i}\oint_c \frac{\mathcal{A}(s',t)}{s'-s} ds'. \tag{1.18}$$

If we assume that

$$\mathcal{A}(s,t) \to 0 \;\text{ as }\; |s| \to \infty, \tag{1.19}$$

then we can deform the contours, resulting in the only non-zero contributions from around the (two) branch cuts. Therefore

$$\mathcal{A}(s,t) = \frac{1}{\pi}\int_{s_0^+}^{\infty} \frac{\mathrm{Im}\mathcal{A}(s',t)}{(s'-s)} ds' + \frac{1}{\pi}\int_{-\infty}^{s_0^-} \frac{\mathrm{Im}\mathcal{A}(s',t)}{(s'-s)} ds'. \tag{1.20}$$

This type of relation relating real and imaginary parts is called a dispersion relation. Where the scattering amplitude does not obey (1.19) we must make subtractions; we divide by factors of $s - s_i$ to make the contribution at infinity vanish. For example, a scattering amplitude that diverges more weakly than s can be written

$$\frac{\mathcal{A}(s,t)}{s-s_0} = \frac{1}{2\pi i}\oint_{C_s} \frac{\mathcal{A}(s',t)}{(s'-s)(s'-s_0)}ds'. \tag{1.21}$$

Deforming the contour picks up a new contribution from the new pole at s_0 in addition to the cut contributions. We can subtract as many times as required. A scattering amplitude that diverges more weakly than s^2 is guaranteed to converge with two subtractions. Deforming the contour around the cuts we find,

$$\begin{aligned}\mathcal{A}(s,t) &= \frac{(s-s_1)}{(s_0-s_1)}\mathcal{A}(s_0,t) + \frac{(s-s_0)}{(s_1-s_0)}\mathcal{A}(s_1,t)\\ &+\frac{(s-s_0)(s-s_1)}{\pi}\int_{s_+}^{\infty} ds' \frac{\operatorname{Im}\mathcal{A}(s',t)}{(s'-s)(s'-s_0)(s'-s_1)}\\ &+\frac{(s-s_0)(s-s_1)}{\pi}\int_{-\infty}^{s_-} ds' \frac{\operatorname{Im}\mathcal{A}(s',t)}{(s'-s)(s'-s_0)(s'-s_1)}.\end{aligned} \tag{1.22}$$

These type of relations are useful because in principle we need only find the imaginary component to find the whole scattering amplitude.

1.3 Regge theory

Consider the two-to-two scattering of $a\bar{c} \to \bar{b}d$ with $\sqrt{s}$ much greater than the masses of the external particles. The scattering amplitude can be written as a partial wave expansion in Legendre polynomials, $P_l(\cos\theta)$, where θ is the centre-of-mass frame scattering angle, which in our approximation, can be expressed

$$\cos\theta = 1 + 2t/s. \tag{1.23}$$

The partial wave expansion is then

$$\mathcal{A}_{a\bar{c}\to\bar{b}d}(s,t) = \sum_{l=0}^{\infty}(2l+1)a_l(s)P_l(1+2t/s), \tag{1.24}$$

where $a_l(s)$ are the partial wave amplitudes. We can cross this process, using the properties of the S-matrix, to obtain

$$\mathcal{A}_{ab\to cd}(s,t) = \sum_{l=0}^{\infty}(2l+1)a_l(t)P_l(1+2s/t), \tag{1.25}$$

where we have permuted $s \leftrightarrow t$. An interesting technique can be applied here to re-express the sum as a complex integral. Note that $\sin \pi l$ has zeros for integer l and its inverse has residues $(-1)^l/\pi$. Relation 8.916:3 from [5] introduces a Gaussian hypergeometric function and gives us

$$(-1)^l P_l(1+2s/t) = {}_2F_1(l+1,-l;1;1+s/t), \tag{1.26}$$

allowing us to analytically continue and write the amplitude

$$\mathcal{A}_{ab\to cd}(s,t) = \frac{1}{2i}\oint_C dl(2l+1)\frac{a(l,t)}{\sin \pi l}\,{}_2F_1(l+1,-l;1;1+s/t), \tag{1.27}$$

where the contour must envelop the positive real axis in such a way as not to enclose any poles other than at integer l. This is called a Sommerfeld-Watson transform and successfully analytically continues angular momentum into the complex plane[2]. The use of this representation becomes apparent when we deform the contour. Let us deform this contour into a line integral, a vanishing contribution from infinity and the sum of the residues of the poles of the integrand that we have passed in the complex plane. We get

$$\begin{aligned}\mathcal{A}_{ab\to cd}(s,t) &= \frac{1}{2i}\int_{1/2-i\infty}^{1/2+i\infty} dl(2l+1)\frac{a(l,t)}{\sin \pi l}\,{}_2F_1(l+1,-l;1;1+s/t)\\ &+\pi\sum_n(2\alpha_n+1)\frac{a(\alpha_n,t)}{\sin \pi\alpha_n}{}_2F_1(\alpha_n+1,-\alpha_n;1;1+s/t).\end{aligned} \tag{1.28}$$

In this study we shall be interested in the Regge region where $s \gg |t|$. Relation in 9.132:2 in [5] gives us

$${}_2F_1(l+1,-l;1;1+s/t)|_{s\to\infty} \to \frac{\Gamma(2l+1)}{\Gamma^2(l+1)}\left(\frac{s}{|t|}\right)^l. \tag{1.29}$$

[2]In fact there is a problem with the uniqueness of $a(l,t)$. The solution to this problem introduces the concept of signature [1]. This complication does not affect the gist of the following analysis, so we neglect to complicate matters here.

As $s \to \infty$ the asymptotic contribution will be from the pole with the largest real component. We shall assume that we are in the Regge region strongly enough that we require only a finite set of pole contributions. That is,

$$\mathcal{A}^{Regge}_{ab\to cd}(s,t) = \sum_n \beta_n(t)\, s^{\alpha_n(t)} \tag{1.30}$$

where

$$\beta_n(t) = \pi(2\alpha_n(t)+1)\,\frac{a(\alpha_n(t),t)}{\sin\pi\alpha_n(t)}\frac{\Gamma(2l+1)}{\Gamma^2(l+1)}|t|^{-l}. \tag{1.31}$$

The poles on the real axis of the complex angular momentum plane correspond to the bound states of physical particles. What do the poles off the real axis correspond to? They cannot be stable particles, since they lie off the real axis. More than that, they can't in general correspond to physical particles at all, since they do not possess integer angular momentum. Nevertheless, we refer to the path mapped out in t by $\alpha_n(t)$ a Regge trajectory and the associated exchange, the exchange of a reggeon.

If we consider this process crossed into the t-channel, rather than reggeon exchange, we have reggeon resonance formation. Chew and Frautschi noticed that if a family of physical meson resonances were plotted, they lay on a straight line of spin versus square mass, $\alpha(m_i^2) = J_i$ [6]. In the t-channel we have resonance formation with $t = m_i^2$. We can interpret this as the physical values of angular momentum on a Regge trajectory. Further, at least at small positive t, we can write a Regge trajectory

$$\alpha(t) = \alpha(0) + \alpha' t. \tag{1.32}$$

It is an empirical observation that the total cross-sections of most scattering processes mediated by the strong force in the Regge region exhibit a falling cross-section that turns over into an asymptotic rise at higher s [7]. The example of $p\bar{p}$ scattering is illustrated in figure 1.2. The total cross-section for any two particle interaction is proportional to the forward elastic scattering of the two particles divided by s *i.e.* $\sigma_{tot} \propto \sum_n s^{\alpha_n(0)-1}$ (equation (1.12)). We see that if we were to try to interpret the empirical observation in terms of Regge theory, we would have to posit the existence of one or more Regge trajectories with $\alpha(0) > 1$ and at least one of

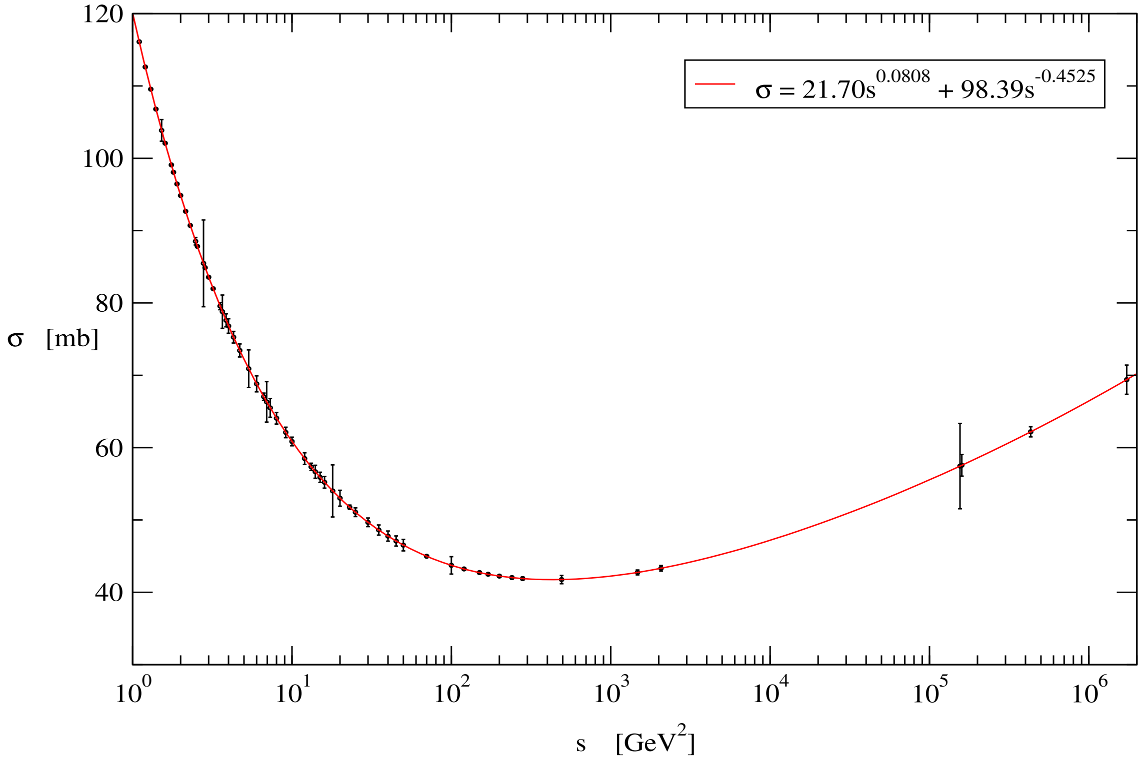

Figure 1.2: The total $p\bar{p}$ cross-section and the fit of [8]. The data only show statistical errors and are taken from [7].

$\alpha(0) < 1$. The authors of [8] were able to fit an impressive range of cross-sections with the two trajectories

$$\alpha(t) = 0.55 + 0.86t \tag{1.33}$$

and

$$\alpha_p(t) = 1.08 + 0.25t. \tag{1.34}$$

The theories of Pomeranchuk [9] and Okun and Pomeranchuk [10] tell us that any cross-section that does not asymptotically vanish must involve the exchange of the quantum number of the vacuum. Such a trajectory with $\alpha(0) > 1$ is called a pomeron. No physical particles have been firmly identified as yet for such a trajectory, though particles consisting purely of glue are a hypothesised possibility. Because the exchange of a pomeron involves the net exchange of no quantum numbers, it is a mechanism for diffractive scattering and thus diffractive scattering is commonly associated with a cross-section rising with s. Note, however, that for t more than a fraction of a

GeV^2, the reggeon trajectory becomes negative. This means that the Regge pomeron of equation (1.34) corresponds to a contribution that falls with s for $-t \geq 1\ \mathrm{GeV}^2$. The possibility of further pomeron trajectories with a higher intercept and a smaller slope, remains. Ultimately, an important aim in the particle physics of the strong force would be to reproduce Regge type behaviour in a perturbative field theory of the strong interaction, such as QCD, in the perturbative Regge region, where $s \gg -t \gg 1\ \mathrm{GeV}^2$. This 'reggeisation' can be defined as deriving behaviour that can be parameterised

$$\mathcal{A} \propto s^{\alpha(t)} \tag{1.35}$$

where for fundamental particles of the field theory

$$\alpha(m^2) = J. \tag{1.36}$$

1.4 QCD in the Regge region

In perturbative quantum field theory it is the Lagrangian that is the instruction booklet. Working in the Feynman gauge the relevant part of the QCD Lagrangian for our purposes is[3]

$$\mathcal{L} = -\frac{1}{4}(F^a_{\mu\nu})^2 + \bar{\psi}(i\not{D} - m)\psi \tag{1.37}$$

where

$$F^a_{\mu\nu} = [\partial_\mu A^a_\nu - \partial_\nu A^a_\mu] + (g f^{abc} A^b_\mu A^c_\nu) \tag{1.38}$$

and

$$D_\mu = \partial_\mu - \{ig A^a_\mu t^a_r\}. \tag{1.39}$$

The indices a, b and c are colour indices corresponding to the generators of the gauge group, t^a are the corresponding representation matrices and f^{abc} correspond to the structure constants. A^a_ν is the gauge boson, or gluon, field and ψ is the fermion field. Reading off the Feynman rules we get the results displayed in figure 1.3 and to these

	initial state	final state
fermion	$\psi\lvert\mathbf{p}, s\rangle = u_s(p)$	$\langle\mathbf{p}\ , s\rvert\bar{\psi} = \bar{u}_s(p)$
anti-fermion	$\bar{\psi}\lvert\mathbf{p}, s\rangle = \bar{v}_s(p)$	$\langle\mathbf{p}\ , s\rvert\psi = v_s(p)$
boson	$A_\mu\lvert\mathbf{p}\rangle = e_\mu^{(\lambda)}$	$\langle\mathbf{p}\rvert A_\mu = e_\mu^{(\lambda)\,*}$

Table 1.1: The initial and final state Feynman rules for external states. The symbol linking the fields and states indicates that they are contracted together. See for example [11].

we must add the rules for initial and final states listed in table 1.1. Although these Feynman rules appear in any textbook on quantum field theory, we make the point of listing them here for ease of reference in the following chapter.

Now let us consider QCD in the light of the results of the previous sections. In perturbation theory the formula (1.11) leads to the Cutkosky cutting rules with

$$\mathrm{Im}\mathcal{A}_{ab\to cd} = \frac{1}{2}\sum_n \int d(\Pi_n)\mathcal{A}_{ab\to X_n}(k)\mathcal{A}^\dagger_{cd\to X_n}(k-q), \tag{1.40}$$

where $\mathcal{A}_{ab\to X_n}$ is the $a+b\to X_n$ scattering amplitude and we integrate over the phase space of n intermediate on-shell particles. Note that for convenience we have absorbed the δ-function of (1.11) into the Π integral; Π_n is then the $2\to n$ phase space integral. The amplitudes on the right-hand side of (1.40) are physical (external legs are on-shell) and the equality means we can relate it to the diagram of the amplitude on the left-hand side. The equality tells us that to find the imaginary part of $\mathcal{A}_{ab\to cd}$ we take the diagram of $ab\to cd$ and sum over all the ways we can cut through the diagram leaving it fully connected, replacing the cut propagators with on-shell enforcing δ-functions. For example,

$$\begin{aligned}\int d(\Pi_2) &= \int d(P.S.^2)\,(2\pi)^4\delta^{(4)}(p_1+p_2-l-l')\\ &= \int \frac{d^4l}{(2\pi)^3}\frac{d^4l'}{(2\pi)^3}\delta(l^2)\delta(l'^2)(2\pi)^4\delta^{(4)}(p_1+p_2-l-l'),\end{aligned} \tag{1.41}$$

[3] We neglect ghosts here. Feynman rules and therefore a Lagrangian is required for these unphysical particles at the loop level. We shall construct all our scattering amplitudes from subamplitudes which have no loops and onshell final states. Ghosts do not contribute.

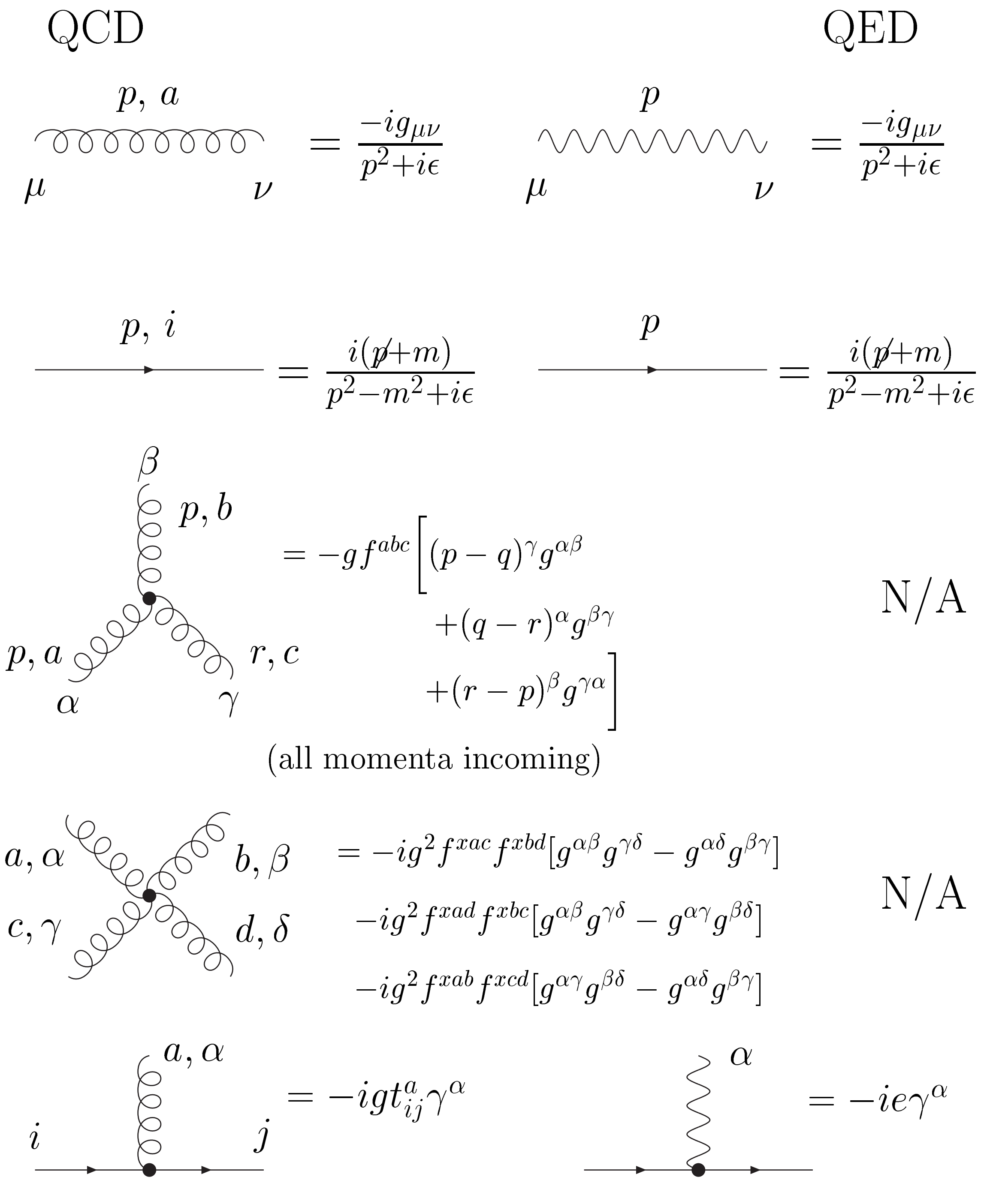

Figure 1.3: The QCD and QED Feynman rules in the Feynman gauge. The boson-boson couplings do not occur in QED because it is an abelian theory.

where l and l' are the momenta of cut particles. Equation (1.41) is indeed the $2 \to 2$ phase space. See [11] for more details and a proof of equation (1.40).

Calculations in QCD in general are more demanding than in QED. There are more Feynman rules and hence more diagrams, a problem that becomes accentuated the higher we go in order. In addition the colour algebra complicates. Higher order calculations are more difficult, but due to the largeness of the strong coupling, higher orders are often far more crucial than in QED. It is a struggle to test QCD quantitatively against nature and we have to look to where it is best to try.

Diffraction provides one avenue. Diffraction is typified by momentum exchanges much less than the centre-of-mass energy; $s \gg -t$. This, as we have seen, is precisely the Regge region, and as observed in the previous section, diffraction is mediated by colour singlet exchange. In QCD we will also refer to this exchanged 'object' as the pomeron. A single strongly interacting particle in QCD is coloured, therefore the pomeron must be a compound object, the simplest being two gluons. We can hope to use our large disparity in scales to our advantage in perturbation theory by systematically making approximations. One such important approximation is the eikonal, which neglects $t = -q^2$ next to s in a spinor. It gives us

$$\bar{u}_s(p_1)\gamma^\mu u_{s'}(p_1 - q) \sim \bar{u}_s(p_1)\gamma^\mu u_{s'}(p_1) = 2p_1^\mu \delta_{ss'}. \tag{1.42}$$

In many cases this approximation drastically simplifies Dirac algebra. We can also, potentially, throw whole classes of diagrams away because they are subleading with respect to another set in s/t. In the Feynman gauge for example, it turns out that all the diagrams with fermion loops that contribute to the perturbative pomeron are subleading [1].

Let us consider first only the lowest order in perturbation theory. In Chapter 2 we derive the lowest order colour-singlet exchange amplitude, two-gluon exchange, for the general process $a + b \to c + d$. The leading s contribution to the amplitude for this process can be written,

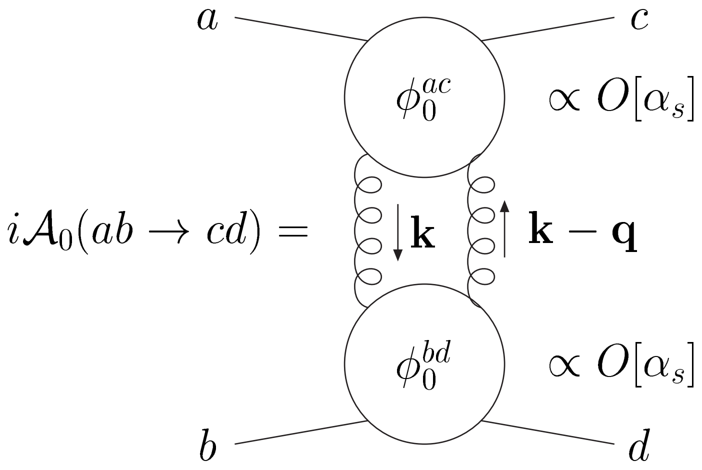

Figure 1.4: The lowest order impact factor representation of QCD colour singlet amplitude; two gluon exchange.

$$\mathcal{A}_0(ab \to cd) = is \int \frac{\phi_0^{ac}(\mathbf{k})\phi_0^{bd}(-\mathbf{k})}{\mathbf{k}^2(\mathbf{k}-\mathbf{q})^2}\frac{d^2\mathbf{k}}{(2\pi)^2} \tag{1.43}$$

where ϕ_0^{ac} contains the lowest order transition of $a \to c$ (see figure 1.4). This object is called an 'impact factor'. The impact factor representation first appeared in a set of pioneering papers by Cheng and Wu [12]. Observe that the Lorentz structure factorises between the two transitions that occur through the exchange of two gluons. Notice also that the transverse momenta integral has factorised from the other components, those being absorbed into the impact factors. This is also a feature beyond leading order in α_s. Despite the simplification possible in the Regge diffractive region there are some disadvantages. The largeness of s/t can compensate for the smallness of α_s. It becomes necessary to sum up to higher orders in a new expansion parameter, $z \propto \alpha_s \ln(s/|t|)$. When we talk about a leading s approximation we will mean we keep the 'leading log' terms, throwing away terms for example $\propto \alpha_s^n \ln^{n-1}(s/|t|)$.

When we want to calculate to higher orders, that is exchange a more complicated 'pomeron', our amplitude corresponds to that represented in figure 1.5. We find that

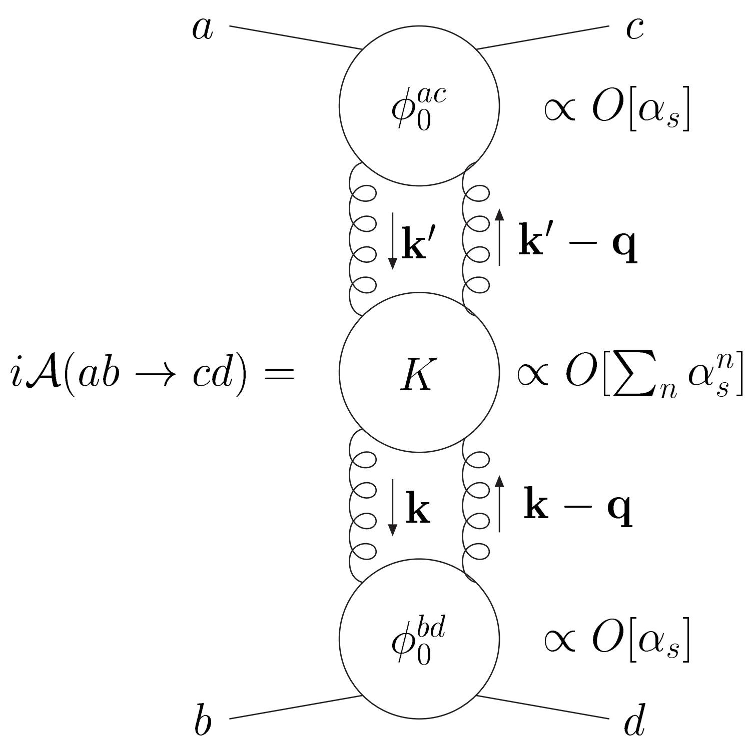

Figure 1.5: The impact factor representation of QCD colour singlet amplitude; leading log QCD pomeron exchange.

the structure of the two-gluon result generalises;

$$\mathcal{A} = is \int \phi_0^{ac}(\mathbf{k}) K(\mathbf{k},\mathbf{k}') \phi_0^{bd}(-\mathbf{k}') \frac{d^2\mathbf{k} d^2\mathbf{k}'}{(2\pi)^4} \tag{1.44}$$

$$= is \int \phi_0^{ac}(\mathbf{k}) \left(\sum_{n=0}^{\infty} K_n(\mathbf{k},\mathbf{k}') \frac{z^n}{n!} \right) \phi_0^{bd}(-\mathbf{k}') \frac{d^2\mathbf{k} d^2\mathbf{k}'}{(2\pi)^4}$$

$$\equiv is \int \frac{\phi_0^{ac}(\mathbf{k}) \left(\sum_{n=0}^{\infty} \phi_n^{bd}(-\mathbf{k}) \frac{z^n}{n!} \right)}{\mathbf{k}^2 (\mathbf{k}-\mathbf{q})^2} \frac{d^2\mathbf{k}}{(2\pi)^2}, \tag{1.45}$$

where we have defined $\phi_n^{bd}(-\mathbf{k}') \equiv K_n(\mathbf{k},\mathbf{k}') \phi_0^{bd}(-\mathbf{k}')\, \mathbf{k}^2 (\mathbf{k}-\mathbf{q})^2$ and have seen that

$$K_0(\mathbf{k},\mathbf{k}') = (2\pi)^2 \frac{\delta^{(2)}(\mathbf{k}-\mathbf{k}')}{\mathbf{k}^2(\mathbf{k}-\mathbf{q})^2}. \tag{1.46}$$

The extension of the calculation beyond leading orders is involved. It turns out that the exchanged pomeron is a ladder-like object consisting of diagrams with gluon 'struts' exchanged between incident particles, with these 'struts' interacting with each other via gluon 'rungs'.

Considering octet rather than singlet exchange for a moment, it turns out that summing all the leading s diagrams to all orders for colour octet exchange can be more neatly expressed as the sum over the number of gluons exchanged between external particles and interactions between these gluons via an effective three gluon vertex

$$\Gamma^{\sigma}_{\mu\nu}(k_1, k_2) = \delta_{+\mu}\delta_{-\nu} \left[\left(k_1^+ + \frac{\mathbf{k_1}^2}{k_2^-} \right) \delta^{+\sigma} + \left(k_2^- + \frac{\mathbf{k}_2^2}{k_1^+} \right) \delta^{-\sigma} - (k_1 + k_2)^{\sigma}_{\perp} \right]. \tag{1.47}$$

See, for example, [1] for further details. We have expressed the vertex in light-cone coordinates (see section 2.1.2 for more on light-cone coordinates) with

$$\begin{aligned} p_1^\mu &= (\sqrt{s/2}, 0, \mathbf{0}) \quad \text{(incoming particle momentum)}, \\ p_2^\mu &= (0, \sqrt{s/2}, \mathbf{0}) \quad \text{(incoming particle momentum)}, \\ \text{and} \quad k_i^\mu &= (k^+, k^-, \mathbf{k}) \quad \text{(momenta of struts)}. \end{aligned} \tag{1.48}$$

Figure 1.6 illustrates the summed diagrams; for more details we again refer the reader to [1]. Note that such diagrams are no longer Feynman diagrams, strictly speaking, once we have introduced the effective vertex Γ. The result of performing the sum of diagrams is that we find the gluon reggeises. In fact the amplitude for colour octet exchange becomes

$$\mathcal{A}^{(8)} \propto \left(\frac{s}{\Lambda^2} \right)^{\alpha_G(t)} \tag{1.49}$$

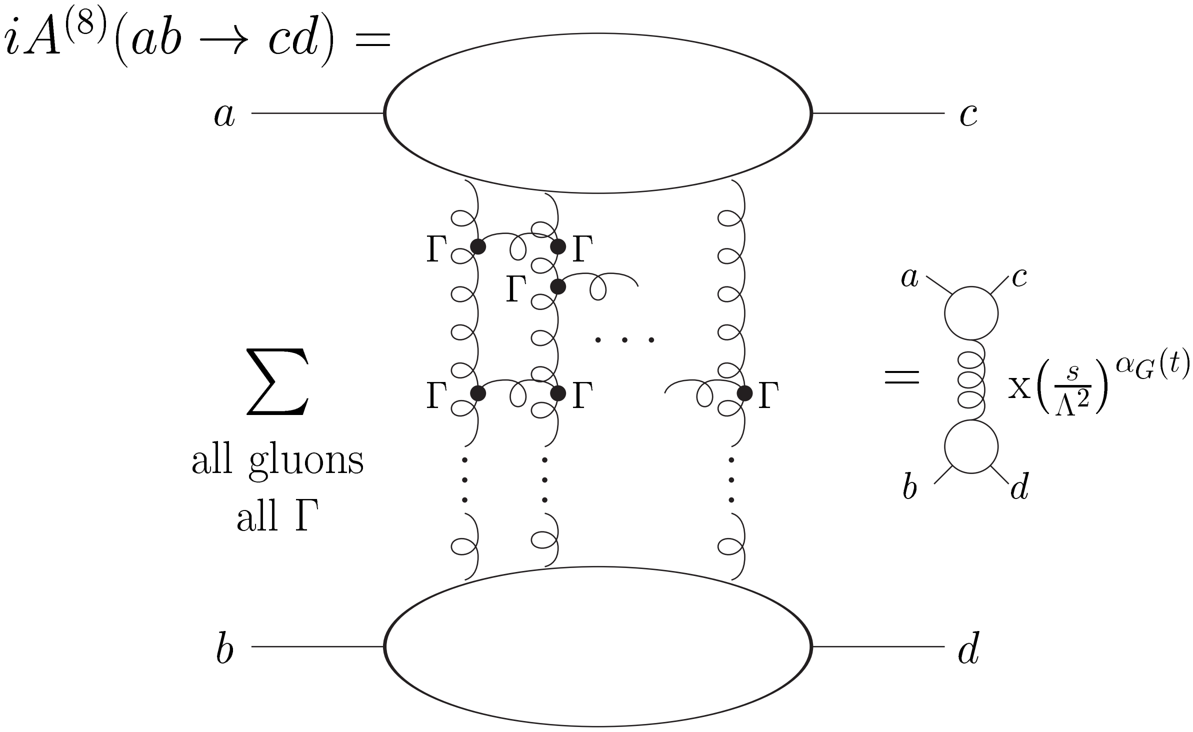

Figure 1.6: The gluon ladder consisting of gluons and the effective three-gluon vertex Γ. The sum over all possible gluon exchanges and all possible Γ couplings results in the reggeisation of the gluon.

where

$$\alpha_G(-\mathbf{q}^2) = 1 - \frac{N\alpha_s \mathbf{q}^2}{(2\pi)^{2+\epsilon}} \int \frac{d^{2+\epsilon}\mathbf{k}}{\mathbf{k}^2(\mathbf{k}-\mathbf{q})^2}. \tag{1.50}$$

Λ^2 can only depend on the scales in the problem, all much less than s, and we have dimensionally regularised α_G. The reggeisation of the (massless) gluon requires that $\alpha_G(0) = 1$ and this is clearly satisfied.

Colour octet exchange is complicated but generates a simple result. The colour singlet exchange of diffractive scattering has no such simplification. The neat exponentiation of octet exchange is spoiled by the differing colour algebra [1]. We can still build it up, at finite order in α_s, by considering the exchange of reggeised gluons and their interactions via the three-gluon effective vertex. The summation to all orders is difficult. Balitsky, Fadin, Kuraev and Lipatov constructed an integral equation that allows us to find the nth order impact factor iteratively from the zeroth one [13]. Their result can be written,

$$\begin{aligned}\phi_i(\mathbf{k}_i, z_i) = &\frac{1}{\pi}\int_0^{z_i} dz' \int \frac{d^2\mathbf{k}_{i-1}}{(\mathbf{k}_i - \mathbf{k}_{i-1})^2} \times \\ &\Bigg(\phi_{i-1}(\mathbf{k}_{i-1}, z_{i-1})\left[\frac{\hat{\mathbf{k}}_i^2}{\hat{\mathbf{k}}_{i-1}^2} + \frac{\mathbf{k}_i^2}{\mathbf{k}_{i-1}^2} - \mathbf{q}^2\frac{(\mathbf{k}_i - \mathbf{k}_{i-1})^2}{\hat{\mathbf{k}}_{i-1}^2\mathbf{k}_{i-1}^2}\right] \\ &-\phi_{i-1}(\mathbf{k}_i, z_{i-1})\left[\frac{\mathbf{k}_i^2}{\mathbf{k}_{i-1}^2 + (\mathbf{k}_i - \mathbf{k}_{i-1})^2} + \frac{\hat{\mathbf{k}}_i^2}{\hat{\mathbf{k}}_{i-1}^2 + (\mathbf{k}_i - \mathbf{k}_{i-1})^2}\right]\Bigg)\end{aligned} \tag{1.51}$$

where

$$z = \frac{3\alpha_s}{2\pi}\ln\left(\frac{s}{\Lambda^2}\right) \tag{1.52}$$

and we have used the notation $\hat{\mathbf{k}} = \mathbf{k} - \mathbf{q}$. This is the BFKL equation. Lipatov succeeded in solving this equation to perform the complete summation of all orders in z [14]. His result for non-zero t can be written as

---

$$\begin{aligned}K(\mathbf{k}, \mathbf{k}') = &\frac{1}{(2\pi)^4}\sum_{n=-\infty}^{n=\infty}\int_{-\infty}^{\infty} d\nu \, \frac{\nu^2 + n^2/4}{[\nu^2 + (n-1)^2/4][\nu^2 + (n+1)^2/4]} e^{\chi_n(\nu) z} \\ &\times \left(\int d^2\rho_1 \, d^2\rho_2 \; E_{n,\nu}(\rho_1, \rho_2) e^{ik\cdot\rho_1} e^{i(q-k)\cdot\rho_2}\right)\left(\int d^2\rho_1' \, d^2\rho_2' \; E_{n,\nu}(\rho_1', \rho_2') e^{ik'\cdot\rho_1'} e^{i(q-k')\cdot\rho_2'}\right)\end{aligned} \tag{1.53}$$

where

$$\chi_n(\nu) \;=\; 4\mathrm{Re}\Big(\psi(1) - \psi(1/2 + |n|/2 + i\nu)\Big) \tag{1.54}$$

and

$$E_{n,\nu}(\rho_1, \rho_2) \;=\; \left(\frac{\rho_1 - \rho_2}{\rho_1 \rho_2}\right)^{-\tilde{\mu}+1/2} \left(\left(\frac{\rho_1 - \rho_2}{\rho_1 \rho_2}\right)^*\right)^{-\mu+1/2} \tag{1.55}$$

with $\mu = n/2 - i\nu$ and $\tilde{\mu} = -n/2 - i\nu$.

This result is the Leading Log BFKL (LL BFKL) pomeron. It will be the focus of this work and the formulae ((1.53), (1.54), (1.55)) will appear several times. For more details see [1, 3] or [15]. The summation variable, n, is referred to as 'conformal spin'. An important observation is that given the result of Lipatov, if we can calculate the impact factor for a process at lowest order, we can immediately generalise to all orders in α_s, within the LL approximation. For us to apply this solution consistently, we require a hard scale much larger than the characteristic scale of QCD, $\Lambda_{QCD} \sim 0.2\, GeV$, above which perturbative calculations makes sense. We also require that this large scale is much smaller than $\sqrt{s}$. A large momentum exchange $q^2 = -t$, where $\Lambda^2_{QCD} \ll |t| \ll s$, can provide the required hard scale. In such a kinematic region, for reasons discussed in the previous section, we would not expect the Regge pomeron to provide a large background.

1.5 Vector meson photoproduction

In the previous sections we have discussed general considerations applying to strong scattering in the Regge region. In this section we will narrow our focus to a specific process and put it in its experimental and historical perspective. The subject of this thesis is the process $\gamma p \to VX$, where V is a vector meson.

We are considering the perturbative Regge region, where $s \gg -t \gg \Lambda^2_{QCD}$. We apply both the solution to the LL BFKL equation and finite order calculations to the process. The two gluon calculation was developed by Ginzburg, Panfil and Serbo (GPS) [17, 18] and the BFKL model was introduced by Forshaw and Ryskin [19] and developed by Bartels, Forshaw, Lotter and Wüstoff (FR&BFLW) [20]. FR&BFLW anticipated the possibility of experimental verification at HERA. The fact that data have now been published by both the ZEUS and H1 groups at HERA [21, 22] makes this process an important test of QCD and BFKL physics. The BFKL model of FR&BFLW was compared to this (preliminary) data in [23, 24]. Despite the theoretical crudity of assuming that the quark and anti-quark leaving the hard scatter have equal momenta, it was shown that the total differential cross-section could be fitted for the ρ, ϕ and J/Ψ, with an appropriate choice of BFKL scale. This was surprising; the approximation was expected to be poor for the light mesons. The model could never give a complete description of the data, however. The measurements of ZEUS for the lighter two mesons show small but non-zero helicity-flip contributions to the cross-section; the BFKL model of FR&BFLW demands helicity conservation between the photon and meson. An understanding of why we can fit the data at all in such a crude approximation could only come from investigating a proper treatment of the meson matrix elements. Ivanov, Kirschner, Schäfer and Szymanowski (IKSS) attempted such an analysis for the light mesons [25] (in fact previously to [23, 24]). They failed to predict the correct t-dependence in the differential cross-section. Despite being a large step forward their work suffered from the fact that it was a leading order (two-gluon) calculation. The main task of this thesis is to extend the calculation to higher orders through the application of the solution to the BFKL equation. In doing so we shall attempt to make a synthesis of all the work to date.

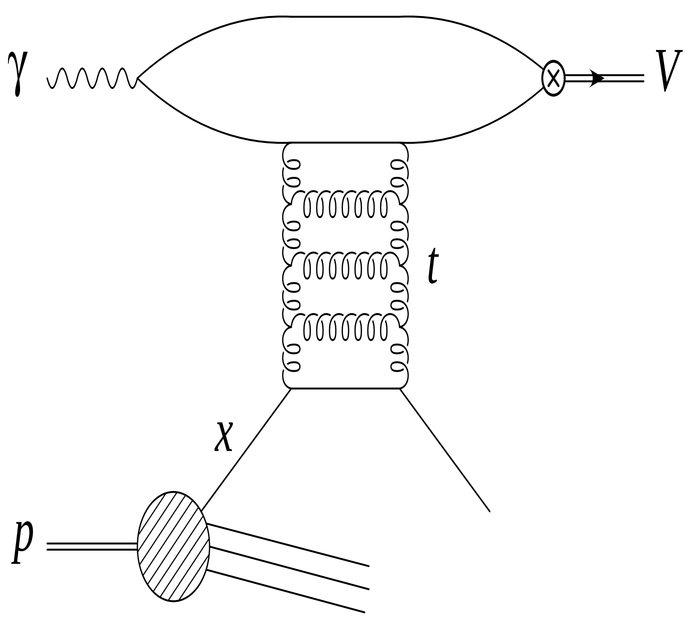

Figure 1.7: Diffractive vector meson photoproduction at large momentum transfer.

The process is assumed to occur as follows (see figure 1.7). A photon and proton approach each other with very high energies, the photon makes a transition to a quark and anti-quark pair which then scatter from the parton content of the proton, via colour singlet (pomeron) exchange. The outgoing quarks then make a transition to a bound state neutral vector meson[4] and the outgoing parton and the proton remnants hadronise to form X. As yet, however, there are no γp colliders, so experimentally the situation is not this simple. HERA is an ep collider so the data for $\gamma p \to VX$ must be unfolded from the measured data for $ep \to eVX$.

The data available from the ZEUS collaboration are for the following experimental situation (see figure 1.8) [21, 26, 27]. The electron and proton approach each other with very high energies from opposite directions along the z-axis. The electron emits a photon, which then interacts with the proton in the manner described above. The trigger condition for detection is that the scattered electron is recorded in a purpose built calorimeter, 44 m down the beam pipe from the 'interaction point' and 3 cm from the beam axis. An electron of zero deflection would force the emitted photon to

[4]We are dealing with the exchange of an object with the quantum numbers of the vacuum, therefore the outgoing meson must have the same spin and parities as the photon i.e. $J^{PC} = 1^{--}$.

be exactly on-shell. The extremely small scattering angle in this experimental set-up imposes $Q_\gamma^2 \simeq 0.01$ GeV^2 [21] *i.e.* we are dealing with vector meson photoproduction. The data come from events recorded that fitted the criteria of (1) two well measured tracks in the central tracking detector with an invariant mass consistent with that of the meson under study (2) no energy in the calorimeter that is not associated with either the two tracks or the proton remnant system (3) an electron detected in the special tagger and (4) $-t > 1$ GeV^2. This last condition ensures that the contribution from the elastic process $ep \to eVp$ is small. The reason for this is suppression from the proton form factor and that due to the Regge pomeron trajectory becoming negative. The suppression of elastic scattering is one reason why this is a clean process theoretically. This experimental set-up also allows a relatively easy determination of t for the γp system since, $t_{\gamma p} \simeq t_{ep} \simeq -p_T^2$ where p_T is the transverse momentum of the meson. Therefore it is also a clean process experimentally; we need only measure the vector meson decay products to reconstruct the momentum exchanged and need not measure X. This is good since, as characteristic for diffraction, much of the proton remnants are lost down the beam pipe where they cannot be measured. The data are for the region $80 < W_{\gamma p} < 120$ GeV, with $\langle W_{\gamma p} \rangle \sim 100$ GeV.

The H1 collaboration focuses on the heavy meson J/ψ and selected different tagging conditions [22, 29]. These imposed a less stringent constraint on the photon virtuality, but had the advantage of allowing measurements of higher momentum exchanges than were achievable in the ZEUS experiment.

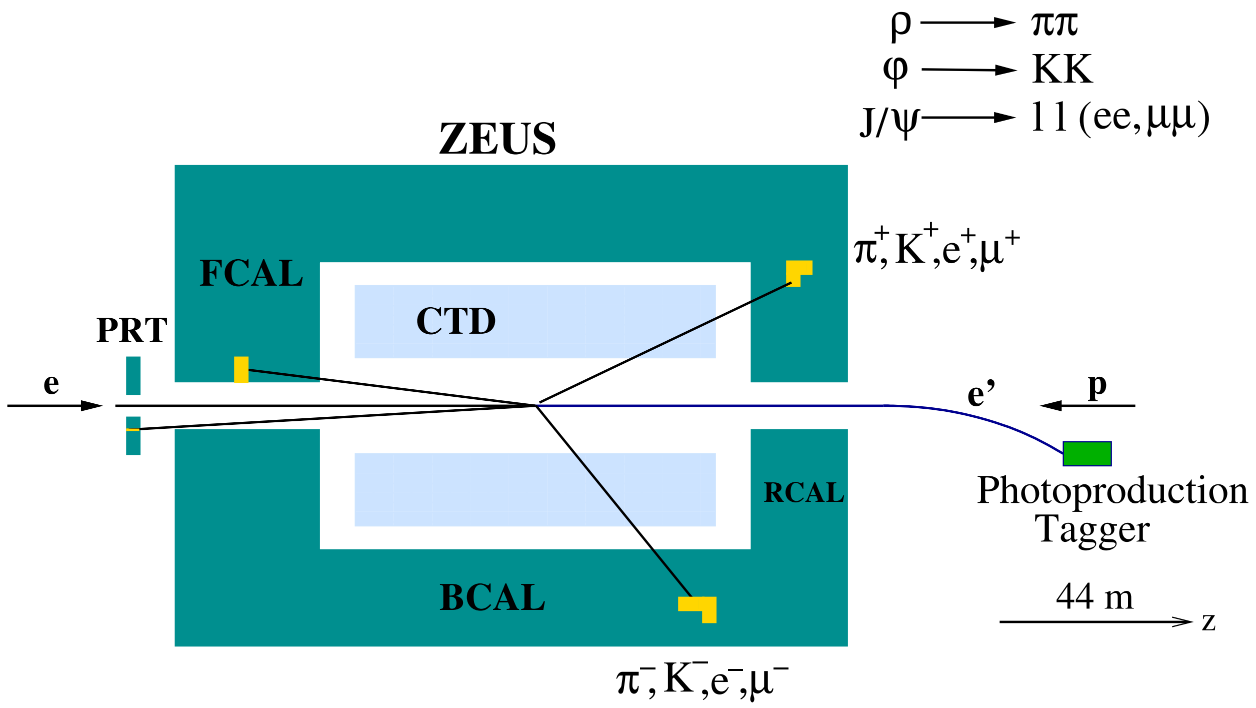

Figure 1.8: The experimental arrangement for the ZEUS detector at HERA for observation of the process $e^+p \to e^+VX$. The mesons are tagged by the decays $\rho \to \pi\pi$, $\phi \to KK$ and $J/\psi \to ll$. The components indicated are the proton remnant tagger (PRT), the forward, rear and back calorimeter (FCAL, RCAL, BCAL) and the central tracking detector (CTD). The plot is taken from [28].

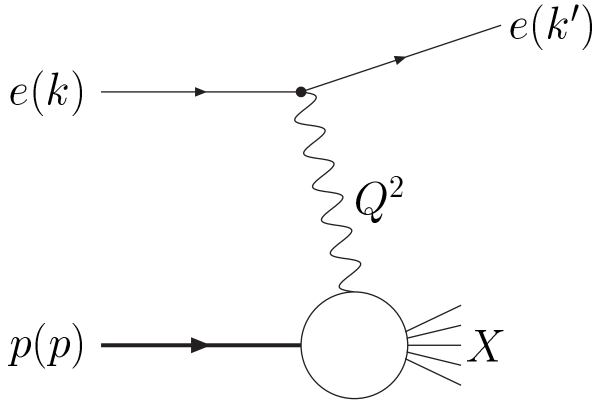

Figure 1.9: Deeply inelastic scattering (DIS) of an electron from a proton.

1.6 From hadrons to partons and back again

There is an obvious gap that needs to be bridged between the discussion in the last section and that of earlier in this chapter. Perturbative field theory deals with the interaction of fundamental particles. In QCD and QED this means leptons, quarks and the gauge bosons, photons and gluons, which can all be considered 'partons'. In the experiment as discussed, we see compound and non-perturbative particles both entering and leaving the interaction in the form of an initial state proton and final state meson. These strongly bound compound particles are hadrons. We need to get from hadrons to partons and back again.

We will consider the initial state proton first. Let us think about Deep Inelastic Scattering (DIS). This process is depicted in figure 1.9. The following analysis is partly inspired by [30]. We can parameterise this scattering process in terms of the following set of Lorentz invariant variables:

$$Q^2 = -q^2, \tag{1.56}$$

$$x = \frac{Q^2}{2p \cdot q}, \tag{1.57}$$

$$s = (k+p)^2, \tag{1.58}$$

$$W^2 = (p+q)^2 = Q^2 \frac{1-x}{x}, \tag{1.59}$$

$$\text{and} \quad y = \frac{p \cdot q}{p \cdot k} = \frac{Q^2}{xs}. \tag{1.60}$$

We will consider the deep ($Q^2 \gg m_p^2$) and inelastic ($W^2 \gg m_p^2$) limits. Further let us concentrate on the region: $m_p^2 \ll Q^2 \ll xs < s$. This will allow us to make some approximations. We parameterise the matrix element for a proton of momentum p to absorb a photon of momentum q and Lorentz index μ to produce a set of hadrons X of momenta p_X as

$$eT_\mu(p, q; p_X). \tag{1.61}$$

We also define the matrix element for an electron of momentum k to emit a photon of momentum q and Lorentz index μ,

$$eU_\mu(k, q) = \bar{u}(k)(-ie\gamma^\mu)u(k-q) \tag{1.62}$$

where we suppress spin. The matrix element for the DIS process is therefore

$$\frac{1}{4}|\mathcal{M}|^2 = \frac{1}{4} U^\mu(k,q) U^{\nu\,*}(k,q) \frac{e^4}{Q^4} T_\mu(p,q;p_X) T_\nu^*(p,q;p_X). \tag{1.63}$$

Now we define the lepton and hadron tensors, the first of which we know from perturbation theory;

$$L^{\mu\nu} = U^\mu(k,q) U^{\nu\,*}(k,q) \sim 4k^\mu k^\nu, \tag{1.64}$$

where we have used the eikonal approximation and again suppressed spin. The phase space for the process $ep \to eX$ can be written

$$d(P.S.^{n+1}) = \frac{Q^2}{16\pi^2 s x^2} dQ^2 dx d(P.S.^X) \tag{1.65}$$

where $d(P.S.^X)$ is the n-body phase-space. The hadron tensor is a non-perturbative object, nevertheless, we can parameterise our ignorance in terms of the two possible four-vectors it can depend on;

$$H_{\mu\nu} = \sum_X \int d(P.S.^X) T_\mu(p,q;p_X) T_\nu^*(p,q;p_X) \tag{1.66}$$

$$= h_1 g_{\mu\nu} + h_2 \frac{p_\mu p_\nu}{Q^2} + h_3 \frac{p_\mu q_\nu + q_\mu p_\nu}{Q^2} \tag{1.67}$$

where we have imposed symmetry in $\mu \leftrightarrow \nu$, as required by a parity conserving theory. The scalars h_i can only depend on the two independent Lorentz scalars constructed out of the two four vectors; $q^2 = -Q^2$ and $p \cdot q = Q^2/2x$ (noting $p^2 \sim 0$). In our kinematic region therefore we can write the leading term of the hadronic tensor as

$$H_{\mu\nu} \sim h_2 \frac{p_\mu p_\nu}{Q^2}. \tag{1.68}$$

Under the assumption that the interaction of the photon with the proton only involves one dimensionful scale, Q^2, then h_2, which is dimensionless, is independent of Q^2 [5]. How do we interpret the object (1.68)? We know that we will have a jet of hadrons in the final state, so the proton is not acting as a perturbative object, *i.e.* we do not get $ep \to ep$. Notice the similarity of form of equations (1.68) and (1.64); it is suggestive. If the photon was resolving perturbative constituents inside the proton we would get the same result. It is as if we were plucking out perturbative objects from inside the proton. Figure 1.10 illustrates this interpretation of DIS. If we assume this is so and we can pull out these partons, then we can factorise out the perturbative part corresponding to parton scattering from the hadronic matrix element. Let us do so; these particles will have a momentum fraction of the proton, η. There may be many types of these particles. We are dealing with QCD so we would have to sum over the flavours of quarks and the gluon[6]. Pulling the quark lines out from the unknown part

[5] By assuming that Q^2 is the only dimensionful scale, we are assuming that $Q^2 \gg m_p^2$, where m_p is the mass of the proton. We are assuming that the partons within the proton are resolved as point-like particles, since we are probing distances $r \sim 1/\sqrt{Q} \ll r_p$, where r_p is the size of the proton.

[6] Note that the gluon also obeys the eikonal approximation, with a differing colour factor.

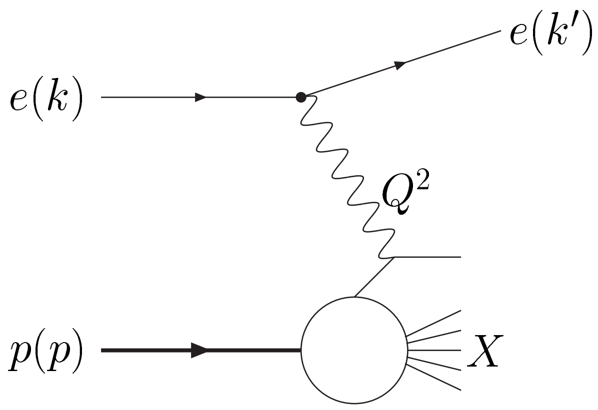

Figure 1.10: Deeply inelastic scattering (DIS) of an electron from a proton. Q^2 is of sufficient magnitude that it probes distances $r \sim 1/|Q| \ll r_p$, where r_p is the size of a proton and $r_p \sim 1/m_p$ where m_p is the mass of a proton. The photon therefore resolves the internal structure of the proton.

of the hadronic tensor, along with its corresponding phase space;

$$e^2 H_{\mu\nu} = \sum_f \int_0^1 d\eta \, |\bar{u}(\eta p)(-ie\, e_f \gamma_\mu) u(\eta p)|^2 \int d(P.S.^1)\, H_f(\eta) \tag{1.69}$$

$$= e^2 \frac{2\pi x}{Q^2} \sum_f \int_0^1 d\eta \, P_{\mu\nu}(\eta p)\, \delta(\eta - x)\, e_f^2 H_f(\eta) \tag{1.70}$$

$$= e^2 \frac{2\pi}{Q^2} \sum_f P_{\mu\nu}(\eta p)\, e_f^2 x H_f(x) \tag{1.71}$$

$$= 8\pi e^2 \frac{p_\mu p_\nu}{Q^2} \sum_f e_f^2 x^3 H_f(x), \tag{1.72}$$

where we define $P_{\mu\nu}$ (equivalent to $L_{\mu\nu}$) as the parton tensor. This allows us to find the cross-section in terms of the non-perturbative function H_f[7];

$$\frac{d^2\sigma(e+p)}{dx dQ^2} = \frac{1}{2s} \frac{Q^2}{16\pi^2 s x^2} |\mathcal{M}(e+p)|^2 = \frac{e^4}{32\pi^2 s^2 x^2 Q^2} L^{\mu\nu} H_{\mu\nu} \tag{1.73}$$

$$= \sum_f \frac{e^4}{16\pi s^2 x^2 Q^4} L^{\mu\nu} P_{\mu\nu} e_f^2 x H_f(x) = \sum_f \frac{d\sigma(e+q_f)}{dQ^2} x H_f(x) \tag{1.74}$$

[7]Note that since we have suppressed spin in the eikonal approximation we now should not spin average. In effect we have chosen initial state spins, or spin averaged already, depending on how you want to look at it.

We have argued that the cross-section for the process $ep \to eX$ can be written as the sum of convolutions of that for the process $eq \to eq$ with the function $xH_f(x) \equiv q_f(x)$, referred to as a parton distribution function (PDF). The independence of H_f on Q^2 is called Bjorken Scaling and is weakly violated beyond lowest order in perturbation theory. This violation occurs because beyond leading order in QCD a scale Λ^2_{QCD} appears. Even though PDFs cannot be calculated perturbatively, they can be measured in experiment, such as in DIS. PDFs are universal, that is a proton is a proton, regardless of the different particles it can interact with. We can use their measurements from other processes and apply them to our own. We are concerned with $\gamma p \to VX$; for this process the analog to the photon is the pomeron and the analogs to the initial and final state electrons are the photon and vector meson respectively. We will use the proton PDF determined elsewhere to get from the hadron to partons and our work is done regarding the proton; since we are dealing with an inclusive final state X, we needn't worry about putting the proton back together again.

We do have to worry about putting a meson together in the final state, however. We are considering the diffractive process $\gamma p \to VX$; to lowest order that means we want to turn a quark and anti-quark into a meson. We have the tools already to calculate up to $\gamma p \to q\bar{q}X$, but the transition $q\bar{q} \to V$ remains an unknown. We have to 'explain' how a quark and anti-quark in a certain momentum configuration make the transition to a non-perturbative object, a meson. Assuming we are able to factorise this soft transition from the hard subprocess, this will again involve a convolution over the momentum of two factorised parts. Figure 1.11 illustrates the $q\bar{q} \to V$ transition. Note the difference between the case of picking partons out of hadrons and this case of going from partons to a hadron. In the the former case we only wanted information about one parton and required no knowledge of the remaining piece. Here we want to know everything before and everything after. As we shall show in the following chapter, we will need to have knowledge of the objects

$$\langle V(p,\lambda)|\bar{\psi}(-x)\Gamma_t\psi(x)|0\rangle, \tag{1.75}$$

which correspond to the factorised soft transition and are referred to as the meson

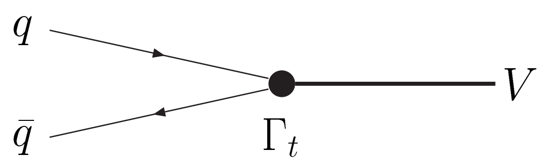

Figure 1.11: The $q\bar{q} \to V$ transition. Γ_t is the possible Dirac structure of the coupling of the meson to the $q\bar{q}$ pair; $\Gamma_t \in \{1, -i\gamma_5, \gamma_\mu, -\gamma_\mu\gamma_5, \sigma_{\mu\nu}\}$.

hadronic matrix elements[8], where $\Gamma_t \in \{1, \gamma_\mu, -i\gamma_5, -\gamma_\mu\gamma_5, \sigma_{\mu\nu}\}$, the complete basis of Dirac matrices.

Even though understanding the meson state transition requires the use of non-perturbative techniques beyond the remit of this work, we are able to deduce some information about the structure of the matrix elements. We have in the object (1.75), a quark field and anti-quark field describing particles separated by a distance $r = 2x$. Assuming the quark and anti-quark are a small dipole, corresponding to a perturbative process, we can expand the hadronic matrix element out in a Taylor expansion about $x^2 = 0$.

$$\langle V(p\lambda)|\bar{\psi}(-x)\Gamma_t\psi(x)|0\rangle = a_{(0)\,t} + \frac{a_{(1)\,t}}{1!}x^2 + \cdots \tag{1.76}$$

This is called a light-cone expansion since $x^2 = 0$ is a light-like vector. We shall make the approximation that $x^2 = 0$ exactly, corresponding to taking only the zeroth term. $f_{(0)\,t}$ can only depend on x through it being dotted with another 4-vector; there are a limited number of such 4-vectors. We have a final state meson of momentum p and polarisation λ. The wave function must have a linear dependence on the polarisation vector, from the very fact that the meson is an external state. For concreteness let us consider the example, $\Gamma_t = \gamma_\mu$. There can only be three pieces, corresponding to the three possible variables with the correct Dirac structure, x_μ, p_μ and $e^{(\lambda)\,*}_{V\,\mu}$. Therefore

[8]We choose the normalisation of a momentum state as GeV^{-1}, giving the object (1.75) the units GeV^2.

(to zeroth order)

$$\langle V(p\lambda)|\bar{\psi}(-x)\gamma_\mu\psi(x)|0\rangle = e^{(\lambda)}_{V\,\mu} a_1(p\cdot x, m_V)$$
$$+p_\mu\,(e^{(\lambda)}_V\cdot x)\,a_2(p\cdot x, m_V) + x_\mu\,(e^{(\lambda)}_V\cdot x)\,a_3(p\cdot x, m_V). \tag{1.77}$$

We can still say more about the form of the hadronic matrix elements. They must be of units GeV^2 and so the powers of $p^2 = m_V^2$ appearing in each piece are restricted. Note also that we are dealing with a non-perturbative transition. The non-perturbative physics introduces an extra dimensionful scale f_V; the matrix elements are defined to be proportional to this. So

$$\langle V(p\lambda)|\bar{\psi}(-x)\gamma_\mu\psi(x)|0\rangle = m_V f_V\Bigg(e^{(\lambda)}_{V\,\mu} b_1(p\cdot x)$$
$$+p_\mu\,(e^{(\lambda)}_V\cdot x)\,b_2(p\cdot x) + m_V^2\,x_\mu\,(e^{(\lambda)}_V\cdot x)\,b_3(p\cdot x)\Bigg), \tag{1.78}$$

where the b_i functions are dimensionless. We can also say something about the dependence of the matrix elements on the dimensionless contraction $p\cdot x$. A matrix element corresponds to the transition of an initial state quark and anti-quark to a vector meson via a coupling of Dirac structure Γ_t. We might expect, therefore, that the matrix element can be written as proportional to incoming plane-waves corresponding to the quark and anti-quark, integrated over their momenta. We shall give the quark the fraction u of the final meson momentum[9]. Therefore we will get an integral in u with a transform of type

$$\int du\, e^{-iup\cdot x} e^{-i(1-u)p\cdot(-x)} f(u) = \int du\, e^{-i\xi p\cdot x} f(u), \tag{1.79}$$

where we define $\xi = 2u-1$. u is the analogue of the x that appears in the PDFs. We still have an unspecified dependence on powers of $p\cdot x$, but the requirement that the matrix element is finite and non-zero for $x=0$ eliminates this freedom[10]. We arrive

[9] More precisely we define u to be the fraction of the $+$ momentum component. If we assume that the transverse momentum of the quark with respect to the meson direction is small, then for a relativistic quark of momentum l, $l\cdot x \sim up\cdot x$.

[10] A direct consequence of the matrix element not being finite and non-zero is that the electronic decay rate of the meson would not be finite and non-zero. Appendix B shows this explicitly.

at

$$\langle 0|\bar{\psi}(-x)\gamma_\mu\psi(x)|V(p,\lambda)\rangle = m_V f_V \Bigg(c_1 e^{(\lambda)\,*}_{V\,\mu} \int_0^1 du\, e^{-i\xi(p\cdot x)}\mathcal{D}_1(u)$$
$$+c_2 p_\mu \frac{(e^{(\lambda)\,*}_V\cdot x)}{p\cdot x}\int_0^1 du\, e^{-i\xi(p\cdot x)}\mathcal{D}_2(u) + c_3 x_\mu m_V^2 \frac{(e^{(\lambda)\,*}_V\cdot x)}{(p\cdot x)^2}\int_0^1 du\, e^{-i\xi(p\cdot x)}\mathcal{D}_3(u)\Bigg). \tag{1.80}$$

We choose the definitions of c_i and $\mathcal{D}_i$ such that $\int_0^1 du\,\mathcal{D}_i = 1$ for all i. These $\mathcal{D}_i$ functions are referred to as distribution amplitudes (DA). The form of these and the relations between them has been systematically explored in [31, 33, 32] for all the basis set of Dirac matrices. We shall use their results in this work.

Chapter 2

Two gluon exchange

The aim of this chapter is to introduce or derive all the machinery necessary to be able to write down the scattering amplitude for $\gamma q \to Vq$, via two gluon colour singlet exchange. To this end we shall:

- Section 2.1. Argue that the amplitude can, in the diffractive limit, be factorised into a convolution of two separate and unentangled quantities. One is essentially the hard subprocess $\gamma q \to q'\bar{q}'q$ and the other is the soft transition $q'\bar{q}' \to V$.
- Section 2.2. Derive high energy factorisation, the impact factor representation and subsequently the $q \to q$ and $\gamma \to q'\bar{q}'$ impact factors.
- Section 2.3. Introduce the light-cone hadronic matrix elements, identifying these with the soft transition, and simplify these in the appropriate approximations.
- Section 2.4. Put all this together to arrive at the impact factor for $\gamma \to V$ and therefore implicitly the scattering amplitude of $\gamma q \to Vq$ via two gluon exchange.
- Section 2.5. Summarise our results.

2.1 Factorisation formulae

2.1.1 The $\gamma q \to Vq$ amplitude

We chose a real initial state photon of (+) polarisation with momentum, p_1 and an incoming quark-parton of momentum p_2. Using the definitions of the T-matrix and the scattering amplitude, $\mathcal{M}$, we would like to be able to write

$$\begin{aligned}
&\delta^{(4)}(p + p_2' - p_1 - p_2)\mathcal{M}(Vq \to \gamma q) \\
&= \langle V(p,\lambda), q(p_2')|\mathrm{T}\left(\exp\left[-i\int d^4x\mathcal{H}_I\right]\right)|\gamma(p_1)q(p_2)\rangle \\
&= \langle V(p,\lambda), q(p_2')|T|\gamma(p_1)q(p_2)\rangle \\
&= (\text{sum of all connected diagrams})\,,
\end{aligned} \tag{2.1}$$

analogous to that we would get for free-particle final states, where T is the time-ordered operator, T is the T-matrix and $\mathcal{H}_I$ is the QED and QCD interaction Hamiltonian density. We have a problem, however. How do we apply the rules of Feynman diagrams when we have a bound state? Perturbation theory corresponds to expanding out the exponential in a power series of the interaction Hamiltonian. In the case of free-particle final states we would use Wick's theorem at a particular order in perturbation theory and choose only the combinations of contractions of fields in which the external states are contracted with fields and all the other fields are contracted to each other. These combinations would correspond to the fully connected diagrams. In our case we don't know how to contract fields with bound states, *i.e.* we don't know what Feynman rules we should be using. A physical picture helps to factorise out this problem. We will assume that we have a hard sub-process with a scale of the hard momentum exchange q, followed by a soft-transition to a vector meson a long time later; the lowest order transition is that of a $q\bar{q} \to V$. This is illustrated in figure 2.1. Let us start with the matrix element

$$\langle V(p,\lambda), q(p_2')|T|\gamma(p_1')q(p_2)\rangle. \tag{2.2}$$

We can insert a complete set of states. Assuming that the transition to a vector meson occurs via the lowest order Fock state, the only state that has overlap with the vector

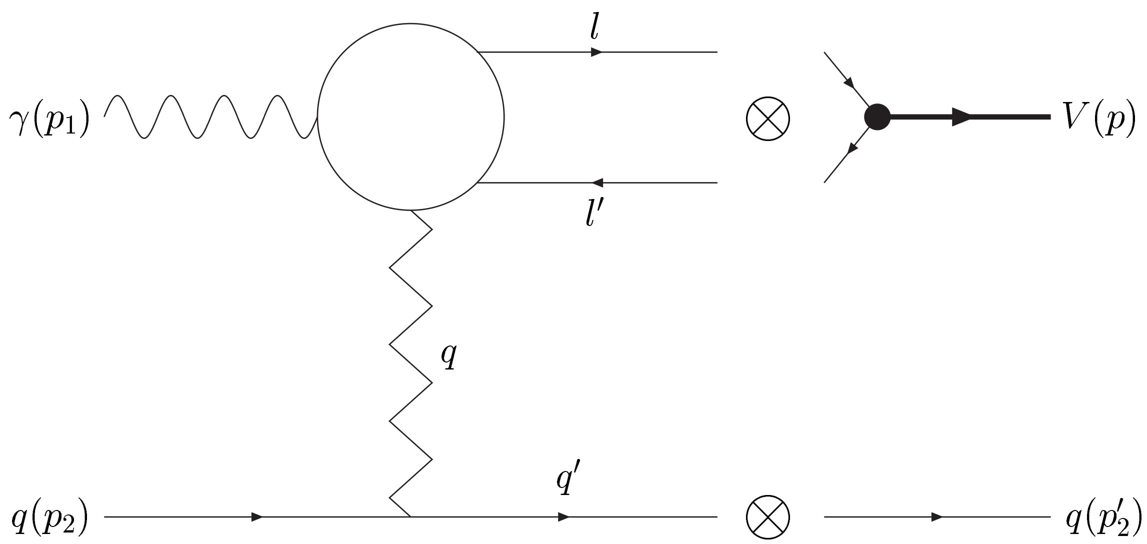

Figure 2.1: The process $\gamma q \to Vq$. This process is depicted as factorised into the convolution of the hard subprocess $\gamma q \to q'\bar{q}'q$ with the soft transition $q'\bar{q}' \to V$. The soft transition is assumed to occur at a time $t' \gg t$ where t is the time of the hard interaction, allowing factorisation. The zig-zag object is the colour singlet exchange mediator; the pomeron.

meson (and a quark) is that of a quark and anti-quark (and another quark). Thus

$$\begin{aligned}\langle V(p,\lambda), q(p_2')|T|\gamma(p_1')q(p_2)\rangle &= \int \frac{d^3l}{2E_l(2\pi)^3}\frac{d^3l'}{2E_{l'}(2\pi)^3}\frac{d^3q'}{2E_{q'}(2\pi)^3} \\ \times\langle V(p,\lambda), q(p_2')|q_f(l),\bar{q}_f(l'),q(q')\rangle&\langle q_f(l),\bar{q}_f(l'),q(q')|T|\gamma(p_1')q(p_2)\rangle. \end{aligned} \tag{2.3}$$

The quark q is a spectator in the soft transition and therefore it can be factored out to give

$$\begin{aligned}\langle V(p,\lambda), q(p_2')|T|\gamma(p_1')q(p_2)\rangle &= \int \frac{d^3l}{2E_l(2\pi)^3}\frac{d^3l'}{2E_{l'}(2\pi)^3}\frac{d^3q'}{2E_{q'}(2\pi)^3}\langle q(p_2')|q(q')\rangle \\ \times\langle V(p,\lambda)|q_f(l),\bar{q}_f(l')\rangle&\langle q_f(l),\bar{q}_f(l'),q(q')|T|\gamma(p_1')q(p_2)\rangle. \end{aligned} \tag{2.4}$$

Using the fact that

$$\langle q(p)|q(p')\rangle = 2E_p(2\pi)^3\,\delta^{(3)}(p-p') \tag{2.5}$$

we find that

$$\begin{aligned}\langle V(p,\lambda), q(p_2')|T|\gamma(p_1')q(p_2)\rangle &= \int \frac{d^3l}{2E_l(2\pi)^3}\frac{d^3l'}{2E_{l'}(2\pi)^3} \\ \times\langle V(p,\lambda)|q_f(l),\bar{q}_f(l')\rangle&\langle q_f(l),\bar{q}_f(l'),q(q')|T|\gamma(p_1')q(p_2)\rangle. \end{aligned} \tag{2.6}$$

We now have two matrix elements; one is that of the overlap of a quark anti-quark and a vector meson, the second is that of $\gamma(p')q(p_2) \to q_f(l)\bar{q}_f(l')q(p_2')$. Writing the latter in terms of its scattering amplitude we find:

$$\begin{aligned}
&\langle V(p,\lambda), q(p_2')|T|\gamma(p_1')q(p_2)\rangle = \\
&\int \frac{d^3l}{2E_l(2\pi)^3}\frac{d^3l'}{2E_{l'}(2\pi)^3}\langle V(p)|q_f(l),\bar{q}_f(l')\rangle\, \delta^{(4)}(l+l'-p')\,\mathcal{A}(l,p'-l') \\
&= \int \frac{d^4l}{(2\pi)^3}\delta(l^2-m^2)\frac{d^4l'}{(2\pi)^3}\delta(l'^2-m^2)\,\langle V(p)|q_f(l),\bar{q}_f(l')\rangle \\
&\qquad\qquad \times\delta^{(4)}(l+l'-p')\mathcal{A}(l,p'-l'),
\end{aligned} \tag{2.7}$$

where $p' = p_1 + p_2 - p_2'$. The scattering amplitude $\mathcal{A}$ has a quark and anti-quark in the final state and so must contain the spinors $\bar{u}(l)$ and $v(l')$. Therefore we can write

$$\begin{aligned}
&\int \frac{d^4l}{(2\pi)^3}\delta(l^2-m^2)\frac{d^4l'}{(2\pi)^3}\delta(l'^2-m^2)\,\langle V(p)|q_f(l),q_f(l')\rangle \\
&\qquad\qquad \times\delta^{(4)}(l+l'-p')\bar{u}_\alpha(l)\mathcal{A}_{\alpha\beta}(l,p'-l')v_\beta(l').
\end{aligned} \tag{2.8}$$

Now note the basic field theory results that

$$\delta(l^2-m^2)\bar{u}_\alpha(l)|q_f(l)\rangle = \delta(l^2-m^2)\bar{u}_\alpha(l)a_l^\dagger|0\rangle = \int\frac{d^4x}{(2\pi)}\bar{\psi}(x)|0\rangle\, e^{-ilx} \tag{2.9}$$

and

$$\delta(l'^2-m^2)v_\beta(l')|\bar{q}_f(l')\rangle = \delta(l'^2-m^2)v_\beta(l')a_{l'}^\dagger|0\rangle = \int\frac{d^4x'}{(2\pi)}\psi(x')|0\rangle\, e^{-il'x'}. \tag{2.10}$$

Therefore

$$\begin{aligned}
\langle V(p)q(p_2')|T|\gamma(p_1)q(p_2)\rangle &= \int d^4x d^4x' \int \frac{d^4l}{(2\pi)^4}\frac{d^4l'}{(2\pi)^4}e^{-ilx}e^{-il'x'} \\
&\times\langle V(p)|\bar{\psi}_\alpha(x)\psi_\beta(x')|0\rangle\, \delta^{(4)}(l+l'-p')\,\mathcal{A}_{\alpha\beta}(l,l').
\end{aligned} \tag{2.11}$$

Eliminating the l' integral we get

$$\begin{aligned}
\langle V(p)q(p_2')|T|\gamma(p_1)q(p_2)\rangle &= \int \frac{d^4x}{(2\pi)^4}\frac{d^4x'}{(2\pi)^4}d^4l\, e^{-il(x-x')}e^{-ip'x'} \\
&\times\langle V(p)|\bar{\psi}_\alpha(x)\psi_\beta(x')|0\rangle\mathcal{A}_{\alpha\beta}(l,p'-l).
\end{aligned} \tag{2.12}$$

Now let us make the change of variables

$$r = x - x' \quad\text{and}\quad R = \frac{1}{2}(x+x'), \tag{2.13}$$

giving us

$$\langle V(p)q(p_2')|T|\gamma(p_1)q(p_2)\rangle = \int \frac{d^4r}{(2\pi)^4}\frac{d^4R}{(2\pi)^4} d^4l e^{-i(2l-p')\frac{r}{2}} e^{-ip'R}$$
$$\times\langle V(p)|\bar{\psi}_\alpha(R+r/2)\psi_\beta(R-r/2)|0\rangle \mathcal{A}_{\alpha\beta}(l,p'-l). \tag{2.14}$$

The variable R is the centre-of-mass position. The vector meson is a free external particle described by a plane wave. Therefore

$$\langle V(p)|\bar{\psi}_\alpha(R+r/2)\psi_\beta(R-r/2)|0\rangle = e^{ipR}\langle V(p)|\bar{\psi}_\alpha(r/2)\psi_\beta(-r/2)|0\rangle. \tag{2.15}$$

Using this result and performing the R integral we find

$$\langle V(p)q(p_2')|T|\gamma(p')q(p_2)\rangle = \int \frac{d^4r}{(2\pi)^4} d^4l\, e^{-i(2l-p')\frac{r}{2}}\langle V(p)|\bar{\psi}_\alpha(r/2)\psi_\beta(-r/2)|0\rangle$$
$$\times\delta^{(4)}(p-p')\mathcal{A}_{\alpha\beta}(l,p'-l). \tag{2.16}$$

This therefore gives us the amplitude of $\gamma(p')q(p_2) \to V(p)q(p_2')$:

$$\mathcal{M} = \int \frac{d^4r}{(2\pi)^4} d^4l\, e^{-i(2l-p)\frac{r}{2}}\langle V(p)|\bar{\psi}_\alpha(r/2)\psi_\beta(-r/2)|0\rangle\, \mathcal{A}_{\alpha\beta}(l,p-l). \tag{2.17}$$

We choose to write this

$$\mathcal{M}_{+\lambda} = \int \frac{d^4r}{(2\pi)^4} d^4l\, e^{i(2l-p)\frac{r}{2}}\, \Psi^{(\lambda)}_{\alpha\beta}(r/2,-r/2)\, \mathcal{A}_{\alpha\beta}(l,p-l) \tag{2.18}$$

where

$$\Psi^{(\lambda)}_{\alpha\beta}(r/2,-r/2) = \langle V(p,\lambda)|\bar{\psi}_\alpha(-r/2)\psi_\beta(r/2)|0\rangle \tag{2.19}$$

---

and we assume an initial state photon of (+) polarisation and the polarisation of the vector meson is (λ).

This is a neat formula. We can do more though. We can disentangle the spinor dependences between $\mathcal{A}_{\alpha\beta}$ and $\Psi_{\alpha\beta}$ using a Fierz identity. Before doing this we shall show that the hard diffractive limit allows approximate factorisation and evaluation of some of the integration variables.

2.1.2 Diffractive factorisation

Diffractive factorisation relies on the limit $l_+ \gg l_-$, where l_+ and l_- are light-cone momenta. l is the momentum of the quark in the dipole that exits the hard subprocess and as such it is the daughter of the initial state photon. For the initial state photon of momentum p_1 with $p_{1+} \gg p_{1-}$, in a leading approximation we expect its daughter particles to obey the analogous limit. In this limit we can factorise the integration variables into different parts of the amplitude. It proves useful to rewrite these formulae in terms of the light cone variables

$$l_\pm = \frac{1}{\sqrt{2}}(l_0 \pm l_3) \tag{2.20}$$

$$d^4l = dl_+ dl_- d^2\mathbf{l} \tag{2.21}$$

$$l_+ = up_+ \tag{2.22}$$

$$\bar{u} = 1 - u \tag{2.23}$$

$$\text{and} \quad \xi = 2u - 1. \tag{2.24}$$

p is the momentum of the final state vector meson. We are free to choose to work in a specific frame where (in light-cone coordinates)

$$p^\mu = (\tilde{p}_+, 0, \mathbf{0}). \tag{2.25}$$

We shall denote components in this frame from now with a 'tilde'. Then the transverse component of the quark momentum, $\tilde{\mathbf{l}}$, and its conjugate, $\tilde{\mathbf{r}}$, are transverse with respect to the meson momentum. The advantage of this frame is that we have, $p \cdot r = \tilde{p}_+ \tilde{r}_-$, exactly.

The diffractive limit tells us that the hard scattering amplitude $A_{\alpha\beta}$ depends only weakly on $\tilde{l}_-$. Neglecting this dependence we generate a δ-function in $\tilde{r}_+$ from the $\tilde{l}_-$ integral, which renders the $\tilde{r}_+$ integral trivial. This approximation yields the result:

$$\mathcal{M}_{+\lambda} = 2\int \mathcal{A}_{\alpha\beta}(l, p-l) e^{-i\tilde{\mathbf{l}}\tilde{\mathbf{r}}} \frac{d^2\tilde{\mathbf{l}} d^2\tilde{\mathbf{r}}}{(2\pi)^2} du \Psi^{(\lambda)}_{\alpha\beta}(u, r), \tag{2.26}$$

$$\Psi^{(\lambda)}_{\alpha\beta}(u, r) = \int \frac{d(\tilde{p}_+\tilde{r}_-/2)}{2\pi} e^{i\tilde{p}_+\tilde{r}_-\xi/2} \Psi^{(\lambda)}_{\alpha\beta}(r/2, -r/2). \tag{2.27}$$

2.1.3 Fierz factorising

We now make use of the Fierz identity

$$\delta_{\alpha\alpha'}\delta_{\beta\beta'} = \frac{1}{4}\Gamma_{t\,\beta\alpha}\Gamma^{t}_{\alpha'\beta'}, \tag{2.28}$$

appearing in most textbooks on QFT (*e.g.* [11]), where $\Gamma^t = \{1,\, \gamma^\mu,\, \gamma^\mu\gamma_5,\, \sigma^{\mu\nu},\, i\gamma_5\}$. The inverse of Γ^t is defined, $\Gamma_t = (\Gamma^t)^{-1} = \{1,\, \gamma_\mu,\, -\gamma_\mu\gamma_5,\, \sigma_{\mu\nu},\, -i\gamma_5\}$. Note that the summation in equation (2.28) over t is over *independent* matrices. There are sixteen such: one scalar, four vector, four pseudovector, six tensor and one pseudovector. Antisymmetry in the Lorentz structure reduces the tensor component to six independent matrices from sixteen. Note that $\sigma_{01}\sigma^{01} = \sigma_{10}\sigma^{10}$, so when Lorentz contracting the tensor component we must be careful not to double count independent matrices.

Inserting equation (2.28) into (2.26) we factorise the helicity dependence and arrive at

$$\mathcal{M}_{+\lambda} = 2\int \mathcal{A}_{\alpha\beta}(l,p-l)e^{-i\tilde{\mathbf{l}}\tilde{\mathbf{r}}}\frac{d^2\tilde{\mathbf{l}}d^2\tilde{\mathbf{r}}}{(2\pi)^2}du\Psi^{(\lambda)}_{\alpha\beta}(u,r) \tag{2.29}$$

$$= 2\int \mathcal{A}_{\alpha\beta}(l,p-l)e^{-i\tilde{\mathbf{l}}\tilde{\mathbf{r}}}\frac{d^2\tilde{\mathbf{l}}d^2\tilde{\mathbf{r}}}{(2\pi)^2}du(\delta_{\alpha\alpha'}\delta_{\beta\beta'})\Psi^{(\lambda)}_{\alpha'\beta'}(u,r) \tag{2.30}$$

$$= 2\int \mathcal{A}_{\alpha\beta}(l,p-l)e^{-i\tilde{\mathbf{l}}\tilde{\mathbf{r}}}\frac{d^2\tilde{\mathbf{l}}d^2\tilde{\mathbf{r}}}{(2\pi)^2}du(\frac{1}{4}\Gamma_{t\,\beta\alpha}\Gamma^{t}_{\alpha'\beta'})\Psi^{(\lambda)}_{\alpha'\beta'}(u,r) \tag{2.31}$$

$$= 2\int \frac{1}{4}[\mathcal{A}_{\alpha\beta}(l,p-l)\Gamma_{t\,\beta\alpha}]\, e^{-i\tilde{\mathbf{l}}\tilde{\mathbf{r}}}\frac{d^2\tilde{\mathbf{l}}d^2\tilde{\mathbf{r}}}{(2\pi)^2}du\,[\Gamma^{t}_{\alpha'\beta'}\Psi^{(\lambda)}_{\alpha'\beta'}(u,r)]. \tag{2.32}$$

We choose to write this

$$\mathcal{M}_{+\lambda} = 2\int d^2\tilde{\mathbf{r}}du\,\frac{1}{4}Tr[\mathcal{A}(u,\tilde{\mathbf{r}})\Gamma_t]\,\Psi^{(\lambda)\,t}(u,r) \tag{2.33}$$

where

$$\Psi^{(\lambda)\,t}(u,r) = \Gamma^{t}_{\alpha'\beta'}\Psi^{(\lambda)}_{\alpha'\beta'}(u,r) \tag{2.34}$$

and

$$\mathcal{A}_{\alpha\beta}(u,\tilde{\mathbf{r}}) = \int \mathcal{A}_{\alpha\beta}(l,p-l)\,e^{-i\tilde{\mathbf{l}}\tilde{\mathbf{r}}}\frac{d^2\tilde{\mathbf{l}}}{(2\pi)^2}. \tag{2.35}$$

The hard subprocess amplitude and the vector meson transition are now only coupled via a summation in Fierz elements and convolutions in u (the fraction of the final meson's + momentum that the quark possesses prior to the transition), and r (the transverse size of the quark/anti-quark dipole). Notice that the object (2.34) is the Fourier transform of the object we encountered in section 1.6. For example

$$\Psi^{(\lambda)\,\gamma^\mu}(u,r) = \int \frac{d(\tilde{p}_+\tilde{r}_-/2)}{2\pi} e^{i\tilde{p}_+\tilde{r}_-\xi/2} \langle V(p,\lambda)|\bar{\psi}(-r/2)\gamma^\mu\psi(r/2)|0\rangle. \qquad (2.36)$$

2.2 The hard scattering amplitude

We now proceed to calculate the lowest order QCD contribution to the hard scattering subprocess and shall assume it is hard, diffractive, and in the Regge limit. The initial state photon has (+) polarisation with a momentum p_1 and the incoming quark-parton of momentum p_2. The photon fluctuates to a quark/anti-quark pair that subsequently undergoes a hard scatter off the quark-parton to produce a longitudinal or transverse meson of momentum p. Let us define the momentum of the quark leaving the hard scatter to be $q_1 = l$. The momentum of the antiquark is therefore $q_2 = p - l$. We define the centre-of-mass energy squared for this interaction s[1].

We shall derive the hard scattering amplitude for $\gamma q \to q'\bar{q}'q$. We shall do so in several stages. First we shall consider the simplest QCD amplitude, the process $qq \to qq$ mediated by single gluon exchange. Using this result and the Cutkosky cutting rules, we shall arrive at the imaginary part of the two gluon exchange amplitude. Utilising dispersion relation theory and the analytic properties of the amplitude we shall obtain the full amplitude. We shall then consider projecting out the colour singlet exchange part, which turns out to be purely imaginary. We shall then show

[1]In this, and the next two chapters, we focus exclusively on parton level calculations, with only passing reference to the fact that the quark-parton originated in a proton. It suits us to define s as the photon-parton centre-of mass energy squared. In Chapter 5, however, when we come to compare to data, we must convolute with PDFs. We will then make the replacement $s \to \hat{s}$. Then we will define s to be the photon-proton centre-of mass energy squared and $\hat{s} = xs$ will be the photon-parton centre-of-mass energy squared, with x Bjorken-x.

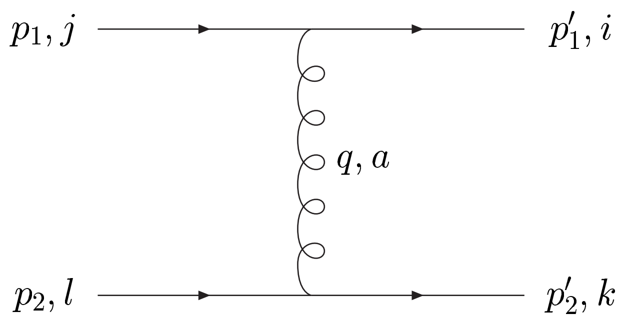

Figure 2.2: One gluon exchange.

that we can generalise the result to generic processes, in which, in the high-energy limit, we can assign a scalar factor to each side of the colour singlet exchange. We call these scalar factors impact factors. The result that such amplitudes can be written as the product of scalar factors is called high-energy factorisation. We then rederive the $q \to q$ impact factor, showing that this corresponds with our earlier result, and proceed to calculate that of $\gamma \to q'\bar{q}'$. This completes the aim of the section.

2.2.1 $qq \to qq$: one gluon exchange

Consider the single gluon exchange between quarks illustrated in figure 2.2 We will work in light-cone coordinates,

$$q = (q_+, q_-, \mathbf{q}), \tag{2.37}$$

where we define

$$q_\pm = \frac{q_0 \pm q_3}{\sqrt{2}}. \tag{2.38}$$

The centre-of-mass energy squared is given by,

$$s = 2p_1 \cdot p_2 \tag{2.39}$$

and the momentum transfer squared by,

$$t = q^2 = 2q_+q_- - \mathbf{q}^2. \tag{2.40}$$

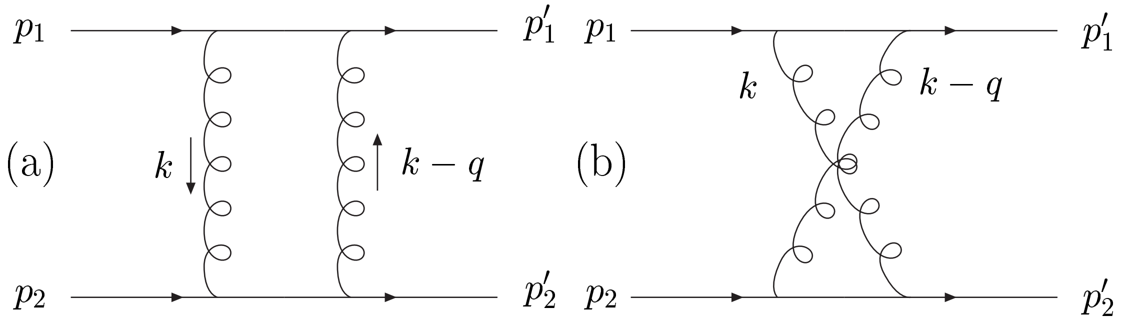

Figure 2.3: Two gluon exchange. (a) is the s-channel diagram. (b) is the $s \leftrightarrow u$ crossed diagram with respect to (a).

The on-mass-shell conditions for the external particles enforce,

$$p_1'^2 = (p_1 - q)^2 = -2\left(\sqrt{\frac{s}{2}} - q_+\right) q_- - \mathbf{q}^2 = 0, \tag{2.41}$$

$$p_2'^2 = (p_2 + q)^2 = 2q_+\left(\sqrt{\frac{s}{2}} + q_-\right) - \mathbf{q}^2 = 0, \tag{2.42}$$

which in turn imply

$$q_+ = |q_-| \sim \frac{\mathbf{q}^2}{\sqrt{2s}} \ll \sqrt{\frac{s}{2}} \;\text{ and }\; q^2 \sim -\mathbf{q}^2. \tag{2.43}$$

The application of the QCD Feynman rules gives us the single-gluon exchange amplitude,

$$iA_{1g}(s,t) = ig_s^2 t_{ij}^a t_{kl}^a \bar{u}_s(p_1')\gamma^\mu u_{s'}(p_1)\frac{g_{\mu\nu}}{q^2}\bar{u}_t(p_2')\gamma^\nu u_{t'}(p_2). \tag{2.44}$$

We shall now apply a high-energy limit approximation to this amplitude; the eikonal approximation (equation (1.42)). Applying this twice we get our final result,

$$\begin{aligned} iA_{1g}(s,t) &\sim ig_s^2 t_{ij}^a t_{kl}^a 2p_1^\mu \delta_{ss'}\frac{g_{\mu\nu}}{q^2} 2p_2^\nu \delta_{tt'} \\ &= 8\pi i\alpha_s t_{ij}^a t_{kl}^a \delta_{ss'}\delta_{tt'}\frac{s}{t}. \end{aligned} \tag{2.45}$$

2.2.2 $qq \to qq$: two gluon exchange

We want to calculate the amplitude for the two diagrams shown in figure 2.3. We shall find the amplitude corresponding to the first diagram first. Note that the difference between the first and second is a 'crossing' of the two gluons such that they couple to

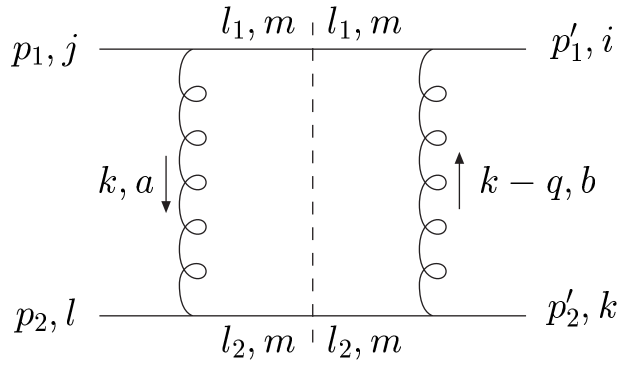

Figure 2.4: The s-channel two gluon exchange diagram. The dashed line is the Cutkosky cut.

the opposite vertex in the lower quark line. The two diagrams are related by $s \leftrightarrow u$. It is worth pointing out that this crossing is not exact, since the quark line direction is such that the two diagrams cannot be deformed into each other. The difference between the diagrams is more than just colour algebra and crossing. However, the quark line direction becomes irrelevant in the eikonal approximation, and, in this limit, we can take a $s \leftrightarrow u$ crossing relation with the appropriate adjustment in colour algebra.

The imaginary part of the uncrossed diagram

The Cutkosky cutting rules allow us to express the imaginary part of the two-gluon exchange amplitude in terms of the one for single-gluon exchange (equation (1.40));

$$\operatorname{Im} \mathcal{A}_{2g}(s,t) = \frac{1}{2} \int d\Pi_2 \, \mathcal{A}_{1g}(s,k^2) \mathcal{A}^{\dagger}_{1g}(s,(k-q)^2), \tag{2.46}$$

where the two-body phase space integral is given by

$$\begin{aligned}
\int d\Pi_2 &= \int \frac{d^4 l_1}{(2\pi)^3} \frac{d^4 l_2}{(2\pi)^3} \delta(l_1^2)\delta(l_2^2)(2\pi)^4 \delta(p_1 + p_2 - l_1 - l_2) \\
&= \int \frac{d^4 k}{(2\pi)^2} \delta((p_1 - k)^2)\delta((p_2 + k)^2) \\
&= \int \frac{dk_+ dk_- d^2\mathbf{k}}{(2\pi)^2} \delta\left(-2k_- \left(\sqrt{\frac{s}{2}} - k_+\right) + \mathbf{k^2}\right) \delta\left(2k_+ \left(\sqrt{\frac{s}{2}} + k_-\right) - \mathbf{k^2}\right).
\end{aligned} \tag{2.47}$$

This is depicted diagrammatically in figure 2.4. Consideration of the on-shell conditions of the cut quarks gives

$$\begin{aligned}
&k_+ = |k_-| \sim \frac{\mathbf{k}^2}{\sqrt{2s}} \ll \sqrt{\frac{s}{2}}, \\
&k^2 \sim -\mathbf{k}^2,\ (k-q)^2 \sim -(\mathbf{k}-\mathbf{q})^2, \\
&\mathbf{k}^2 \sim (\mathbf{k}-\mathbf{q})^2 \sim \mathbf{q}^2,
\end{aligned} \tag{2.48}$$

which in turn allow us to approximate the phase space integral as

$$\begin{aligned}
&\int d\Pi_2 = \int \frac{dk_+ dk_- d^2\mathbf{k}}{(2\pi)^2} \delta\left(-k_-\sqrt{2s} + \mathbf{k}^2\right) \delta\left(k_+\sqrt{2s} - \mathbf{k}^2\right) \\
&= \frac{1}{2s}\frac{1}{(2\pi)^2} \int d^2\mathbf{k}.
\end{aligned} \tag{2.49}$$

The imaginary part of diagram a then directly follows as

$$\operatorname{Im} \mathcal{A}_{2g\,a}(s,t) = 4\alpha_s^2 (t^a t^b)_{ij} (t^a t^b)_{kl}\, s \int \frac{d^2\mathbf{k}}{\mathbf{k}^2(\mathbf{k}-\mathbf{q})^2}. \tag{2.50}$$

Finding full amplitudes

We will make use of a dispersion relation to find the real part of the desired amplitude (for more detail on dispersion relations see [34, 35]). The s dependence of the imaginary part requires that we utilise the doubly subtracted dispersion relation (equation (1.22))

$$\begin{aligned}
\mathcal{A}(s,t) &= \frac{(s-s_1)}{(s_0-s_1)}\mathcal{A}(s_0,t) + \frac{(s-s_0)}{(s_1-s_0)}\mathcal{A}(s_1,t) \\
&+ \frac{(s-s_0)(s-s_1)}{\pi} \int_{s_+}^{\infty} ds' \frac{\operatorname{Im}\mathcal{A}(s',t)}{(s'-s)(s'-s_0)(s'-s_1)} \\
&+ \frac{(s-s_0)(s-s_1)}{\pi} \int_{-\infty}^{s_-} ds' \frac{\operatorname{Im}\mathcal{A}(s',t)}{(s'-s)(s'-s_0)(s'-s_1)},
\end{aligned} \tag{2.51}$$

which follows simply from the analytic properties of $\mathcal{A}$. We shall go through this calculation explicitly, because it is often alluded to but rarely shown.

The full amplitude is the sum of two contributions,

$$\mathcal{A} = \mathcal{A}_a + \mathcal{A}_b. \tag{2.52}$$

In general the relation between $\mathcal{A}_a$ and $\mathcal{A}_b$ is non trivial. However, in the leading s approximation the direction of fermion lines becomes irrelevant and we can identify $\mathcal{A}_b$ with the analytic continuation of $\mathcal{A}_a$ into the region $s \leq s_-$, where it represents the u-crossed process. Note that the colour structure of a and b will be different. The dispersion relations for the two diagrams are therefore

$$\begin{aligned} \mathcal{A}_a(s,t) &= \frac{(s-s_1)}{(s_0-s_1)}\mathcal{A}_a(s_0,t) + \frac{(s-s_0)}{(s_1-s_0)}\mathcal{A}_a(s_1,t) \\ &+ \frac{(s-s_0)(s-s_1)}{\pi}\int_{s_+}^{\infty} ds' \frac{\operatorname{Im}\mathcal{A}_a(s',t)}{(s'-s)(s'-s_0)(s'-s_1)} \end{aligned} \tag{2.53}$$

$$\begin{aligned} \text{and} \quad \mathcal{A}_b(s,t) &= \frac{(s-s_1)}{(s_0-s_1)}\mathcal{A}_b(s_0,t) + \frac{(s-s_0)}{(s_1-s_0)}\mathcal{A}_b(s_1,t) \\ &- \frac{(s-s_0)(s-s_1)}{\pi}\int_{-s_-}^{\infty} ds' \frac{\operatorname{Im}\mathcal{A}_b(s',t)}{(s'+s)(s'+s_0)(s'+s_1)}, \end{aligned} \tag{2.54}$$

where we have defined $\mathcal{A}_{a/b}$ to be zero below the physical threshold, $s_+/-s_-$, and we have used $\mathcal{A}_b(s,t) \sim \mathcal{A}_a(u,t) \sim \mathcal{A}_a(-s,t)$ (modulo colour factors). Partial fractions gives us the relation,

$$\frac{(s-s_0)(s-s_1)s'}{(s'-s)(s'-s_0)(s'-s_1)} = \frac{s}{(s'-s)} + \frac{s_0(s-s_1)}{(s_1-s_0)(s'-s_0)} + \frac{s_1(s_0-s)}{(s_1-s_0)(s'-s_1)}. \tag{2.55}$$

Let us consider a possible s dependence for the amplitude $\operatorname{Im}\mathcal{A}_a = s\ln^n s$, our lowest order calculation corresponding to $n = 0$. Equation (2.55) and the preceding result allow us to write,

$$\begin{aligned} &\frac{(s-s_0)(s-s_1)}{\pi}\int_{s_+}^{\infty} ds' \frac{s' \ln^n s'}{(s'-s)(s'-s_0)(s'-s_1)} \\ &= \frac{1}{\pi}\int_{s_+}^{\infty} ds' \left[\frac{s\ln^n s'}{s'-s} + \frac{s_0(s-s_1)}{s_1-s_0}\frac{\ln^n s'}{(s'-s_0)} + \frac{s_1(s_0-s)}{s_1-s_0}\frac{\ln^n s'}{(s'-s_1)}\right] \end{aligned} \tag{2.56}$$

$$\sim \frac{1}{\pi}\int_{s_+-s}^{\infty} ds' \frac{s\ln^n s'}{s'} + \frac{1}{\pi}\int_{s_+-s_0}^{\infty} ds' \frac{s_0(s-s_1)}{s_1-s_0}\frac{\ln^n s'}{s'} + \frac{1}{\pi}\int_{s_+-s_1}^{\infty} ds' \frac{s_1(s_0-s)}{s_1-s_0}\frac{\ln^n s'}{s'}. \tag{2.57}$$

Since the dominant contributions to the integrals come from the region,

$$s' \sim s_i \quad \text{where} \quad s_i = s,\ s_0 \ \text{ or } \ s_1, \tag{2.58}$$

then the approximation $\ln(s'-s_i) \sim \ln s'$ is correct, to leading log accuracy. Using the result,

$$\int \frac{\ln^n x}{x} dx = \frac{\ln^{n+1} x}{n+1} \tag{2.59}$$

and after cancelling the divergences and neglecting s_+ next to s we find that

$$\begin{aligned}&\frac{(s-s_0)(s-s_1)}{\pi}\int_{s_+}^{\infty} ds' \frac{s' \ln^n s'}{(s'-s)(s'-s_0)(s'-s_1)} \\ &\sim -\frac{1}{\pi(n+1)}\left[s\ln^{n+1}(-s) + \frac{(s-s_1)}{(s_1-s_0)}s_0\ln^{n+1}(-s_0) + \frac{(s_0-s)}{(s_1-s_0)}s_1\ln^{n+1}(-s_1)\right].\end{aligned} \tag{2.60}$$

This result gives us, to leading log accuracy,

$$\begin{aligned}\mathcal{A}_a(s,t) &= \frac{(s-s_1)}{(s_0-s_1)}\mathcal{A}_a(s_0,t) + \frac{(s-s_0)}{(s_1-s_0)}\mathcal{A}_a(s_1,t) \\ &+ \frac{(s-s_0)(s-s_1)}{\pi}\int_{s_+}^{\infty} ds' \frac{\operatorname{Im}\mathcal{A}_a(s',t)}{(s'-s)(s'-s_0)(s'-s_1)} \\ &= -\frac{1}{\pi(n+1)}\, N\mathcal{C}_1 s\ln^{n+1}(-s) \\ &+ \frac{(s-s_1)}{(s_0-s_1)}[\mathcal{A}_a(s_0,t) + \frac{1}{\pi(n+1)}N\mathcal{C}_1 s_0\ln^{n+1}(-s_0)] \\ &+ \frac{(s-s_0)}{(s_1-s_0)}[\mathcal{A}_a(s_1,t) + \frac{1}{\pi(n+1)}N\mathcal{C}_1 s_1\ln^{n+1}(-s_1)],\end{aligned} \tag{2.61}$$

where N is a normalisation factor and $\mathcal{C}_1$ is the colour factor associated with diagram a. Inspection shows the solution of this equation to be,

$$\mathcal{A}_a(s,t) = -\frac{1}{\pi(n+1)}\, N\mathcal{C}_1 s\ln^{n+1}(-s). \tag{2.62}$$

Therefore we also have,

$$\mathcal{A}_b(s,t) = \frac{1}{\pi(n+1)}\, N\mathcal{C}_2 s\ln^{n+1}(s). \tag{2.63}$$

In section 1.4 we noted that the leading behaviour in s of the imaginary part of an amplitude, at a particular order in α_s, was a logarithm to an integer power; we summed in a power series of $z \propto \alpha_s \ln s$. The results directly above show that the real part then depends on s in a logarithm one power higher.

The full two gluon exchange amplitude

Using the results of the previous section with the special case $n = 0$ we obtain the two gluon exchange amplitudes

$$\mathcal{A}_{2g\,a}(s,t) = -\frac{1}{\pi}\, N\mathcal{C}_1 s\ln(-s), \tag{2.64}$$

and

$$\mathcal{A}_{2g\,b}(s,t) = \frac{1}{\pi} N\mathcal{C}_2 s\ln(s). \tag{2.65}$$

Putting these together we obtain,

$$\begin{aligned}\mathcal{A}_{2g}(s,t) &= -\frac{1}{\pi} sN(\mathcal{C}_1\ln(-s) - \mathcal{C}_2\ln(s) \\ &= -\frac{N}{\pi}(\mathcal{C}_1 - \mathcal{C}_2)s\ln s + iN\mathcal{C}_1 s.\end{aligned} \tag{2.66}$$

Now putting the correct normalisation in, obtained from the imaginary part of diagram a (equation (2.50)), and putting in the explicit form of the colour factors, we arrive at the result for two gluon exchange,

$$\mathcal{A}_{2g} = -4\frac{\alpha_s^2}{\pi}(t^a t^b)_{ij}\left[[t^a,t^b]_{kl}s\ln\left(\frac{s}{|t|}\right) - i\pi(t^a t^b)_{kl}s\right]\int\frac{d^2\mathbf{k}}{\mathbf{k^2(k-q)^2}}. \tag{2.67}$$

The projection out of the octet and singlet parts

The amplitude that we have derived for two gluon exchange has, in general, to leading logs, non-zero real and imaginary parts. Closer analysis reveals that enforcing colour singlet exchange ($k = l$) leaves the amplitude purely imaginary. In addition, enforcing octet exchange ($k \neq l$) leaves the amplitude purely real. The first of these results is a general feature of leading s amplitudes for singlet exchange; exact cancellation occurs between the real parts of the s and u channel contributions. The second result is a special case. We can derive a weaker condition for the octet exchange, however.

An amplitude can be written

$$\mathcal{A} = [\mathcal{C}_s^{(8)}\mathcal{A}_s^{(8)} + \mathcal{C}_u^{(8)}\mathcal{A}_u^{(8)}]_{kl} + [\mathcal{C}_s^{(0)}\mathcal{A}_s^{(0)} + \mathcal{C}_u^{(0)}\mathcal{A}_u^{(0)}]_{kl} \tag{2.68}$$

where the colour indices, k and l, are associated with the colour factors $\mathcal{C}$. Now let us impose singlet exchange. The crossed diagram colour factor simply has reversed ordered colour matrices with respect to the uncrossed one. When we impose singlet exchange we get a trace, so reversibility of traces gives

$$\begin{aligned}\mathcal{A} &= (Tr[\mathcal{C}_s^{(8)}]\mathcal{A}_s^{(8)} + Tr[\mathcal{C}_u^{(8)}]\mathcal{A}_u^{(8)}) + (Tr[\mathcal{C}_s^{(0)}]\mathcal{A}_s^{(0)} + Tr[\mathcal{C}_u^{(0)}]\mathcal{A}_u^{(0)}) \\ &= Tr[\mathcal{C}_s^{(8)}](\mathcal{A}_s^{(8)} + \mathcal{A}_u^{(8)}) + Tr[\mathcal{C}_s^{(0)}](\mathcal{A}_s^{(0)} + \mathcal{A}_u^{(0)}) \\ &= Tr[\mathcal{C}_s^{(0)}](\mathcal{A}_s^{(0)} + \mathcal{A}_u^{(0)}),\end{aligned} \tag{2.69}$$

where the last equality follows by definition. Therefore we can say, in general, that

$$\mathcal{A}_s^{(8)} = -\mathcal{A}_u^{(8)}. \tag{2.70}$$

Summarising this, to leading s we have

$$\mathcal{A}_u(s,t) = \mathcal{A}_s(u,t) \sim \mathcal{A}_s(-s,t), \tag{2.71}$$

$$\mathcal{A}_s^{(8)} = -\mathcal{A}_u^{(8)}, \tag{2.72}$$

$$\mathcal{A}^{(0)} = i\mathrm{Im}\,\mathcal{A}^{(0)}. \tag{2.73}$$

For our purposes we are concerned with the singlet amplitude, leaving our amplitude purely imaginary. We can write our $qq \to qq$ amplitude

---

$$\begin{aligned}\mathcal{A}_0^{(0)} &= 4i\alpha_s^2 Tr[t^a t^b]^2 s \int \frac{d^2\mathbf{k}}{\mathbf{k^2(k-q)^2}} \\ &= is \int \frac{\phi_{qq}\phi_{qq}}{\mathbf{k^2(k-q)^2}} \frac{d^2\mathbf{k}}{(2\pi)^2},\end{aligned} \tag{2.74}$$

where we define

$$\phi_{qq} = 2\alpha_s\, Tr[t^a t^b] = 2\pi\alpha_s \frac{\delta_{ab}}{N}. \tag{2.75}$$

The subscript on the amplitude indicates the order above lowest. From now on we will drop the superscript indicating singlet exchange and this will be assumed. It is worth pointing out that this result for the amplitude for this process is not infra-red finite. This problem can be resolved by appealing to higher orders, for example BFKL, where the infra-red divergences cancel. At finite order we can appeal to physical arguments, for example noting that the gluons must probe a quark within a hadron of size r, so that they must carry greater than a minimum transverse momentum square, $\mathbf{k}_{min}^2 \sim 1/\mathbf{r}^2 \sim 1\,\mathrm{GeV}^2$. This problem is not an issue for us, however, since we will not ultimately be concerned with this particular process.

The value of the notation ϕ_{qq} will be seen in the next section, where we generalise to more complicated processes. These will still be mediated by two gluon exchange, but will be between more complicated external states.

2.2.3 Generalised Processes

So far we have discussed only the process $qq \to qq$. This was for thematic purposes, as the structure of the results are largely process independent. However, $qq \to qq$ scattering is not the process that is the focus of this thesis. We now proceed to discuss the generalisation of the results so far attained for generic processes, then we will apply ourselves to the particular case of $\gamma q \to q'\bar{q}'q$. We do so by first considering the leading kinematic regions. This allows us to derive the generalisation of equation (2.74) and then the $\gamma \to q'\bar{q}'$ impact factor. Note that analysis of leading regions is difficult to make rigorous, we attempt no rigour here, we simply use heuristic arguments and demand self-consistency.

Kinematics and leading regions

Consider the diagram depicted in figure (2.5), representing generic incoming particles producing an unprescribed number of daughter particles, which then diffractively scatter via two gluon colour singlet exchange. Remember that scattering amplitudes for colour singlet exchange at leading s are purely imaginary. This allows us to get the complete leading s amplitude directly from the Cutkosky rules. This technique is useful for analysing kinematics since by expressing the amplitude in terms of cut diagrams we put the (cut) daughter particles on shell. The gluon on the left side of the cut must couple to a particle and we will now consider the momentum of this gluon. We shall make two assumptions. One is that the daughter particles of momentum $q_{\{i\}}$ and mass $m_{\{i\}}$, in our leading approximation, are dominated by the same momentum component as their initial parent particle. That is they conform to either

$$|q_{\{i\}+}| \gg |q_{\{i\}-}| \qquad \text{or} \qquad |q_{\{j\}-}| \gg |q_{\{j\}+}|, \tag{2.76}$$

as appropriate. We will take the particles in the top half diagram to be i type particles and the bottom half, j. We will also assume that the momenta of the individual gluons exchanged obey the Regge region criteria ($\mathbf{k}^2$, $(\mathbf{k}-\mathbf{q})^2 \ll s$), in addition to the overall momentum exchange doing so. Besides making physical sense, we note that if this were not the case we would require a large cancellation in momentum. That would

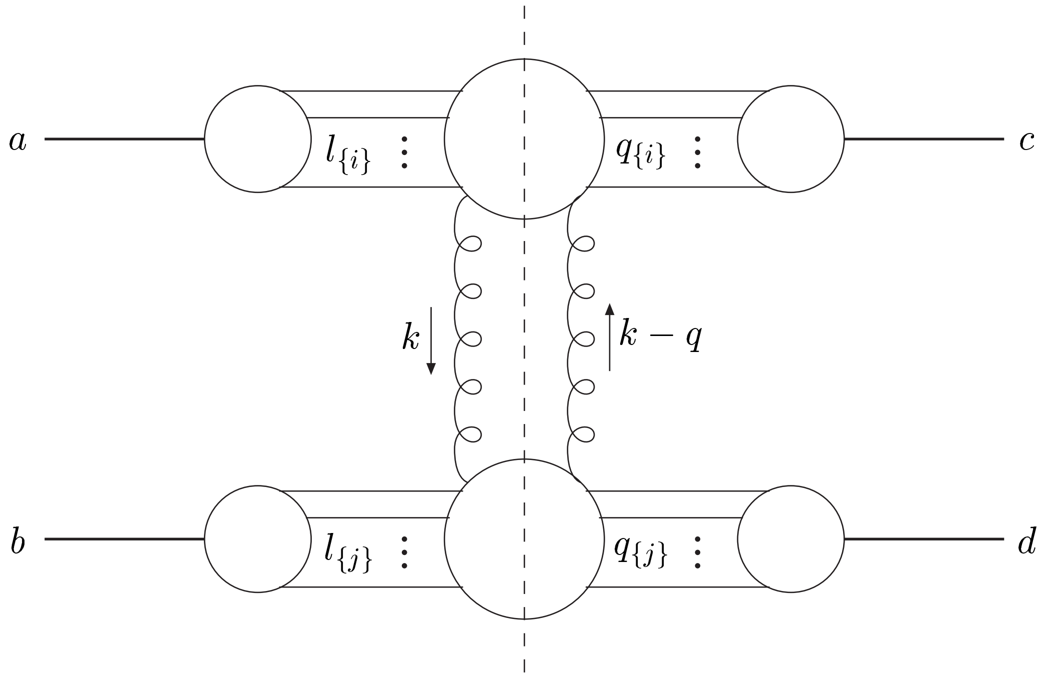

Figure 2.5: A generalised process $ab \to cd$, mediated by two-gluon colour singlet exchange. The dashed-line is the cut of the Cutkosky rules. $\{i\}$ and $\{j\}$ are the daughter particles of a and b respectively.

result in two propagators with large denominators suppressing our amplitude.

We shall define the momentum of the daughter particle before coupling to the gluon, $l^2_{\{i\}}$ in the upper block and $l^2_{\{j\}}$ in the lower. We shall define the $+/-$ components

$$l_{k\in i\,+} = \zeta_k\, p_1 \quad \text{with} \quad l_{k-} = 0 \tag{2.77}$$

$$\text{and} \qquad l_{k\in j\,+} = \zeta_k\, p_2 \quad \text{with} \quad l_{k+} = 0, \tag{2.78}$$

where $\zeta_k \sim 1-\zeta_k \sim 1$. We shall also assume that the transverse part of these momenta are much smaller than s. The requirement that final state particles do so makes this assumption sensible. Thus,

$$m_k^2 = (l_{k\in i} - k)^2 \quad \rightarrow \quad \Delta^2_{k\in i} + \mathbf{k}^2 \sim 2(k_+ - \sqrt{s/2})k_-, \tag{2.79}$$

$$m_k^2 = (l_{k\in j} + k)^2 \quad \rightarrow \quad \Delta^2_{k\in j} + \mathbf{k}^2 \sim 2(k_- + \sqrt{s/2})k_+, \tag{2.80}$$

where

$$\Delta^2_{k\in i} = m_k^2 - l_k^2 - 2\mathbf{k}\cdot\mathbf{l}_k - 2k_-\sqrt{s/2}\,(1-\zeta_k). \tag{2.81}$$

and

$$\Delta^2_{k\in j} = m_k^2 - l_k^2 - 2\mathbf{k}\cdot\mathbf{l}_k + 2k_+\sqrt{s/2}\,(1-\zeta_k). \tag{2.82}$$

Equations ((2.79), (2.80)) are the analogues to ((2.41), (2.42)). Further assuming that

$$\Delta^2_{\{i\}} \sim \Delta^2_{\{j\}} \sim \Delta^2, \tag{2.83}$$

we can use these equations to find,

$$k_+ \sim -k_-. \tag{2.84}$$

Reminding ourselves that we are in the Regge region $|k^2| \ll s$, we find that

$$k^2 = 2k_+k_- - \mathbf{k}^2 \sim -2k_+^2 - \mathbf{k}^2 \quad \Rightarrow \quad k_+ \ll \sqrt{s}. \tag{2.85}$$

Utilising this in conjunction with equations (2.81) and (2.82) we end up with,

$$k_+ \sim \frac{\Delta^2 + \mathbf{k}^2}{\sqrt{2s}} \tag{2.86}$$

and

$$k_- \sim -\frac{\Delta^2 + \mathbf{k}^2}{\sqrt{2s}}, \tag{2.87}$$

which also imply

$$k^2 \sim -\mathbf{k}^2. \tag{2.88}$$

Analysis of the other side of the cut line is completely analogous. We find,

$$k_+ - q_+ \sim \frac{\Delta^2 + (\mathbf{k} - \mathbf{q})^2}{\sqrt{2s}} \tag{2.89}$$

and

$$k_- - q_- \sim -\frac{\Delta^2 + (\mathbf{k} - \mathbf{q})^2}{\sqrt{2s}}, \tag{2.90}$$

which also imply

$$(k - q)^2 \sim -(\mathbf{k} - \mathbf{q})^2. \tag{2.91}$$

These results are a justification of the assumption that there are no scales comparable with s, since $\Delta^2 \ll s$.

High energy factorisation

We now apply the kinematic analysis above to the generalised two-gluon exchange amplitude. We wish to calculate the leading s component of the generalised process depicted in figure 2.5. Following [17], and working directly from the Feynman rules, we write the amplitude for a general process $AB \to A'B'$,

$$\mathcal{A}_0^{AB \to A'B'}(q) = \frac{i}{2} \int A^{\mu\nu}_{A \to A'}(-k, k - q) A^{\alpha\beta}_{B \to B'}(k, -k + q) \frac{-ig_{\mu\alpha}}{k^2} \frac{-ig_{\nu\beta}}{(k - q)^2} \frac{d^4k}{(2\pi)^4}. \tag{2.92}$$

The sub-amplitudes or 'blocks' correspond to the amplitudes of gluon Compton scattering off the initial state particles. The factor of one-half is needed in (2.92), since by crossing the gluons in both the upper and lower blocks we are double counting diagrams. As previously mentioned, we shall assume that any particles produced from particle A should, to a first approximation, possess similar momentum configurations. By this we mean that if p_1 is dominated by the p_+ component, then so should the momentum q_i of any daughter particles. Let us define the momenta

$$k^\mu = (k_+, k_-, \mathbf{k}), \quad q^\mu = (q_+, q_-, \mathbf{q}),$$
$$q_k^\mu = (q_{k\,+}, q_{k\,-}, \mathbf{q}), \quad p_1^\mu = (\sqrt{s/2}, 0, \mathbf{0}), \quad p_2 = (0, \sqrt{s/2}, \mathbf{0}), \tag{2.93}$$

where again we denote the momenta of the daughter particles as $q_{\{j\}}$ for the lower block, as opposed to $q_{\{i\}}$ for the upper block. Then we can state the assumption of like-to-like momentum as,

$$q_{i\,+} \sim q_{j\,-} \sim \sqrt{\frac{s}{2}}. \tag{2.94}$$

The kinematic analysis done previously for on-shell conditions yielded the leading log region,

$$|q_+|,\ |q_-|,\ |k_+|,\ |k_-|,\ |q_{i\,-}|,\ |q_{j\,+}| \sim \frac{\Delta^2 + \mathbf{q}^2}{\sqrt{2s}} \ll \sqrt{\frac{s}{2}} \tag{2.95}$$

where q is the overall transverse momentum exchange and we have assumed $\mathbf{k}^2 \sim (\mathbf{k} - \mathbf{q})^2 \sim \mathbf{q}^2$. These limits and (2.94) allow us to neglect k_+ in the upper block and k_- in the lower one; that is we can neglect k_+ next to $q_{\{i\}+}$ and k_- next to $q_{\{j\}-}$. Thus the momentum integrals in the amplitude factorise. These limits also allow us to make the further approximation in the gluon propagators such that,

$$k^2 = 2k_+k_- - \mathbf{k}^2 \sim -\mathbf{k}^2 \ \text{ and } \ (k - q)^2 \sim -(\mathbf{k} - \mathbf{q})^2. \tag{2.96}$$

The final step in the proof of high energy factorisation is to show that the Lorentz structure factorises to give fully contracted scalar factors. To see this we note the easily verifiable fact that we can write the (light-cone) metric

$$g_{\mu\alpha} = \delta_{\mu+}\delta_{\alpha-} + \delta_{\mu-}\delta_{\alpha+} + g_{\perp\,\mu\alpha}, \tag{2.97}$$

where $\delta^{\mu+}g_{\mu\nu} = \delta_\nu^+ = \delta_{\nu-}$. Leading s contributions will only arise from the $\delta_{\mu+}\delta_{\alpha-}$ or $\delta_{\mu-}\delta_{\alpha+}$ parts. They are not s dependent themselves, but they will be the only pieces to give non-zero contractions with the leading s parts of the blocks. The upshot is that we can throw the transverse piece of the metric away. The factorisation is complete and we can write the amplitudes in the form

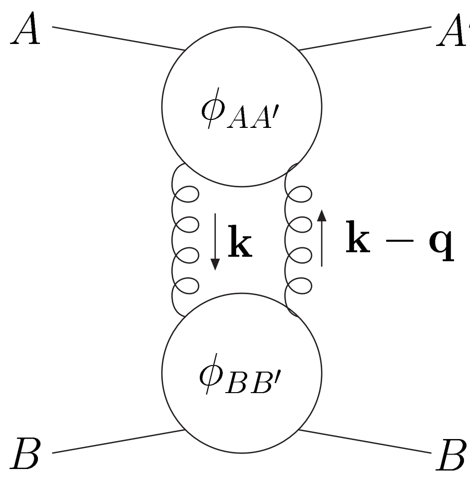

Figure 2.6: The two-gluon exchange impact factor representation of QCD colour singlet amplitude.

$$\mathcal{A}_0^{AB\to A'B'}(q) = is\int \frac{\phi_{AA'}(-\mathbf{k},\mathbf{k}-\mathbf{q})\phi_{BB'}(\mathbf{k},-\mathbf{k}+\mathbf{q})}{\mathbf{k^2}(\mathbf{k}-\mathbf{q})^\mathbf{2}}\frac{d^2\mathbf{k}}{(2\pi)^2}, \tag{2.98}$$

where

$$\phi_{AA'}(-\mathbf{k},\mathbf{k}-\mathbf{q}) = \frac{1}{\sqrt{2s}}\int A^{\mu\nu}_{AA'}(-k,k-q)\delta_{\mu+}\delta_{\nu+}\frac{dk_-}{2\pi i} \tag{2.99}$$

$$\text{and}\quad \phi_{BB'}(\mathbf{k},-\mathbf{k}+\mathbf{q}) = \frac{1}{\sqrt{2s}}\int A^{\alpha\beta}_{BB'}(k,-k+q)\delta_{\alpha-}\delta_{\beta-}\frac{dk_+}{2\pi i}. \tag{2.100}$$

We have derived the impact factor representation promised in section 1.4, illustrated again in figure 2.6. Note that these 'impact factors' will depend only on $\mathbf{k}$, $\mathbf{q}_i$, $q_{i\,+}/\sqrt{s}$ or on $\mathbf{k}$, $\mathbf{q}_j$, $q_{j\,-}/\sqrt{s}$, but not on s.

The qq impact factor

The amplitude corresponding to the $q \to q$ transition is depicted in figure 2.7. Applying

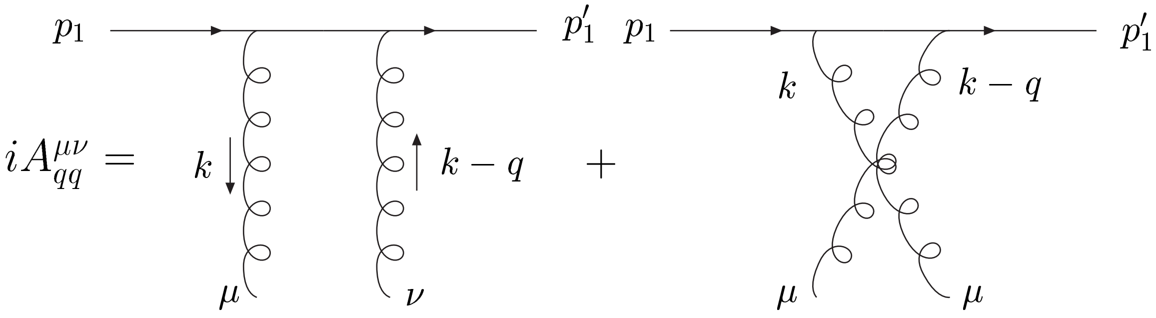

Figure 2.7: The amplitude for $q \to q$ via gluon Compton scattering, amputated in the final state gluon polarisations.

the Feynman rules for QCD to the first diagram we obtain,

$$\begin{aligned}
&\mathcal{A}^{\mu\nu}_{qq\,a}(-k,k-q)\delta_{\mu+}\delta_{\nu+} = \bar{u}_s(p_1-q)\frac{\gamma^\mu(\not{p}_1 - \not{k} - m)\gamma^\nu}{(p_1-k)^2 - m^2 + i\epsilon}u_{s'}(p_1)(-ig)^2\frac{Tr[t^a t^b]}{N}\delta_{\mu+}\delta_{\nu+} \\
&= \frac{4p_1^+p_1^+}{p_1^2 - 2k_-p_{1+} - \mathbf{k}^2 - m^2 + i\epsilon}(-ig)^2\frac{Tr[t^a t^b]}{N}\delta_{ss'} \\
&= -\sqrt{2s}(-ig)^2\frac{Tr[t^a t^b]}{N}\delta_{ss'}\frac{1}{k_- + \frac{\mathbf{k^2}}{\sqrt{2s}} - i\epsilon},
\end{aligned} \tag{2.101}$$

where we have applied the eikonal and relevant kinematic approximations. Note that the contour integration will force k_- to take on a value compatible with our kinematic analysis. We obtain the result[2]

$$\begin{aligned}
\phi_{qq\,a} &= g^2\frac{Tr[t^2 t^b]}{N}\delta_{ss'}\int_{-\infty}^{\infty}\frac{1}{k_- + \frac{\mathbf{k^2}}{\sqrt{2s}} - i\epsilon}\frac{dk_-}{2\pi i} \\
&= g^2\frac{Tr[t^2 t^b]}{N}\delta_{ss'} \\
&= g^2\frac{\delta_{ab}}{2N}\delta_{ss'} = \phi_{qq},
\end{aligned} \tag{2.102}$$

which is identical to that derived earlier for the $qq \to qq$ process. We still have diagram b to consider, but note that to get a non-zero contribution from a we were forced to

[2]Strictly speaking this integral does not converge, but the integrand is only valid in our kinematic range. Our assumption that we can close the contour is equivalent to saying that there is large k_- behaviour which saves convergence but does not give the leading contribution to the amplitude.

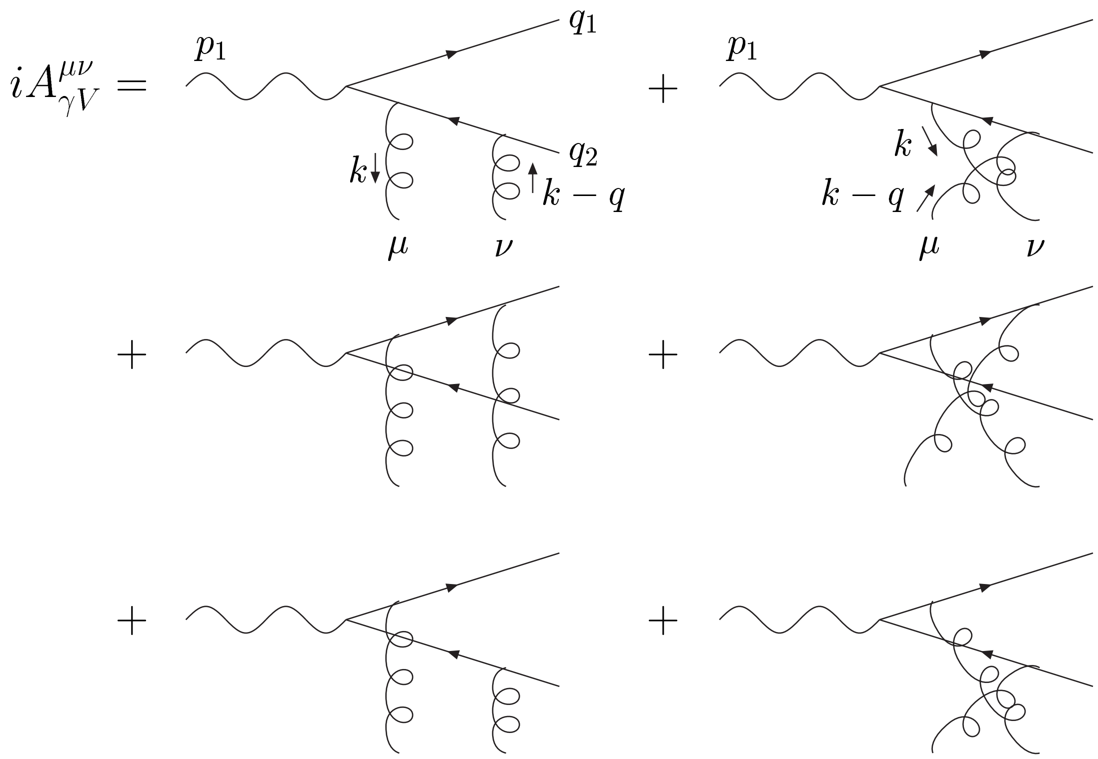

Figure 2.8: The amplitude for the $\gamma \to q\bar{q}$ transition via gluon emission/absorption, amputated in the final state gluon polarisations.

close the contour in the upper-half plane. Diagram b has no pole in the upper-half plane (since $k \to -k+q$) and is therefore zero. We were justified in writing $\phi_{qq\,a} = \phi_{qq}$.

The $\gamma q\bar{q}$ impact factor

The amplitude corresponding to the $\gamma \to q\bar{q}$ transition is depicted in figure 2.8. This impact factor is essential to our later calculation. The charge of the quark coupling to the photon is taken as ee_q[3]. Potentially, to lowest order, six diagrams contribute. Let us define them,

$$\phi_{\gamma q\bar{q}} = \frac{1}{\sqrt{2s}} \int (A^{\mu\nu} + B^{\mu\nu} + C^{\mu\nu} + A'^{\mu\nu} + B'^{\mu\nu} + C'^{\mu\nu})\delta_{\mu+}\delta_{\nu+}\frac{dk_-}{2\pi i}. \quad (2.103)$$

[3]Note that when we have a meson of mixed quark states we must average over these states. This accounted for by the substitution $e_q \to Q_V$. For example the ρ is the state $(u\bar{u} - d\bar{d})/\sqrt{2}$; therefore $Q_V = (e_u - e_d)/\sqrt{2} = 1/\sqrt{2}$.

Consider the first diagram first;

$$iA^{\mu\nu} = (-iee_q)(-ig)^2\frac{Tr[t^at^b]}{N}$$
$$\times\bar{u}_s(q_1)\ \not{e}\frac{i(\not{q}_1-\ \not{p}_1+m)}{(q_1-p_1)^2-m^2}\gamma^\mu\frac{i(\not{q}_1-\ \not{p}_1+\ \not{k}+m)}{(q_1-p_1+k)^2-m^2+i\epsilon}\gamma^\nu v_{s'}(q_2). \quad (2.104)$$

Therefore,

$$\phi^A_{\gamma q\bar{q}} = \frac{1}{i}\frac{1}{\sqrt{2s}}\int(-iee_q)(-ig)^2\frac{Tr[t^at^b]}{N}$$
$$\times\bar{u}_s(q_1)\ \not{e}\frac{i(\not{q}_1-\ \not{p}_1+m)}{(q_1-p_1)^2-m^2}\gamma^\mu\frac{i(\not{q}_1-\ \not{p}_1+\ \not{k}+m)}{(q_1-p_1+k)^2-m^2+i\epsilon}\gamma^\nu v_{s'}(q_2)$$
$$\times\delta_{\mu+}\delta_{\nu+}\frac{dk_-}{2\pi i}$$
$$= -\frac{ee_qg^2}{\sqrt{2s}}\frac{\delta^{ab}}{2N}\bar{u}_s(q_1)\ \not{e}\frac{(\not{q}_1-\ \not{p}_1+m)}{(q_1-p_1)^2-m^2}F_A\, v_{s'}(q_2), \quad (2.105)$$

where

$$F_A = \int\frac{dk_-}{2\pi i}\ \not{\delta}_+\frac{(\not{q}_1-\ \not{p}_1+\ \not{k}+m)}{(q_1-p_1+k)^2-m^2+i\epsilon}\ \not{\delta}_+. \quad (2.106)$$

We use the notation, $\not{\delta}_+ = \gamma^\mu\delta_{\mu+}$. Using the fact that $\not{\delta}_+\ \not{\delta}_+ = 0$ (just as $\not{p}_2^2 = 0$) we can rewrite this as,

$$F_A = \int\frac{dk_-}{2\pi i}\frac{(2\delta_+\cdot q_1-2\delta_+\cdot p_1+2\delta_+\cdot k)}{(q_1-p_1+k)^2-m^2+i\epsilon}\ \not{\delta}_-$$
$$= \sqrt{\frac{2}{s}}\int\frac{dk_-}{2\pi i}\frac{\sqrt{\frac{s}{2}}-q_{1+}-k_+}{(k_-+q_{1-})(1-\sqrt{2/s}\,(q_{1+}+k_+))+\frac{(\mathbf{q}_1+\mathbf{k})^2+m^2}{\sqrt{2s}}-i\epsilon}\ \not{\delta}_+$$
$$= \not{\delta}_+. \quad (2.107)$$

This leaves us with the following Dirac structure to analyse:

$$\bar{u}_s(q_1)\ \not{e}(\not{q}_1-\ \not{p}_1+m)\ \not{\delta}_+v_{s\prime}(q_2)$$
$$= \bar{u}_s(q_1)(-\ \not{e}\ \not{p}_1+2e\cdot q_{1\perp})\ \not{\delta}_+v_{s\prime}(q_2)$$
$$= \bar{u}_s(q_1)\left(-\ \not{e}\frac{\not{q}_1-\sqrt{2/s}\,q_{1-}\ \not{p}_2-\ \not{q}_{1\perp}}{\sqrt{2/s}\,q_{1+}}+2e\cdot q_1\right)\ \not{\delta}_+v_{s\prime}(q_2)$$
$$= \bar{u}_s(q_1)\left(-\ \not{e}\frac{\not{q}_1-\ \not{q}_{1\perp}}{\sqrt{2/s}\,q_{1+}}+2e\cdot q_1\right)\ \not{\delta}_+v_{s\prime}(q_2)$$
$$= \bar{u}_s(q_1)\left(\frac{\not{q}_1-\ \not{q}_{1\perp}}{\sqrt{2/s}\,q_{1+}}\ \not{e}+2e\cdot q_1\right)\ \not{\delta}_+v_{s\prime}(q_2)$$
$$= \bar{u}_s(q_1)\left(\frac{m-\ \not{q}_{1\perp}}{\sqrt{2/s}\,q_{1+}}\ \not{e}+2e\cdot q_1\right)\ \not{\delta}_+v_{s\prime}(q_2), \quad (2.108)$$

where we have used

$$\begin{aligned}
&\bar{u}_s(q_1)\,\not{q}_1 = m, \\
&\not{p}_2\,\not{\delta}_+ = 0, \\
&e\cdot q_1 = e\cdot q_{1\perp}, \\
&\text{and}\quad q_1 = \sqrt{\frac{2}{s}}q_{1+}p_1 + \sqrt{\frac{2}{s}}q_{1-}p_2 + q_{1\perp}.
\end{aligned} \tag{2.109}$$

Note also that since both p_1 and q_1 are on shell we can write,

$$(q_1-p_1)^2 - m^2 = -\sqrt{2s}q_{1-} = -\frac{(\mathbf{q}_1^2+m^2)}{\sqrt{2/s}\,q_{1+}}. \tag{2.110}$$

Putting this together we find,

$$\begin{aligned}
\phi^A_{\gamma q\bar{q}} &= -\frac{ee_q g^2}{\sqrt{2s}}\frac{\delta^{ab}}{2N}\bar{u}_s(q_1)\,\not{e}\frac{(\not{p}_1-\not{q}_1+m)}{(p_1-q_1)^2-m^2}\,F_A\,v_{s'}(q_2) \\
&= \frac{ee_q g^2}{\sqrt{2s}}\frac{\delta^{ab}}{2N}\frac{\bar{u}_s(q_1)\left((m-\not{q}_{1\perp})\,\not{e} + 2\sqrt{2/s}\,q_{1+}eq_{1\perp}\right)\,\not{\delta}_+ v_{s\prime}(q_2)}{\mathbf{q}_1^2+m^2}.
\end{aligned} \tag{2.111}$$

The list of other diagrams is:

$$\begin{aligned}
iB^{\mu\nu} &= (-iee_q)(-ig)^2\frac{Tr[t^at^b]}{N} \\
&\times\bar{u}_s(q_1)\gamma^\nu\frac{i(\not{p}_1-\not{q}_2-\not{k}+m)}{(p_1-q_2-k)^2-m^2+i\epsilon}\gamma^\mu\frac{i(\not{p}_1-\not{q}_2+m)}{(p_1-q_2)^2-m^2}\,\not{e}v_{s'}(q_2),
\end{aligned} \tag{2.112}$$

$$\begin{aligned}
iC^{\mu\nu} &= (-iee_q)(-ig)^2\frac{Tr[t^at^b]}{N} \\
&\times\bar{u}_s(q_1)\gamma^\mu\frac{i(\not{q}_1+\not{k}+m)}{(q_1+k)^2-m^2+i\epsilon}\,\not{e}\frac{i(\not{q}_1-\not{p}_1+\not{k}+m)}{(q_1-p_1+k)^2-m^2+i\epsilon}\gamma^\nu v_{s'}(q_2),
\end{aligned} \tag{2.113}$$

$$\begin{aligned}
iA'^{\mu\nu} &= (-iee_q)(-ig)^2\frac{Tr[t^at^b]}{N} \\
&\times\bar{u}_s(q_1)\,\not{e}\frac{i(\not{q}_1-\not{p}_1+m)}{(q_1-p_1)^2-m^2}\gamma^\nu\frac{i(\not{q}_1-\not{p}_1-\not{k}+\not{q}+m)}{(q_1-p_1-k+q)^2-m^2+i\epsilon}\gamma^\mu v_{s'}(q_2),
\end{aligned} \tag{2.114}$$

$$\begin{aligned}
iB'^{\mu\nu} &= (-iee_q)(-ig)^2\frac{Tr[t^at^b]}{N} \\
&\times\bar{u}_s(q_1)\gamma^\mu\frac{i(\not{p}_1-\not{q}_2+\not{k}-\not{q}+m)}{(p_1-q_2+k-q)^2-m^2+i\epsilon}\gamma^\nu\frac{i(\not{p}_1-\not{q}_2+m)}{(p_1-q_2)^2-m^2}\,\not{e}v_{s'}(q_2),
\end{aligned} \tag{2.115}$$

$$\begin{aligned}
iC'^{\mu\nu} &= (-iee_q)(-ig)^2\frac{Tr[t^at^b]}{N} \\
&\times\bar{u}_s(q_1)\gamma^\nu\frac{i(\not{p}_1-\not{q}_2-\not{k}+m)}{(p_1-q_2-k)^2-m^2+i\epsilon}\,\not{e}\frac{i(-\not{q}_2-\not{k}+m)}{(q_2+k)^2-m^2+i\epsilon}\gamma^\mu v_{s'}(q_2).
\end{aligned} \tag{2.116}$$

An analogous calculation to diagram A for diagram B yields

$$F_B = -\not{\delta}_+, \tag{2.117}$$

where

$$\begin{aligned}\phi^B_{\gamma q\bar{q}} &= -\frac{ee_q g^2}{\sqrt{2s}}\frac{\delta^{ab}}{2N}\bar{u}_s(q_1)\, F_B\, \frac{(\not{p}_1 - \not{q}_2 + m)}{(p_1-q_2)^2 - m^2}\,\not{e} v_{s'}(q_2) \\ &= \frac{ee_q g^2}{\sqrt{2s}}\frac{\delta^{ab}}{2N}\frac{\bar{u}_s(q_1)\,\not{\delta}_+\left((-m - \not{q}_{2\perp})\,\not{e} + 2\sqrt{2/s}\,q_{2+}e\cdot q_{2\perp}\right)v_{s'}(q_2)}{\mathbf{q}_2^2 + m^2}.\end{aligned} \tag{2.118}$$

Commuting the δ_+ to the right and using the constraint $q_{1+} + q_{2+} = p_{1+} = \sqrt{s/2}$ we obtain the result,

$$\phi^B_{\gamma q\bar{q}} = \frac{ee_q g^2}{\sqrt{2s}}\frac{\delta^{ab}}{2N}\frac{\bar{u}_s(q_1)\left((m + \not{q}_{2\perp})\,\not{e} - 2\sqrt{2/s}\,q_{1+}e\cdot q_{2\perp}\right)\,\not{\delta}_+ v_{s'}(q_2)}{\mathbf{q}_2^2 + m^2}. \tag{2.119}$$

Note that the primed amplitudes can be found from the unprimed ones by the substitution $k,\mu \to -k+q,\nu$. In the cases of A' and B', note that the integration variable k appears in only one propagator, the change in the sign of k in the primed substitution therefore means that if we close the contour to pick up non-zero A and B contributions, A' and B' are necessarily zero. That is, we are left with only the C and C' to calculate. These diagrams are more complicated than A and B due to the appearance of k in both quark line propagators and the position of the polarisation vector between the $\not{\delta}_+$'s. Let us consider C first. Note that we are working in the regime where we put $k_+ \to 0$ in this impact factor. This allows us to write,

$$\begin{aligned}k_\mu &= \sqrt{\frac{2}{s}}k_+\,p_{1\,\mu} + \sqrt{\frac{2}{s}}k_-\,p_{2\,\mu} + k_\perp \\ &\simeq \sqrt{\frac{2}{s}}k_-\,p_{2\,\mu} + k_\perp.\end{aligned} \tag{2.120}$$

This result combined with the fact that the ks in the propagators also lie next to a $\not{\delta}_+$, allows us to rewrite C

$$\begin{aligned}iC^{\mu\nu} &\to (-iee_q)(-ig)^2\frac{Tr[t^a t^b]}{N} \\ &\times \bar{u}_s(q_1)\gamma^\mu \frac{i(\not{q}_1 + \not{k}_\perp + m)}{(q_1+k)^2 - m^2 + i\epsilon}\,\not{e}\,\frac{i(\not{q}_1 - \not{p}_1 + \not{k}_\perp + m)}{(q_1 - p_1 + k)^2 - m^2 + i\epsilon}\gamma^\nu v_{s'}(q_2).\end{aligned} \tag{2.121}$$

Analysis shows that only the second of the propagators has a pole in the upper-half plane, and, in fact, this propagator is identical to the one appearing in A. Permuting the γ^μ and $\not{e}$ across the first propagator and each other we find

$$
\begin{aligned}
&iC^{\mu\nu}\delta_{+\mu}\delta_{+\nu} = (-iee_q)(-ig)^2\frac{Tr[t^a t^b]}{N} \\
&\times\bar{u}_s(q_1)\frac{i2q_+\not{e}}{(q_1+k)^2-m^2+i\epsilon}\frac{i(\not{q}_1-\not{p}_1+\not{k}_\perp+m)}{(q_1-p_1+k)^2-m^2+i\epsilon}\not{\delta}_+ v_{s'}(q_2) \\
&+(-iee_q)(-ig)^2\frac{Tr[t^a t^b]}{N} \\
&\times\bar{u}_s(q_1)\frac{i\not{k}_\perp\not{e}\not{\delta}_+}{(q_1+k)^2-m^2+i\epsilon}\frac{i(\not{q}_1-\not{p}_1+\not{k}_\perp+m)}{(q_1-p_1+k)^2-m^2+i\epsilon}\not{\delta}_+ v_{s'}(q_2),
\end{aligned}
\tag{2.122}
$$

yielding the result,

$$
\begin{aligned}
\phi^C_{\gamma q\bar{q}} &= -\frac{ee_q g^2}{\sqrt{2s}}\frac{\delta^{ab}}{2N}\left[\bar{u}_s(q_1)\frac{\not{k}_\perp\not{e}}{(q_1+k)^2-m^2+i\epsilon}F_A\, v_{s'}(q_2)\right. \\
&+\left.\int\frac{dk_-}{2\pi i}\bar{u}_s(q_1)\frac{2q_+\not{e}}{(q_1+k)^2-m^2+i\epsilon}\frac{(\not{q}_1-\not{p}_1+\not{k}_\perp+m)}{(q_1-p_1+k)^2-m^2+i\epsilon}\not{\delta}_+ v_{s'}(q_2)\right] \\
&= -\frac{ee_q g^2}{\sqrt{2s}}\frac{\delta^{ab}}{2N}\bar{u}_s(q_1)\frac{\left(\not{k}_\perp\not{e}\not{\delta}_+ + \frac{2q_{1+}\not{e}(\not{q}_1-\not{p}_1+\not{k}_\perp+m)\not{\delta}_+}{2(\sqrt{\frac{s}{2}}-q_{1+})}\right)}{(q_1+k)^2-m^2+i\epsilon}v_{s'}(q_2).
\end{aligned}
\tag{2.123}
$$

Using the facts that:

$$q_1^2 = m^2, \tag{2.124}$$

$$k_- = -q_{1-} - \frac{(\mathbf{q}_1+\mathbf{k})^2+m^2}{2(\sqrt{s/2}-q_{1+})} \quad \text{(imposed by contour integration)}, \tag{2.125}$$

$$\text{and} \quad q_{1-} = \frac{\mathbf{q}_1^2+m^2}{2q_{1+}}, \tag{2.126}$$

we can show that we may then approximate the propagator denominator by

$$\frac{1}{(q_1+k)^2-m^2} \sim -\frac{\sqrt{s/2}}{\sqrt{s/2}-q_{1+}}\frac{1}{(\mathbf{q}_1+\mathbf{k})^2+m^2}. \tag{2.127}$$

Some more manipulation gives us the final answer for diagram C,

$$\phi^C_{\gamma q\bar{q}} = -\frac{ee_q g^2}{\sqrt{2s}}\frac{\delta^{ab}}{2N}\bar{u}_s(q_1)\frac{(m-\not{q}_{1\perp}-\not{k}_\perp)\not{e}+2\sqrt{2/s}\,q_{1+}e\cdot(q_{1\perp}+k_\perp)}{(\mathbf{q}_1+\mathbf{k})^2+m^2}\not{\delta}_+ v_{s'}(q_2). \tag{2.128}$$

A completely analogous calculation for C' gives,

$$\phi^{C'}_{\gamma q\bar{q}} = -\frac{ee_q g^2}{\sqrt{2s}}\frac{\delta^{ab}}{2N}\bar{u}_s(q_1)\ \not{\delta}_+\frac{(-m-\ \not{q}_{2\perp}-\ \not{k}_\perp)\ \not{e}+2\sqrt{2/s}\,q_{2+}e\cdot(q_{2\perp}+k_\perp)}{(\mathbf{q}_2+\mathbf{k})^2+m^2}v_{s'}(q_2)$$
$$= -\frac{ee_q g^2}{\sqrt{2s}}\frac{\delta^{ab}}{2N}\bar{u}_s(q_1)\frac{(m+\ \not{q}_{2\perp}+\ \not{k}_\perp)\ \not{e}-2\sqrt{2/s}\,q_{1+}e\cdot(q_{2\perp}+k_\perp)}{(\mathbf{q}_2+\mathbf{k})^2+m^2}\ \not{\delta}_+v_{s'}(q_2). \quad (2.129)$$

Note that we have the following relations between the four non-zero diagrams,

$$\phi^{B}_{\gamma q\bar{q}} = \phi^{A}_{\gamma q\bar{q}}(q_{1\perp}\to -q_{2\perp}), \quad (2.130)$$
$$\phi^{C}_{\gamma q\bar{q}} = -\phi^{A}_{\gamma q\bar{q}}(q_{1\perp}\to q_{1\perp}+k_\perp) \quad (2.131)$$
$$\text{and}\quad \phi^{C'}_{\gamma q\bar{q}} = -\phi^{B}_{\gamma q\bar{q}}(q_{2\perp}\to q_{2\perp}+k_\perp). \quad (2.132)$$

Putting these results together we find that we can express the total impact factor as,

---

$$\phi_{\gamma q\bar{q}}(-\mathbf{k},\mathbf{q}_1,\mathbf{q}_2) = \frac{ee_q g^2}{\sqrt{2s}}\frac{\delta^{ab}}{2N}\bar{u}_s(q_1)[2u\,P\cdot e-\ \not{P}\ \not{e}+m\,R\ \not{e}]\ \not{\delta}_+v_{s'}(q_2), \quad (2.133)$$

where we define,

$$u = \sqrt{2/s}\,q_{1+} = q_{1+}/p_{1+} \quad (2.134)$$
$$P = (0,\mathbf{P},0) \quad (2.135)$$
$$\mathbf{P} = \left(\frac{\mathbf{q}_1}{\mathbf{q}_1^2+m^2}+\frac{-\mathbf{k}-\mathbf{q}_1}{(\mathbf{k}+\mathbf{q}_1)^2+m^2}\right)-(\mathbf{q}_1\to\mathbf{q_2}) \quad (2.136)$$
$$R = \left(\frac{1}{\mathbf{q}_1^2+m^2}-\frac{1}{(\mathbf{k}+\mathbf{q}_1)^2+m^2}\right)+(\mathbf{q}_1\to\mathbf{q_2}). \quad (2.137)$$

For later purposes we will define the impact factor with the spinors amputated as

---

$$\hat{Q}^{\gamma q\bar{q}}_{\alpha\beta}(\mathbf{k},\mathbf{q}_1,\mathbf{q}_2) = \frac{ee_q g^2}{\sqrt{2s}}\frac{\delta^{ab}}{2N}[2u\,P\cdot e-\ \not{P}\ \not{e}+m\,R\ \not{e}]\ \not{\delta}_+. \quad (2.138)$$

We have obtained the $\gamma \to q\bar{q}$ impact factor. We stress that we have obtained by working in the frame where the initial state photon and quark define the z-axis. Note that we have written the impact factor as a function of $-\mathbf{k}$ with $\mathbf{q}_1 + \mathbf{q}_2 = -\mathbf{q}$. If we take this as the bottom impact factor then we merely substitute $\mathbf{k} \to -\mathbf{k}$ and $\mathbf{q} \to -\mathbf{q}$ within the factor. This is the equivalent to changing the definition of the direction of momentum exchange.

2.2.4 The hard subprocess Fierz trace

The $\gamma q \to q'\bar{q}'q$ amplitude

The results of the previous subsections give us

$$\mathcal{A}(\gamma q \to q'\bar{q}'q) = is \int \frac{\phi_{qq}(-\mathbf{k}, -\mathbf{q})\phi_{\gamma q'\bar{q}'}(\mathbf{k}, \mathbf{q_1}, \mathbf{q_2})}{\mathbf{k^2}(\mathbf{k}-\mathbf{q})^2} \frac{d^2\mathbf{k}}{(2\pi)^2}, \tag{2.139}$$

and amputated

$$\mathcal{A}_{\alpha\beta}(\gamma q \to q'\bar{q}'q) = is \int \frac{\phi_{qq}(-\mathbf{k}, -\mathbf{q})\hat{Q}^{\gamma q\bar{q}}_{\alpha\beta}(\mathbf{k}, \mathbf{q}_1, \mathbf{q}_2)}{\mathbf{k^2}(\mathbf{k}-\mathbf{q})^2} \frac{d^2\mathbf{k}}{(2\pi)^2}. \tag{2.140}$$

We need to take the trace of this last result in spinor space, with the various γ-matrix combinations (see result (2.33)).

The traces

The only Dirac algebra in the amplitude is within $\hat{Q}^{\gamma q\bar{q}}$. The quantities we need to evaluate are therefore (dropping the superscript)

$$Tr[\hat{Q}\Gamma_t] \quad \text{where,} \quad \Gamma_t \in \{1, \gamma_\mu, -\gamma_\mu\gamma_5, \sigma_{\mu\nu}, -i\gamma_5\}. \tag{2.141}$$

Using the usual Dirac identities we easily find[4],

$$
\begin{aligned}
Tr[\hat{Q}] &= \frac{ee_q g^2}{s}\frac{\delta^{ab}}{2N} m\, Tr[\not{e}\ \not{p}_2] \\
&= \frac{ee_q g^2}{s}\frac{\delta^{ab}}{2N} 4m\,(e\cdot p_2) = 0, && (2.142)\\
Tr[i\gamma_5\hat{Q}] &= 0, && (2.143)\\
Tr[\gamma_\mu\hat{Q}] &= \frac{ee_q g^2}{s}\frac{\delta^{ab}}{2N} Tr[\gamma_\mu(2u(P\cdot e) - \not{P}\ \not{e})p_2] \\
&= \frac{ee_q g^2}{s}\frac{\delta^{ab}}{2N} 4(1-2u)(\mathbf{P}\cdot\mathbf{e})p_{2\mu}, && (2.144)\\
Tr[-\gamma_\mu\gamma_5\hat{Q}] &= \frac{ee_q g^2}{s}\frac{\delta^{ab}}{2N} Tr[\gamma_\mu\gamma_5\ \not{P}\ \not{e}\ \not{p}_2] \\
&= \frac{ee_q g^2}{s}\frac{\delta^{ab}}{2N} 4i\epsilon_{\mu\nu\sigma\tau}P^\nu e^\sigma p_2^\tau, && (2.145)\\
Tr[\sigma_{\mu\nu}\hat{Q}] &= \frac{ee_q g^2}{s}\frac{\delta^{ab}}{2N} mR\, Tr[\sigma_{\mu\nu}\ \not{e}\ \not{p}_2] \\
&= \frac{ee_q g^2}{s}\frac{\delta^{ab}}{2N} 4mi\, R(p_{2\mu}e_\nu - e_\mu p_{2\nu}). && (2.146)
\end{aligned}
$$

We have now calculated all the necessary quantities of the hard subprocess.

[4]We adopt the convention $\gamma_5 = i\gamma^0\gamma^1\gamma^2\gamma^3$. The convention $\gamma_5 = i\gamma_0\gamma_1\gamma_2\gamma_3$ would introduce a relative minus sign here for the $\gamma_\mu\gamma_5$ element (that would be cancelled out by another in the relevant light-cone hadronic matrix element).

2.3 From partons to mesons

We now turn to the soft transition of $q\bar{q} \to V$. The calculation of the light-cone matrix elements is beyond the aims of this work. The authors of [33] have presented results for the Fourier transform of the quantities we require and we shall utilise their results.

2.3.1 The soft subprocess Fierz traces: The light-cone matrix elements

The spins of the quark and anti-quark can be aligned or anti-aligned along their directions of motion. Where they are aligned the configuration is referred to as chiral odd. Where they are anti-aligned the configuration is referred to as chiral even. The chiral even terms are associated with the Dirac structures $\Gamma_t = \gamma_\mu,\, \gamma_\mu\gamma_5$, the chiral odd with $\Gamma_t = \sigma_{\mu\nu}$ [33]. The authors of [33] provide us with the light-cone matrix elements,

$$\begin{aligned}\langle V(p,\lambda)|\bar{\psi}(-r/2)\gamma_\mu\psi(r/2)|0\rangle = f_V m_V \Bigg[&\frac{e_V^{(\lambda)*}\cdot r}{p\cdot r} p_\mu \int_0^1 du\, e^{-i\xi(p\cdot r/2)}\phi_\parallel(u) \\ &+ \left(e_{V\mu}^{(\lambda)*} - p_\mu \frac{e_V^{(\lambda)*}\cdot r}{p\cdot r}\right) \int_0^1 du\, e^{-i\xi(p\cdot r/2)} g_\perp^{(v)}(u)\Bigg],\end{aligned} \tag{2.147}$$

$$\langle V(p,\lambda)|\bar{\psi}(-r/2)\gamma_\mu\gamma_5\psi(r/2)|0\rangle = -\frac{1}{4} f_V m_V\, \epsilon_{\mu\nu\alpha\beta}\, e_V^{(\lambda)*\,\nu} p^\alpha r^\beta \int_0^1 du\, e^{-i\xi(p\cdot r/2)} g_\perp^{(a)}(u), \tag{2.148}$$

$$\begin{aligned}\langle V(p,\lambda)|\bar{\psi}(-r/2)\sigma_{\mu\nu}\psi(r/2)|0\rangle &= -if_V^T \left[(e_{V\mu}^{(\lambda)*} p_\nu - e_{V\nu}^{(\lambda)*} p_\mu) \int_0^1 du\, e^{-i\xi(p\cdot r/2)}\phi_\perp(u)\right] \\ -if_V^T &\left[(p_\mu r_\nu - p_\nu r_\mu) \frac{e_V^{(\lambda)*}\cdot r}{(p\cdot r)^2} m_V^2 \int_0^1 du\, e^{-i\xi(p\cdot r/2)} \left(h_\parallel^{(t)}(u) - \frac{1}{2}\phi_\perp(u) - \frac{1}{2}h_3(u)\right)\right] \\ -if_V^T &\left[\frac{1}{2}(e_{V\mu}^{(\lambda)*} r_\nu - e_{V\nu}^{(\lambda)*} r_\mu) \frac{m_V^2}{p\cdot r} \int_0^1 du\, e^{-i\xi(p\cdot r/2)} (h_3(u) - \phi_\perp(u))\right].\end{aligned} \tag{2.149}$$

The stated matrix elements are the conjugates[5] of the ones listed in [33]. It is important to note that the polarisations appearing above are the polarisations of

[5]Note that $\gamma_5^\dagger = \gamma_5$, $\bar{\gamma}_\mu = \gamma_0\gamma_\mu^\dagger\gamma_0 = \gamma_\mu$ and $\sigma_{\mu\nu}^\dagger = \sigma_{\mu\nu}$.

the vector meson *not* the photon. We neglect to distinguish between the two in notation henceforth because to leading logs in the Regge region, where we will be working, they are the same. That is $\cos\theta \sim 1$ where θ is the angle between the incoming photon and outgoing meson. This allows us to make such approximations as $e^{(+)} \cdot e_V^{(-)*} \sim e^{(+)} \cdot e^{(-)*} = 0$.

2.3.2 Inputting the polarisation vector

We will work in the 'tilde' frame where the meson momentum defines the z-axis and $p \cdot r = \tilde{p}_+\tilde{r}_-$. We denote the polarisation vectors of the photon and transversely polarised meson as

$$\tilde{\mathbf{e}}^{\lambda=\pm 1} = \mp\frac{1}{\sqrt{2}}(1, \pm i) \tag{2.150}$$

and the polarisation vector of a longitudinal meson (see Appendix A) as

$$e^{\lambda=0} = \frac{p_\mu}{m_V}, \tag{2.151}$$

where, as observed above, to leading log accuracy, we are able to equate the components of polarisation vectors in the 'tilde' frame and the frame where the photon-quark define the z-axis. Then, putting these polarisations explicitly into the light-cone matrix element expressions, we find

$$\begin{aligned}
&\langle V(p,\lambda=0)|\bar{\psi}(-r/2)\gamma_\mu\psi(r/2)|0\rangle = \\
&f_V m_V \left[\frac{\tilde{p}_+\tilde{r}_-/m_V}{\tilde{p}_+\tilde{r}_-} p_\mu \int_0^1 du\, e^{-i\xi(\tilde{p}_+\tilde{r}_-/2)}\phi_\parallel(u) \right. \\
&\qquad \left. + \left(\frac{p_\mu}{m_V} - p_\mu\frac{\tilde{p}_+\tilde{r}_-/m_V}{\tilde{p}_+\tilde{r}_-}\right)\int_0^1 du\, e^{-i\xi(\tilde{p}_+\tilde{r}_-/2)} g_\perp^{(v)}(u)\right], \\
&= f_V p_\mu \int_0^1 du\, e^{-i\xi(\tilde{p}_+\tilde{r}_-/2)}\phi_\parallel(u),
\end{aligned} \tag{2.152}$$

$$\begin{aligned}
&\langle V(p,\lambda=T)|\bar{\psi}(-r/2)\gamma_\mu\psi(r/2)|0\rangle = \\
&-f_V m_V p_\mu \frac{\tilde{\mathbf{e}}^{(T)*}\cdot\tilde{\mathbf{r}}}{\tilde{p}_+\tilde{r}_-}\int_0^1 du\, e^{-i\xi(\tilde{p}_+\tilde{r}_-/2)}(\phi_\parallel(u) - g_\perp^{(v)}(u)) \\
&\qquad + \left\{ f_V m_V e_\mu^{(T)*}\int_0^1 du\, e^{-i\xi(\tilde{p}_+\tilde{r}_-/2)} g_\perp^{(v)}(u)\right\},
\end{aligned} \tag{2.153}$$

$$\langle V(p,\lambda=0)|\bar{\psi}(-r/2)\gamma_\mu\gamma_5\psi(r/2)|0\rangle = -\frac{1}{4}f_V\,\epsilon_{\mu\nu\alpha\beta}\,p^\nu\,p^\alpha r^\beta\int_0^1 du\,e^{-i\xi(\tilde{p}_+\tilde{r}_-/2)}g_\perp^{(a)}(u),$$
$$= 0, \tag{2.154}$$

$$\langle V(p,\lambda=T)|\bar{\psi}(-r/2)\gamma_\mu\gamma_5\psi(r/2)|0\rangle =$$
$$-\frac{1}{4}f_V m_V\,\epsilon_{\mu\nu\alpha\beta}\,e^{(T)*\,\nu}p^\alpha r^\beta\int_0^1 du\,e^{-i\xi(\tilde{p}_+\tilde{r}_-/2)}g_\perp^{(a)}(u), \tag{2.155}$$

$$\langle V(p,\lambda=0)|\bar{\psi}(-r/2)\sigma_{\mu\nu}\psi(r/2)|0\rangle =$$
$$-if_V^T(p_\mu r_\nu - p_\nu r_\mu)\frac{m_V}{\tilde{p}_+\tilde{r}_-}\int_0^1 du\,e^{-i\xi(\tilde{p}_+\tilde{r}_-/2)}\left(h_\parallel^{(t)}(u)-\phi_\perp(u)\right) \tag{2.156}$$

and

$$\langle V(p,\lambda=T)|\bar{\psi}(-r/2)\sigma_{\mu\nu}\psi(r/2)|0\rangle =$$
$$-if_V^T\left[(e_\mu^{(T)*}p_\nu - e_\nu^{(T)*}p_\mu)\int_0^1 du\,e^{-i\xi(\tilde{p}_+\tilde{r}_-/2)}\phi_\perp(u)\right]$$
$$+if_V^T\left[(p_\mu r_\nu - p_\nu r_\mu)\frac{\tilde{\mathbf{e}}^{(T)*}\cdot\tilde{\mathbf{r}}}{(\tilde{p}_+\tilde{r}_-)^2}m_V^2\int_0^1 du\,e^{-i\xi(\tilde{p}_+\tilde{r}_-/2)}\left(h_\parallel^{(t)}(u)-\frac{1}{2}\phi_\perp(u)-\frac{1}{2}h_3(u)\right)\right]$$
$$-if_V^T\left\{\frac{1}{2}(e_\mu^{(T)*}r_\nu - e_\nu^{(T)*}r_\mu)\frac{m_V^2}{\tilde{p}_+\tilde{r}_-}\int_0^1 du\,e^{-i\xi(\tilde{p}_+\tilde{r}_-/2)}(h_3(u)-\phi_\perp(u))\right\}. \tag{2.157}$$

We will need the Fourier transforms of these quantities from r space to u space. The objects in the curly brackets of equation (2.153) and (2.157) are subleading in s and shall be disregarded.

2.3.3 Transform to Fourier space

We define the Fourier transform of the light-cone matrix elements as,

$$\psi_t^{(\lambda)}(u,\tilde{\mathbf{r}}) = \frac{1}{2}\int\frac{d(\tilde{p}_+\tilde{r}_-)}{2\pi}e^{i(\tilde{p}_+\tilde{r}_-/2)\xi}\langle V(p,\lambda)|\bar{\psi}(-r/2)\Gamma_t\psi(r/2)|0\rangle. \tag{2.158}$$

The appearance of powers of $\tilde{p}_+\tilde{r}_-$ complicate the transforms. We can eliminate these factors by introducing an extra integration via integration by parts. We rely on the following properties of the distribution amplitudes (denoted here generically, $\mathcal{D}$);

$$\int_0^1\mathcal{D}(u)du = 1 \quad \text{(normalisation)} \tag{2.159}$$
$$\mathcal{D}(1-u) = \mathcal{D}(u) \quad \text{(flavour symmetry)}. \tag{2.160}$$

Using these properties we can write:

$$
\begin{aligned}
&\langle V(p,\lambda=T)|\bar{\psi}(-r/2)\gamma_\mu\psi(r/2)|0\rangle = \\
&-f_V m_V p_\mu \frac{\tilde{\mathbf{e}}^{(T)*}\cdot\tilde{\mathbf{r}}}{\tilde{p}_+\tilde{r}_-}\int_0^1 du\, e^{-i\xi(\tilde{p}_+\tilde{r}_-/2)}(\phi_\parallel(u)-g_\perp^{(v)}(u)) \\
&= -f_V m_V p_\mu \frac{\tilde{\mathbf{e}}^{(T)*}\cdot\tilde{\mathbf{r}}}{\tilde{p}_+\tilde{r}_-}\left[e^{-i\xi(\tilde{p}_+\tilde{r}_-/2)}\int_0^u dv(\phi_\parallel(v)-g_\perp^{(v)}(v))\right]_0^1 \\
&-f_V m_V p_\mu \frac{\tilde{\mathbf{e}}^{(T)*}\cdot\tilde{\mathbf{r}}}{\tilde{p}_+\tilde{r}_-}\int_0^1 du\, i(\tilde{p}_+\tilde{r}_-)e^{-i\xi(\tilde{p}_+\tilde{r}_-/2)}\int_0^u dv(\phi_\parallel(v)-g_\perp^{(v)}(v)) \\
&= -if_V m_V p_\mu \tilde{\mathbf{e}}^{(T)*}\cdot\tilde{\mathbf{r}}\int_0^1 du\, e^{-i\xi(\tilde{p}_+\tilde{r}_-/2)}\int_0^u dv(\phi_\parallel(v)-g_\perp^{(\nu)}(v)).
\end{aligned}
\tag{2.161}
$$

Such a process can be applied as many times as required to eliminate all powers of $(\tilde{p}_+\tilde{r}_-)$ in a particular formula. Doing so we find,

$$\psi^{(0)}_{\gamma_\mu}(u,\tilde{\mathbf{r}}) = \frac{1}{2}p_\mu f_V\phi_\parallel(u), \tag{2.162}$$

$$\psi^{(T)}_{\gamma_\mu}(u,\tilde{\mathbf{r}}) = -\frac{i}{2}f_V m_V p_\mu \tilde{\mathbf{e}}^{(T)*}\cdot\tilde{\mathbf{r}}\left(\int_0^u dv(\phi_\parallel(v)-g_\perp^{(v)}(v))\right), \tag{2.163}$$

$$\psi^{(0)}_{\gamma_\mu\gamma_5}(u,\tilde{\mathbf{r}}) = 0, \tag{2.164}$$

$$\psi^{(T)}_{\gamma_\mu\gamma_5}(u,\tilde{\mathbf{r}}) = -\frac{1}{8}f_V m_V \epsilon_{\mu\nu\alpha\beta}e^{(T)\,\nu*}p^\alpha r^\beta\, g_\perp^{(a)}(u), \tag{2.165}$$

$$\psi^{(0)}_{(\sigma_{\mu\nu})}(u,\tilde{\mathbf{r}}) = \frac{1}{2}f_V^T(p_\mu r_\nu - p_\nu r_\mu)m_V\int_0^u dv\left(h_\parallel^{(t)}(v)-\phi_\perp(v)\right), \tag{2.166}$$

and

$$
\begin{aligned}
&\psi^{(T)}_{\sigma_{\mu\nu}}(u,\tilde{\mathbf{r}}) = -i\frac{f_V^T}{2}\left(e_\mu^{(T)*}p_\nu - e_\nu^{(T)*}p_\mu\right)\phi_\perp(u) \\
&-i\frac{f_V^T}{2}\left(p_\mu r_\nu - p_\nu r_\mu\right)(\tilde{\mathbf{e}}_\mu^{(T)*}\cdot\tilde{\mathbf{r}})m_V^2\int_0^u dv\int_0^v d\eta\left(h_\parallel^{(t)}(\eta)-\frac{1}{2}\phi_\perp(\eta)-\frac{1}{2}h_3(\eta)\right).
\end{aligned}
\tag{2.167}
$$

2.3.4 Lorentz contraction of the hard subprocess with the light-cone matrix elements

Equation (2.33) tells us that we need to contract ((2.144), (2.145), (2.146)) with corresponding matrix elements ((2.162, 2.163), (2.164, 2.165), (2.166, 2.167)). The contractions between these Fierz factorised pieces requires the following contractions of kinematic variables,

$$\gamma: \qquad \frac{p_2^\mu}{s} p_\mu \sim \frac{p_2^\mu}{s} p_{2\,\mu} = \frac{1}{2} \tag{2.168}$$

$$\gamma\gamma_5: \qquad \frac{1}{s}\epsilon_{\mu\nu\sigma\tau} P^\nu e^{(+)\sigma} p_2^\tau \epsilon^{\mu\alpha\beta\gamma} e_\alpha^{(T)*} p_\beta r_\gamma \tag{2.169}$$

$$= \frac{1}{2}[\,(P\cdot e^{(T)*})(r\cdot e^{(+)}) - (P\cdot r)(e^{(T)*}\cdot e^{(+)})\,]$$

$$= \frac{1}{2}[\,(\tilde{\mathbf{P}}\cdot\tilde{\mathbf{e}}^{(T)*})(\tilde{\mathbf{r}}\cdot\tilde{\mathbf{e}}^{(+)}) - (\tilde{\mathbf{P}}\cdot\tilde{\mathbf{r}})\cdot(\tilde{\mathbf{e}}^{(T)*}\cdot\tilde{\mathbf{e}}^{(+)})\,] \tag{2.170}$$

$$\sigma: \qquad \frac{1}{s}(p_{2\mu}e_\nu^{(+)} - p_{2\nu}e_\mu^{(+)})(p_\mu r_\nu - p_\nu r_\mu) = -(\tilde{\mathbf{r}}\cdot\tilde{\mathbf{e}}^{(+)}) \tag{2.171}$$

$$\frac{1}{s}(p_{2\mu}e_\nu^{(+)} - p_{2\nu}e_\mu^{(+)})(e_\mu^{(T)*}p_\nu - e_\nu^{(T)*}p_\mu) = (\tilde{\mathbf{e}}^{(+)}\cdot\tilde{\mathbf{e}}^{(T)*}), \tag{2.172}$$

where we have made use of the identity,

$$\epsilon^{\mu\nu\sigma\tau}\epsilon_{\mu\alpha\beta\gamma} = -\delta_\alpha^\nu\delta_\beta^\sigma\delta_\gamma^\tau + \delta_\alpha^\nu\delta_\gamma^\sigma\delta_\beta^\tau + \delta_\beta^\nu\delta_\alpha^\sigma\delta_\gamma^\tau - \delta_\beta^\nu\delta_\gamma^\sigma\delta_\alpha^\tau - \delta_\gamma^\nu\delta_\alpha^\sigma\delta_\beta^\tau + \delta_\gamma^\nu\delta_\beta^\sigma\delta_\alpha^\tau \tag{2.173}$$

and the constraint

$$\tau = \beta \qquad \text{(leading } s \text{ approximation).} \tag{2.174}$$

Here and subsequently, the photon polarisation vector can be distinguished from the vector meson vector by the fact that it takes a definite transverse polarisation, (+). Moving on, we find, in our approximations, that:

$$\frac{1}{4}Tr[\gamma_\mu\hat{Q}]\psi_{\gamma_\mu}^{(0)}(u,\tilde{\mathbf{r}}) = ee_q\frac{g^2\delta_{ab}}{2N}(1-2u)(\tilde{\mathbf{P}}\cdot\tilde{\mathbf{e}}^{(+)})\frac{f_V}{4}\phi_\parallel(u), \tag{2.175}$$

$$\frac{1}{4}Tr[\gamma_\mu\hat{Q}]\psi_{\gamma_\mu}^{(T)}(u,\tilde{\mathbf{r}}) = ee_q\frac{g^2\delta_{ab}}{2N}(1-2u)(\tilde{\mathbf{P}}\cdot\tilde{\mathbf{e}}^{(+)})\frac{-if_V m_V}{4}(\tilde{\mathbf{r}}\cdot\tilde{\mathbf{e}}^{(T)*})$$
$$\times\int_0^u dv\,(\phi_\parallel(v) - g_\perp^{(v)}(v)) \tag{2.176}$$

and

$$\frac{1}{4}Tr[-\gamma_\mu\gamma_5\hat{Q}]\psi^{(T)}_{\gamma_\mu\gamma_5}(u,\tilde{\mathbf{r}}) =$$
$$-ee_q\frac{g^2\delta_{ab}}{2N}\frac{if_V m_V}{4}\left[(\tilde{\mathbf{P}}\cdot\tilde{\mathbf{e}}^{(T)*})(\tilde{\mathbf{r}}\cdot\tilde{\mathbf{e}}^{(+)}) - (\tilde{\mathbf{P}}\cdot\tilde{\mathbf{r}})(\tilde{\mathbf{e}}^{(T)*}\cdot\tilde{\mathbf{e}}^{(+)})\right]\frac{g_\perp^{(a)}(u)}{4}. \quad (2.177)$$

$$\frac{1}{4}Tr[\sigma_{\mu\nu}\hat{Q}]\psi^{(0)}_{\sigma_{\mu\nu}}(u,\tilde{\mathbf{r}}) =$$
$$ee_q\frac{g^2\delta_{ab}}{2N}(-i)m\,\tilde{R}\,m_V\frac{f_V^T}{2}(\tilde{\mathbf{r}}\cdot\tilde{\mathbf{e}}^{(+)})\int_0^u dv\,(h_\parallel^{(t)}(v)-\phi_\perp(v)) \quad (2.178)$$

$$\frac{1}{4}Tr[\sigma_{\mu\nu}\hat{Q}]\psi^{(T)}_{\sigma_{\mu\nu}}(u,\tilde{\mathbf{r}}) = ee_q\frac{g^2\delta_{ab}}{2N}(\tilde{\mathbf{e}}^{(T)*}\cdot\tilde{\mathbf{e}}^{(+)})m\,\tilde{R}\,\frac{f_V^T}{2}\phi_\perp(u)$$
$$-ee_q\frac{g^2\delta_{ab}}{2N}(\tilde{\mathbf{r}}\cdot\tilde{\mathbf{e}}^{(+)})(\tilde{\mathbf{r}}\cdot\tilde{\mathbf{e}}^{(T)*})m\,\tilde{R}\,\frac{f_V^T}{2}m_V^2\int_0^u dv\int_0^v d\eta\left(h_\parallel^{(t)}(\eta)-\frac{1}{2}\phi_\perp(\eta)-\frac{1}{2}h_3(\eta)\right) \quad (2.179)$$

Summing over the chiral odd and even Fierz decompositions separately for specific meson polarisations we get:

Even

$$V^{(0)}_{even}(\mathbf{k},\mathbf{q}_1,\mathbf{q}_2;\tilde{\mathbf{r}},u) \equiv \sum_{t\in even}\frac{1}{4}Tr[\Gamma_t\hat{Q}]\psi^{(0)}_{\Gamma^t}(u,\tilde{\mathbf{r}}) = ee_q\frac{g^2\delta_{ab}}{2N}(1-2u)(\tilde{\mathbf{P}}\cdot\tilde{\mathbf{e}}^{(+)})\frac{f_V}{4}\phi_\parallel(u), \quad (2.180)$$

$$V^{(+)}_{even}(\mathbf{k},\mathbf{q}_1,\mathbf{q}_2;\tilde{\mathbf{r}},u) \equiv \sum_{t\in even} \frac{1}{4} Tr[\Gamma_t \hat{Q}]\psi^{(+)}_{\Gamma^t}(u,\tilde{\mathbf{r}}) = ee_q \frac{g^2\delta_{ab}}{2N}\frac{-if_V m_V}{4}$$
$$\times\Bigg[(\tilde{\mathbf{P}}\cdot\tilde{\mathbf{e}}^{(+)})(\tilde{\mathbf{r}}\cdot\tilde{\mathbf{e}}^{(+)*})(1-2u)\int_0^u dv\,(\phi_\parallel(v)-g_\perp^{(v)}(v))$$
$$+[(\tilde{\mathbf{P}}\cdot\tilde{\mathbf{e}}^{(+)*})(\tilde{\mathbf{r}}\cdot\tilde{\mathbf{e}}^{(+)})-(\tilde{\mathbf{P}}\cdot\tilde{\mathbf{r}})]\frac{g_\perp^{(a)}(v)}{4}\Bigg] \tag{2.181}$$

and

$$V^{(-)}_{even}(\mathbf{k},\mathbf{q}_1,\mathbf{q}_2;\tilde{\mathbf{r}},u) \equiv \sum_{t\in even} \frac{1}{4} Tr[\Gamma_t \hat{Q}]\psi^{(-)}_{\Gamma^t}(u,\tilde{\mathbf{r}}) = ee_q \frac{g^2\delta_{ab}}{2N}\frac{-if_V m_V}{4}$$
$$\times\Bigg[(\tilde{\mathbf{P}}\cdot\tilde{\mathbf{e}}^{(+)})(\tilde{\mathbf{r}}\cdot\tilde{\mathbf{e}}^{(-)*})(1-2u)\int_0^u dv\,(\phi_\parallel(v)-g_\perp^{(v)}(v))$$
$$+(\tilde{\mathbf{P}}\cdot\tilde{\mathbf{e}}^{(-)*})(\tilde{\mathbf{r}}\cdot\tilde{\mathbf{e}}^{(+)})\frac{g_\perp^{(a)}(v)}{4}\Bigg] \tag{2.182}$$

where things simplify a little in the $T=-$ case, since $\tilde{\mathbf{e}}^{(-)*}\cdot\tilde{\mathbf{e}}^{(+)}=0$.

Odd

Here we divide by two in the sum to account for double counting of independent matrices (see section 2.1.3) giving,

$$V^{(0)}_{odd}(\mathbf{k},\mathbf{q}_1,\mathbf{q}_2;\tilde{\mathbf{r}},u) \equiv \frac{1}{2}\sum_{t\in odd} \frac{1}{4} Tr[\Gamma_t \hat{Q}]\psi^{(0)}_{\Gamma^t}(u,\tilde{\mathbf{r}}) = ee_q \frac{g^2\delta_{ab}}{2N}(-i)m\,\tilde{R}\,m_V\frac{f_V^T}{4}(\tilde{\mathbf{r}}\cdot\tilde{\mathbf{e}}^{(+)})$$
$$\times\int_o^u dv\,(h_\parallel^{(t)}(v)-\phi_\perp(v)), \tag{2.183}$$

$$V^{(+)}_{odd}(\mathbf{k},\mathbf{q}_1,\mathbf{q}_2;\tilde{\mathbf{r}},u) \equiv \frac{1}{2}\sum_{t\in odd} \frac{1}{4} Tr[\Gamma_t \hat{Q}]\psi^{(+)}_{\Gamma^t}(u,\tilde{\mathbf{r}}) = ee_q \frac{g^2\delta_{ab}}{2N}\,m\,\tilde{R}\,\frac{f_V^T}{4}\phi_\perp(u)$$
$$-ee_q\frac{g^2\delta_{ab}}{2N}|\tilde{\mathbf{r}}\cdot\tilde{\mathbf{e}}^{(+)}|^2\,m\,\tilde{R}\,\frac{f_V^T}{4}m_V^2\int_0^u dv\int_0^v d\eta\left(h_\parallel^{(t)}(\eta)-\frac{1}{2}\phi_\perp(\eta)-\frac{1}{2}h_3(\eta)\right)$$
$$=-ee_q\frac{g^2\delta_{ab}}{2N}\,m\,\tilde{R}\,\frac{f_V^T}{4}\phi_\perp(u)\left(1+O(|\tilde{\mathbf{r}}|^2)\right)\simeq ee_q\frac{g^2\delta_{ab}}{2N}\,m\,\tilde{R}\,\frac{f_V^T}{4}\phi_\perp(u) \tag{2.184}$$

and

$$V^{(-)}_{odd}(\mathbf{k},\mathbf{q}_1,\mathbf{q}_2;\tilde{\mathbf{r}},u) \equiv \frac{1}{2}\sum_{t\in odd} \frac{1}{4} Tr[\Gamma_t \hat{Q}]\psi^{(-)}_{\Gamma^t}(u,\tilde{\mathbf{r}}) = -ee_q \frac{g^2\delta_{ab}}{2N}(\tilde{\mathbf{r}}\cdot\tilde{\mathbf{e}}^{(+)})(\tilde{\mathbf{r}}\cdot\tilde{\mathbf{e}}^{(-)*})$$
$$\times m\,\tilde{R}\,\frac{f_V^T}{4}m_V^2\int_0^u dv\int_0^v d\eta\left(h_\parallel^{(t)}(\eta)-\frac{1}{2}\phi_\perp(\eta)-\frac{1}{2}h_3(\eta)\right). \tag{2.185}$$

2.4 Vector meson photoproduction: the story so far

We have all the ingredients to write down the amplitude for vector meson photoproduction via two gluon exchange. Recall the results of Fierz factorising, (2.33), high energy factorisation, (2.98), and the results for the particular impact factors (2.102, 2.133). We find that we can write,

$$\begin{aligned}\mathcal{M}_{+\lambda}(\gamma q \to Vq) &= 2\int \frac{1}{4} Tr[\mathcal{A}(u,\tilde{\mathbf{r}})\Gamma_t]\Psi^{(\lambda)}_{\Gamma^t}(u,\tilde{\mathbf{r}})]d^2\tilde{\mathbf{r}}du \\ &= is\int \frac{\phi_{qq}(-\mathbf{k},-\mathbf{q})\phi^{+\lambda}_{\gamma V}(\mathbf{k},\mathbf{q}_1,\mathbf{q}_2)}{\mathbf{k}^2(\mathbf{k}-\mathbf{q})^2}\frac{d^2\mathbf{k}}{(2\pi)^2} \end{aligned}\tag{2.186}$$

with the definition (2.35),

$$\mathcal{A}_{\alpha\beta}(u,\tilde{\mathbf{r}}) = \int \mathcal{A}_{\alpha\beta}(l,p-l)\, e^{-i\tilde{\mathbf{l}}\tilde{\mathbf{r}}}\frac{d^2\tilde{\mathbf{l}}}{(2\pi)^2}. \tag{2.187}$$

Therefore we can write

$$\begin{aligned}\mathcal{A}_{\alpha\beta}(u,\tilde{\mathbf{r}}) &= is\int \frac{\phi_{qq}(-\mathbf{k},-\mathbf{q})\hat{Q}^{\gamma q'\bar{q}'}(\mathbf{k},\mathbf{q}_1,\mathbf{q}_2)}{\mathbf{k}^2(\mathbf{k}-\mathbf{q})^2}\frac{d^2\mathbf{k}}{(2\pi)^2}\, e^{-i\tilde{\mathbf{l}}\tilde{\mathbf{r}}}\frac{d^2\tilde{\mathbf{l}}}{(2\pi)^2} \\ &= is\int \frac{\phi_{qq}(-\mathbf{k},-\mathbf{q})}{\mathbf{k}^2(\mathbf{k}-\mathbf{q})^2}\frac{d^2\mathbf{k}}{(2\pi)^2}\int \hat{Q}^{\gamma q'\bar{q}'}(\mathbf{k},\mathbf{q}_1,\mathbf{q}_2)\, e^{-i\tilde{\mathbf{l}}\tilde{\mathbf{r}}}\frac{d^2\tilde{\mathbf{l}}}{(2\pi)^2} \\ &= is\int \frac{\phi_{qq}(-\mathbf{k},-\mathbf{q})\hat{Q}^{\gamma q'\bar{q}'}(u,\mathbf{k},\tilde{\mathbf{r}})}{\mathbf{k}^2(\mathbf{k}-\mathbf{q})^2}\frac{d^2\mathbf{k}}{(2\pi)^2},\end{aligned}\tag{2.188}$$

with the definition

$$\hat{Q}^{\gamma q'\bar{q}'}(u,\mathbf{k},\tilde{\mathbf{r}}) \equiv \int \hat{Q}^{\gamma q'\bar{q}'}(\mathbf{k},\mathbf{q}_1,\mathbf{q}_2)\, e^{-i\tilde{\mathbf{l}}\tilde{\mathbf{r}}}\frac{d^2\tilde{\mathbf{l}}}{(2\pi)^2}, \tag{2.189}$$

where $\mathbf{q}_1$ and $\mathbf{q}_2$ are implicitly functions of $\tilde{\mathbf{l}}$. This gives us the γV impact factor as

$$\begin{aligned}\phi^{+\lambda}_{\gamma V}(\mathbf{k},\mathbf{q}) &\equiv \phi^{\gamma(+)V(\lambda)}_{even}(\mathbf{k},\mathbf{q}) + \phi^{\gamma(+)V(\lambda)}_{odd}(\mathbf{k},\mathbf{q}) \\ &= 2\int \frac{1}{4}Tr[\hat{Q}_{\gamma q'\bar{q}'}(u,\mathbf{k},\tilde{\mathbf{r}}))\Gamma_t]Tr[\Gamma^t\Psi^\lambda(u,\tilde{\mathbf{r}})]d^2\tilde{\mathbf{r}}du \\ &= 2\int d^2\tilde{\mathbf{r}}du\left(\int [V^\lambda_{even}(\mathbf{k},\mathbf{q}_1,\mathbf{q}_2;\tilde{\mathbf{r}},u) + V^\lambda_{odd}(\mathbf{k},\mathbf{q}_1,\mathbf{q}_2;\tilde{\mathbf{r}},u)]e^{-i\tilde{\mathbf{l}}\tilde{\mathbf{r}}}\frac{d^2\tilde{\mathbf{l}}}{(2\pi)^2}\right) \\ &\equiv 2\int d^2\mathbf{r}du[\hat{V}^\lambda_{even}(\mathbf{k},\tilde{\mathbf{r}},u) + \hat{V}^\lambda_{odd}(\mathbf{k},\tilde{\mathbf{r}},u)],\end{aligned}\tag{2.190}$$

where we take the last line as a definition. We have arrived at an explicit formula for the γV impact factor, which is expressed in terms of quantities we have previously obtained. We now catalogue the zoo of these. There are 2 (odd or even) times 3 (physical polarisation states) = 6 such impact factors, and three distinct amplitudes corresponding to those polarisation states. Note first that there is no dependence on the variable l outside the $\tilde{\mathbf{P}}$ and $\tilde{R}$ functions. We define their Fourier transforms

$$\tilde{\mathbf{P}}(\tilde{\mathbf{r}}, u) = \int \frac{d^2\mathbf{l}}{(2\pi)^2} e^{-i\tilde{\mathbf{l}}\tilde{\mathbf{r}}} \tilde{\mathbf{P}}(\mathbf{q}_1, \mathbf{q}_2) \tag{2.191}$$

and

$$\tilde{R}(\tilde{\mathbf{r}}, u) = \int \frac{d^2\tilde{\mathbf{l}}}{(2\pi)^2} e^{-i\tilde{\mathbf{l}}\tilde{\mathbf{r}}} \tilde{R}(\mathbf{q}_2, \mathbf{q}_2). \tag{2.192}$$

The catalogue of impact factors is then:

$$\phi_{even}^{\gamma(+)V(0)}(\mathbf{k}, \mathbf{q}) = ee_q \frac{g^2\delta_{ab}}{2N} \frac{f_V}{2} \int d^2\tilde{\mathbf{r}} du\, (1-2u)(\tilde{\mathbf{P}}(\tilde{\mathbf{r}}, u) \cdot \tilde{\mathbf{e}}^{(+)})\, \phi_{||}(u), \tag{2.193}$$

$$\begin{aligned}\phi_{even}^{\gamma(+)V(+)}(\mathbf{k}, \mathbf{q}) &= -iee_q \frac{g^2\delta_{ab}}{2N} \frac{f_V m_V}{2} \int d^2\tilde{\mathbf{r}} du \\ &\times \Bigg[(\tilde{\mathbf{P}}(\tilde{\mathbf{r}}, u) \cdot \tilde{\mathbf{e}}^{(+)})(\tilde{\mathbf{r}} \cdot \tilde{\mathbf{e}}^{(+)*})(1-2u) \int_0^u dv\, (\phi_{||}(v) - g_\perp^{(v)}(v)) \\ &\quad + [\, (\tilde{\mathbf{P}}(\tilde{\mathbf{r}}, u) \cdot \tilde{\mathbf{e}}^{(+)*})(\tilde{\mathbf{r}} \cdot \tilde{\mathbf{e}}^{(+)}) - (\tilde{\mathbf{P}}(\tilde{\mathbf{r}}, u) \cdot \tilde{\mathbf{r}})\,]\, \frac{g_\perp^{(a)}(v)}{4} \Bigg],\end{aligned} \tag{2.194}$$

$$\begin{aligned}\phi_{even}^{\gamma(+)V(-)}(\mathbf{k}, \mathbf{q}) &= -iee_q \frac{g^2\delta_{ab}}{2N} \frac{f_V m_V}{2} \int d^2\tilde{\mathbf{r}} du \\ &\times \Bigg[(\tilde{\mathbf{P}}(\tilde{\mathbf{r}}, u) \cdot \tilde{\mathbf{e}}^{(+)})(\tilde{\mathbf{r}} \cdot \tilde{\mathbf{e}}^{(-)*})(1-2u) \int_0^u dv\, (\phi_{||}(v) - g_\perp^{(v)}(v)) \\ &\quad + (\tilde{\mathbf{P}}(\tilde{\mathbf{r}}, u) \cdot \tilde{\mathbf{e}}^{(-)*})(\tilde{\mathbf{r}} \cdot \tilde{\mathbf{e}}^{(+)})\, \frac{g_\perp^{(a)}(v)}{4} \Bigg],\end{aligned} \tag{2.195}$$

$$\phi_{odd}^{\gamma(+)V(0)}(\mathbf{k},\mathbf{q}) = -iee_q \frac{g^2\delta_{ab}}{2N} m\, m_V \frac{f_V^T}{2} \int d^2\tilde{\mathbf{r}}(\tilde{\mathbf{r}}\cdot\tilde{\mathbf{e}}^{(+)})$$
$$\times \int du\, \tilde{R}(\tilde{\mathbf{r}},u) \int_0^u dv\, (h_{\|}^{(t)}(v) - \phi_\perp(v)), \tag{2.196}$$

$$\phi_{odd}^{\gamma(+)V(+)}(\mathbf{k},\mathbf{q}) = ee_q \frac{g^2\delta_{ab}}{2N}\, m\, \frac{f_V^T}{2} \int d^2\tilde{\mathbf{r}} du\, \tilde{R}(\tilde{\mathbf{r}},u)\, \phi_\perp(u), \tag{2.197}$$

and

$$\phi_{odd}^{\gamma(+)V(-)}(\mathbf{k},\mathbf{q}) = -ee_q \frac{g^2\delta_{ab}}{2N}\, m\, m_V^2 \frac{f_V^T}{2} \int d^2\tilde{\mathbf{r}}(\tilde{\mathbf{r}}\cdot\tilde{\mathbf{e}}^{(+)})(\tilde{\mathbf{r}}\cdot\tilde{\mathbf{e}}^{(-)*})$$
$$\times \int du\, \tilde{R}(\tilde{\mathbf{r}},u) \int_0^u dv \int_0^v d\eta \left(h_{\|}^{(t)}(\eta) - \frac{1}{2}\phi_\perp(\eta) - \frac{1}{2}h_3(\eta) \right). \tag{2.198}$$

2.5 Summary

In section 2.1 we showed that the amplitude can, in the diffractive limit, be factorised into a convolution of two separate and unentangled quantities. One is the hard subprocess $\gamma q \to q'\bar{q}'q$ and the other is the soft transition $q'\bar{q}' \to V$. In section 2.2 we started by considering $qq \to qq$ scattering. We derived high energy factorisation, the impact factor representation and subsequently the $q \to q$ and $\gamma \to q'\bar{q}'$ impact factors. In section 2.3 we introduce the light-cone matrix elements, identifying these with the soft transition, and simplified these in the appropriate approximations. In section 2.4 we put all this together to arrive at the impact factor for $\gamma \to V$. We find six distinct contributions corresponding to chiral odd and chiral even contributions of the three possible meson polarisations.

The impact factors listed in section 2.4 combined with equation (2.186) give us the two-gluon exchange helicity amplitudes. We do not write their explicit expression here (they appear later in section 4.1.4). These amplitudes were all explicitly or implicitly first derived in [25]. We could now proceed to investigate the phenomenology of two-gluon exchange by confronting the helicity amplitudes with data. We choose to postpone this, however, until we have extended the calculation to higher orders.

Chapter 3

BFKL calculation 1: heavy and collinear quarks

In the previous chapter we derived the scattering amplitude for two gluon colour singlet exchange. In this and the subsequent chapter we shall extend our calculation to higher orders. We can do this since we have already derived the $\gamma \to V$ impact factor. The difficulty is in analytic manipulation of our higher order formulae. We apply the solution to the BFKL equation for non-zero momentum exchange. This is the sum of leading log contributions in s to all orders in α_s, as discussed in Chapter 1, section 1.4. In this chapter we make two approximations that make analytic calculation easier. Firstly, we assume that the quark/anti-quark pair exiting the hard sub-process are collinear. To subsequently make a transition to a vector meson this must be approximately true and therefore is potentially a fair approximation. Secondly, we shall make a non-relativistic assumption with regard to the meson in its rest frame. We shall assume that the quarks have no relative motion. The rest-mass of each quark is therefore half the rest-mass of the meson. This should be a good approximation for heavy mesons where it is true that $m_q \sim m_V/2$. The outline of the chapter is:

- Section 3.1. We apply the collinear approximation to the impact factors. We use this to explicitly write down the two-gluon exchange helicity amplitudes in this approximation.

- Section 3.2. We extend the calculation of the helicity amplitudes in the collinear approximation to higher orders by using the solution to the BFKL equation. We check that our result reproduces the two-gluon exchange prediction in the appropriate limit.

- Section 3.3. We summarise our results.

3.1 Two gluon exchange

3.1.1 Collinear quark and anti-quark

When we derived the impact factor for the $\gamma q \to q'\bar{q}'q$, we made no explicit mention of the form of $\mathbf{q}_1$ and $\mathbf{q}_2$, the momenta of the quark and anti-quark. These momenta will only depend on $\tilde{\mathbf{l}}$, $\mathbf{q}$ and u. In section 2.1.2 we defined $\tilde{\mathbf{l}}$ as the transverse momentum of the quark with respect to the meson momentum, p; by definition then this transverse vector is zero in the collinear approximation. $\mathbf{q}_1$ and $\mathbf{q}_2$, however, are defined as transverse to the initial photon direction. First we will impose collinearity, that is put $\tilde{\mathbf{l}} = 0$. We shall work in canonical space-time coordinates here to aid intuition. In the frame where the photon-proton define the z-axis, to our level of approximation, $q_{1z} = \epsilon_1$, where ϵ_1 is the quark energy. So, the 4-momenta of the quark and anti-quark produced by the hard scatter in the lab-frame can be approximated as,

$$q_1 = (\epsilon_1, \mathbf{q}_1, \epsilon_1) \;\text{ and }\; q_2 = (\epsilon_2, \mathbf{q}_2, \epsilon_2), \tag{3.1}$$

where $\mathbf{q} = \mathbf{q}_1 + \mathbf{q}_2$, $\epsilon_1 + \epsilon_2 = E$ and E is their combined energy. If we assume the quark and anti-quark are collinear we can relate their 3-momenta,

$$\frac{\mathbf{q}_1}{|\mathbf{q}_1|} = \frac{\mathbf{q}_2}{|\mathbf{q}_2|} \quad \to \quad \frac{\mathbf{q}_1}{\epsilon_1} = \frac{\mathbf{q}_2}{\epsilon_2}, \tag{3.2}$$

which in turn implies,

$$\mathbf{q}_1 = \mathbf{q}\frac{\epsilon_1}{\epsilon_1 + \epsilon_2} = \frac{\epsilon_1}{E}\mathbf{q} \sim \frac{\tilde{l}_+}{\tilde{p}_+}\mathbf{q} = u\mathbf{q}. \tag{3.3}$$

Therefore,

$$\mathbf{q}_1 = u\mathbf{q} \tag{3.4}$$

$$\mathbf{q}_2 = (1-u)\mathbf{q} = \bar{u}\mathbf{q}. \tag{3.5}$$

Then in the collinear approximation $\mathbf{q}_1$ and $\mathbf{q}_2$ are only functions of $\mathbf{q}$ and u.

3.1.2 The $\tilde{\mathbf{P}}(\tilde{\mathbf{r}}, u)$ and $\tilde{R}(\tilde{\mathbf{r}}, u)$ functions

We remind ourselves that the impact factors depend on either the quantity,

$$\tilde{\mathbf{P}}(\tilde{\mathbf{r}}, u) = \int \frac{d^2\tilde{\mathbf{l}}}{(2\pi)^2} e^{-i\tilde{\mathbf{l}}\tilde{\mathbf{r}}} \tilde{\mathbf{P}}(\tilde{\mathbf{l}}, u) \tag{3.6}$$

or the quantity,

$$\tilde{R}(\tilde{\mathbf{r}}, u) = \int \frac{d^2\tilde{\mathbf{l}}}{(2\pi)^2} e^{-i\tilde{\mathbf{l}}\tilde{\mathbf{r}}} \tilde{R}(\tilde{\mathbf{l}}, u). \tag{3.7}$$

In the collinear approximation we obtain,

$$\tilde{\mathbf{P}}(\tilde{\mathbf{r}}, u) = \int \frac{d^2\tilde{\mathbf{l}}}{(2\pi)^2} e^{-i\tilde{\mathbf{l}}\tilde{\mathbf{r}}} \tilde{\mathbf{P}}(\mathbf{0}, u) = \delta^{(2)}(\tilde{\mathbf{r}}) \tilde{\mathbf{P}}(\tilde{\mathbf{l}} = \mathbf{0}, u) \tag{3.8}$$

and

$$\tilde{R}(\tilde{\mathbf{r}}, u) = \int \frac{d^2\tilde{\mathbf{l}}}{(2\pi)^2} e^{-i\tilde{\mathbf{l}}\tilde{\mathbf{r}}} \tilde{R}(\mathbf{0}, u) = \delta^{(2)}(\tilde{\mathbf{r}}) \tilde{R}(\tilde{\mathbf{l}} = \mathbf{0}, u). \tag{3.9}$$

3.1.3 The impact factors

The catalogue (2.193-2.198) now becomes (where we drop the unnecessary tilde from the polarisation vector)

$$\begin{aligned}\phi_{even}^{\gamma(+)V(0)}(\mathbf{k},\mathbf{q}) &= ee_q \frac{g^2\delta_{ab}}{2N}\frac{f_\rho}{2}\int du(1-2u)(\tilde{\mathbf{P}}(\tilde{\mathbf{l}}=\mathbf{0},u)\cdot\mathbf{e}^{(+)})\phi_{\parallel}(u) \\ &= ee_q \frac{g^2\delta_{ab}}{2N}\frac{f_\rho}{2}\int du\,(1-2u)\phi_{\parallel}(u) \\ &\times\left[\left(\frac{u\mathbf{q}}{u^2\mathbf{q}^2+m^2}+\frac{\mathbf{k}-u\mathbf{q}}{(\mathbf{k}-u\mathbf{q})^2+m^2}\right)-(u\to 1-u)\right]\cdot\mathbf{e}^{(+)}\end{aligned} \tag{3.10}$$

$$\phi_{even}^{\gamma(+)V(+)}(\mathbf{k},\mathbf{q}) = 0, \tag{3.11}$$

$$\phi_{even}^{\gamma(+)V(-)}(\mathbf{k},\mathbf{q}) = 0, \tag{3.12}$$

$$\phi_{odd}^{\gamma(+)V(0)}(\mathbf{k},\mathbf{q}) = 0, \tag{3.13}$$

$$\begin{aligned}\phi_{odd}^{\gamma(+)V(+)}(\mathbf{k},\mathbf{q}) &= ee_q \frac{g^2\delta_{ab}}{2N}\,m\,\frac{f_\rho^T}{2}\int du\,\tilde{R}(|\tilde{\mathbf{l}}|=0,u)\,\phi_\perp(u) \\ &= ee_q \frac{g^2\delta_{ab}}{2N}\,m\,\frac{f_\rho^T}{2}\int du\,\phi_\perp(u)\left[\left(\frac{1}{u^2\mathbf{q}^2+m^2}-\frac{1}{(\mathbf{k}-u\mathbf{q})^2+m^2}\right)+(u\to 1-u)\right]\end{aligned} \tag{3.14}$$

and

$$\phi_{odd}^{\gamma(+)V(-)}(\mathbf{k},\mathbf{q}) = 0. \tag{3.15}$$

3.1.4 The two-gluon exchange amplitudes

Our collinear impact factors give us the two gluon exchange amplitudes

$$
\begin{aligned}
\mathcal{M}_{+0}^{even\,2g} &= isee_q\alpha_s^2\frac{N^2-1}{N^2}\frac{f_\rho}{2}\int\frac{d^2\mathbf{k}}{\mathbf{k}^2(\mathbf{k}-\mathbf{q})^2}\,du\,(1-2u)\phi_\parallel(u) \\
&\times\left[\left(\frac{u\mathbf{q}}{u^2\mathbf{q}^2+m^2}+\frac{\mathbf{k}-u\mathbf{q}}{(\mathbf{k}-u\mathbf{q})^2+m^2}\right)-(u\to 1-u)\right]\cdot\mathbf{e}^{(+)}
\end{aligned}
\tag{3.16}
$$

and

$$
\begin{aligned}
\mathcal{M}_{++}^{odd\,2g} &= isee_q\alpha_s^2\frac{N^2-1}{N^2}\,m\,\frac{f_\rho^T}{2}\int\frac{d^2\mathbf{k}}{\mathbf{k}^2(\mathbf{k}-\mathbf{q})^2}\,du\,\phi_\perp(u) \\
&\times\left[\left(\frac{1}{u^2\mathbf{q}^2+m^2}-\frac{1}{(\mathbf{k}-u\mathbf{q})^2+m^2}\right)+(u\to 1-u)\right],
\end{aligned}
\tag{3.17}
$$

with all others zero.

If we identify the Brodsky-Lepage wave-functions[1] with those in equations (3.16) and (3.17) arising within the light-cone approach, we find the above amplitudes correspond exactly with those arrived at by Ginzburg, Panfil and Serbo outside the light-cone formalism [17]. They explicitly make the collinear approximation in their work. This approximation is an approximation of leading 'twist'. 'Twist' refers to suppression in powers of $|\mathbf{q}|$, higher twist being more highly suppressed. It is also worth noting that since the light-cone matrix elements that survive have no $\tilde{\mathbf{r}}$ dependence (the ones that do being higher twist), the collinear approximation is automatically enforced by the $d^2\tilde{\mathbf{l}}$ integration. The collinear approximation therefore consists *not* in imposing approximations on $\mathcal{M}_{+0}^{even}$ and $\mathcal{M}_{++}^{odd}$, but in *throwing away* the other helicity amplitudes.

[1]For a review of which see [36]

3.1.5 The heavy meson approximation

The heavy meson approximation consists of imposing $m_q = m_V/2$, requiring zero relative momentum of the quark and anti-quark in the meson rest-frame. The distribution amplitudes must therefore be a δ-functions. The correct normalisation requires

$$\phi_\perp(u) = \phi_{||}(u) = \delta(u - 1/2). \tag{3.18}$$

This choice of distribution amplitude gives us,

$$\phi^{\gamma(+)V(0)}_{even\,\delta} = 0 \tag{3.19}$$

and

$$\begin{aligned}\phi^{\gamma(+)V(+)}_{odd\,\delta} &= ee_q g^2 \frac{\delta_{ab}}{2N}\frac{f_V^T}{2}\frac{m_V}{2}\,\tilde{R}(\tilde{\mathbf{l}} = \mathbf{0}, u = 1/2)\\ &= ee_q g^2 \frac{\delta_{ab}}{2N}\frac{f_V^T}{2} m_V \left(\frac{1}{\mathbf{q}^2/4 + M_V^2/4} - \frac{1}{(\mathbf{k}-\mathbf{q}/2)^2 + M_V^2/4}\right),\end{aligned} \tag{3.20}$$

which in turn gives us the amplitude,

$$\begin{aligned}\mathcal{M}^{odd\,2g\,\delta}_{++} &= isee_q\alpha_s^2\frac{N^2-1}{N^2}\, m_V\, \frac{f_\rho^T}{2}\int \frac{d^2\mathbf{k}}{\mathbf{k}^2(\mathbf{k}-\mathbf{q})^2}\\ &\quad\times\left(\frac{1}{\mathbf{q}^2/4 + m_V^2/4} - \frac{1}{(\mathbf{k}-\mathbf{q}/4)^2 + m_V^2/4}\right).\end{aligned} \tag{3.21}$$

This formula is exactly that appearing in [19]. We observe that only the chiral odd configuration of spins survives and that the helicity of the photon is conserved: a (+) polarised photon becomes a (+) polarised meson.

3.2 Beyond two-gluon exchange

Now we shall use the BFKL summation of the leading s component to all orders in α_s. Note that from here on we shall often represent two-dimensional vectors by complex numbers; thus $\mathbf{k} \to k$. This proves beneficial analytically.

3.2.1 The BFKL solution

We know the impact factors for $\gamma \to V$. We are therefore able to generalise straight away to the BFKL leading log summation [14], using the results of Lipatov quoted in Chapter 1. Results ((1.45), (1.53-1.55)) give us

$$\mathcal{M}_{AB}^{BFKL}(z,q) = \frac{is}{(2\pi)^4} \sum_{n=-\infty}^{n=\infty} \int_{-\infty}^{\infty} d\nu \, \frac{\nu^2 + n^2/4}{[\nu^2 + (n-1)^2/4][\nu^2 + (n+1)^2/4]} \times \exp[\chi_n(\nu) z] \; I_{n,\nu}^A(q) \, (I_{n,\nu}^B(q))^* \tag{3.22}$$

where

$$\chi_n(\nu) = 4\mathcal{R}\mathrm{e} \Big(\psi(1) - \psi(1/2 + |n|/2 + i\nu) \Big) \tag{3.23}$$

is proportional to the eigenvalues of the BFKL kernel, and

$$I_{n,\nu}^A(q) = \int \frac{d^2k}{(2\pi)^2} \phi_A(k,q) \int d^2\rho_1 \, d^2\rho_2 \; E_{n,\nu}(\rho_1,\rho_2) \exp(ik\cdot\rho_1 + i(q-k)\cdot\rho_2), \tag{3.24}$$

with an analogous result for the index B. We shall refer to these $I_{n,\nu}$ factors as the projections of the impact factors. The eigenfunctions are given by

$$E_{n,\nu}(\rho_1,\rho_2) = \left(\frac{\rho_1-\rho_2}{\rho_1\rho_2}\right)^{-\tilde{\mu}+1/2} \left(\left(\frac{\rho_1-\rho_2}{\rho_1\rho_2}\right)^*\right)^{-\mu+1/2} \tag{3.25}$$

where $\mu = n/2 - i\nu$ and $\tilde{\mu} = -n/2 - i\nu$. Here k and q are transverse two dimensional momentum vectors, and ρ_1 and ρ_2 are position space vectors in the complex representation, $\rho_i = \rho_{i\,x} + i\rho_{i\,y}$. The variable z is a rapidity variable,

$$z = \frac{3\alpha_s}{2\pi} \ln\left(\frac{s}{\Lambda^2}\right), \tag{3.26}$$

where s is the parton level centre-of-mass energy and Λ^2 is not prescribed in the leading log approximation but must depend on the scales in the problem. For the photoproduction of collinear quarks the only two relevant scales are m_V and q. The functions $\phi_A = \phi^{\gamma(\lambda)V(\lambda')}$ and $\phi_B = \phi_{qq}$ are the impact factors.

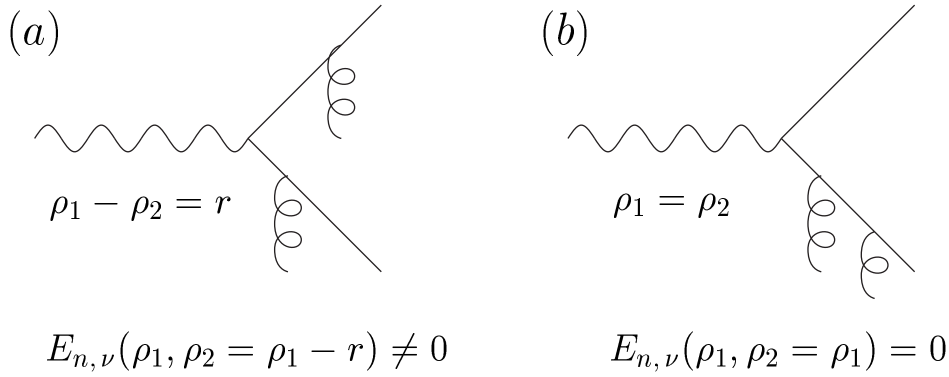

Figure 3.1: The types of diagram that contribute to the colour dipole impact factor: (a) the pomeron couples to two separate partons ($2p$); (b) the pomeron couples to one parton ($1p$). The BFKL eigenfunction takes on a non-zero value for diagrams of type (a), but is forced to zero for type (b).

3.2.2 The projection of the $q \to q$ impact factor

The BFKL eigenfunction of equation (3.25) is only appropriate for a colourless particle. This is fine for the coupling of the pomeron to a colour dipole such a meson, but for our calculation we also need to consider the case of scattering from a coloured object; a quark. The variables ρ_1 and ρ_2 are impact parameter vectors conjugate to the gluon momenta, and the quantity $\rho_1 - \rho_2$ relates to the transverse size of the object being probed by the pomeron. For a point-like object, like a quark, this will be zero and the eigenfunction (3.25) gives no contribution. This is also true for diagrams where the pomeron couples to a single parton within a colourless object (see figure 3.1). So what eigenfunction is appropriate for a coloured particle?

Let us first consider how the pomeron couples to a dipole. We make a clear distinction here. We define the size of the object probed by the pomeron to be of size $\rho \equiv \rho_1 - \rho_2$. The transverse size of the colourless object, however, corresponds to the vector $\mathbf{r}$, as discussed in Chapter 2[2]. We have, approximately[3], $|\mathbf{r}| \sim max\{\frac{1}{u|\mathbf{q}|}, \frac{1}{\bar{u}|\mathbf{q}|}\}$.

[2]Note that to leading logs the transverse size of a dipole with respect to its centre-of-mass direction is the same as its size defined transverse to the initial state particle momenta.

[3]We refer ahead to Chapter 4 and the expression (4.12). Under the assumption that the quark mass is not much larger than $u(1-u)|\mathbf{q}|$, then this object ensures that the major contributions arise from where $u\mathbf{q} \cdot \mathbf{r} \sim 1$ and $\bar{u}\mathbf{q} \cdot \mathbf{r} \sim 1$.

If we have a perturbative colourless object, *e.g.* from $\gamma \to q\bar{q}$, we expect it to be neither point-like nor very large, and the pomeron to couple to the 'whole thing' and therefore $|\mathbf{r}| \sim \frac{1}{|\mathbf{q}|}$. But we must ask ourselves what happens as $u(1-u) \to 0$? We would expect the amplitude to be dominated by the large $|\mathbf{r}|$ region. Consider what happens in this limit,

$$\begin{aligned} E_{n,\nu}(\rho_1,\rho_2) &\sim E_{n,\nu}(\rho_1 \to \infty, \rho_2) + E_{n,\nu}(\rho_1, \rho_2 \to \infty) \\ &\to \left(\frac{1}{\rho_2}\right)^{-\widetilde{\mu}+1/2} \left(\left(\frac{1}{\rho_2}\right)^*\right)^{-\mu+1/2} + \left(\frac{-1}{\rho_1}\right)^{-\widetilde{\mu}+1/2} \left(\left(\frac{-1}{\rho_1}\right)^*\right)^{-\mu+1/2}. \end{aligned} \tag{3.27}$$

We find independence of the 'large' impact parameter. Consequently, under integration of the impact factors we get the δ-functions, either $\delta^{(2)}(\mathbf{k})$ or $\delta^{(2)}(\mathbf{q}-\mathbf{k})$. These δ-functions cannot arise in perturbation theory. The Feynman rules simply could not produce them. The properties of colourless impact factors ensure that the contributions from these are zero, however. This is manifest through the condition

$$\phi(\mathbf{k}=0,\mathbf{q}) = \phi(\mathbf{k}=\mathbf{q},\mathbf{q}) = 0. \tag{3.28}$$

This ensures a zero contribution from the δ-function pieces (in practise this occurs as a complete cancellation between diagrams). So the BFKL eigenfunction makes sense by itself for colourless objects. Note that we could, in principle, add an arbitrary amount of the asymptotic eigenfunction (3.27) to our original one and it would not affect our answer. In fact this is exactly what Lipatov did in obtaining his solution to the BFKL equation. He added δ-functions in momentum to restore conformal invariance and solve the equation [14]. This was fine for colourless particles, as we have observed, but the BFKL eigenfunction cannot be appropriate for coloured particles. Coloured impact factors do not, in general, obey condition (3.28) (see for example (2.102)). The δ-functions that Lipatov introduced affect the result in coloured scattering. The question of what eigenfunction is appropriate for a coloured particle can now be stated more precisely. What do we need to subtract from the BFKL eigenfunction to remove the spurious momentum δ-functions? The answer is the asymptotic eigenfunction. Let us subtract this asymptotic piece, then we get the object,

$$E_{n,\nu}^{MT}(\rho_1,\rho_2) = \left(\frac{\rho_1-\rho_2}{\rho_1\rho_2}\right)^{-\tilde{\mu}+1/2}\left(\left(\frac{\rho_1-\rho_2}{\rho_1\rho_2}\right)^*\right)^{-\mu+1/2}$$
$$-\left(\frac{1}{\rho_2}\right)^{-\tilde{\mu}+1/2}\left(\left(\frac{1}{\rho_2}\right)^*\right)^{-\mu+1/2} - \left(\frac{-1}{\rho_1}\right)^{-\tilde{\mu}+1/2}\left(\left(\frac{-1}{\rho_1}\right)^*.\right)^{-\mu+1/2}. \quad (3.29)$$

This has the desired cancellation in the limits $\rho_1 \to \infty$ or $\rho_2 \to \infty$ and is called the Mueller-Tang subtraction [37]. It is a generalised prescription. The properties of the eigenfunction pieces are such that the original BFKL piece, (3.25), generates no contributions when combined with a coloured impact factor and the subtracted pieces generate no contribution when combined with a colourless impact factor. This subtraction prescription is discussed at greater length in [38].

A consequence of the Mueller-Tang subtraction is interesting, from a physics perspective. Consider the scattering of a pomeron off a colour dipole. The non-zero contribution to the amplitude would come from the diagrams where gluons couple to both the quark and anti-quark, and consequently from the original BFKL eigenfunction (see figure 3.1 (a)). However, in the large $|\mathbf{r}|$ limit, we have to question whether we can legitimately call the colour dipole a colourless object, the quark and anti-quark are eventually separated by such a large distance that they cannot be resolved as such. In such a limit we might propose an alternative method of interaction, in which the pomeron sees only either the quark or anti-quark in isolation from its partner. Now only the diagrams where the pomeron couples to one or the other will contribute and therefore only the subtracted eigenfunctions (see figure 3.1 (b)). Let us split the impact factor into two pieces, one corresponding to single parton coupling and a second to where the pomeron couples to the whole dipole. We have

$$\phi(\mathbf{k},\mathbf{q}) = \phi_{2p}(\mathbf{k},\mathbf{q}) + \phi_{1p}(\mathbf{q}). \quad (3.30)$$

Note that the $1p$ part has no $\mathbf{k}$ dependence; this can be seen as a consequence of the eikonal approximation. The parts of the impact factor are related by,

$$\phi_{2p}(\mathbf{k}=\mathbf{q},\mathbf{q}) = \phi_{2p}(\mathbf{k}=\mathbf{0},\mathbf{q}) = -\phi_{1p}(\mathbf{q}). \quad (3.31)$$

Our two approaches to the dipole scattering are either to take the (3.25) eigenfunction in conjunction with the ϕ_{2p} piece, or the subtracted eigenfunction piece with the ϕ_{1p}

piece. The consequence of (3.31), the ensuing δ-functions and the minus sign of the Mueller-Tang subtraction, is that both contributions are asymptotically equal. In the limit $|\mathbf{r}| \to \infty$ (or equivalently $u \to 0$), the scattering of the dipole tends to the result that would be obtained by considering the process as the scattering of the pomeron off the coloured partonic content of the dipole. It seems that the colourless scattering is telling us what the coloured should be. The Mueller-Tang subtraction is suitable for scattering off a dipole, whether resolved as coloured or colourless.

We have only been talking about colour dipoles. The pomeron, however, in coloured coupling, only resolves a parton as a parton. It doesn't matter whether it's in a dipole or a proton, since for a pomeron probing a parton within 'the rest' we will have $|\mathbf{r}| \gg |\rho|$. This reinforces the argument that we have found the correct eigenfunction for the coupling of the BFKL pomeron to a general coloured object.

At last we can proceed and calculate the projection, (4.28), of the $q \to q$ impact factor for arbitrary conformal spin. The $n = 0$ calculation was first performed in [20] and generalised in [39].

$$\begin{aligned}
I^{qq}_{n,\nu}(q) &= \int \frac{d^2k}{(2\pi)^2}\phi_{qq}(k,q) \int d^2\rho_1\, d^2\rho_2\; E^{MT}_{n,\nu}(\rho_1,\rho_2)\exp(ik\cdot\rho_1 + i(q-k)\cdot\rho_2)\\
&= \frac{g^2\delta_{ab}}{2N}\int \frac{d^2k}{(2\pi)^2}\int d^2\rho_1\, d^2\rho_2\; E^{MT}_{n,\nu}(\rho_1,\rho_2)\exp(ik\cdot\rho_1 + i(q-k)\cdot\rho_2)\\
&= -\frac{g^2\delta_{ab}}{2N}\int d^2k \left(\delta^{(2)}(k)\int d^2\rho_2\, e^{i(q-k)\cdot\rho}\,\frac{1}{|\rho_2|^{1+2i\nu}}\left(\frac{\rho_2}{|\rho_2|}\right)^n\right.\\
&\qquad\left. +\delta^{(2)}(q-k)\int d^2\rho_1\, e^{ik\cdot\rho}\,\frac{1}{|\rho_1|^{1+2i\nu}}\left(\frac{-\rho_1}{|\rho_1|}\right)^n\right)\\
&= -\frac{g^2\delta_{ab}}{2N}\left(\int d^2\rho_2\, e^{iq\cdot\rho}\,\frac{1}{|\rho_2|^{1+2i\nu}}\left(\frac{\rho_2}{|\rho_2|}\right)^n + \int d^2\rho_1\, e^{iq\cdot\rho}\,\frac{1}{|\rho_1|^{1+2i\nu}}\left(\frac{-\rho_1}{|\rho_1|}\right)^n\right)\\
&= -\frac{g^2\delta_{ab}}{N}\,(1+(-1)^n)\int d^2\rho_2\, e^{iq\cdot\rho}\,\frac{1}{|\rho_2|^{1+2i\nu}}\left(\frac{\rho_2}{|\rho_2|}\right)^n. \qquad (3.32)
\end{aligned}$$

Using the integral definition of the Bessel function,

$$J_n(z) = \frac{1}{2\pi}\int_{-\pi}^{+\pi} d\theta\, e^{-ni\theta + iz\sin\theta}, \qquad (3.33)$$

the property,

$$J_{-n}(z) = (-1)^n\, J_n(z) \qquad (3.34)$$

and the result 6.561.14 from [5],

$$\int_0^\infty dx\, x^\mu J_\nu(ax) = 2^\mu a^{-\mu-1}\frac{\Gamma(\frac{1+\nu+\mu}{2})}{\Gamma(\frac{1+\nu-\mu}{2})}, \tag{3.35}$$

we arrive at

$$\boxed{I^{qq}_{n,\nu}(q) \;=\; -\frac{g^2\delta_{ab}}{2N}\frac{4\pi\, i^n}{|q|}\left(\frac{|q|^2}{4}\right)^{i\nu}\left(\frac{q^*}{q}\right)^{n/2}\frac{\Gamma(1/2+n/2-i\nu)}{\Gamma(1/2+n/2+i\nu)}} \tag{3.36}$$

for even n and $I^{qq}_{n,\nu} = 0$ for odd n.

3.2.3 The projection of the $\gamma \to V$ impact factor

In this subsection we compute the projection of the impact factor for the chiral odd contribution to $A = \gamma(+) \to V(+)$ transition for all conformal spins, n. The following integrals are to be evaluated

$$\begin{aligned} I^A_{n,\nu}(q) \;&=\; \int \frac{d^2k}{(2\pi)^2}\,\phi_A(k,q)\int d^2\rho_1\, d^2\rho_2\; E_{n,\nu}(\rho_1,\rho_2) \\ &\times \exp(ik^*\rho_1/2 + ik\rho_1^*/2 + i(q^*-k^*)\rho_2/2 + i(q-k)\rho_2^*/2). \end{aligned} \tag{3.37}$$

Changing variables to $\rho_1 = R + \rho/2$, $\rho_2 = R - \rho/2$ and integrating over d^2k we get

$$I^A_{n,\nu}(q) = \int d^2\rho\;\phi^q_A(\rho)\;\int d^2R\; E_{n,\nu}(R,\rho)e^{iq\cdot R}, \tag{3.38}$$

where $\phi^q_A(\rho)$ is the Fourier transform of the momentum space impact factor, $\phi_A(k,q)$ and

$$\phi^q_A(\rho) = \int \frac{d^2k}{(2\pi)^2}\phi_A(k,q)e^{i(k-q/2)\cdot\rho}. \tag{3.39}$$

The integration over R in (3.53) was first performed for $n=0$ by Forshaw and Sutton [40]. The generalisation to higher conformal spin was done in [41].

$$I^A_{n,\nu}(q) = \int d^2\rho\;\Phi^A_q(\rho)\;\hat{E}^q_{n,\nu}(\rho), \tag{3.40}$$

where the mixed representation eigenfunction $E^q_{n,\nu}(\rho)$ is given by

$$\begin{aligned} \hat{E}^q_{n,\nu}(\rho) \;&=\; \frac{(-1)^n}{2\pi^2}\,b_{n,\nu}\left(\frac{|q|}{8}\right)^{2i\nu}\left(\frac{q^*}{q}\right)^{n/2}\Gamma(1-i\nu-n/2)\Gamma(1-i\nu+n/2) \\ &\times\;\; |\rho|\,[J_\mu(q^*\rho/4)\;J_{\tilde\mu}(q\rho^*/4) - (-1)^n\;J_{-\mu}(q^*\rho/4)\;J_{-\tilde\mu}(q\rho^*/4)] \end{aligned} \tag{3.41}$$

and

$$b_{n,\nu} = \frac{2^{4i\nu}\pi^3}{|n/2| - i\nu} \frac{\Gamma(|n|/2 - i\nu + 1/2)\Gamma(|n|/2 + i\nu)}{\Gamma(|n|/2 + i\nu + 1/2)\Gamma(|n|/2 - i\nu)}. \tag{3.42}$$

The Fourier transform of the impact factor

The Fourier transform of the impact factor was performed in [19]. Standard integrals give us

$$\begin{aligned}
&\phi_{odd}^{\gamma(+)V(+)}(\rho) = \int \frac{d^2k}{(2\pi)^2} e^{(k-q/2)\cdot\rho} \phi_{odd}^{\gamma(+)V(+)}(k,q) \\
&= ee_q g^2 \frac{\delta_{ab}}{2N} f_V^T \frac{m_V}{2} \int \frac{d^2k}{(2\pi)^2} e^{(k-q/2)\cdot\rho} \left(\frac{1}{q^2/4 + M_V^2/4} - \frac{1}{(k-q/2)^2 + M_V^2/4} \right) \\
&= ee_q g^2 \frac{\delta_{ab}}{2N} \frac{f_V^T}{2} m_V \left[\frac{1}{q^2/4 + M_V^2/4} \delta^{(2)}(\rho) - \frac{1}{2\pi} K_0(m_v|\rho|/2) \right],
\end{aligned} \tag{3.43}$$

where K_0 is the McDonald function[4]. The properties of the eigenfunction (3.25) are such that the δ-function component does not contribute to the $I_{n,\nu}^{\gamma V}$ factor. Thus we arrive at

$$\begin{aligned}
&I_{n,\nu}^{\gamma(+)V(+)}(q) = -\frac{1}{2\pi} ee_q g^2 \frac{\delta_{ab}}{2N} \frac{f_V^T}{2} m_V \int d^2\rho \, \hat{E}_{n,\nu}^q(\rho) \, K_0(m_v\rho/2) \\
&= -ee_q g^2 \frac{\delta_{ab}}{2N} \frac{f_V^T}{2} m_V \frac{(-1)^n}{4\pi^3} \, b_{n,\nu} \left(\frac{|q|}{8} \right)^{2i\nu} \left(\frac{q^*}{q} \right)^{n/2} \Gamma(1 - i\nu - n/2)\Gamma(1 - i\nu + n/2) \\
&\int d^2\rho \, |\rho| \, K_0(m_v|\rho|/2) \, [J_\mu(q^*\rho/4) \; J_{\tilde{\mu}}(q\rho^*/4) - (-1)^n \; J_{-\mu}(q^*\rho/4) \; J_{-\tilde{\mu}}(q\rho^*/4)] \\
&= -ee_q g^2 \frac{\delta_{ab}}{2N} \frac{f_V^T}{2} m_V \frac{(-1)^n}{4\pi^3} \, b_{n,\nu} \left(\frac{|q|}{8} \right)^{2i\nu} \left(\frac{q^*}{q} \right)^{n/2} \\
&\times \Gamma(1 - i\nu - n/2)\Gamma(1 - i\nu + n/2) \, I_n(\nu, q),
\end{aligned} \tag{3.44}$$

where we define

$$\begin{aligned}
I_n(\nu, q) \quad &= \frac{m_V}{2} \int d^2\rho \; \rho^{1/2} \rho^{*\,1/2} \, K_0(m_V|\rho|/2) \\
&\times [J_\mu(q^*\rho/4) J_{\tilde{\mu}}(q\rho^*/4) - (-1)^n \; J_{-\mu}(q^*\rho/4) J_{-\tilde{\mu}}(q\rho^*/4)].
\end{aligned} \tag{3.45}$$

[4]Note that the δ-function piece comes from the diagrams where the pomeron couples to one parton. The other part where ρ, the size of the probed object, is not forced to be zero comes from diagrams where the pomeron couples to more than one particle.

Analytic manipulation and evaluation

To find the projection of the impact factor, we need to evaluate a double integral over $d^2\rho = |\rho|\, d|\rho|\, d\phi$. Such an integral is not straightforward. We shall exchange the complication of special functions for the complication of power series that we could hope to truncate at finite order. We represent the Bessel functions by their power series expansions $J_\sigma(z) = (z/2)^\sigma \sum_{k=0}^\infty (-1)^k\, (z/2)^{2k}/[\Gamma(k+1)\Gamma(\sigma+k+1)]$ and obtain

$$J_{n/2-i\nu}(q^*\rho/4)\, J_{-n/2-i\nu}(q\rho^*/4) \;-\; (-1)^n\, J_{-n/2+i\nu}(q^*\rho/4)\, J_{n/2+i\nu}(q\rho^*/4) \;= \\ \left[\sum_{k=0}^\infty \sum_{l=0}^\infty \frac{(-1)^{k+l}\,(|q||\rho|/8)^{2k+2l-2i\nu}\, \exp[i\phi(2l-2k+n)]}{\Gamma(k+1)\,\Gamma(l+1)\,\Gamma(1+l+n/2-i\nu)\,\Gamma(1+k-n/2-i\nu)}\right] - \Big[c.c.\Big]. \quad (3.46)$$

Both the ϕ and $|\rho|$ integrations in (3.45) are performed term by term in the sums (3.46). All the ϕ dependence of the integrand in (3.45) occurs in (3.46) where only integer powers of $\exp(i\phi)$ appear. Therefore, after the angular integration, only terms with $n - 2k + 2l = 0$ contribute, and one of the summations in equation (3.46) may be trivially performed giving

$$\int_0^{2\pi} d\phi \left[J_{n/2-i\nu}(q^*\rho/4)\, J_{-n/2-i\nu}(q\rho^*/4) \;-\; (-1)^n\, J_{-n/2+i\nu}(q^*\rho/4)\, J_{n/2+i\nu}(q\rho^*/4)\right] \\ = \left[\;2\pi \sum_{l=0}^\infty \frac{(-1)^{|n|/2}\,(|q||\rho|/8)^{4l+|n|-2i\nu}}{\Gamma(1+l)\,\Gamma(1+l+|n|/2)\,\Gamma(1+l-i\nu)\,\Gamma(1+l+|n|/2-i\nu)}\right] - \Big[c.c.\Big]. \quad (3.47)$$

Note that the odd n contributions are all zero; the $n-2k+2l = 0$ cannot be fulfilled. Using (3.47) and performing the remaining $|\rho|$ integration in equation (3.45), we have

$$\int_0^\infty d|\rho|\, |\rho|^2\, K_0(m_V|\rho|/2) \int_0^{2\pi} d\phi \\ \times\left[J_{n/2-i\nu}(q^*\rho/4)\, J_{-n/2-i\nu}(q\rho^*/4) \;-\; (-1)^n\, J_{-n/2+i\nu}(q^*\rho/4)\, J_{n/2+i\nu}(q\rho^*/4)\right] \\ = \left[\frac{4\pi}{(m_V/2)^3} \sum_{l=0}^\infty \frac{(-1)^{|n|/2}\,\Gamma^2(3/2-i\nu+2l+|n|/2)\,(|q|/2m_V)^{4l+|n|-2i\nu}}{\Gamma(1+l)\,\Gamma(1+l+|n|/2)\,\Gamma(1+l-i\nu)\,\Gamma(1+l+|n|/2-i\nu)}\right] - \Big[c.c.\Big]. \quad (3.48)$$

The obtained series is convergent for $|q|/2m_V < 1$ and the infinite sum gives the value of the integral. We need to continue analytically the result to $|q|/2m_V \geq 1$. Towards this end we represent this infinite sum of terms $\mathcal{A}(l)$ as an integral over complex l

using a Sommerfeld-Watson type transform. A contour $\mathcal{C}_1$ in the complex l plane is introduced enclosing the half-plane $\mathcal{R}e\,(l) > -1/2$ where $\mathcal{A}(l)$ has no poles. It is possible to construct a function $\mathcal{D}(l)$ with a pole structure and with residues such that the contour integral of $\mathcal{D}(l)\mathcal{A}(l)/(2\pi i)$ along $\mathcal{C}_1$, evaluated using the Cauchy theorem, reproduces the initial sum over the index l. It is easy to verify that

$$\mathcal{D}(l) \;=\; -\pi\frac{\sin\pi i\nu}{\sin\pi l\sin\pi(l-i\nu)} \;=\; \frac{\Gamma(l)\Gamma(1-l)\Gamma(l-i\nu)\Gamma(1-l+i\nu)}{\Gamma(i\nu)\Gamma(1-i\nu)} \tag{3.49}$$

has the desired properties. Thus one has

$$\begin{aligned}&\left[\frac{4\pi}{(m_V/2)^3}\sum_{l=0}^{\infty}\frac{(-1)^{|n|/2}\,\Gamma^2(3/2-i\nu+2l+|n|/2)\,(|q|/2m_V)^{4l+|n|-2i\nu}}{\Gamma(1+l)\,\Gamma(1+l+|n|/2)\,\Gamma(1+l-i\nu)\,\Gamma(1+l+|n|/2-i\nu)}\right]-\Big[c.c.\Big]\\ &=\frac{4\pi}{(m_V/2)^3}\oint_{\mathcal{C}_1}\frac{dl\,\mathcal{D}(l)}{2\pi i}\frac{(-1)^{|n|/2}\,(|q|/2m_V)^{4l+|n|-2i\nu}\,\Gamma^2(3/2-i\nu+2l+|n|/2)}{\Gamma(1+l)\,\Gamma(1+l+|n|/2)\,\Gamma(1+l-i\nu)\,\Gamma(1+l+|n|/2-i\nu)}.\end{aligned} \tag{3.50}$$

The contribution from the region of complex $l\to\infty$ vanishes in the limit, so the value of the contour integral is given by a line integral

$$\begin{aligned}&\left[\frac{4\pi}{(m_V/2)^3}\sum_{l=0}^{\infty}\frac{(-1)^{|n|/2}\,\Gamma^2(3/2-i\nu+2l+|n|/2)\,(|q|/2m_V)^{4l+|n|-2i\nu}}{\Gamma(1+l)\,\Gamma(1+l+|n|/2)\,\Gamma(1+l-i\nu)\,\Gamma(1+l+|n|/2-i\nu)}\right]-\Big[c.c.\Big]\\ &=-\frac{4\pi}{(m_V/2)^3}(-1)^{|n|/2}\int_{-1/2-i\infty}^{-1/2+i\infty}\frac{dl}{2\pi i}\,(|q|/2m_V)^{4l+|n|-2i\nu}\\ &\times\frac{\Gamma(l-i\nu)\,\Gamma(1-l+i\nu)}{\Gamma(i\nu)\,\Gamma(1-i\nu)}\;\frac{\Gamma(l)\,\Gamma(1-l)}{\Gamma(1+l)\,\Gamma(1+l-i\nu)}\;\frac{\Gamma^2(3/2+2l+|n|/2-i\nu)}{\Gamma(1+l+|n|/2)\,\Gamma(1+l+|n|/2-i\nu)}.\end{aligned} \tag{3.51}$$

This form is suggestive of the $n=0$ result of [20]. Substituting $s=2l+1-i\nu$, $\tau=q^2/m_V^2$ and using the Euler Γ-function relations such as the doubling formula $2^{2z-1}\Gamma(z)\Gamma(z+1/2)=\sqrt{\pi}\,\Gamma(2z)$ allows simplification of the integrand. Inserting (3.51) into (3.45) and using the identity $(-1)^{|n|/2}\frac{\Gamma(i\nu+|n|/2)\,\Gamma(1-i\nu-|n|/2)}{\Gamma(i\nu)\,\Gamma(1-i\nu)}=1$ for even n, we obtain the final answer,

$$\begin{aligned}I_{n,\nu}^{\gamma(\lambda)V(\lambda)}(q) = ee_qg^2\frac{\delta_{ab}}{2N}\frac{f_V^T}{2}m_V\frac{16\pi^2}{|q|^3}\left(\frac{|q|^2}{4}\right)^{i\nu}\left(\frac{q^*}{q}\right)^{n/2}\left(\frac{1}{4}\right)^{|n|/2}\frac{\Gamma(1/2-i\nu+|n|/2)}{\Gamma(1/2+i\nu+|n|/2)}\\ \times\int_{-i\infty}^{i\infty}\frac{ds}{2\pi i}\,\tau^{1/2+s+|n|/2}\,\frac{\Gamma(1-s-i\nu)\,\Gamma(1-s+i\nu)}{\Gamma(1-s/2-i\nu/2)\,\Gamma(1-s/2+i\nu/2)}\\ \times\frac{\Gamma^2(1/2+s+|n|/2)}{\Gamma(1/2+s/2-i\nu/2+|n|/2)\,\Gamma(1/2+s/2+i\nu/2+|n|/2)}\end{aligned} \tag{3.52}$$

for even n and $I_{n,\nu}^{\gamma(\lambda)V(\lambda)} = 0$ for odd n. This agrees with the corresponding expression of Bartels *et al.* for $n = 0$ [20]. The r.h.s. of equation (3.52) is the desired analytic continuation of the sum of the infinite power series (c.f. (3.48)) which holds for all values of τ.

3.2.4 Result: the BFKL amplitude

Introducing the notation $m = n/2$, and using the result for $I_{n,\nu}^{qq}$, we arrive at the amplitude

$$
\begin{aligned}
\mathcal{M}_{++}^{odd\,\delta} &= is\frac{8\pi}{t^2}\frac{N^2-1}{N^2}\,ee_q f_V m_V\,\alpha_s^2 \\
&\times \sum_{m=-\infty}^{m=\infty}\left(-\frac{1}{4}\right)^{|m|}\int d\nu\,\frac{\nu^2+m^2}{(\nu^2+(m-1/2)^2)(\nu^2+(m+1/2)^2)}\,e^{\chi_m(\nu)z} \\
&\times \int_{-i\infty}^{i\infty}\frac{ds}{2\pi i}\,\tau^{1/2+s+|m|}\,\frac{\Gamma(1-s-i\nu)\,\Gamma(1-s+i\nu)}{\Gamma(1-s/2-i\nu/2)\,\Gamma(1-s/2+i\nu/2)} \\
&\times \frac{\Gamma^2(1/2+s+|m|)}{\Gamma(1/2+s/2-i\nu/2+|m|)\,\Gamma(1/2+s/2+i\nu/2+|m|)},
\end{aligned}
\tag{3.53}
$$

which can be written as

$$
\begin{aligned}
\mathcal{M}_{++}^{odd\,\delta} &= is\frac{16}{t^2}\frac{N^2-1}{N^2}\,ee_q f_V m_V \alpha_s^2 \\
&\times \sum_{m=-\infty}^{m=\infty}(-1)^m\int d\nu\,\frac{\nu^2+m^2}{(\nu^2+(m-1/2)^2)(\nu^2+(m+1/2)^2)}\,e^{\chi_m(\nu)z} \\
&\times \int_{-i\infty}^{i\infty}\frac{ds}{2\pi i}\left(\frac{\tau}{4}\right)^{1/2+s+|m|}\frac{\Gamma(1/2-s/2+i\nu/2)\,\Gamma^2(1/2+s+|m|)\,\Gamma(1/2-s/2-i\nu/2)}{\Gamma(1/2+s/2-i\nu/2+|m|)\,\Gamma(1/2+s/2+i\nu/2+|m|)}.
\end{aligned}
\tag{3.54}
$$

These results for general conformal spin were first obtained by Enberg, Motyka and Poludniowski [24]. Note that the m contribution is equal to the $-m$ contribution. Note again that the former expression reproduces the result of [19] for the $m = 0$ component. The phenomenology of this component was explored in Forshaw and Poludniowski [23].

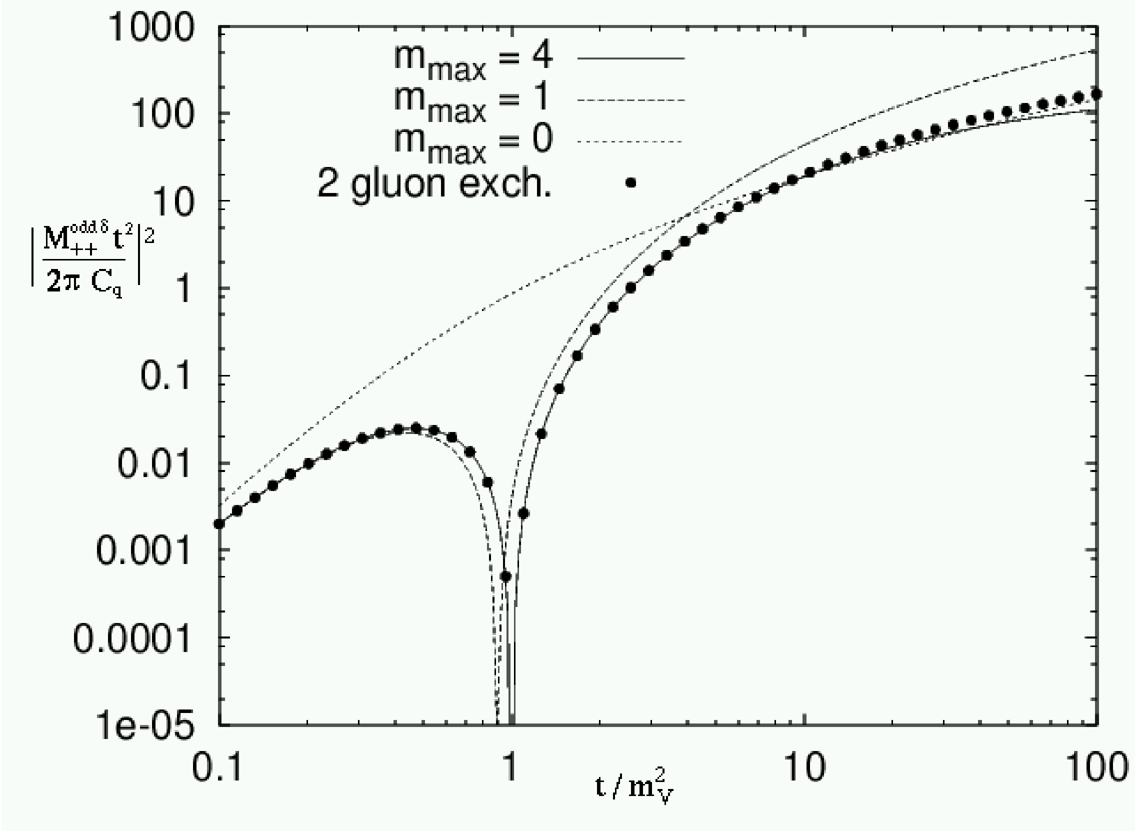

Figure 3.2: The $\gamma(+)q \to V(+)q$ heavy meson amplitude for $z = 0$. The dots correspond to two-gluon exchange. The sum over conformal spins builds up the two-gluon in the $z \to 0$ limit. The constant, $C_q = s\alpha_s^2(N^2 - 1/N^2)f_V m_V e e_q$.

3.2.5 The two-gluon exchange limit

A cross-check that is interesting to perform is that of the limit $z \to 0$. The full BFKL result summed over conformal spin contains two-gluon exchange, and all other contributions vanish in the $z \to 0$ limit. In the limit $z(\alpha_s) \to 0$, the BFKL result should reproduce two-gluon exchange. Figure 3.2 shows how the sum over conformal spins builds up the two gluon result in the zero rapidity limit. Note that the asymptotic BFKL component, that is the $m = 0$ component, cannot reproduce the dip that occurs in the two-gluon cross-section at $m_V^2 = q^2$. Higher conformal spin is required; the oscillation between successive non-zero contributions provides the possibility of cancellation.

3.3 Summary

In section 3.1 we applied the collinear approximation to the impact factors and then explicitly wrote down the two-gluon exchange helicity amplitudes in this approximation. We found that only two survived, the $\mathcal{M}_{+0}^{even\,2g\delta}$ and $\mathcal{M}_{++}^{odd\,2g\delta}$. These amplitudes correspond exactly to those found by [17, 18]. These are the 'leading twist' contributions. For these amplitudes the outgoing quark and anti-quark are naturally forced to be collinear by their light-cone hadronic matrix elements (they are $\mathbf{r}$ independent, so the $\tilde{\mathbf{r}}$ integral gives a δ-function in $\mathbf{l}$.). When the additional heavy meson approximation of a δ-function distribution amplitude was applied, only $\mathcal{M}_{++}^{odd\,2g\delta}$ was non-zero. The result of [19] was recovered. In section 3.2 we extended the calculation of the helicity amplitudes in the collinear approximation to higher orders by using the solution to the BFKL equation. This reproduced the results of [20, 24]. We checked that the result for all conformal spins reproduced the two-gluon exchange prediction in the $z \to 0$ limit.

Chapter 4

BFKL calculation 2: generic non-collinear quarks

The object of this chapter is to repeat the calculation of the previous chapter, with the collinear and heavy-meson approximations relaxed. The analytic calculation is more involved in this case. The outline of the chapter is:

- Section 4.1. We consider the kinematics of the quark and anti-quark with the collinear and heavy meson approximations relaxed. We then explicitly write down the full two-gluon exchange helicity amplitudes. This is the culmination of the work in Chapter 2. We observe that [25] found the $\mathcal{M}_{++}^{even\,2g}$ amplitude to have logarithmic divergent contributions from the end-points in u, that is where $u(1-u) \to 0$.

- Section 4.2. We extend the calculation to higher orders again using the solution to the BFKL equation. We demonstrate that the $\mathcal{M}_{++}^{even}$ amplitude is now finite.

- Section 4.3. We summarise our results.

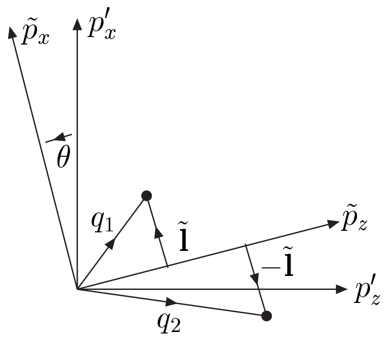

$$q'_{1x} = \tilde{l}_z \sin\theta + \tilde{l}_x \cos\theta$$
$$q'_{1y} = \tilde{l}_y$$

$$q'_{2x} = \tilde{l}_z \sin\theta - \tilde{l}_x \cos\theta$$
$$q'_{2y} = -\tilde{l}_y$$

Figure 4.1: The quark and anti-quark coordinate systems in momentum space. The quark and anti-quark have 4-momenta q_1 and q_2 respectively and these need not lie in the $x-z$ plane. The primed coordinate system is that where the initial state photon and proton define the z-axis. The 'tilde' coordinate system is that where the outgoing meson direction defines the z-axis. We have defined the momentum given to the meson, q, to be in the x direction; therefore $\sin\theta \simeq \frac{2|q|}{\sqrt{s}} \to \cos\theta \sim 1 + \frac{2t}{s}$. This result corresponds to (1.23), quoted in Chapter 1.

4.1 Two gluon exchange

4.1.1 Collinear quark and anti-quark

In section 3.1.1 we observed that in the collinear approximation, $\mathbf{q}_1$ and $\mathbf{q}_2$ are only functions of $\mathbf{q}$ and u. Now that we relax this approximation we will get an additional dependence on $\tilde{\mathbf{l}}$. We will again work in canonical space-time coordinates to aid intuition. The momentum given to the quark and anti-quark pair through the scattering causes the centre-of-mass of the pair to exit the interaction at an angle θ to the initial photon. $\tilde{\mathbf{l}}$ is defined as transverse to the outgoing meson. We need to find $\mathbf{q}_1$ and $\mathbf{q}_2$, which are defined as transverse to the initial photon. We have to deal with a rotation of coordinate systems. The rotation is illustrated in figure 4.1, in which (for convenience) we have defined $q^2 = -q_x^2$. In our kinematic approximation, the 4-momenta of the quark and anti-quark in the photon-proton frame after scattering, can be approximated by,

$$q_1 = (\epsilon_1, \mathbf{q}_1, \epsilon_1) \tag{4.1}$$
$$q_2 = (\epsilon_2, \mathbf{q}_2, \epsilon_2)$$

where $\mathbf{q} = \mathbf{q}_1 + \mathbf{q}_2$, $\epsilon_1 + \epsilon_2 = E$ and E is their combined energy. The rotation gives us

$$\begin{aligned}
\mathbf{q_1} &= (q'_{1x}, q'_{1y}) = (\tilde{l}_x \cos\theta + \tilde{l}_z \sin\theta, \tilde{l}_y) \\
&= (\tilde{l}_x \cos(1 + 2t/s) + \tilde{l}_z \sin(2\sqrt{-t/s}), \tilde{l}_y) \\
&\simeq (\tilde{l}_x + 2\tilde{l}_z \sqrt{-t/s}, \tilde{l}_y) = \tilde{\mathbf{l}} + (2\tilde{l}_z q_x/\sqrt{s}, 0) \\
&= \tilde{\mathbf{l}} + u\mathbf{q} \qquad (4.2)
\end{aligned}$$

The condition $\mathbf{q}_1 + \mathbf{q}_2 = \mathbf{q}$, then straight away gives us

$$\mathbf{q_2} = -\tilde{\mathbf{l}} + (1-u)\mathbf{q}. \qquad (4.3)$$

This explicit treatment of the rotation of coordinate systems makes it transparent why, unlike in the case of polarisation vectors, we cannot to leading log accuracy equate transverse momentum vectors before and after rotation. $\mathbf{q_2} \neq \tilde{\mathbf{l}}$, because the largeness of the z component of the quark momentum compensates for the smallness of the rotation angle. That is why we bothered with the 'tilde' notation! In summary, we have the result

---

$$\mathbf{q}_1(u, \mathbf{q}, \tilde{\mathbf{l}}) = \tilde{\mathbf{l}} + u\mathbf{q} \qquad (4.4)$$

$$\mathbf{q}_2(u, \mathbf{q}, \tilde{\mathbf{l}}) = -\tilde{\mathbf{l}} + (1-u)\mathbf{q} = -\tilde{\mathbf{l}} + \bar{u}\mathbf{q}. \qquad (4.5)$$

We expressed the hadronic matrix elements in the 'tilde' frame, where the outgoing meson direction defined the z-axis. We derived the $\mathbf{P}(\mathbf{r}, u)$ and $R(\mathbf{r}, u)$ functions of the hard scatter in the frame where the photon-proton defined the z-axis. Through relations (4.4-4.5), we know how to relate these frames.

4.1.2 The $\tilde{\mathbf{P}}(\tilde{\mathbf{r}}, u)$ and $\tilde{R}(\tilde{\mathbf{r}}, u)$ functions

We again remind ourselves that the impact factors depend on either the quantity,

$$\tilde{\mathbf{P}}(\tilde{\mathbf{r}}, u) = \int \frac{d^2\tilde{\mathbf{l}}}{(2\pi)^2} e^{-i\tilde{\mathbf{l}}\tilde{\mathbf{r}}} \tilde{\mathbf{P}}(\tilde{\mathbf{l}}, u) \qquad (4.6)$$

or the quantity,

$$\tilde{R}(|\tilde{\mathbf{r}}|,u) = \int \frac{d^2\tilde{\mathbf{l}}}{(2\pi)^2} e^{-i\tilde{\mathbf{l}}\tilde{\mathbf{r}}} \tilde{R}(|\tilde{\mathbf{l}}|,u). \tag{4.7}$$

Equations (2.136) and (2.137) give us[1],

$$\tilde{\mathbf{P}} = \left(\frac{\mathbf{q}_1}{\mathbf{q}_1^2+m^2} + \frac{\mathbf{k}-\mathbf{q}_1}{(\mathbf{k}-\mathbf{q}_1)^2+m^2} \right) - (\mathbf{q}_1 \to \mathbf{q_2}) \tag{4.8}$$

and

$$\tilde{R} = \left(\frac{1}{\mathbf{q}_1^2+m^2} - \frac{1}{(\mathbf{k}-\mathbf{q}_1)^2+m^2} \right) + (\mathbf{q}_1 \to \mathbf{q_2}). \tag{4.9}$$

Shifting variables and using standard integrals we obtain,

$$\begin{aligned}\tilde{\mathbf{P}}(\tilde{\mathbf{r}},u) &= \int \frac{d^2\tilde{\mathbf{l}}}{(2\pi)^2} e^{-i\tilde{\mathbf{l}}\tilde{\mathbf{r}}} \tilde{\mathbf{P}}(\tilde{\mathbf{r}},u) = \int \frac{d^2\tilde{\mathbf{l}}}{(2\pi)^2} \frac{\tilde{\mathbf{l}}}{\tilde{\mathbf{l}}^2+m^2} e^{-i\tilde{\mathbf{l}}\tilde{\mathbf{r}}} f^d \\ &= -\frac{im}{2\pi} K_1(|\tilde{\mathbf{r}}|m) \frac{\tilde{\mathbf{r}}}{|\tilde{\mathbf{r}}|} f^d\end{aligned} \tag{4.10}$$

and

$$\begin{aligned}\tilde{R}(|\tilde{\mathbf{r}}|,u) &= \int \frac{d^2\tilde{\mathbf{l}}}{(2\pi)^2} e^{-i\tilde{\mathbf{l}}\tilde{\mathbf{r}}} \tilde{R}(|\tilde{\mathbf{r}}|,u) = \int \frac{d^2\tilde{\mathbf{l}}}{(2\pi)^2} \frac{1}{\tilde{\mathbf{l}}^2+m^2} e^{-i\tilde{\mathbf{l}}\tilde{\mathbf{r}}} f^d \\ &= \frac{1}{2\pi} K_0(|\tilde{\mathbf{r}}|m) f^d,\end{aligned} \tag{4.11}$$

where

$$f^d = e^{iu\mathbf{q}\tilde{\mathbf{r}}}(1-e^{-i\mathbf{k}\tilde{\mathbf{r}}}) + e^{-i\bar{u}\mathbf{q}\tilde{\mathbf{r}}}(1-e^{i\mathbf{k}\tilde{\mathbf{r}}}). \tag{4.12}$$

From now on we drop the 'tilde' notation on the vector $\mathbf{r}$. It has served its purpose. Unlike the $\tilde{\mathbf{l}}$ vector, to leading logs, we can identify $\mathbf{r}$ as the transverse vector in both the frame defined by the photon-proton and that by the vector meson direction[2].

[1] Note that the we have used $\phi_{\gamma q\bar{q}}(\mathbf{k},\mathbf{q})$ rather than $\phi_{\gamma q\bar{q}}(-\mathbf{k},-\mathbf{q})$, which entails the reversal of $\mathbf{k}$ and $\mathbf{q}$ in (2.136, 2.137).

[2] In our approximation r_+ is exactly zero. Also, r_- is constrained to be small by the fact that the dominant contributions arise from where $\tilde{p}_+\tilde{r}_- \sim 1$. There is no large '$z$' component analogous to that appearing in (4.4).

4.1.3 The impact factors

We remind ourselves of the definitions of transverse polarisations,

$$e^{\lambda=\pm1} = \mp\frac{1}{\sqrt{2}}(0,1,\pm i,0). \tag{4.13}$$

These definitions along with the transforms of $\tilde{\mathbf{P}}$ and $\tilde{R}$ give us:

$$\phi_{even}^{\gamma(+)V(0)}(\mathbf{k},\mathbf{q}) = im\, e_q\frac{g^2\delta_{ab}}{2N}f_\rho\int\frac{d^2\mathbf{r}du}{4\pi}K_1(|r|m)\frac{r}{|r|}\frac{f^d}{\sqrt{2}}(1-2u)\phi_{\parallel}(u), \tag{4.14}$$

$$\begin{aligned}\phi_{even}^{\gamma(+)V(+)}(\mathbf{k},\mathbf{q}) &= m\, e_q\frac{g^2\delta_{ab}}{2N}\frac{f_\rho}{2}m_\rho\int\frac{d^2\mathbf{r}du}{4\pi}\,K_1(|r|m)|r|f^d\\ &\times\left(\frac{g_\perp^{(a)}(u)}{4}-(1-2u)\int_0^u dv(\phi_\parallel(v)-g_\perp^{(v)}(v))\right),\end{aligned} \tag{4.15}$$

$$\begin{aligned}\phi_{even}^{\gamma(+)V(-)}(\mathbf{k},\mathbf{q}) &= m\, e_q\frac{g^2\delta_{ab}}{2N}\frac{f_\rho}{2}m_\rho\int\frac{d^2\mathbf{r}du}{4\pi}\,K_1(|r|m)\frac{r^2}{|r|}f^d\\ &\times\left(\frac{g_\perp^{(a)}(u)}{4}+(1-2u)\int_0^u dv(\phi_\parallel(v)-g_\perp^{(v)}(v))\right),\end{aligned} \tag{4.16}$$

$$\begin{aligned}\phi_{odd}^{\gamma(+)V(0)}(\mathbf{k},\mathbf{q}) &= ie_q\frac{g^2\delta_{ab}}{2N}m\,m_\rho f_\rho^T\int\frac{d^2\mathbf{r}du}{4\pi}\frac{r}{\sqrt{2}}K_0(|r|m)f^d\\ &\times\int_0^u dv(h_\parallel^{(t)}(v)-\phi_\perp(v)),\end{aligned} \tag{4.17}$$

$$\phi_{odd}^{\gamma(+)V(+)}(\mathbf{k},\mathbf{q}) = e_q \frac{g^2\delta_{ab}}{2N}\, m\, f_\rho^T \int \frac{d^2\mathbf{r}du}{4\pi} K_0(|r|m) f^d\, \phi_\perp(u), \tag{4.18}$$

and

$$\begin{aligned}\phi_{odd}^{\gamma(+)V(-)}(\mathbf{k},\mathbf{q}) = e_q \frac{g^2\delta_{ab}}{2N}\, m\, m_\rho^2 \frac{f_\rho^T}{2} \int \frac{d^2\mathbf{r}du}{4\pi} r^2 K_0(|r|m) f^d \\ \times \int_0^u dv \int_0^v d\eta \left(h_\parallel^{(t)}(\eta) - \frac{1}{2}\phi_\perp(\eta) - \frac{1}{2} h_3(\eta) \right),\end{aligned} \tag{4.19}$$

where r is complex notation, $r = r_x + ir_y$ and we note that, for example, $\mathbf{r}\cdot\mathbf{e}^{(+)} = -r/\sqrt{2}$.

4.1.4 The two-gluon exchange amplitudes

The full list of amplitude could have been written down explicitly at the end of Chapter 2. We do so now and the list is:

$$\begin{aligned}\mathcal{M}_{+0}^{even\,2g} = -s\, m\, e_q \alpha_s^2 \frac{N^2-1}{N^2} f_\rho \int \frac{d^2\mathbf{k}}{\mathbf{k}^2(\mathbf{k}-\mathbf{q})^2} \frac{d^2\mathbf{r}du}{4\pi} \\ \times K_1(|r|m) \frac{r}{|r|} \frac{f^d}{\sqrt{2}} (1-2u)\phi_\parallel(u),\end{aligned} \tag{4.20}$$

$$\begin{aligned}\mathcal{M}_{++}^{even\,2g} = is\, m\, e_q \alpha_s^2 \frac{N^2-1}{N^2} \frac{f_\rho}{2} m_\rho \int \frac{d^2\mathbf{r}du}{4\pi} \frac{d^2\mathbf{k}}{\mathbf{k}^2(\mathbf{k}-\mathbf{q})^2} K_1(|r|m)|r| f^d \\ \times \left(\frac{g_\perp^{(a)}(u)}{4} - (1-2u) \int_0^u dv (\phi_\parallel(v) - g_\perp^{(v)}(v)) \right),\end{aligned} \tag{4.21}$$

$$\mathcal{M}^{even\,2g}_{+-} = is\,m\,e_q\alpha_s^2\frac{N^2-1}{N^2}\frac{f_\rho}{2}m_\rho\int\frac{d^2\mathbf{k}}{\mathbf{k}^2(\mathbf{k}-\mathbf{q})^2}\frac{d^2\mathbf{r}du}{4\pi}\,K_1(|r|m)\frac{r^2}{|r|}f^d \times\left(\frac{g_\perp^{(a)}(u)}{4}+(1-2u)\int_0^u dv(\phi_\parallel(v)-g_\perp^{(v)}(v))\right), \tag{4.22}$$

$$\mathcal{M}^{odd\,2g}_{+0} = -s\,e_q\alpha_s^2\frac{N^2-1}{N^2}m\,m_\rho f_\rho^T\int\frac{d^2\mathbf{k}}{\mathbf{k}^2(\mathbf{k}-\mathbf{q})^2}\frac{d^2\mathbf{r}du}{4\pi}\frac{r}{\sqrt{2}}K_0(|r|m)f^d \times\int_0^u dv(h_\parallel^{(t)}(v)-\phi_\perp(v)), \tag{4.23}$$

$$\mathcal{M}^{odd\,2g}_{++} = is\,e_q\alpha_s^2\frac{N^2-1}{N^2}\,m\,f_\rho^T\int\frac{d^2\mathbf{k}}{\mathbf{k}^2(\mathbf{k}-\mathbf{q})^2}\frac{d^2\mathbf{r}du}{4\pi}K_0(|r|m)f^d\,\phi_\perp(u), \tag{4.24}$$

and

$$\mathcal{M}^{odd\,2g}_{+-} = is\,e_q\alpha_s^2\frac{N^2-1}{N^2}\,m\,m_\rho^2\frac{f_\rho^T}{2}\int\frac{d^2\mathbf{k}}{\mathbf{k}^2(\mathbf{k}-\mathbf{q})^2}\frac{d^2\mathbf{r}du}{4\pi}r^2K_0(|r|m)f^d \times\int_0^u dv\int_0^v d\eta\left(h_\parallel^{(t)}(\eta)-\frac{1}{2}\phi_\perp(\eta)-\frac{1}{2}h_3(\eta)\right). \tag{4.25}$$

These expressions are in agreement with the work of [25].

4.2 Beyond two-gluon exchange

4.2.1 The BFKL solution

We know the impact factors for $\gamma \to V$. We are therefore again able to generalise straight away to the BFKL leading log summation, using the result of [14]. We list this result yet again to save referring back:

$$\mathcal{M}^{AB}_{BFKL}(z,q) = \frac{is}{(2\pi)^4} \sum_{n=-\infty}^{n=\infty} \int_{-\infty}^{\infty} d\nu \, \frac{\nu^2 + n^2/4}{[\nu^2 + (n-1)^2/4][\nu^2 + (n+1)^2/4]} \times \exp[\chi_n(\nu) z] \; I^A_{n,\nu}(q) \, (I^B_{n,\nu}(q))^* \tag{4.26}$$

where as usual

$$\chi_n(\nu) = 4\mathcal{R}\mathrm{e}\Big(\psi(1) - \psi(1/2 + |n|/2 + i\nu)\Big) \tag{4.27}$$

is proportional to the eigenvalues of the BFKL kernel, and where

$$I^A_{n,\nu}(q) = \int \frac{d^2k}{(2\pi)^2} \phi_A(k,q) \int d^2\rho_1 \, d^2\rho_2 \; E_{n,\nu}(\rho_1,\rho_2) \exp(ik\cdot\rho_1 + i(q-k)\cdot\rho_2), \tag{4.28}$$

with an analogous result for the index B. The eigenfunctions are given by

$$E_{n,\nu}(\rho_1,\rho_2) = \left(\frac{\rho_1-\rho_2}{\rho_1\rho_2}\right)^{-\tilde{\mu}+1/2} \left(\left(\frac{\rho_1-\rho_2}{\rho_1\rho_2}\right)^*\right)^{-\mu+1/2} \tag{4.29}$$

where $\mu = n/2 - i\nu$ and $\tilde{\mu} = -n/2 - i\nu$. Here k and q are transverse two-dimensional momentum vectors, and ρ_1 and ρ_2 are position space vectors in the standard complex representation. The variable z is as before:

$$z = \frac{3\alpha_s}{2\pi} \ln\left(\frac{s}{\Lambda^2}\right), \tag{4.30}$$

The functions $\phi_A = \phi^{\gamma(\lambda)V(\lambda')}$ and $\phi_B = \phi_{qq}$ are the impact factors.

4.2.2 The projection of the $q \to q$ impact factor

The projection of the quark impact factor was found in the previous chapter (see section 3.2.2 equation (4.31)). We restate the result,

$$I^{qq}_{n,\nu}(q) = -\frac{g^2\delta_{ab}}{2N}\frac{4\pi\, i^n}{|q|}\left(\frac{|q|^2}{4}\right)^{i\nu}\left(\frac{q^*}{q}\right)^{n/2}\frac{\Gamma(1/2+n/2-i\nu)}{\Gamma(1/2+n/2+i\nu)} \tag{4.31}$$

for even n and $I^{qq}_{n,\nu} = 0$ for odd n.

4.2.3 The projection of the $\gamma \to V$ impact factor

In this subsection we compute the projection of the impact factor for both the chiral even and odd contribution to $A = \gamma(+) \to V(\lambda')$ transition for all conformal spins, n. The following integrals are to be evaluated:

$$I^A_{n,\nu}(q) = \int \frac{d^2k}{(2\pi)^2}\, \phi_A(k,q) \int d^2\rho_1\, d^2\rho_2\; E_{n,\nu}(\rho_1,\rho_2) \\ \times \exp(ik^*\rho_1/2 + ik\rho_1^*/2 + i(q^*-k^*)\rho_2/2 + i(q-k)\rho_2^*/2). \tag{4.32}$$

Changing variables to $\rho_1 = R + \rho/2$, $\rho_2 = R - \rho/2$ and integrating over d^2k we get

$$I^A_{n,\nu}(q) = \int d^2\rho\; \Phi^A_q(\rho)\; \hat{E}^q_{n,\nu}(\rho), \tag{4.33}$$

where $\phi^q_A(\rho)$ is the Fourier transform of the impact factor in the momentum space $\phi_A(k,q)$,

$$\phi^q_A(\rho) = \int \frac{d^2k}{(2\pi)^2} \phi_A(k,q) e^{i(k-q/2)\cdot\rho} \tag{4.34}$$

and $\hat{E}^q_{n,\nu}(\rho)$ was presented as (3.41) in section 3.2.3.

The Fourier transform of the impact factor

The integral over k of impact factors (4.14, 4.15, 4.16) and (4.17, 4.18, 4.19) may be easily performed since k appears only in f^d (see (4.12)). The integral over f^d gives,

$$\int \frac{d^2k}{(2\pi)^2} e^{i(k-q/2)\cdot\rho}\, f^d = e^{-iq\cdot\rho/2}\Big[\delta^{(2)}(\rho)e^{iuq\cdot r} - \delta^{(2)}(r-\rho)e^{iuq\cdot r} \\ -\delta^{(2)}(r+\rho)e^{-i\bar{u}q\cdot r} + \delta^{(2)}(\rho)e^{-i\bar{u}q\cdot r}\Big]. \tag{4.35}$$

Due to the resulting δ functions $\delta(\rho)$, $\delta(r-\rho)$ and $\delta(r+\rho)$ the integration over r is trivial[3]. We arrive at the impact factors,

$$\phi^{\gamma(+)V(0)}_{even}(\rho) = -im\, e_q \frac{g^2\delta_{ab}}{2N} f_\rho\, K_1(|\rho| m) \frac{\rho}{|\rho|} \\ \times \int \frac{du}{4\pi} \frac{e^{i\frac{\xi}{2}q\cdot\rho} - e^{-i\frac{\xi}{2}q\cdot\rho}}{\sqrt{2}} (1-2u)\phi_\parallel(u), \tag{4.36}$$

[3] Note that we again see non-contributing $\delta^{(2)}(\rho)$ functions arising from the coupling of the pomeron to single partons. The multi-parton couplings *i.e.* to both quark and anti-quark, are associated with $\delta^{(2)}(r-\rho)$; the pomeron couples to the 'whole' dipole.

$$\phi^{\gamma(+)V(+)}_{even}(\rho) = -m\, e_q \frac{g^2\delta_{ab}}{2N}\frac{f_\rho}{2} m_\rho\, K_1(|\rho|m)|\rho| \int \frac{du}{4\pi}(e^{i\frac{\xi}{2}q\cdot\rho} + e^{-i\frac{\xi}{2}q\cdot\rho})$$
$$\times \left(\frac{g_\perp^{(a)}(u)}{4} - (1-2u)\int_0^u dv(\phi_\|(v) - g_\perp^{(v)}(v))\right), \quad (4.37)$$

$$\phi^{\gamma(+)V(-)}_{even}(\rho) = -m\, e_q \frac{g^2\delta_{ab}}{2N}\frac{f_\rho}{2} m_\rho\, K_1(|\rho|m)\frac{\rho^2}{|\rho|} \int \frac{du}{4\pi}(e^{i\frac{\xi}{2}q\cdot\rho} + e^{-i\frac{\xi}{2}q\cdot\rho})$$
$$\times \left(\frac{g_\perp^{(a)}(u)}{4} + (1-2u)\int_0^u dv(\phi_\|(v) - g_\perp^{(v)}(v))\right), \quad (4.38)$$

$$\phi^{\gamma(+)V(0)}_{odd}(\rho) = -ie_q \frac{g^2\delta_{ab}}{2N} m\, m_\rho f_\rho^T\, \frac{\rho}{\sqrt{2}} K_0(|\rho|m) \int \frac{du}{4\pi}(e^{i\frac{\xi}{2}q\cdot\rho} - e^{-i\frac{\xi}{2}q\cdot\rho})$$
$$\times \int_0^u dv(h_\|^{(t)}(v) - \phi_\perp(v)), \quad (4.39)$$

$$\phi^{\gamma(+)V(+)}_{odd}(\rho) = -e_q \frac{g^2\delta_{ab}}{2N}\, m\, f_\rho^T\, K_0(|\rho|m) \int \frac{du}{4\pi}(e^{i\frac{\xi}{2}q\cdot\rho} + e^{-i\frac{\xi}{2}q\cdot\rho})\, \phi_\perp(u), \quad (4.40)$$

and

$$\phi^{\gamma(+)V(-)}_{odd}(\rho) = -e_q \frac{g^2\delta_{ab}}{2N}\, m\, m_\rho^2 \frac{f_\rho^T}{2}\, \rho^2 K_0(|\rho|m) \int \frac{du}{4\pi}(e^{i\frac{\xi}{2}q\cdot\rho} + e^{-i\frac{\xi}{2}q\cdot\rho})$$
$$\times \int_0^u dv \int_0^v d\eta \left(h_\|^{(t)}(\eta) - \frac{1}{2}\phi_\perp(\eta) - \frac{1}{2}h_3(\eta)\right), \quad (4.41)$$

where we define the shorthand $\xi = 2u-1$. Using the fact that $\hat{E}^q_{n,\nu}(\rho) = 0$ for $\rho = 0$, and

$$\hat{E}^q_{n,\nu}(\rho) = (-1)^n \hat{E}^q_{n,\nu}(-\rho), \quad (4.42)$$

which can be seen from, for example, the series expansion of the Bessel functions in $\hat{E}$. One arrives at the projections (with superscripts E and O denoting even and odd contributions respectively),

$$
\begin{aligned}
I_{n,\nu}^{\gamma(+)V(0)\,E}(q) &= -im\, e_q \frac{g^2\delta_{ab}}{2N} f_\rho\,(1+(-1)^n) \int d^2\rho\, \hat{E}^q_{n,\nu}(\rho)\, K_1(|\rho|m) \frac{\rho}{|\rho|} \\
&\qquad \times \int \frac{du}{4\pi} \frac{e^{i\frac{\xi}{2}q\cdot\rho}}{\sqrt{2}} (1-2u)\phi_{\parallel}(u) \\
&= -ie_q \frac{g^2\delta_{ab}}{2N} f_\rho\,(1+(-1)^n) \\
&\times \frac{(-1)^n}{2\pi^2}\, b_{n,\nu} \left(\frac{|q|}{8}\right)^{2i\nu} \left(\frac{q^*}{q}\right)^{n/2} \Gamma(1-i\nu-n/2)\Gamma(1-i\nu+n/2) \\
&\qquad \times \int \frac{du}{4\pi} \frac{1}{\sqrt{2}} (1-2u)\phi_{\parallel}(u) I_{0-1}(\nu,n,q,u;1),
\end{aligned} \tag{4.43}
$$

$$
\begin{aligned}
I_{n,\nu}^{\gamma(+)V(+)\,E}(q) &= -m\, e_q \frac{g^2\delta_{ab}}{2N} \frac{f_\rho}{2} m_\rho\,(1+(-1)^n) \int d^2\rho\, \hat{E}^q_{n,\nu}(\rho)\, K_1(|\rho|m) |\rho| \\
&\qquad \times \int \frac{du}{4\pi} e^{i\frac{\xi}{2}q\cdot\rho} \left(\frac{g_\perp^{(a)}(u)}{4} - (1-2u)\int_0^u dv(\phi_{\parallel}(v) - g_\perp^{(v)}(v)) \right) \\
&= -e_q \frac{g^2\delta_{ab}}{2N} \frac{f_\rho}{2} m_\rho\,(1+(-1)^n) \\
&\times \frac{(-1)^n}{2\pi^2}\, b_{n,\nu} \left(\frac{|q|}{8}\right)^{2i\nu} \left(\frac{q^*}{q}\right)^{n/2} \Gamma(1-i\nu-n/2)\Gamma(1-i\nu+n/2) \\
&\times \int \frac{du}{4\pi} \left(\frac{g_\perp^{(a)}(u)}{4} - (1-2u)\int_0^u dv(\phi_{\parallel}(v) - g_\perp^{(v)}(v)) \right) I_{00}(\nu,n,q,u;1),
\end{aligned} \tag{4.44}
$$

$$
\begin{aligned}
I_{n,\nu}^{\gamma(+)V(-)\,E}(q) &= -m\, e_q \frac{g^2\delta_{ab}}{2N} \frac{f_\rho}{2} m_\rho\,(1+(-1)^n) \int d^2\rho\, \hat{E}^q_{n,\nu}(\rho)\, K_1(|\rho|m) \frac{\rho^2}{|\rho|} \\
&\qquad \times \int \frac{du}{4\pi} e^{i\frac{\xi}{2}q\cdot\rho} \left(\frac{g_\perp^{(a)}(u)}{4} + (1-2u)\int_0^u dv(\phi_{\parallel}(v) - g_\perp^{(v)}(v)) \right) \\
&= -e_q \frac{g^2\delta_{ab}}{2N} \frac{f_\rho}{2} m_\rho\,(1+(-1)^n) \\
&\times \frac{(-1)^n}{2\pi^2}\, b_{n,\nu} \left(\frac{|q|}{8}\right)^{2i\nu} \left(\frac{q^*}{q}\right)^{n/2} \Gamma(1-i\nu-n/2)\Gamma(1-i\nu+n/2) \\
&\times \int \frac{du}{4\pi} \left(\frac{g_\perp^{(a)}(u)}{4} + (1-2u)\int_0^u dv(\phi_{\parallel}(v) - g_\perp^{(v)}(v)) \right) I_{1-1}(\nu,n,q,u;1),
\end{aligned} \tag{4.45}
$$

$$
\begin{aligned}
I^{\gamma(+)V(0)\,O}_{n,\nu}(q) &= -ie_q \frac{g^2\delta_{ab}}{2N} m\, m_\rho f^T_\rho\,(1+(-1)^n) \int d^2\rho\, \hat{E}^q_{n,\nu}(\rho) \frac{\rho}{\sqrt{2}} K_0(|\rho|m) \\
&\quad \times \int \frac{du}{4\pi} e^{i\frac{\xi}{2}q\cdot\rho} \int_0^u dv (h^{(t)}_{\parallel}(v) - \phi_\perp(v)) \\
&= -ie_q \frac{g^2\delta_{ab}}{2N}\, m_\rho f^T_\rho\,(1+(-1)^n) \\
&\times \frac{(-1)^n}{2\pi^2}\, b_{n,\nu} \left(\frac{|q|}{8}\right)^{2i\nu} \left(\frac{q^*}{q}\right)^{n/2} \Gamma(1-i\nu-n/2)\Gamma(1-i\nu+n/2) \\
&\times \int \frac{du}{4\pi} \int_0^u dv (h^{(t)}_{\parallel}(v) - \phi_\perp(v))\, I_{\frac{1}{2}-\frac{1}{2}}(\nu,n,q,u;0)
\end{aligned}
\tag{4.46}
$$

$$
\begin{aligned}
I^{\gamma(+)V(+)\,O}_{n,\nu}(q) &= -e_q \frac{g^2\delta_{ab}}{2N}\, m\, f^T_\rho\,(1+(-1)^n) \int d^2\rho\, \hat{E}^q_{n,\nu}(\rho)\, K_0(|\rho|m) \\
&\quad \times \int \frac{du}{4\pi} e^{i\frac{\xi}{2}q\cdot\rho}\, \phi_\perp(u) \\
&= -e_q \frac{g^2\delta_{ab}}{2N}\, f^T_\rho\,(1+(-1)^n) \frac{(-1)^n}{2\pi^2}\, b_{n,\nu} \left(\frac{|q|}{8}\right)^{2i\nu} \left(\frac{q^*}{q}\right)^{n/2} \\
&\times \Gamma(1-i\nu-n/2)\Gamma(1-i\nu+n/2) \int \frac{du}{4\pi}\, \phi_\perp(u)\, I_{-\frac{1}{2}-\frac{1}{2}}(\nu,n,q,u;0)
\end{aligned}
\tag{4.47}
$$

and

$$
\begin{aligned}
I^{\gamma(+)V(-)\,O}_{n,\nu}(q) &= -e_q \frac{g^2\delta_{ab}}{2N}\, m\, m^2_\rho \frac{f^T_\rho}{2}\,(1+(-1)^n) \int d^2\rho\, \hat{E}^q_{n,\nu}(\rho)\, \rho^2 K_0(|\rho|m) \\
&\times \int \frac{du}{4\pi} e^{i\frac{\xi}{2}q\cdot\rho} \int_0^u dv \int_0^v d\eta \left(h^{(t)}_{\parallel}(\eta) - \frac{1}{2}\phi_\perp(\eta) - \frac{1}{2}h_3(\eta)\right) \\
&= -e_q \frac{g^2\delta_{ab}}{2N}\, m^2_\rho \frac{f^T_\rho}{2} \frac{(-1)^n}{2\pi^2}\, b_{n,\nu} \left(\frac{|q|}{8}\right)^{2i\nu} \left(\frac{q^*}{q}\right)^{n/2} \Gamma(1-i\nu-n/2)\Gamma(1-i\nu+n/2) \\
&\times (1+(-1)^n) \int \frac{du}{4\pi} \int_0^u dv \int_0^v d\eta \left(h^{(t)}_{\parallel}(\eta) - \frac{1}{2}\phi_\perp(\eta) - \frac{1}{2}h_3(\eta)\right) I_{\frac{3}{2}-\frac{1}{2}}(\nu,n,q,u;0)
\end{aligned}
\tag{4.48}
$$

where

$$
\begin{aligned}
I_{\alpha\beta}(\nu,n,q,u;a) &= m \int d^2\rho\, \rho^{\alpha+1} \rho^{*\,\beta+1}\, K_a(m|\rho|) e^{\frac{i\xi}{4}[q^*\rho + q\rho^*]} \\
&\quad \times [J_\mu(q^*\rho/4) J_{\tilde{\mu}}(q\rho^*/4) - (-1)^n\, J_{-\mu}(q^*\rho/4) J_{-\tilde{\mu}}(q\rho^*/4)]
\end{aligned}
\tag{4.49}
$$

and $K_a(x)$ is the modified Bessel function, displaying effects of the quark mass. The parameter a equals 1 for the chiral even and 0 for the chiral odd impact factors of (see

(4.10), (4.11) and section 2.2.4). Note that in all cases the projections vanish for odd conformal spin.

Analytic manipulation and evaluation

It is convenient to use the variable $\xi = u - \bar{u} = 2u - 1$ rather than u, and to compute the integral for ξ as an arbitrary complex number and then continue analytically into the physical region $-1 < \xi < 1$. We can then write the parts of (4.49), using $2i\, d^2\rho = d\rho\, d\rho^*$ and suppressing α and β, as

$$\mathcal{I}_\pm = m \int \frac{d\rho\, d\rho^*}{2i}\ \rho^{\alpha+1} \rho^{*\,\beta+1}\ K_a(m|\rho|)\ e^{\frac{i}{4}(\xi^* \rho^* q + \xi \rho q^*)}\ J_{\pm\mu}(q^*\rho/4)\ J_{\pm\widetilde{\mu}}(q\rho^*/4) \tag{4.50}$$

so that $\mathcal{I} = \mathcal{I}_+ - (-1)^n\, \mathcal{I}_-$.

Let us start by computing the integral (4.50) for massive quarks. The massless case will be obtained in a suitable limit.

The Bessel functions J are defined with a cut, but the products appearing here are single-valued. To make the cut structure of the integral more explicit it is convenient to represent the Bessel functions in terms of confluent hypergeometric functions, which are individually single-valued, by using the relation 8.440 of [5]

$$J_{\sigma-1/2}(z) = \phi(\sigma, 2\sigma; -2iz)\ \left(\frac{z}{2}\right)^{\sigma-1/2} \frac{e^{iz}}{\Gamma(\sigma+1/2)}. \tag{4.51}$$

Inserting this into equation (4.50) we have

$$\begin{aligned}
\mathcal{I}_+ \ &= \ \frac{64^{i\nu}\ q^{*\,\mu} q^{\widetilde{\mu}}}{\Gamma(\mu+1)\Gamma(\widetilde{\mu}+1)}\ m \int \frac{d\rho\, d\rho^*}{2i} \rho^{\alpha+1+\mu} \rho^{*\,\beta+1+\widetilde{\mu}} \\
&\times\ \exp\left[i\,\frac{\xi+1}{4} q^* \rho + i\,\frac{\xi^*+1}{4} q \rho^* \right] K_a(m|\rho|) \\
&\times\ \phi\left(\mu + \tfrac{1}{2}, 2\mu+1; -\tfrac{i}{2} q^* \rho\right)\ \phi\left(\widetilde{\mu} + \tfrac{1}{2}, 2\widetilde{\mu}+1; -\tfrac{i}{2} q \rho^*\right).
\end{aligned} \tag{4.52}$$

The Bessel function K_a can be replaced with the line integral representation[4]

$$K_a(x) = \frac{1}{2} \left(\frac{2}{x}\right)^b \int_{C-i\infty}^{C+i\infty} \frac{dz}{2\pi i}\ \Gamma(b/2 + a/2 - z)\Gamma(b/2 - a/2 - z)\ \left(\frac{x^2}{4}\right)^z \tag{4.53}$$

[4]This can be seen either by the inverse Mellin transformation or by expressing K_a as a Meijer G function and using its line integral representation.

for $C \leq Re[b/2 + a/2]$, $Re[b/2 - a/2]$. Substituted into Eq. (4.52), we now get the following integral:

$$\begin{aligned} \mathcal{I}_+ &= \frac{64^{i\nu}\, q^{*\mu} q^{\widetilde{\mu}}}{\Gamma(\mu+1)\Gamma(\widetilde{\mu}+1)} \frac{m}{2} \int_{C'-i\infty}^{C'+i\infty} \frac{d\zeta}{2\pi i} \Gamma(a/2-\zeta)\Gamma(-a/2-\zeta) \left(\frac{m^2}{4}\right)^{\zeta} \\ &\times \int \frac{d\rho\, d\rho^*}{2i} \rho^{\alpha+1+\mu+\zeta} \rho^{*\,\beta+1+\widetilde{\mu}+\zeta} \exp\left[i\,\frac{\xi+1}{4} q^* \rho + i\,\frac{\xi^*+1}{4} q \rho^* \right] \\ &\times \phi\left(\mu+\tfrac{1}{2}, 2\mu+1; -\tfrac{i}{2} q^* \rho\right) \phi\left(\widetilde{\mu}+\tfrac{1}{2}, 2\widetilde{\mu}+1; -\tfrac{i}{2} q \rho^*\right) \end{aligned} \tag{4.54}$$

where we have changed to the integration variable $\zeta = z - b/2$.

The ρ and ρ^* dependence of the integrand is clearly factorised, but to disentangle the integrals we have to consider carefully the analytic structure. It is convenient to rescale the integration variables,

$$W = \frac{q^*(\xi+1)}{4i} \rho \tag{4.55}$$

$$Z = \frac{q(\xi^*+1)}{4i} \rho^*, \tag{4.56}$$

giving

$$\begin{aligned} \mathcal{I}_+ &= \frac{64^{i\nu}\, q^{*\mu} q^{\widetilde{\mu}}}{\Gamma(\mu+1)\Gamma(\widetilde{\mu}+1)} \frac{m}{2} \int_{C'-i\infty}^{C'+i\infty} \frac{d\zeta}{2\pi i} \Gamma(a/2-\zeta)\Gamma(-a/2-\zeta) \left(\frac{m^2}{4}\right)^{\zeta} \\ &\times \int \frac{dW\, dZ}{2i} W^{\alpha+1+\mu+\zeta}\, Z^{\beta+1+\widetilde{\mu}+\zeta}\, e^{-(W+Z)} \\ &\times \left(\frac{4i}{q^*(\xi+1)}\right)^{2+\alpha+\mu+\zeta} \left(\frac{4i}{q(\xi^*+1)}\right)^{2+\beta+\widetilde{\mu}+\zeta} \\ &\times \phi\left(\mu+\frac{1}{2}, 2\mu+1; \frac{2W}{\xi+1}\right) \phi\left(\widetilde{\mu}+\frac{1}{2}, 2\widetilde{\mu}+1; \frac{2Z}{\xi^*+1}\right). \end{aligned} \tag{4.57}$$

Our analysis of the cut structure of the integrand now follows a similar path to [42]. Let us fix Z to be a constant real number. If $Z > 0$ there is a branch cut along the positive real axis from zero to infinity in the complex W plane, and if $Z < 0$ the cut is along the negative real axis. For the integral to converge Z must be positive, and so to get a non-zero contribution we have to close the contour around the cut in the right half-plane, finding the discontinuity across the cut. Keeping Z fixed, the W integral can be written as

$$\oint_C dW (-WZ)^u e^{-W} e^{-Z} F(W) \tag{4.58}$$

where u is a non-integer complex exponent and $F(W)$ is the non-problematic, single-valued part of the integrand. Let the contour C be the two rays $W_\pm = re^{\pm i\delta}$, where r is integrated from 0 to infinity and δ is a positive real number, anticipating the limit $\delta \to 0$. We then have

$$
\begin{aligned}
&\oint_C dW(-WZ)^u e^{-W} e^{-Z} F(W) \\
&= \lim_{\delta\to 0} \int_0^\infty dr[(-ZW_-)^u e^{-W_-} - (-ZW_+)^u e^{-W_+}] e^{-Z} F(W) \\
&= -2i \sin(\pi u)\, Z^u e^{-Z} \int_0^\infty dr\, r^u e^{-r} F(r).
\end{aligned}
\tag{4.59}
$$

That is, factorising the two integrals, we get an extra factor $\sin(\pi u)$ ensuring that the expression is single-valued. Note that we have chosen the direction of the contour to give the correct overall sign. Applying this result to (4.57), with $u = \alpha + \mu + \zeta$, and using the fact that $\mu - \widetilde{\mu} = n$ and $\alpha - \beta$ are both integers, leads to

$$
\begin{aligned}
\mathcal{I}_+ &= \frac{64^{i\nu}\, q^{*\mu} q^{\widetilde{\mu}}}{\Gamma(\mu+1)\Gamma(\widetilde{\mu}+1)} \frac{m}{2} \int_{C'-i\infty}^{C'+i\infty} \frac{d\zeta}{2\pi i} \Gamma(a/2-\zeta)\Gamma(-a/2-\zeta) \left(\frac{m^2}{4}\right)^\zeta \\
&\times \left(\frac{4}{q^*(\xi+1)}\right)^{2+\alpha+\mu+\zeta} \left(\frac{4}{q(\xi^*+1)}\right)^{2+\beta+\widetilde{\mu}+\zeta} \sin\pi(\alpha+\mu+\zeta)\, (-i)^{\alpha-\beta+n} \\
&\times \int_0^\infty dW\, W^{\alpha+1+\mu+\zeta}\, e^{-W} \phi\left(\mu+\frac{1}{2}, 2\mu+1; \frac{2W}{\xi+1}\right) \\
&\times \int_0^\infty dZ\, Z^{\beta+1+\widetilde{\mu}+\zeta}\, e^{-Z} \phi\left(\widetilde{\mu}+\frac{1}{2}, 2\widetilde{\mu}+1; \frac{2Z}{\xi^*+1}\right).
\end{aligned}
\tag{4.60}
$$

The last two integrals are instances of the standard integral 7.621:4 in [5]

$$
\int_0^\infty du\, e^{-u} u^b \phi(a, 2a, ku) = \Gamma(b+1)\, {}_2F_1(a, b+1; 2a; k), \tag{4.61}
$$

and when using this, (4.60) is reduced to the single line integral

$$
\begin{aligned}
\mathcal{I}_+ &= \frac{64^{i\nu}\, q^{*\mu} q^{\widetilde{\mu}}}{\Gamma(\mu+1)\Gamma(\widetilde{\mu}+1)} \frac{m}{2} \int_{C'-i\infty}^{C'+i\infty} \frac{d\zeta}{2\pi i} \Gamma(a/2-\zeta)\Gamma(-a/2-\zeta) \left(\frac{m^2}{4}\right)^\zeta \\
&\times \left(\frac{4}{q^*(\xi+1)}\right)^{2+\alpha+\mu+\zeta} \left(\frac{4}{q(\xi^*+1)}\right)^{2+\beta+\widetilde{\mu}+\zeta} \sin\pi(\alpha+\mu+\zeta)\, (-i)^{\alpha-\beta+n} \\
&\times \Gamma(\alpha+2+\mu+\zeta)\, {}_2F_1\left(\mu+\frac{1}{2},\, \alpha+2+\mu+\zeta;\, 2\mu+1;\, \frac{2}{\xi+1}\right) \\
&\times \Gamma(\beta+2+\widetilde{\mu}+\zeta)\, {}_2F_1\left(\widetilde{\mu}+\frac{1}{2},\, \beta+2+\widetilde{\mu}+\zeta;\, 2\widetilde{\mu}+1;\, \frac{2}{\xi^*+1}\right).
\end{aligned}
\tag{4.62}
$$

We are now ready to express $\mathcal{I}$ in its final form for n even,

$$
\begin{aligned}
&\mathcal{I} = \mathcal{I}_+ - (-1)^n \mathcal{I}_- \\
= \;& \frac{m}{2} \int_{C'-i\infty}^{C'+i\infty} \frac{d\zeta}{2\pi i} \Gamma(a/2-\zeta)\Gamma(-a/2-\zeta)\, \tau_q^{\zeta} \; \left(\frac{4}{|q|}\right)^4 (-i)^{\alpha-\beta+n} \\
&\times \Big[\sin\pi(\alpha+\mu+\zeta)\; B(\alpha,\mu,q^*,\xi,\zeta)\, B(\beta,\widetilde{\mu},q,\xi^*,\zeta) \\
&- \sin\pi(\alpha-\mu+\zeta)\; B(\alpha,-\mu,q^*,\xi,\zeta)\, B(\beta,-\widetilde{\mu},q,\xi^*,\zeta) \Big],
\end{aligned}
\tag{4.63}
$$

where we have introduced the dimensionless parameter $\tau_q = 4m^2/|q|^2$ and the conformal blocks

$$
\begin{aligned}
B(\alpha,\mu,q^*,\xi,\zeta) = & \left(\frac{1}{\xi+1}\right)^{\mu+2+\alpha+\zeta} \left(\frac{4}{q^*}\right)^{\alpha} 2^{-\mu}\, \frac{\Gamma(\alpha+2+\mu+\zeta)}{\Gamma(\mu+1)} \\
& {}_2F_1\left(\mu+\frac{1}{2}\,,\; \mu+2+\alpha+\zeta\,;\; 2\mu+1\,;\; \frac{2}{\xi+1}\right).
\end{aligned}
\tag{4.64}
$$

This expression can be rewritten as

$$
\begin{aligned}
B(\alpha,\mu,q^*,\xi,\zeta) \;=\; & \left(\frac{|\xi|}{\xi}\right)^{\alpha+\mu} (\xi^2-1)^{-(\mu+2+\alpha+\zeta)/2} \left(\frac{4}{q^*}\right)^{\alpha} 2^{-\mu}\, \frac{\Gamma(\mu+2+\alpha+\zeta)}{\Gamma(\mu+1)} \\
& {}_2F_1\left(\frac{\mu+2+\alpha+\zeta}{2}\,,\; \frac{\mu-1-\alpha-\zeta}{2}\,;\; \mu+1\,;\; \frac{1}{1-\xi^2}\right)
\end{aligned}
\tag{4.65}
$$

by using the identities 9.134:1 and 9.131:1 of [5] and assuming n is even, considering that the conformal block will be multiplied with another one. This displays explicitly that the $\xi \leftrightarrow -\xi$ symmetry depends on α and β; there will be an overall factor in the product of conformal blocks,

$$
\left(\frac{|\xi|}{\xi}\right)^{\alpha+\mu} \left(\frac{|\xi^*|}{\xi^*}\right)^{\beta+\widetilde{\mu}} = (\text{sign }\xi)^{\alpha-\beta+n},
\tag{4.66}
$$

when analytically continuing into the physical region $-1 < \xi < 1$.

The results (4.63) and (4.65) show features of earlier calculations of heavy [24] vector meson photoproduction, namely the complex line integral. Also, for $m \to 0$, it gives the amplitudes for light vector meson production in the massless case [25]. Later in this chapter we will show the result in the massless quark limit, and how to obtain it from the present massive quark result.

The obtained expressions for the impact factors are rather complicated and the derivation is rather involved. Therefore we performed an independent test of the results by comparing a direct numerical integration of (4.49) over ρ to the analytical formula for some arbitrary sets of parameters, with the quark mass tending to zero. Full agreement was found in all cases.

Note that when evaluating these expressions numerically it is necessary to carefully consider the branch cut structure of the conformal blocks, which are not single-valued individually. It also proves useful, numerically, to further transform equations (4.64) or (4.65) by *e.g.* using formula 9.132:2 of [5], in the region $4u(1-u) < 0.5$. This also allows explicit isolation the branch cuts outside of the hypergeometric functions. We refer the reader to [43], for a nice exposition of the properties of hypergeometric functions. We refer those with enough enthusiasm to [44].

4.2.4 Results: the BFKL amplitudes

Using the fact that

$$\frac{(-1)^n}{2\pi^2} b_{n,\nu} \left(\frac{|q|}{8}\right)^{2i\nu} \left(\frac{q^*}{q}\right)^{n/2} I_{n,\nu}^{qq^*}(q) \tag{4.67}$$

can be simplified to

$$-\frac{-2\pi^3}{|q|}\frac{1}{\sin \pi i\nu} \tag{4.68}$$

for even n, the helicity amplitudes can be expressed in the following way

$$\mathcal{M}_{+0}^{even} = \frac{isC_V f_V}{4\sqrt{2}|q|} \int_0^1 du\, (1-2u)\phi_{||}(u)$$
$$\sum_{n=-\infty}^{n=+\infty} \int_{-\infty}^{\infty} d\nu \frac{\nu^2+n^2}{[\nu^2+(n-1/2)^2][\nu^2+(n+1/2)^2]} \frac{\exp[\chi_{2n}(\nu)z]}{\sin(i\pi\nu)} I_{0-1}(\nu,2n,q,u;1), \tag{4.69}$$

$$\mathcal{M}^{even}_{++} = \frac{sC_V f_V M_V}{8|q|} \int_0^1 du \left(\frac{g_\perp^{(a)}(u)}{4} - (1-2u) \int_0^u dv (\phi_\parallel(v) - g_\perp^{(v)}(v)) \right)$$
$$\times \sum_{n=-\infty}^{n=+\infty} \int_{-\infty}^{\infty} d\nu \frac{\nu^2+n^2}{[\nu^2+(n-1/2)^2][\nu^2+(n+1/2)^2]} \frac{\exp[\chi_{2n}(\nu)z]}{\sin(i\pi\nu)} I_{00}(\nu,2n,q,u;1), \tag{4.70}$$

$$\mathcal{M}^{even}_{+-} = \frac{sC_V f_V M_V}{8|q|} \int_0^1 du \left(\frac{g_\perp^{(a)}(u)}{4} + (1-2u) \int_0^u dv (\phi_\parallel(v) - g_\perp^{(v)}(v)) \right)$$
$$\times \sum_{n=-\infty}^{n=+\infty} \int_{-\infty}^{\infty} d\nu \frac{\nu^2+n^2}{[\nu^2+(n-1/2)^2][\nu^2+(n+1/2)^2]} \frac{\exp[\chi_{2n}(\nu)z]}{\sin(i\pi\nu)} I_{1-1}(\nu,2n,q,u;1). \tag{4.71}$$

Analogously, one may express the chiral odd amplitudes

$$\mathcal{M}^{odd}_{+0} = \frac{isC_V f_V^T M_V}{4\sqrt{2}|q|} \int_0^1 du \int_0^u dv (h_\parallel^{(t)}(v) - \phi_\perp(v))$$
$$\times \sum_{n=-\infty}^{n=+\infty} \int_{-\infty}^{\infty} d\nu \frac{\nu^2+n^2}{[\nu^2+(n-1/2)^2][\nu^2+(n+1/2)^2]} \frac{\exp[\chi_{2n}(\nu)z]}{\sin(i\pi\nu)} I_{\frac{1}{2}-\frac{1}{2}}(\nu,2n,q,u;0), \tag{4.72}$$

$$\mathcal{M}^{odd}_{++} = \frac{sC_V f_V^T}{4|q|} \int_0^1 du\, \phi_\perp(u)$$
$$\times \sum_{n=-\infty}^{n=+\infty} \int_{-\infty}^{\infty} d\nu \frac{\nu^2+n^2}{[\nu^2+(n-1/2)^2][\nu^2+(n+1/2)^2]} \frac{\exp[\chi_{2n}(\nu)z]}{\sin(i\pi\nu)} I_{-\frac{1}{2}-\frac{1}{2}}(\nu,2n,q,u;0), \tag{4.73}$$

$$\mathcal{M}^{odd}_{+-} = \frac{sC_V f_V^T M_V^2}{8|q|} \int_0^1 du \int_0^u dv \int_0^v d\eta \left(h_{\parallel}^{(t)}(\eta) - \frac{1}{2}\phi_\perp(\eta) - \frac{1}{2}h_3(\eta) \right)$$
$$\times \sum_{n=-\infty}^{n=+\infty} \int_{-\infty}^{\infty} d\nu \frac{\nu^2+n^2}{[\nu^2+(n-1/2)^2][\nu^2+(n+1/2)^2]} \frac{\exp[\chi_{2n}(\nu)z]}{\sin(i\pi\nu)} I_{\frac{3}{2}-\frac{1}{2}}(\nu, 2n, q, u; 0). \tag{4.74}$$

The constant, $C_V = i((N^2-1)/N^2)ee_q\alpha_s^2$. The derivation of integrals (4.49) for integer difference[5] $\alpha-\beta$ was given in the previous section, and the result reads

$$I_{\alpha\beta}(\nu,n,q,u;a) = \frac{m}{2}\int_{C'-i\infty}^{C'+i\infty} \frac{d\zeta}{2\pi i}\Gamma(a/2-\zeta)\Gamma(-a/2-\zeta)\,\tau_q^\zeta\ (i\,\mathrm{sign}\,(1-2u))^{\alpha-\beta+n}$$
$$\times \left(\frac{4}{|q|}\right)^4 \Big[\sin\pi(\alpha+\mu+\zeta)\ B(\alpha,\mu,q^*,u,\zeta)\,B(\beta,\widetilde{\mu},q,u^*,\zeta)$$
$$-(-1)^n\sin\pi(\alpha-\mu+\zeta)\ B(\alpha,-\mu,q^*,u,\zeta)\,B(\beta,-\widetilde{\mu},q,u^*,\zeta)\Big] \tag{4.75}$$

where we have introduced the dimensionless parameter $\tau_q = 4m^2/|q|^2$ and the conformal blocks

$$B(\alpha,\mu,q^*,u,\zeta) = (-4u\bar{u})^{-(\mu+2+\alpha+\zeta)/2}\left(\frac{4}{q^*}\right)^\alpha 2^{-\mu}\,\frac{\Gamma(\mu+2+\alpha+\zeta)}{\Gamma(\mu+1)}$$
$${}_2F_1\left(\frac{\mu+2+\alpha+\zeta}{2}, \frac{\mu-1-\alpha-\zeta}{2}; \mu+1; \frac{1}{4u\bar{u}}\right). \tag{4.76}$$

Note, that the sums are performed over even conformal spins $2n$ due to properties of the quark impact factor (4.31). It turns out that odd conformal spin components of photon-meson impact factors (4.14, 4.15, 4.16, 4.17, 4.18, 4.19) all vanish. The impact factors are symmetric under the coordinate transformation given by ($\rho\to-\rho$, $u\to$

[5]The condition of integer $\alpha-\beta$ is necessary for the amplitudes to be single valued.

$1-u$). The parity behaviour (4.42) of conformal eigenfunctions applied to (4.75) leads to the relation

$$I_{\alpha\beta}(\nu,n,q,u;a)=(-1)^{n+\alpha-\beta}I_{\alpha\beta}(\nu,n,q,1-u;a). \tag{4.77}$$

These results may be combined to give $I_{n,\nu}^{\gamma(\lambda)V(\lambda')}=0$ for odd n.

4.2.5 The massless quark limit

In [25] the formulae corresponding to (4.63) and (4.65) were computed in the approximation of zero quark mass. This corresponds to using the small argument behaviour for the case $a=1$, relevant for the calculation of chiral even amplitudes,

$$mK_1(m|\rho|)\sim 1/|\rho|. \tag{4.78}$$

Then we obtain a simpler result $\mathcal{J}=\mathcal{I}|_{m=0}$ not involving the line integral over ζ:

$$\begin{aligned}\mathcal{J} &= \left(\frac{4}{|q|}\right)^4 (-i)^{\alpha-\beta+n}\ [\sin\pi(\alpha+\mu-1/2)\ C(\alpha,\mu,q^*,\xi)\, C(\beta,\widetilde{\mu},q,\xi^*)\\ &- (-1)^n\sin\pi(\alpha-\mu-1/2)\ C(\alpha,-\mu,q^*,\xi)\, C(\beta,-\widetilde{\mu},q,\xi^*)\ ]\,,\end{aligned} \tag{4.79}$$

where the $C(\alpha,\mu,q^*,\xi)$ conformal blocks are given by[6] $B(\alpha,\mu,q^*,\xi,\zeta=-1/2)$

$$\begin{aligned}C(\alpha,\mu,q^*,\xi)=\left(\frac{|\xi|}{\xi}\right)^{\alpha+\mu}(\xi^2-1)^{-(\mu+3/2+\alpha)/2}\left(\frac{4}{q^*}\right)^{\alpha}2^{-\mu}\,\frac{\Gamma(\mu+3/2+\alpha)}{\Gamma(\mu+1)}\\ {}_2F_1\left(\frac{\mu+3/2+\alpha}{2},\frac{\mu-1/2-\alpha}{2};\mu+1;\frac{1}{1-\xi^2}\right).\end{aligned} \tag{4.80}$$

The calculation proceeds in a similar way to the preceding one and we do not show the details here. It should also, however, be possible to recover the massless result from the massive one by taking the limit $m\to 0$. This can be done by taking the leading pole approximation for the ζ integral in the limit $\tau_q=4m^2/|q|^2\to 0$. The results the reduce to those calculated for the chiral even BFKL helicity amplitudes in the light-quark limit [45]. The product of gamma functions in the integrand becomes $\Gamma(1/2-\zeta)\Gamma(-1/2-\zeta)$ and there is a simple pole at $\zeta=-1/2$ and double poles at

[6]The substitution $\zeta=-1/2$ is made to keep the definitions of α and β the same, because there is a difference by a factor of $|\rho|$ between the massless and massive integrand.

$\zeta = 1/2, 3/2, \ldots$. The double poles, however, vanish in the limit $\tau_q \to 0$, and using the residue theorem for the pole at $\zeta = -1/2$ reproduces the massless result (4.79). Note that formula (4.79) is a generalisation of an integral calculated in [41] for $\alpha = \beta$, and we have checked that our result agrees.

The perturbative chiral-odd photon wave function corresponds to $a = 0$ and is proportional to $mK_0(m|\rho|) \to -m\ln(m|\rho|)$, and therefore vanishes in the massless limit.

We stress that the above formulae (i.e. in the massless limit) are only reliable away from the regions of u close to 0 or 1. Figure 4.2 illustrates this by comparing the full $\mathcal{M}^{even}_{++}$ amplitude (differential in u) to its pole approximation, over a range of u. This particular amplitude was chosen because [25] demonstrated that this amplitude is divergent when the two-gluon and light-quark approximations are taken simultaneously. Note that for $4u(1-u) > 0.5$, the agreement is excellent between the pole approximation and the full result, for all the masses plotted. The pole approximation diverges as $1/u$ as $u \to 0$; this implies a logarithmic divergence in the integrated $\mathcal{M}^{even}_{++}$ amplitude. Anything that diverges more weakly than the pole approximation will give a finite integrated amplitude. Note that for the full expression we get a peak in the differential amplitude at $u \sim m/q$, below which in u, the amplitude falls to zero. The naive expectation that as $m \to 0$, the full expression tends to the pole approximation over the whole u range, is disproved. Observe that as we lower the quark mass to very low values the full result dips increasingly beneath the pole approximation curve. It looks as if the full amplitude is convergent in the limit $m \to 0$. This is in fact the case, as figure 4.3 clearly shows. In effect, the true expansion parameter is more like $m^2/(u(1-u)|q|^2)$ and this is not small at the endpoints. In particular, a careful treatment reveals that there are no endpoint singularities in the full amplitude in the massless limit (see Appendix E).

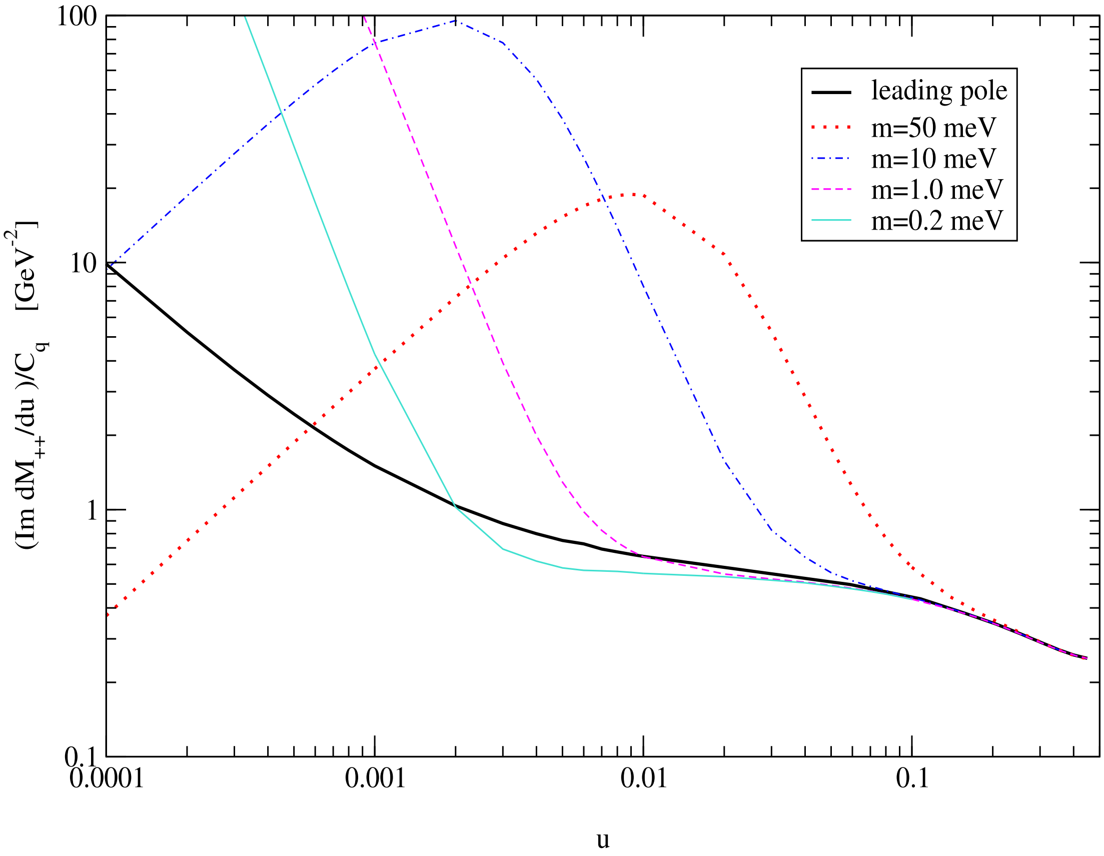

Figure 4.2: The $\mathcal{M}_{++}^{even}$ amplitude differential in u plotted against u. The thick solid line shows the leading pole approximation. The other curves show the full amplitude for different m. The fixed parameter values are $(z, m_V, |t|) = (1.0, m_\rho, 10\,\mathrm{GeV}^2)$. The constant, $C_q = s\alpha_s^2(N^2 - 1/N^2)f_V m_V e e_q$. The asymptotic distribution amplitudes were used.

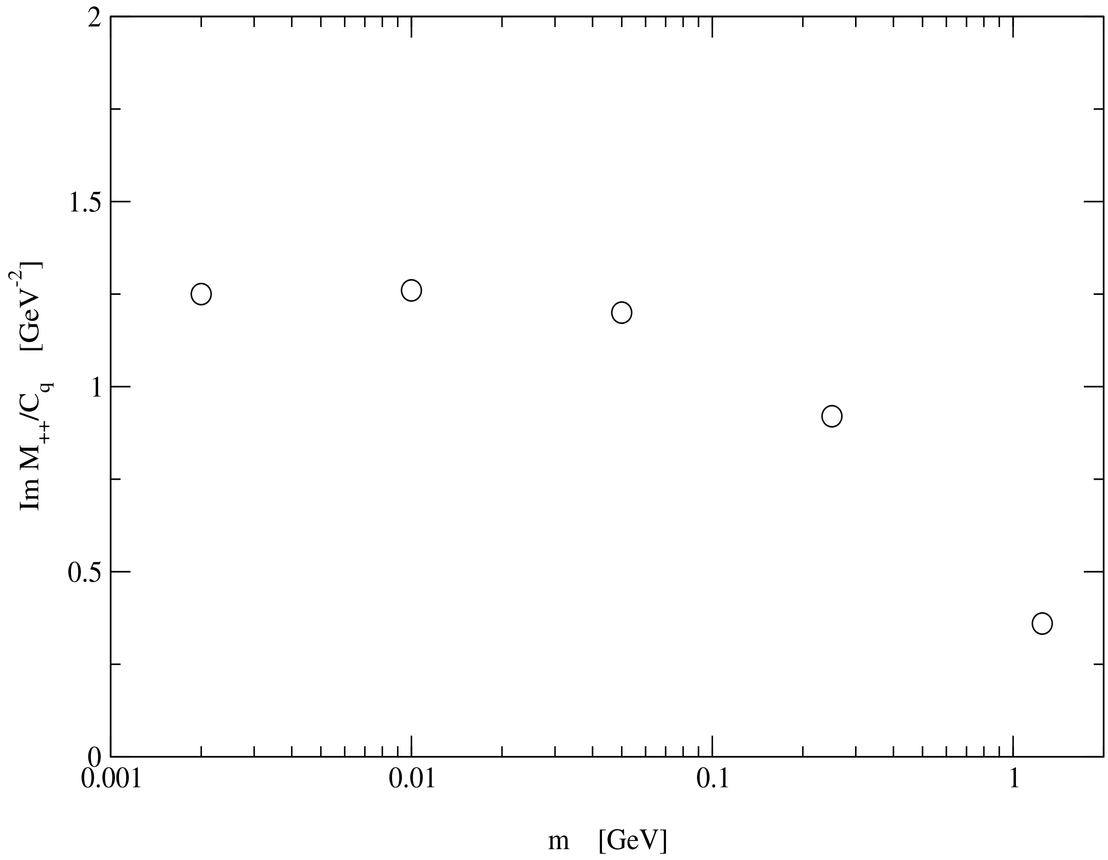

Figure 4.3: The $\mathcal{M}_{++}^{even}$ amplitude against m, the quark mass parameter. The circles are numerical results using the formulae (4.70, 4.75). The fixed parameter values are $(z, m_V, |t|) = (1.0, m_\rho, 10\,\mathrm{GeV}^2)$. The constant, $C_q = s\alpha_s^2(N^2 - 1/N^2)f_V m_V e e_q$. The asymptotic distribution amplitudes were used.

4.3 Summary

In section 4.1. we explicitly wrote down the complete two-gluon exchange helicity amplitudes. This was the culmination of the work done in Chapter 2 and our results agree with those of [25]. The authors of [25] found the $\mathcal{M}_{++}^{even\,2g}$ amplitude to have logarithmic divergent contributions from the end-points in u, that is where $u(1-u) \to 0$. In section 4.2 we extended the calculation to higher orders, again using the solution to the BFKL equation. We demonstrated that the $\mathcal{M}_{++}^{even}$ amplitude is now finite, away from $z = 0$. The results for the full set of helicity amplitudes are new. They have recently been published in [46]. We now finally proceed to consider the phenomenology of our results.

Chapter 5

Phenomenology

5.1 The experiments

It is time to emerge from the mathematics and return to physics. We make a brief recap. Let us remind ourselves of the experimental situation for $\gamma p \to VX$ and enlarge on some details. We consider an incident photon and proton which define our z-axis. The momentum transfered between the two particles we define q; it is dominated by its transverse part: $t = q^2 \simeq -\boldsymbol{q}^2$. We choose to define the momentum exchanged between the two particles to be in the positive x-direction, as illustrated in figure 5.1. This is in agreement with the conventions used by experimentalists [47] and in fact simplifies our theoretical analysis (see Appendix C). The vector meson exiting the interaction defines a coordinate system rotated in $x - z$ with respect to the one defined by the initial state particles.

The initial state photon has a small virtuality and is therefore quasi-real and thus the possible helicity states can be described by the transverse polarisation vectors

$$\boldsymbol{e}^{(\pm)} = \mp \frac{1}{\sqrt{2}}(1, \pm i). \tag{5.1}$$

The rotation due to momentum exchange is small as we are in the Regge region ($\hat{s} \gg |t|$ and $\cos\theta \sim 1 + 2t/\hat{s}$; see section 4.1.1) and so we can make the identification

$$e_V^{(\pm)} \simeq e^{(\pm)}. \tag{5.2}$$

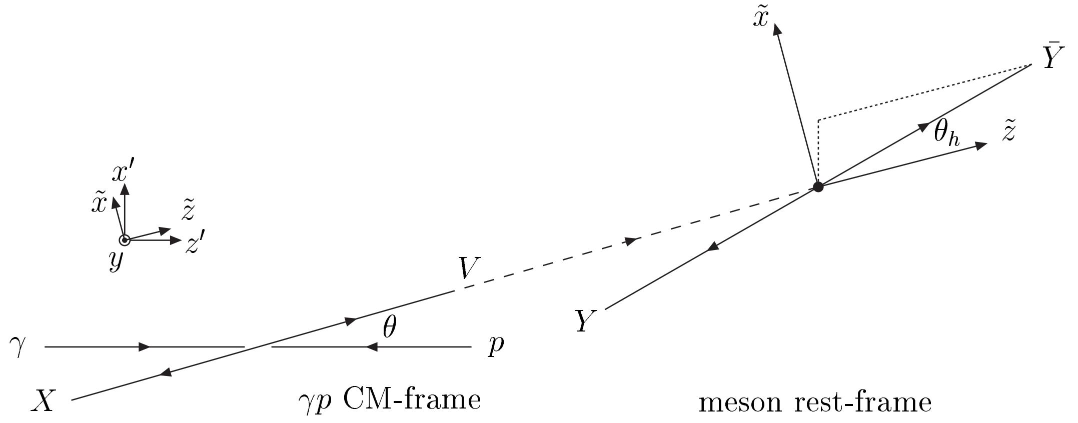

Figure 5.1: The coordinate systems defined by the initial (γp) and final (VX) states.

The vector meson as a massive vector boson has an additional longitudinal degree of freedom; to leading accuracy we can write this (in the centre-of-mass frame)

$$e^{(0)} = \frac{p}{m_V}, \tag{5.3}$$

where p is the 4-momentum of the meson and m_V is its mass (see Appendix A for more details). The possible photon-meson transitions may be described using three independent helicity amplitudes $\mathcal{M}_{++}$ (no-flip), $\mathcal{M}_{+0}$ (single-flip) and $\mathcal{M}_{+-}$ (double-flip), each with both a possible chiral odd (spins aligned) and chiral even (spins anti-aligned) configuration of quark and anti-quark exiting the hard scatter (see section 2.3.1)[1]. So far the details above apply to both the ZEUS and H1 measurements at HERA. We will now enlarge on the particulars of the two experiments.

The ZEUS data are for the energy range $80 < W_{\gamma p} < 100\,\mathrm{GeV}$ with the mean value approximately central. Their measurements are for $1 < -t < 10\,\mathrm{GeV}^2$. Their choice of cut was in $-(m_X^2 - m_p^2)/t$, where m_X is the mass of the proton remnants and

[1]There are also the corresponding amplitudes $\mathcal{M}_{--}$, $\mathcal{M}_{-0}$ and $\mathcal{M}_{-+}$.

m_p the mass of the proton; they imposed $-(m_X^2 - m_p^2)/t < 100\,\mathrm{GeV}^2$. The relation

$$m_X^2 - m_p^2 = -t(1/x - 1) \tag{5.4}$$

translates this to a cut of $x > 0.01$ in the more theoretically useful Bjorken-x variable. The ZEUS collaboration quote a photon virtuality restriction $Q^2 < 0.02\,\mathrm{GeV}^2$ with $\langle Q^2 \rangle \sim 10^{-5}\,\mathrm{GeV}^2$. This smallness allows us to neglect Q^2 in the kinematic relations and in our theoretical calculation. We shall not discuss the details of the event selection (for more details see [21]). We note only that the ρ, ϕ and J/ψ are tagged by their respective two-body decays to $\pi\pi$, KK and ll, where ll is a lepton pair. The events are restricted to those in which the two-body decay has an invariant mass close to the meson in question.

The H1 data are for J/ψ production only, and in the energy range $50 < W_{\gamma p} < 150\,\mathrm{GeV}$ with the mean value approximately central. Their measurements are for $2 < -t < 30\,\mathrm{GeV}^2$ and their choice of cut was in the 'elasticity' variable z, which is related to m_X to a good approximation (for the J/ψ) by

$$z \simeq 1 - (m_X^2 - t)/W_{\gamma p}. \tag{5.5}$$

H1 quote $m_X < 30\,\mathrm{GeV}$ which translates to $z > 0.95$ and $x_{min} \simeq -t/(1-z)s$. H1 quote the photoproduction event sample to have the restriction $Q^2 < 1\,\mathrm{GeV}^2$ with $\langle Q^2 \rangle \sim 0.06\,\mathrm{GeV}^2$, again small enough to consider the process to be photoproduction. The J/ψ two-body decay to leptons (muons) is again the measured decay channel [22].

5.2 The observables

The model we are using for the diffractive process $\gamma p \to VX$ at large momentum transfer t is the exchange of the leading log BFKL pomeron (see figure 5.2). It has been shown that at large momentum transfer, the hard pomeron couples predominantly to individual partons in the proton [19]. This was also discussed in section 1.6 of this thesis. The cross-section may therefore be factorised into a product of the parton level

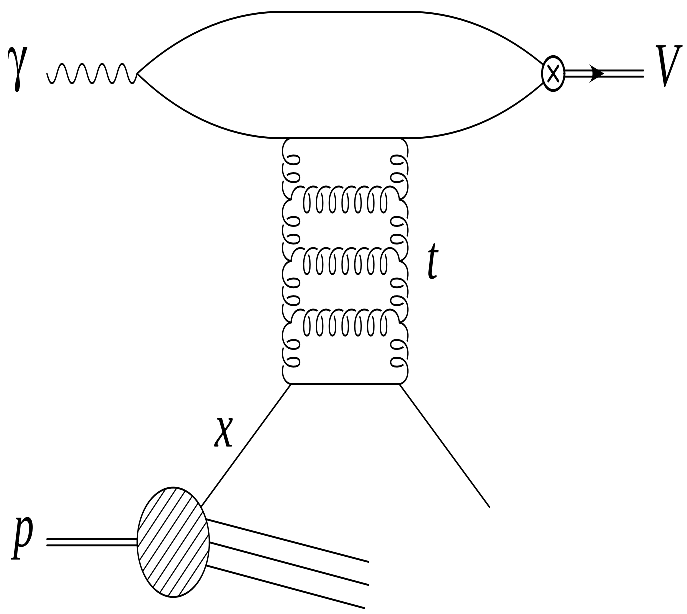

Figure 5.2: Diffractive vector meson photoproduction at large momentum transfer.

cross-section and the parton distribution functions,

$$\frac{d\sigma(\gamma p \to VX)}{dt\, dx_j} = \left(\frac{4N^4}{(N^2-1)^2}G(x_j,t) + \sum_f [q_f(x_j,t) + \bar{q}_f(x_j,t)]\right)\frac{d\sigma(\gamma q \to Vq)}{dt}, \tag{5.6}$$

where $N = 3$, $G(x_j, t)$ and $q_f(x_j, t)$ are the gluon and quark distribution functions respectively[2], and s is the γp centre-of-mass energy squared. The struck parton in the proton, that initiates a jet in the proton hemisphere, carries a fraction x_j of the longitudinal momentum of the incoming proton. For future use, we introduce the integrated quantity

$$\left\langle \frac{d\sigma(\gamma q \to Vq)}{dt} \right\rangle = \int_{\text{cuts}} dx_j \, \frac{d\sigma(\gamma p \to VX)}{dt\, dx_j}. \tag{5.7}$$

The partonic cross-section, characterised by the invariant collision energy squared $\hat{s} = x_j s$ is expressed in terms of the amplitudes $M_{\lambda\lambda'}(\hat{s}, t)$,

---

$$\frac{d\sigma}{dt} = \frac{1}{16\pi \hat{s}^2}\left(|M_{++}(\hat{s},t)|^2 + |M_{+0}(\hat{s},t)|^2 + |M_{+-}(\hat{s},t)|^2\right). \tag{5.8}$$

[2]The relative colour factor between the quark and gluon PDF comes from the eikonal approximations for gluons and quarks. This colour factor has been pulled outside the scattering amplitude definition *i.e.* the parton level amplitudes are defined for $\gamma q \to Vq$ rather than for $\gamma g \to Vg$.

To obtain a value for $d\sigma/dt$, experimentalists measure the number of events in a certain 'bin' of t. This value alone, however, can tell us nothing about the interplay of the helicity amplitudes, only their squared sum. To access this information, the angular distribution of the decay products of the vector meson have also been measured. The reason this helps is that the cross-section for $\gamma p \to VX$ is reconstructed from that of $\gamma p \to VX \to Y\bar{Y}X$, where $Y\bar{Y}$ are the specific two body decay products of the vector meson, V. The polarisation of the intermediate meson is therefore not measured. Quantum mechanics dictates that if we don't measure the state of the intermediate state, then there will be interference effects between all the possible polarisations. Appendix C shows this explicitly and we find that the interference effects result in an angular distribution [47]

$$\frac{d^2\sigma}{d\cos\theta_h\, d\phi_h} \propto \left[\frac{1}{2}(1 \mp r^{04}_{00}) \pm \frac{1}{2}(3r^{04}_{00} - 1)\cos^2\theta_h \right.$$
$$\left. \mp\sqrt{2}\mathrm{Re}[r^{04}_{00}]\,\sin 2\theta_h\,\cos\phi_h \mp r^{04}_{1-1}\,\sin^2\theta_h\,\cos 2\phi_h\right], \tag{5.9}$$

where the upper (lower) signs are for spin-0 (spin-1/2) particles. θ_h and ϕ_h are the decay angles of the positive particle of the two body decay, where the vector meson momentum defines the z-axis and the x-axis is defined to lie in the direction of the hard momentum exchange, $|\mathbf{q}|$. The r-matrix elements can be written [47, 48, 49]

$$r^{04}_{00} = \frac{\langle |M_{+0}|^2\rangle}{\langle |M_{++}|^2 + |M_{+0}|^2 + |M_{+-}|^2\rangle}, \tag{5.10}$$

$$r^{04}_{10} = \frac{1}{2}\frac{\langle M_{++}M^*_{+0} + M_{+-}M^*_{-0}\rangle}{\langle |M_{++}|^2 + |M_{+0}|^2 + |M_{+-}|^2\rangle}, \tag{5.11}$$

$$r^{04}_{1-1} = \frac{1}{2}\frac{\langle M_{++}M^*_{+-} + M_{+-}M^*_{++}\rangle}{\langle |M_{++}|^2 + |M_{+0}|^2 + |M_{+-}|^2\rangle}, \tag{5.12}$$

---

twist	2	3	4
single-flip	$\mathcal{M}^{even}_{+0}$	$\mathcal{M}^{odd}_{+0}$	–
no-flip	$\mathcal{M}^{odd}_{++}$	$\mathcal{M}^{even}_{++}$	–
double-flip	–	$\mathcal{M}^{even}_{+-}$	$\mathcal{M}^{odd}_{+-}$

Table 5.1: Classification of helicity amplitudes in twist.

where r^{04}_{ij} are spin density matrix elements and $\langle ... \rangle$ denotes the integration of the parton level quantities over partonic x_j with the appropriate cuts (as for (5.7)).

Therefore the four observables we wish to confront our analytic formulae with are $d\sigma/dt$ and the set of three r-matrix elements. These observables have all been measured by the ZEUS and H1 collaborations and we compare to their data [21].

For simplicity we chose a single fixed value for the γp centre-of-mass energy in our theoretical predictions: $s = W^2_{\gamma p} = 10^4\,\mathrm{GeV}^2$. The energy dependence of the observables is also in principle an important element to look in to. The QCD pomeron typically has a higher intercept than the Regge pomeron and consequently has a stronger energy dependence.

5.3 Parameters and prescriptions

The vector meson matrix elements have been calculated in an expansion about $\mathbf{r}^2 = 0$, where $\mathbf{r}$ is the transverse size of the dipole. Higher orders in $(m_V\mathbf{r})$ correspond to higher orders in $(m_V/|\mathbf{q}|)$, after integration over size. These factors are referred to as 'twist', one unit of twist corresponding to one factor of $(m_V/|\mathbf{q}|)$. The lowest order contribution to the light-cone hadronic matrix element corresponds to twist-2. The authors of [32, 33] give the complete set of hadronic matrix elements up to twist-4 and they present results for the distribution amplitudes that define them. Table 5.1 gives the classification of the six helicity amplitudes in terms of the lowest non-zero twist contribution to their hadronic matrix element[3].

[3]An inspection of the formula (4.75), in conjunction with expressions (4.69-4.74) for the helicity amplitudes, shows that the scattering amplitudes do indeed have the associated relative suppression in integer powers of $|\mathbf{q}|$, modulo '$m/|\mathbf{q}|$' effects.

Counting twist in the hadronic matrix element alone, however, is not sufficient to gauge the overall pattern of power suppression in $|\mathbf{q}|$ of our observables; the other piece corresponding to the hard scatter may be important. It may boost or suppress certain helicity amplitudes relative to each other. Twist gives us the suppression in $m_V/|\mathbf{q}|$, but through the photon wavefunction we also have dependence on powers of the scale $m/|\mathbf{q}|$, where m is the quark mass[4]. We will not assume that m vanishes, or is small, so we cannot simply identify the affect of these terms. Taking a pragmatic approach we will assume that we can use the twist of the hadronic matrix elements as our criteria for suppression in $|\mathbf{q}|$. We will then test the validity of this assumption by numerical results.

In chapters 3 and 4 we arrived at the complete analytic formulae up-to twist-3 for the helicity amplitudes, to leading log accuracy. To obtain the first non-zero chiral odd contribution to helicity double-flip we were obliged to work to twist-4 in that amplitude. We therefore only have *complete* information to next-to-leading order in twist. We will test the importance of the $|\mathbf{q}|$ suppressed terms we do know, to estimate the sensitivity of our observables to unknown higher twist terms.

The treatment of the quark mass parameter, m, is of crucial importance in this calculation. Strictly, in perturbation theory, we should use the current quark mass. Experimental measurement of the up and down quark masses gives the range $2.5 < \frac{m_u+m_q}{2} < 6\,\text{MeV}$ as appropriate for the ρ meson. Such a small mass renders the chiral odd contribution negligible. A calculation with a small quark mass proves to be incapable of describing the r-matrix elements. Ivanov *et al* in [25] noted the importance of introducing a large chiral odd contribution. The method they employ replaces the perturbative photon wavefunction which is exponentially suppressed in r for large r, with one that is r independent. They then argue for a sizable non-perturbative parameter associated with this non-perturbative photon wavefunction. We shall take a different approach. In past calculations, the replacement of the current

[4]To see this note that in $\mathbf{r}$ space we have integrals over $K_1(m|\mathbf{r}|)$ (even) and $K_0(m|\mathbf{r}|)$ (odd) Bessel functions. Rescaling $\hat{r} = |\mathbf{r}|/\mathbf{q}|$ extracts the powers of $\mathbf{q}$ associated with the twist of the hadronic matrix elements, and leaves dependence on a scale $m/|\mathbf{q}|$, which for fixed m affects the true nature of the power counting. We also see this scale appear when we are in the line integral representation, rather than $\mathbf{r}$ space (see (4.75)).

quark mass with the constituent quark mass has given surprisingly good results, not least for this very process [23]. We shall put $m = m_V/2$; we will also investigate the sensitivity to this parameter.

There are many parameters involved in the calculation of numbers for the observables. Many are associated with just the meson matrix element; f_V and f_V^T are the most important of these. As an exploration of BFKL dynamics, it is the systematic investigation of the effect of the parameters involved with the hard subprocess that is of primary importance in this thesis; this means how we implement the strong coupling, α_s, the BFKL scale and the two scales it could depend on, $\Lambda^2 = \beta m_V^2 - \gamma t$, and finally the quark mass, m. We have already eliminated our freedom with regard to the quark mass parameter by fixing it at the constituent mass. We will also choose at this point to fix, $\beta = 1$. We choose to do this since a change in its value can approximately be traded off with a change in α_s. This simplifies matters a little. We remind the reader that the BFKL Λ^2 scale appears in the definition of 'z' rapidity (see (1.52))

$$z = \frac{3\alpha_s}{2\pi} \ln\left(\frac{xs}{\Lambda^2}\right). \tag{5.13}$$

We note that it is vital to keep our freedom to vary γ within Λ^2, as this has a direct effect on the t dependence of cross-sections.

Notice that α_s appears in two very different places. It appears as $(\alpha_s)^2$ as a constant in front of every helicity amplitude. It also appears in the definition of 'z'. The sources of these two are very different. The overall factor is from the couplings of the two gluons to each impact factor. The 'BFKL' coupling, however, is generated by the gluon couplings inside the gluon ladder. We shall denote them α_S^{IF} and α_s^{BFKL}. How then should we treat these strong couplings? A fixed α_s is appropriate to the level of our calculation, that of leading logs. Next-to-leading logs will cause α_s to run, however. We could still approximately account for this by running α_s globally with $|\mathbf{q}|$ (rather than with the momentum at every vertex). However, arguments exist that the effect of next-to-leading logs is to effectively fix α_s^{BFKL} [50]. Phenomenologically fixing α_s^{BFKL} has proved successful in the past [51, 23]. We will also fix it here. We remain free to run or fix the impact factor coupling, α_s^{IF}, and we shall subsequently make use of this possibility. When we refer to a running coupling in future, we shall be referring to the following expression derived from the one loop β-function [52]:

$$\alpha_s^{IF}(q^2) = \frac{\alpha_s(\mu^2)}{1 + \alpha_s(\mu^2) b \ln\left(\frac{q^2}{\mu^2}\right)}, \tag{5.14}$$

where $b = (33 - 2n_f)/12\pi$ with n_f being the number of active flavours. We choose $n_f = 4$. We will always quote α_s^{IF} at 1 GeV. The next-to-leading order BFKL contributions are expected to mainly affect the normalisation of predictions, rather than the t-dependence, and so choosing the value of α_s^{IF} at 1 GeV is a way of approximately modelling next-to-leading order effects in the cross-section. We note that, as ratios, the r-matrix elements are independent of α_s^{IF}.

In summary, the parameters we shall treat as free for fitting purposes are:

$$\alpha_s^{IF} \qquad \alpha_s^{BFKL} \qquad \text{and} \qquad \Lambda^2 = m_V^2 - \gamma \tag{5.15}$$

We shall also show the sensitivity of our variables to the quark mass

$$m$$

though we shall not treat this as a fitting parameter.

For other parameters, we shall use those either measured by experiment or estimated in the literature. We shall not 'play' with these. The sensitivity of the predictions to higher twist and the form of the distribution amplitude will be tested by testing the importance of $1/|\mathbf{q}|^2$ suppressed and above terms and by employing three different distribution amplitude (DA) prescriptions. The three prescriptions are the δ-function, the asymptotic distribution amplitudes (obtained in the limit $\alpha_s \to 0$) and the distribution amplitudes of Ball and Braun and Ball, Braun, Koike and Tanaka (BBKT)[32, 33]. More details on the distribution amplitude prescriptions can be found in Appendix D.

Finally, we now present the parameters appearing in the literature. All the helicity amplitudes depend on the vector meson coupling constants; either f_V (vector) or f_V^T

	ρ	ϕ	J/ψ
f_V [GeV]	0.216	0.231	0.405
$f_V^T(1\,\mathrm{GeV})$ [GeV]	0.160	0.215	(0.405)

Table 5.2: The meson strong couplings [33].

	ρ	ϕ	J/ψ
Q_V	$1/\sqrt{2}$	$-1/3$	$2/3$

Table 5.3: The meson charge couplings.

(tensor). Table 5.2 presents the vector meson vector and tensor couplings for the relevant mesons. The vector coupling are directly measurable from the electronic decay width of the vector mesons (see Appendix B). The tensor couplings have been calculated at $\mu^2 = 1\,\mathrm{GeV}^2$ using QCD sum rules in [33][5]. Table 5.3 presents the charge coupling associated with the relevant vector mesons. The additional parameters associated with BBKT DA are listed in Appendix D.

[5]The tensor coupling for the J/ψ value is unavailable in the literature and so we, as default, put it equal to the vector coupling.

5.4 Phenomenology for the ρ meson.

We will start with the most crude approximations and relax these systematically.

5.4.1 The collinear and δ-function approximations

This fits of this section are based on the analytic results of Chapter 3, compared with the ZEUS photoproduction data for the ρ.

We remind the reader of the result of section 3.1.1, that the collinear approximation corresponds to putting the transverse momentum of the quark in the dipole, $\tilde{\mathbf{l}}$, with respect to the final state meson direction, to zero, leaving the transverse momenta of the quark and anti-quark with respect to the photon-proton axis, $\mathbf{q}_1$ and $\mathbf{q}_2$, functions of $\mathbf{q}$ and u only (see results (3.5)). The resulting integration over $\tilde{\mathbf{l}}$ in the hard scatter generates δ-functions in $\mathbf{r}$ that force the transverse size of the dipole to zero (see (3.8) and (3.9)). This fact forces all the higher twist helicity amplitudes, which depend on non-zero powers of $\mathbf{r}$, to zero. Only the leading $\mathcal{M}^{even}_{+0}$ and $\mathcal{M}^{odd}_{++}$ of twist-2 survive.

The δ-function approximation for the meson distribution amplitudes is equating

$$\phi_{\|}(u) = \phi_{\perp}(u) = \delta(u - 1/2). \tag{5.16}$$

Only the vector component of the Fierz decomposition contributes to the production of a longitudinal vector meson (see (2.154)). The corresponding part of the trace appearing in the hard subprocess (see (2.144)) has a $(1 - 2u)$ factor. The $\mathcal{M}^{even}_{+0}$ helicity amplitude is therefore zero in the δ-function approximation for the distribution amplitudes. The only non-zero amplitude is $\mathcal{M}^{odd}_{++}$ (see (3.53) in Chapter 3).

The non-zero helicity amplitude in the collinear approximation with δ-function distribution amplitudes

---

$$
\begin{aligned}
\mathcal{M}_{++}^{odd} &= sC_V \frac{8\pi}{t^2} f_V m_V \\
\times \sum_{m=-\infty}^{m=\infty} \left(-\frac{1}{4}\right)^{|m|} &\int d\nu \, \frac{\nu^2 + m^2}{(\nu^2 + (m-1/2)^2)(\nu^2 + (m+1/2)^2)} \, e^{\chi_m(\nu) z} \\
&\times \int_{-i\infty}^{i\infty} \frac{ds}{2\pi i} \, \tau^{1/2+s+|m|} \, \frac{\Gamma(1-s-i\nu)\,\Gamma(1-s+i\nu)}{\Gamma(1-s/2-i\nu/2)\,\Gamma(1-s/2+i\nu/2)} \\
&\times \frac{\Gamma^2(1/2+s+|m|)}{\Gamma(1/2+s/2-i\nu/2+|m|)\,\Gamma(1/2+s/2+i\nu/2+|m|)},
\end{aligned}
\tag{5.17}
$$

where[6], $C_V = i((N^2-1)/N^2) e Q_V \alpha_s^2$.

Figure 5.3 shows the predictions for $d\sigma/dt$ for three different sets of parameter values. Running the scale Λ^2 that appears under s in the BFKL log with t or running α_s^{IF} with t prove to predict t dependencies that are too steep and incompatible with the data presented by ZEUS [21]. Fixing the strong coupling in the impact factor and in the BFKL ladder in addition to the BFKL logarithm yields a good fit. These results agree with those of Forshaw and Poludniowski for the leading conformal spin component $(n = 0)$[7][23].

Since only the $\mathcal{M}_{++}^{odd}$ amplitude is non-zero with the collinear and δ-function approximations imposed, referring to their definitions ((5.10), (5.11), (5.12)), we see that this enforces all the r-matrix elements to zero. Figure 5.4 shows this prediction in comparison to the ZEUS data. We see that zero r-matrix elements are compatible with data for r_{10}^{04}, in fair agreement for r_{10}^{04} and in poor agreement for r_{1-1}^{04}.

[6] We have substituted $e_q \to Q_V$, as noted in the derivation of the $\gamma q\bar{q}$ impact factor.

[7] Note that in [23], the authors implicitly equated the tensor vector meson coupling, f_V^T, to the vector coupling, f_V, rather than using the value estimated from QCD sum rules.

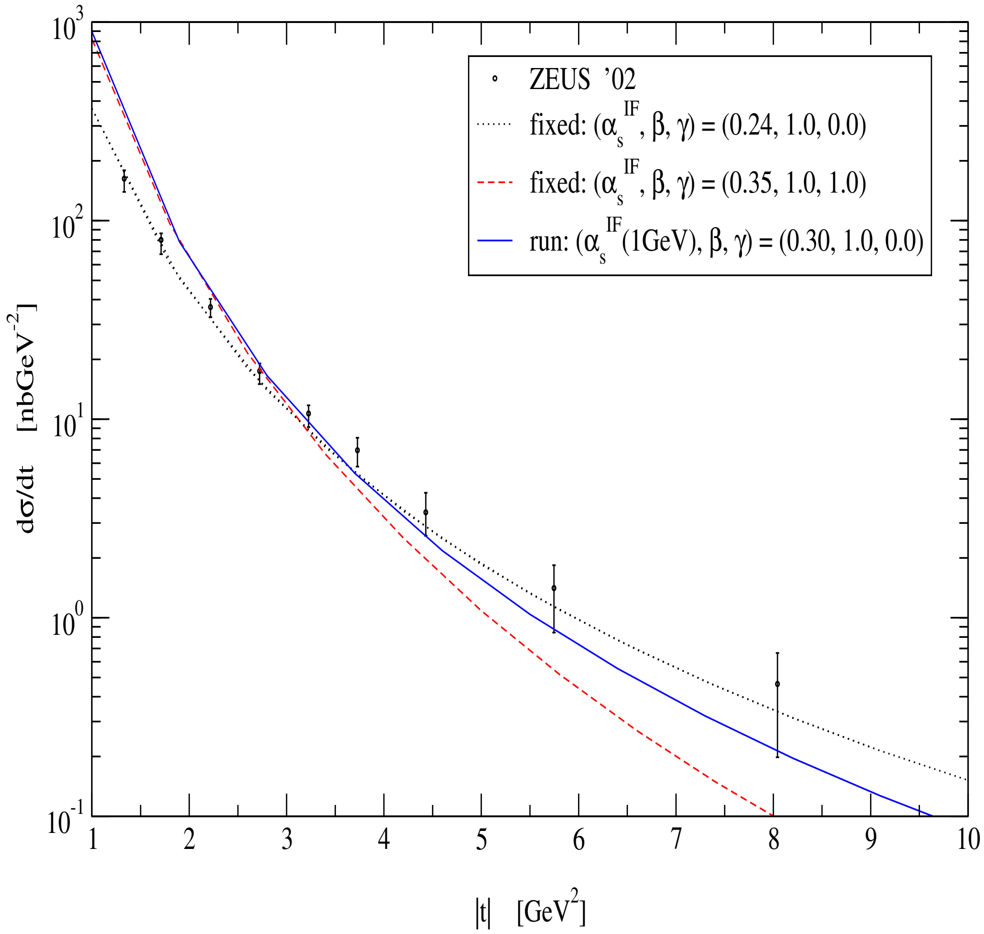

Figure 5.3: Collinear and δ-function approximation: $d\sigma/dt$ for parameter values, $(\alpha_s^{BFKL},\, m) = (0.2,\, m_\rho/2)$.

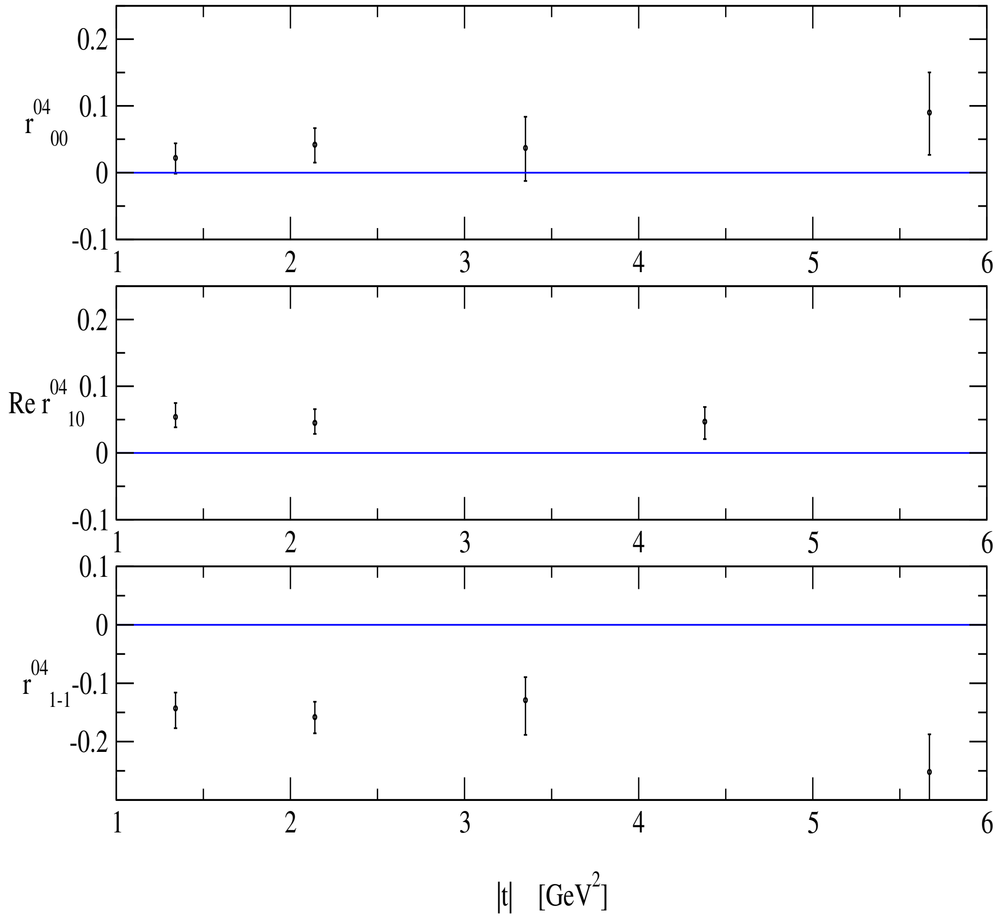

Figure 5.4: Collinear and δ-function approximation: r-matrix elements. The predictions are parameter independent.

5.4.2 Collinear approximation and asymptotic distribution amplitudes

The use of a δ-function distribution amplitude is a crude approximation. For the charm quark and J/ψ meson, $m_c \sim m_{J/\psi}/2$. For this meson, the configurations that provide the dominant contributions should be close to $u \sim 1/2$ *i.e.* we expect the δ-function approximation to be fair. This is not so for the light ρ. The use of the δ-function was motivated purely by past phenomenological success at the cross-section level [23]. To understand this success, and to have any hope of predicting the helicity structure of the cross-section, we must relax the crude distribution amplitude assumption. We maintain the collinear assumption and use the asymptotic distribution amplitudes. The relevant amplitudes are

$$\phi_{\parallel}(u) = \phi_{\perp}(u) = 6u(1-u). \tag{5.18}$$

Now momentum configurations of $u \neq 1/2$ contribute and the the $\mathcal{M}^{even}_{+0}$ helicity amplitude is non-zero. We quote the results ((4.69), (4.73)) of Chapter 4:

The non-zero helicity amplitudes in the collinear approximation with asymptotic DA

$$\mathcal{M}^{even}_{+0} = \frac{isC_V f_V}{4\sqrt{2}|q|} \int_0^1 du\ (1-2u)\, 6u(1-u)$$
$$\sum_{n=-\infty}^{n=+\infty} \int_{-\infty}^{\infty} d\nu \frac{\nu^2+n^2}{[\nu^2+(n-1/2)^2][\nu^2+(n+1/2)^2]} \frac{\exp[\chi_{2n}(\nu)z]}{\sin(i\pi\nu)}\, I_{0\,-1}(\nu, 2n, q, u; 1), \tag{5.19}$$

$$\mathcal{M}^{odd}_{++} = \frac{sC_V f_V^T}{4|q|} \int_0^1 du\ \ 6u(1-u)$$
$$\times \sum_{n=-\infty}^{n=+\infty} \int_{-\infty}^{\infty} d\nu \frac{\nu^2+n^2}{[\nu^2+(n-1/2)^2][\nu^2+(n+1/2)^2]} \frac{\exp[\chi_{2n}(\nu)z]}{\sin(i\pi\nu)}\, I_{-\frac{1}{2}\,-\frac{1}{2}}(\nu, 2n, q, u; 0), \tag{5.20}$$

where $I_{\alpha\beta}$ is also defined in Chapter 4 ((4.75)).

Figure 5.5 shows predictions for the cross-section. The $\mathcal{M}^{even}_{+0}$ amplitude has a less steep t dependence than $\mathcal{M}^{odd}_{++}$[8]. The reason for this difference is that implicit in the formulae above (in fact in the $I_{\alpha\beta}$ factor) are dependencies on powers of $(m/|\mathbf{q}|)$. Though we have assumed that this would not make enough difference to affect our power counting arguments, we would expect the t dependence of an even component to dominate over an odd component at the same twist. This is born out by the observation that the $\mathcal{M}^{even}_{+0}$ amplitude has a less steep t dependence. The r^{04}_{00} element is the ratio of the longitudinal component of the cross-section to the total. Figure 5.6 demonstrates that this longitudinal component is numerically subdominant, but becomes increasingly important with rising $|t|$. The change in the t dependence of the combined cross-section, due to this component, results in the previous fit of $\gamma = 0$ and fixed α_s^{IF} now being marginal. We now fit the data better by either running Λ^2 with t or α_s^{IF} with t.

Note that the amplitude $\mathcal{M}_{+-}$ is still zero in our collinear scheme. This means that the r^{04}_{1-1} r-matrix element is still predicted to be zero. As observed for the case of the δ-function distribution amplitude, this is precisely the r-matrix most incompatible with such a prediction. Figure 5.6 shows the effect on the r-matrix elements of running the Λ^2 scale with t versus keeping it fixed. We observe that both provide a good fit for r^{04}_{00} and poor predictions for r^{04}_{10} and r^{04}_{1-1}[9]. The poor quality of fits to the r-matrix elements motivates the progression to higher twist. Higher twist is the only solution to producing a non-zero $\mathcal{M}_{+-}$ contribution.

---

[8]The higher suppression of the chiral odd term is what we might expect. Note that in the definition of the $I_{\alpha\beta}$ integral in $\mathbf{r}$ space (see (4.50), where $\rho = r$), chiral even amplitudes have a K_1 function and odd a K_0. In the large $\mathbf{q}$ limit we expect $m/|\mathbf{q}| \to 0$ and in this limit $K_1(m\hat{r}/|\mathbf{q}|) \to (|\mathbf{q}|/m\hat{r})$, but $K_0(m\hat{r}/|\mathbf{q}|) \to \log(|\mathbf{q}|/m\hat{r})$, only.

[9]Note that a flip in sign of either $\mathcal{M}_{+0}$ or both $\mathcal{M}_{++}$ and $\mathcal{M}_{+-}$ would flip the sign of our prediction for r^{04}_{00}. We were unable to find an error in our work despite thorough checking. Our two gluon leading twist amplitudes agree with [17] at the Born level and we checked that our BFKL result reduces to the Born prediction in the limit $z \to 0$. In addition we have checked that all our conventions agree with those of ZEUS *i.e.* the direction of $\vec{q} = (|q|, 0, 0)$ in 3-space and we have the correct phases for our polarisation vectors (for more details see Appendix C).

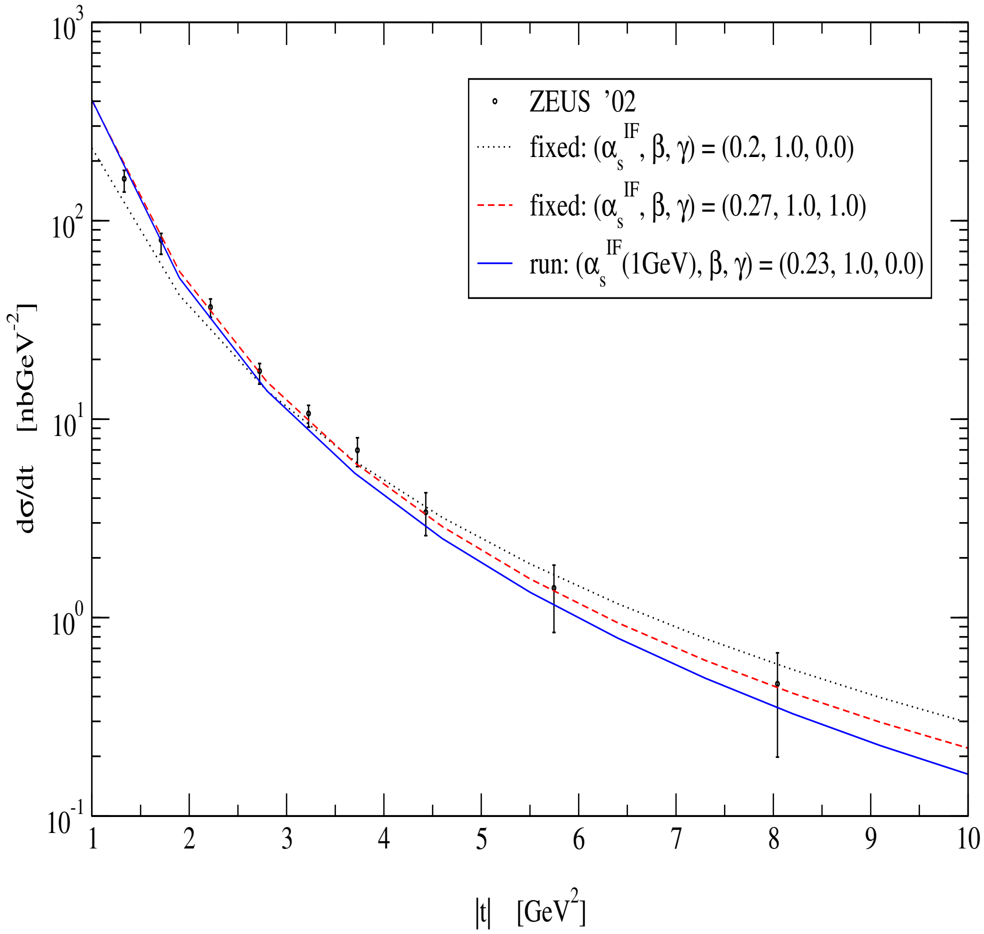

Figure 5.5: Collinear approximation: $d\sigma/dt$ for parameter values, $(\alpha_s^{BFKL}, m) = (0.2, m_\rho/2)$.

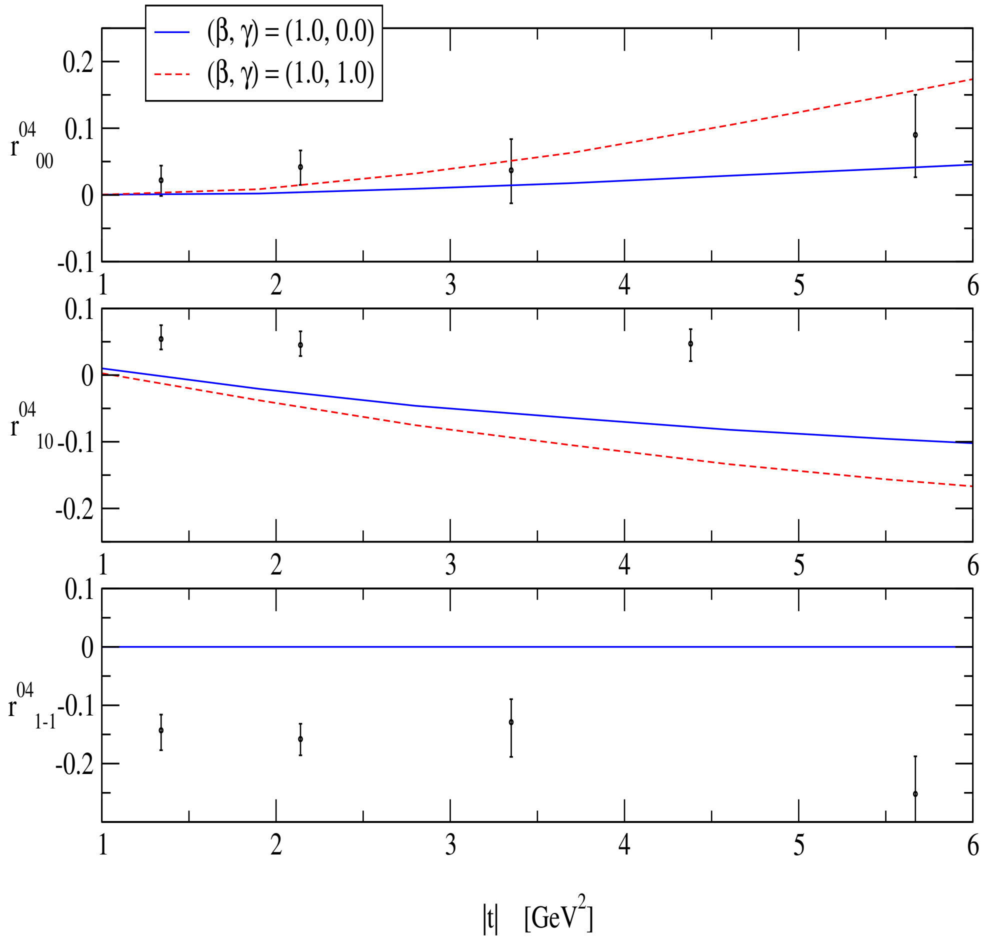

Figure 5.6: Collinear approximation: r-matrix elements for parameter values, $(\alpha_s^{BFKL},\, m) = (0.2,\, m_\rho/2)$.

5.4.3 Higher twist effects

Higher twist effects are introduced by relaxing the assumption that a collinear quark and anti-quark exit the hard subprocess. In section 4.1.1 we showed that the momenta of the quark and anti-quark, $\mathbf{q}_1$ and $\mathbf{q}_2$, are then functions of $\tilde{\mathbf{l}}$ as well as of $\mathbf{q}$ and u. The effect of this is that we no longer have zero sized dipoles and higher-twist terms are no longer forced to be zero. We have to consider, potentially, the full six helicity amplitudes. The complete set of relevant asymptotic distribution amplitudes are

$$\begin{aligned}
&\phi_{\|}(u) = \phi_{\perp}(u) = 6u\bar{u} \\
&g_{\perp}^{(a)}(u) = 6u\bar{u} \qquad g_{\perp}^{(v)}(u) = \frac{3}{4}(1+\xi^2) \\
&h_{\|}^{(s)} = 6u\bar{u} \qquad h_{\|}^{(t)} = 3\xi^2 \\
&h_3(u) = \frac{3}{2}(1-\xi^2),
\end{aligned} \tag{5.21}$$

where $\xi = 2u-1$. Putting these in to the results ((4.69), (4.70), (4.71), (4.72), (4.73), (4.74)) of Chapter 4 we obtain:

All helicity amplitudes with asymptotic distribution amplitudes

---

$$\mathcal{M}_{+0}^{even}[2] = \frac{isC_V f_V}{4\sqrt{2}|q|} \int_0^1 du\ (1-2u)\, 6u\bar{u}$$
$$\sum_{n=-\infty}^{n=+\infty} \int_{-\infty}^{\infty} d\nu \frac{\nu^2+n^2}{[\nu^2+(n-1/2)^2][\nu^2+(n+1/2)^2]} \frac{\exp[\chi_{2n}(\nu)z]}{\sin(i\pi\nu)}\, I_{0-1}(\nu, 2n, q, u; 1), \tag{5.22}$$

$$\mathcal{M}_{++}^{even}[3] = \frac{sC_V f_V M_V}{8|q|} \int_0^1 du\ 3u\bar{u}(u^2+\bar{u}^2)$$
$$\times \sum_{n=-\infty}^{n=+\infty} \int_{-\infty}^{\infty} d\nu \frac{\nu^2+n^2}{[\nu^2+(n-1/2)^2][\nu^2+(n+1/2)^2]} \frac{\exp[\chi_{2n}(\nu)z]}{\sin(i\pi\nu)}\, I_{00}(\nu, 2n, q, u; 1), \tag{5.23}$$

$$\mathcal{M}^{even}_{+-}[3] = \frac{sC_V f_V M_V}{8|q|} \int_0^1 du\, 6u^2\bar{u}^2$$
$$\times \sum_{n=-\infty}^{n=+\infty} \int_{-\infty}^{\infty} d\nu \frac{\nu^2+n^2}{[\nu^2+(n-1/2)^2][\nu^2+(n+1/2)^2]} \frac{\exp[\chi_{2n}(\nu)z]}{\sin(i\pi\nu)}\, I_{1\,-1}(\nu,2n,q,u;1), \tag{5.24}$$

$$\mathcal{M}^{odd}_{+0}[3] = \frac{isC_V f_V^T M_V}{4\sqrt{2}|q|} \int_0^1 du\; 3(1-2u)u\bar{u}$$
$$\times \sum_{n=-\infty}^{n=+\infty} \int_{-\infty}^{\infty} d\nu \frac{\nu^2+n^2}{[\nu^2+(n-1/2)^2][\nu^2+(n+1/2)^2]} \frac{\exp[\chi_{2n}(\nu)z]}{\sin(i\pi\nu)}\, I_{\frac{1}{2}\,-\frac{1}{2}}(\nu,2n,q,u;0), \tag{5.25}$$

$$\mathcal{M}^{odd}_{++}[2] = \frac{sC_V f_V^T}{4|q|} \int_0^1 du\; 6u\bar{u}$$
$$\times \sum_{n=-\infty}^{n=+\infty} \int_{-\infty}^{\infty} d\nu \frac{\nu^2+n^2}{[\nu^2+(n-1/2)^2][\nu^2+(n+1/2)^2]} \frac{\exp[\chi_{2n}(\nu)z]}{\sin(i\pi\nu)}\, I_{-\frac{1}{2}\,-\frac{1}{2}}(\nu,2n,q,u;0), \tag{5.26}$$

$$\mathcal{M}^{odd}_{+-}[4] = \frac{sC_V f_V^T M_V^2}{8|q|} \int_0^1 du\; \frac{3}{2}u^2\bar{u}^2$$
$$\times \sum_{n=-\infty}^{n=+\infty} \int_{-\infty}^{\infty} d\nu \frac{\nu^2+n^2}{[\nu^2+(n-1/2)^2][\nu^2+(n+1/2)^2]} \frac{\exp[\chi_{2n}(\nu)z]}{\sin(i\pi\nu)}\, I_{\frac{3}{2}\,-\frac{1}{2}}(\nu,2n,q,u;0). \tag{5.27}$$

The numbers in the square bracket associated with each helicity amplitude denotes the twist of that amplitude.

We want to see the effect of higher twist terms on our observables by systematically adding suppressed terms. How should we go about this? Any observable is proportional to products of the helicity amplitudes *i.e.* $\mathcal{M}_{ij}\mathcal{M}^*_{kl}$. Consider the (parton level) cross-section for the production of a longitudinal meson:

$$\frac{d\sigma_{+0}}{dt} \propto \mathcal{M}_{+0}\mathcal{M}_{+0}^{*} = \left(\mathcal{M}_{+0}^{even}[2] + \mathcal{M}_{+0}^{odd}[3]\right)\left(\mathcal{M}_{+0}^{even\,*}[2] + \mathcal{M}_{+0}^{odd\,*}[3]\right)$$
$$= \underbrace{\mathcal{M}_{+0}^{even}[2]\mathcal{M}_{+0}^{even\,*}[2]}_{\text{(twist-2 x twist-2)}} + \underbrace{\mathcal{M}_{+0}^{even}[2]\mathcal{M}_{+0}^{odd\,*}[3]}_{\text{(twist-2 x twist-3)}} + \underbrace{\mathcal{M}_{+0}^{odd}[3]\mathcal{M}_{+0}^{even\,*}[2]}_{\text{(twist-2 x twist-3)}} + \underbrace{\mathcal{M}_{+0}^{odd}[3]\mathcal{M}_{+0}^{odd\,*}[3]}_{\text{(twist-3 x twist-3)}}$$

In the expression above we see that the first term is leading twist (twist-2 x twist-2), the second and third $1/|\mathbf{q}|$ suppressed (twist-2 x twist-3), and the fourth $1/|\mathbf{q}|^2$ suppressed (twist-3 x twist-3). Note that a (twist-2 x twist-4) term would also be $1/|\mathbf{q}|^2$ suppressed and that we only worked to twist-3 in Chapter 2. Next-to leading twist in observables is therefore, in general, the highest level of twist for which we have complete knowledge. Note that to next-to-leading twist, the helicity double flip cross-section is zero, but, products linear in $(+-)$ amplitudes, such as r^{04}_{1-1}, are not.

Figure 5.7 shows $d\sigma/dt$ for the varying levels of approximation in twist. The effect on the combined cross-section is predominantly that of normalisation. We see that adding in the (twist-2 x twist-3) to the (twist-2 x twist-2) terms has a significant effect, but that adding the next-to-next-to-leading twist terms that we know has much less effect. This is a pleasing result, since it suggests that the total cross-section is insensitive to the higher twist terms that we have incomplete knowledge of.

Figure 5.8 shows that the observables r^{04}_{00} and r^{04}_{10} are also relatively insensitive to next-to-next-to leading twist. The r^{04}_{1-1} proves more sensitive. Adding the (twist-3 x twist-3) terms has an effect of order 100%. It is not surprising that this observable is the most sensitive to higher twist, since it is zero at leading twist. At first it appears that we cannot trust our predictions for this r-matrix element and that it is therefore not a good observable with which to test the validity of BFKL dynamics. However, figure 5.9, makes it clearer what is happening. It shows the ratios of even to odd helicity amplitudes at $x = 0.1$[10]. In our twist counting scheme, we have ignored the effect of $|\mathbf{q}|$-dependent effects in the hard scatter. The plots in figure 5.9 are a test of the validity of this assumption. If effects of the hard scatter were the same, we would expect twist counting to give us $\mathcal{M}_{+0}^{even}/\mathcal{M}_{+0}^{odd}$ and $\mathcal{M}_{+-}^{even}/\mathcal{M}_{+-}^{odd}$ approximately $\propto \sqrt{-t}$

[10]The mean x values that contribute for each amplitude were found to be $\langle x \rangle \simeq 0.1$

and $\mathcal{M}^{even}_{++}/\mathcal{M}^{odd}_{++} \propto 1/\sqrt{-t}$. Our assumption seems reasonable for the $(+0)$ and $(+-)$ amplitudes, however, for $(++)$ the odd and even terms have a similar t-dependence. $\mathcal{M}^{even}_{++}$ is twist-3 but the $\mathbf{q}$ dependence from the hard scatter boosts its importance to the same significance as the twist-2 pieces. The thick line in the plot of r^{04}_{1-1} in figure 5.8, is the prediction where we, in addition to the $\mathcal{M}^{odd}_{++}[2]\mathcal{M}^{even}_{+-}[3]$ term, kept the $\mathcal{M}^{even}_{++}[3]\mathcal{M}^{even}_{+-}[3]$ term. For t significantly above $1\,\mathrm{GeV}^2$, we can see that the effect of terms genuinely $1/|\mathbf{q}|^2$ suppressed and above, is minimal. Thus, though r^{04}_{1-1} is the most sensitive observable to higher twist effects, we have control over it. We shall therefore, from here on, use our full formulae (4.69-4.74) and not throw away any suppressed pieces. These suppressed contributions should not significantly affect any conclusions. Our control over higher twist suggests that any such effects are unlikely to provide the solution to the fact we cannot fit the complete set of r-matrix elements.

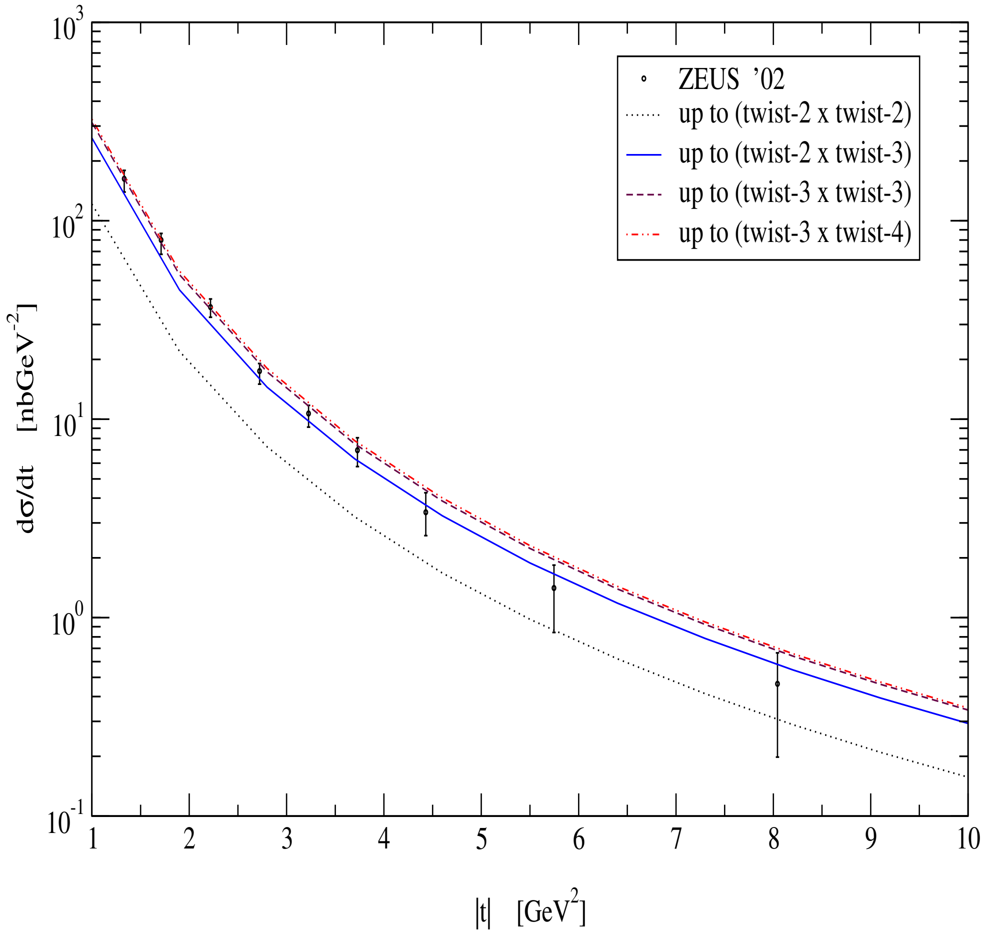

Figure 5.7: Higher twist effects: $d\sigma/dt$ for parameter values, $(\alpha_s^{IF}, \alpha_s^{BFKL},\ \Lambda^2, m) = (0.17,\ 0.2,\ m_V^2,\ m_\rho/2)$.

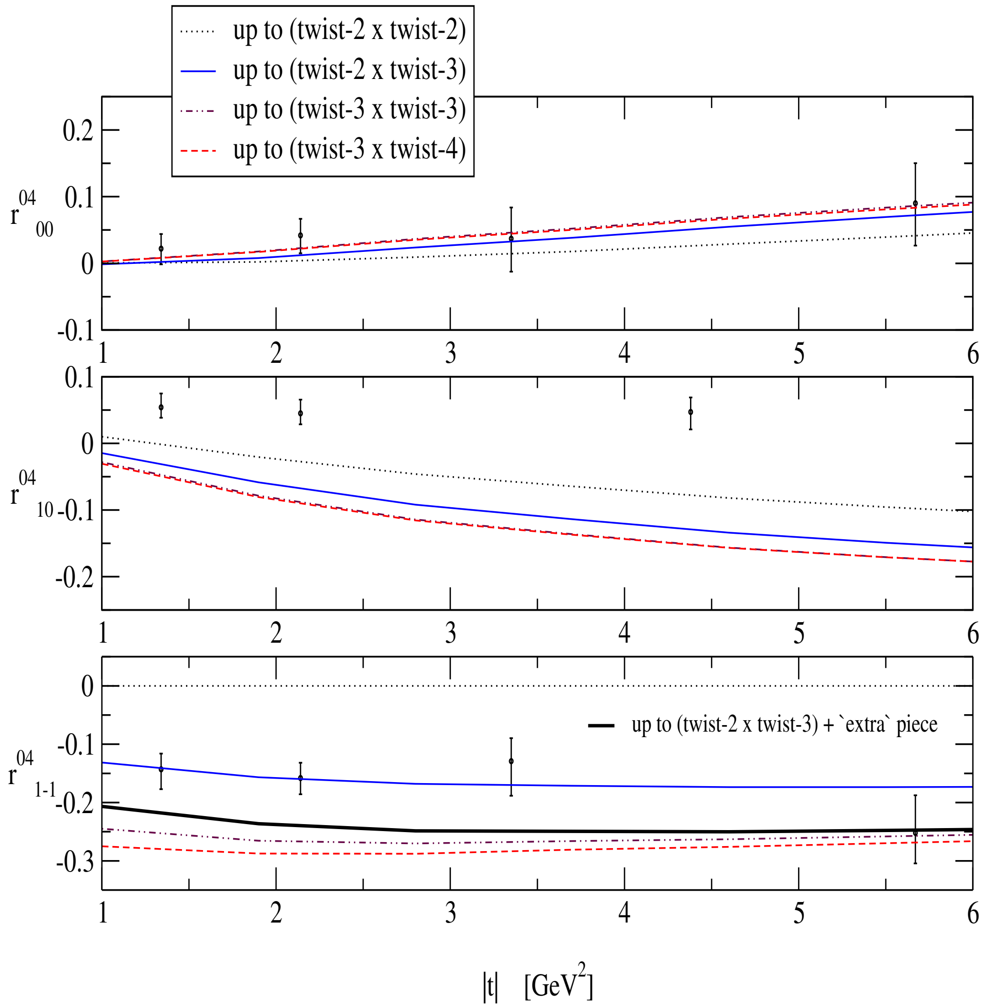

Figure 5.8: Higher twist effects: r-matrix elements for parameter values, $(\alpha_s^{BFKL}, \Lambda^2, m) = (0.2, m_V^2, m_\rho/2)$.

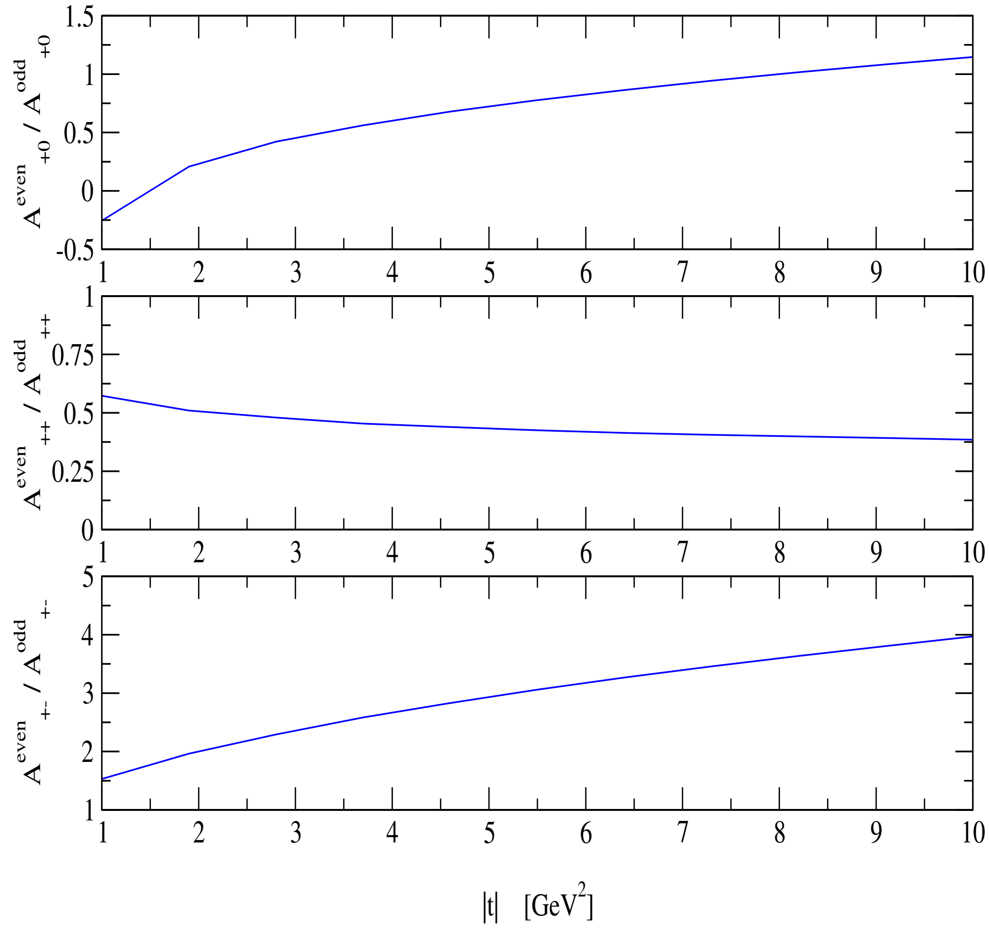

Figure 5.9: Higher twist effects: even to odd amplitude ratios for parameter values, $(\alpha_s^{BFKL},\, \Lambda^2,\, m) = (0.2,\, m_V^2,\, m_\rho/2)$.

5.4.4 The sensitivity of predictions to parameters

We demonstrated in the previous section that, away from low t, our predictions are only weakly sensitive to higher twist corrections. The fit for the r^{04}_{10} r-matrix element remained particularly poor, however. Can we do better through playing with the parameters of the hard scatter? In this section we explore the sensitivity to this. Since we have fixed the BFKL parameter, β, the remaining parameters are

α_s^{IF}	α_s^{BFKL}	$\Lambda^2 = m_V^2 - \gamma t$

We shall use a fixed α_s^{IF}, rendering it purely a normalisation parameter (which cancels in r^{04}_{ij}). We will explore the effect of the other two.

Sensitivity to α_s^{BFKL}

Figure 5.10 shows a central curve corresponding to: $(\alpha_s^{IF},\, \alpha_s^{BFKL},\, \Lambda^2,\, m) =$ $(0.17,\, 0.2,\, m_\rho^2,\, m_\rho/2)$. The two other curves show the effect of varying the value of α_s^{BFKL} by 25%. The effect is primarily that of normalisation.

The r-matrix element predictions are shown in figure 5.11. They are not highly sensitive to α_s^{BFKL}. r^{04}_{00} is the most sensitive, followed in order by r^{04}_{10} and r^{04}_{1-1}. We find r^{04}_{1-1} to be relatively insensitive to this BFKL parameter (whereas we remind the reader that it proved most sensitive to higher twist). We note that while the general quality of the fits for all the r-matrix elements is unaffected by varying α_s^{BFKL} by 25%, a large value of α_s is associated with a larger suppression of the longitudinal cross-section. We also note that the fit to r^{04}_{10} remains poor.

Sensitivity to γ

The default fit, $(\alpha_s^{IF},\, \alpha_s^{BFKL},\, \Lambda^2,\, m) = (0.17,\, 0.2,\, m_\rho^2,\, m_\rho/2)$, that provides the solid curve in figure 5.12, is only marginally compatible with the cross-section data. This is because, as previously noted, the longitudinal contribution becomes increasingly important at higher t and this flattens the t dependence. The dotted curve on the same graph demonstrates that we can fit the data much better by running the BFKL scale, Λ^2.

The predictions in figure 5.13 for the r-matrix elements again show the sign problem in the prediction for r^{04}_{10}. Running Λ^2 has not solved this. Note also that the predictions for r^{04}_{00} and r^{04}_{10} are sensitive to the values of the BFKL parameters and in particular, the quality of the fits becomes worse when Λ^2 is run with t. We see that when Λ^2 is run, the longitudinal fraction grows quicker than is compatible with data. This is not seen when we keep Λ^2 fixed.

Sensitivity to z rapidity

The sensitivity of the r matrix element predictions to α_s^{BFKL} and γ, discussed in the two subsections above, is slightly surprising. We might expect that the effects of higher orders, in this case BFKL, would approximately cancel in ratios. Note that the rapidity variable 'z' increases (decreases) as we raise α_s^{BFKL} (γ). It is really this z variable that we have been investigating. Figure 5.14 contains a plot for each helicity amplitude at the rapidity values, $z = 0.5$, 0.75 and 1.0. The number in the brackets in the legends correspond to the areas underneath the curves. Note that the position of the peaks do not shift as we change rapidity. As z decreases all amplitudes fall, but a look at the integrated values demonstrate that the longitudinal amplitudes fall more slowly. If we lower z we raise the ratio of the longitudinal to the transverse contributions.

This observation allows us to play off the effects of varying α_s^{BFKL} and Λ^2 simultaneously. A non-zero γ value in Λ^2 improves the t dependence of the differential cross-section and in conjunction, increasing α_s^{BFKL} drives the longitudinal component down. The fit values $(\alpha_s^{IF}, \alpha_s^{BFKL}, \Lambda^2) = (0.17, 0.25, m_\rho^2 - t)$ therefore lead to an improved overall fit. The predictions for these values are shown in figures 5.15-5.16.

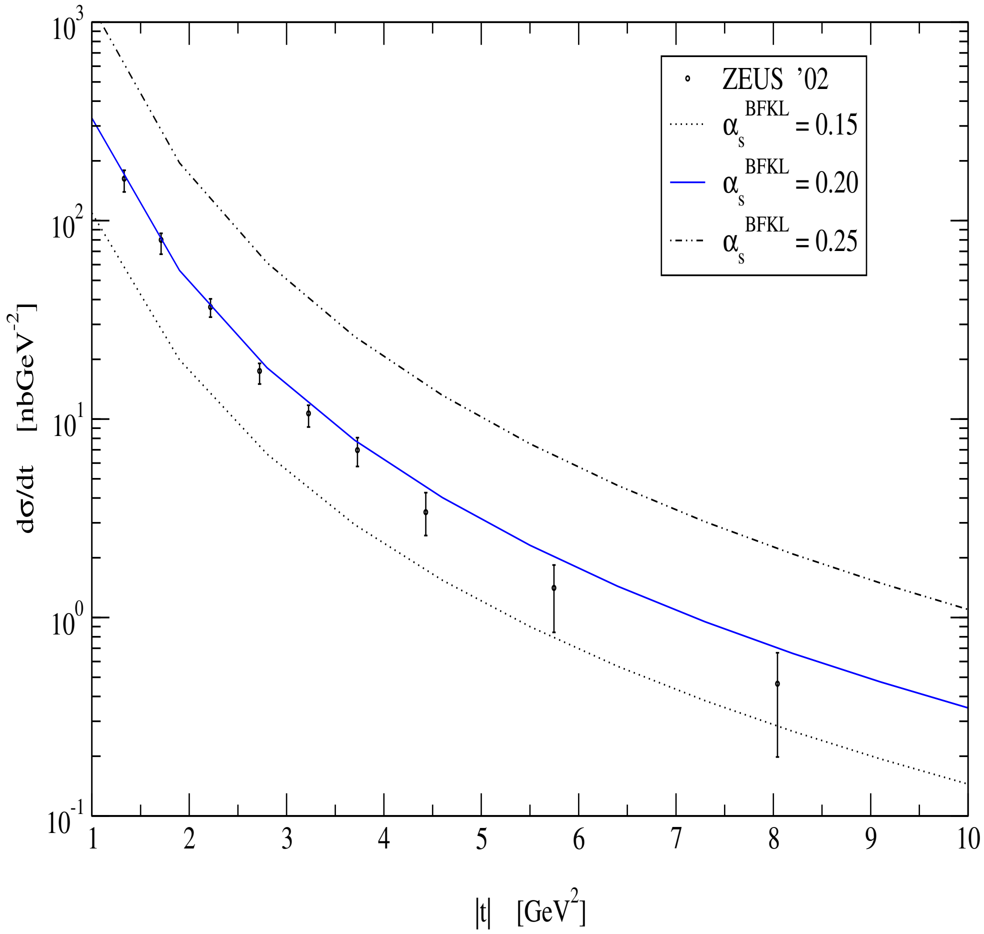

Figure 5.10: The sensitivity to varying α_s^{BFKL}: $d\sigma/dt$ for parameter values, $(\alpha_s^{IF}, \Lambda^2, m) = (0.17, m_\rho^2 - t, m_\rho/2)$.

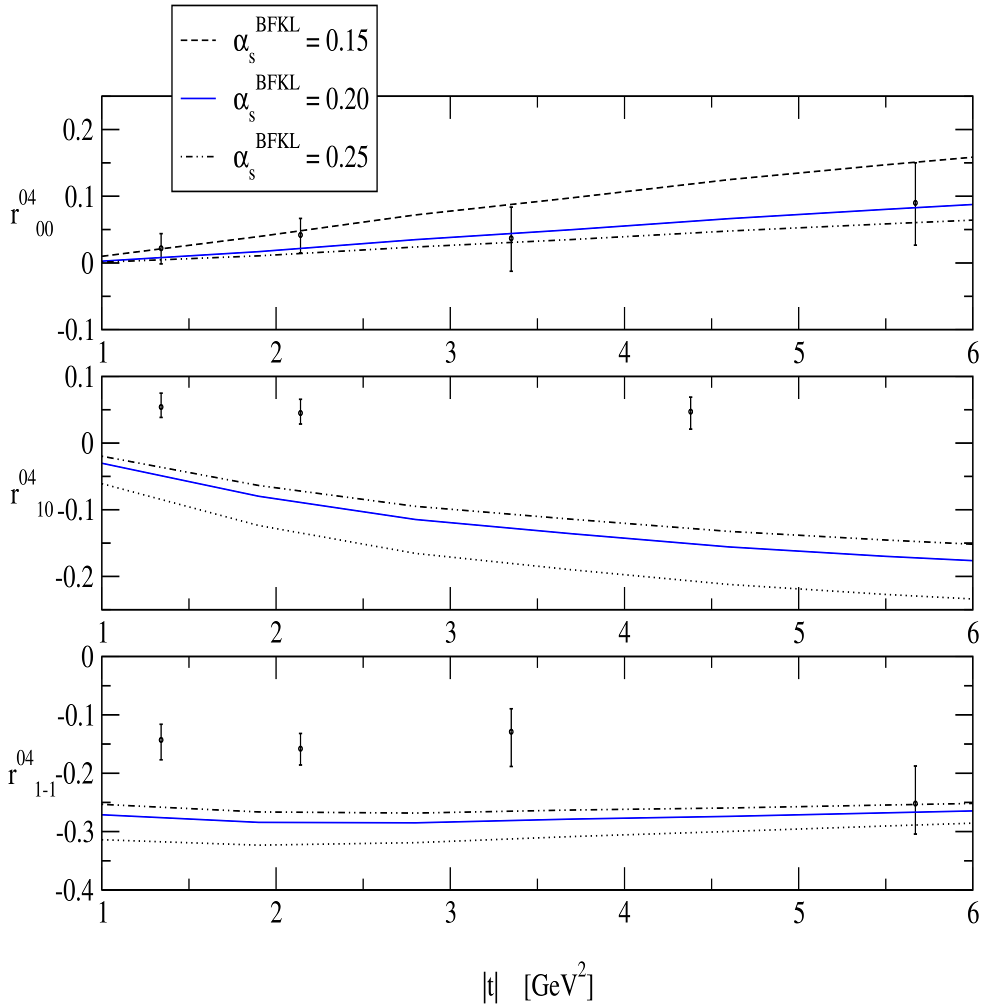

Figure 5.11: The sensitivity to varying α_s^{BFKL}: r-matrix elements for parameter values, $(\Lambda^2,\, m) = (m_\rho^2 - t,\, m_\rho/2)$.

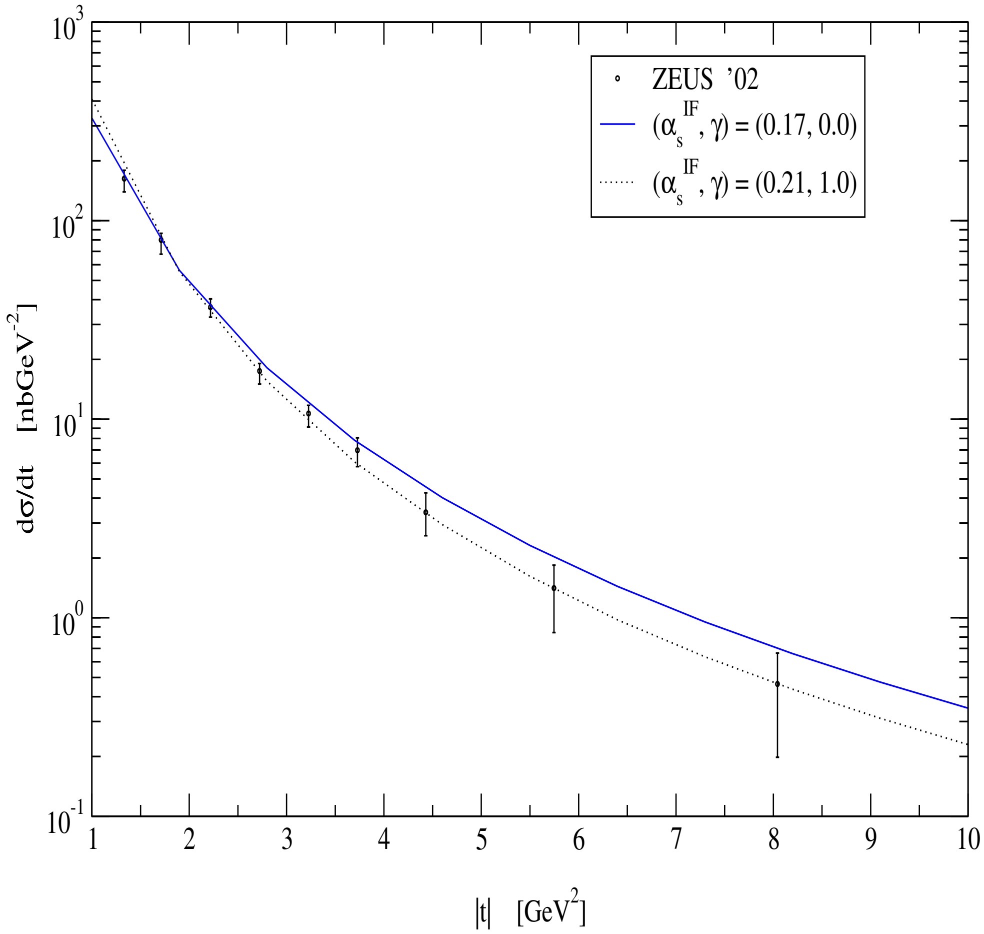

Figure 5.12: The sensitivity to varying γ: $d\sigma/dt$ for parameter values, $(\alpha_s^{IF},\, \alpha_s^{BFKL},\, m) = (0.17,\, 0.2,\, m_\rho/2)$.

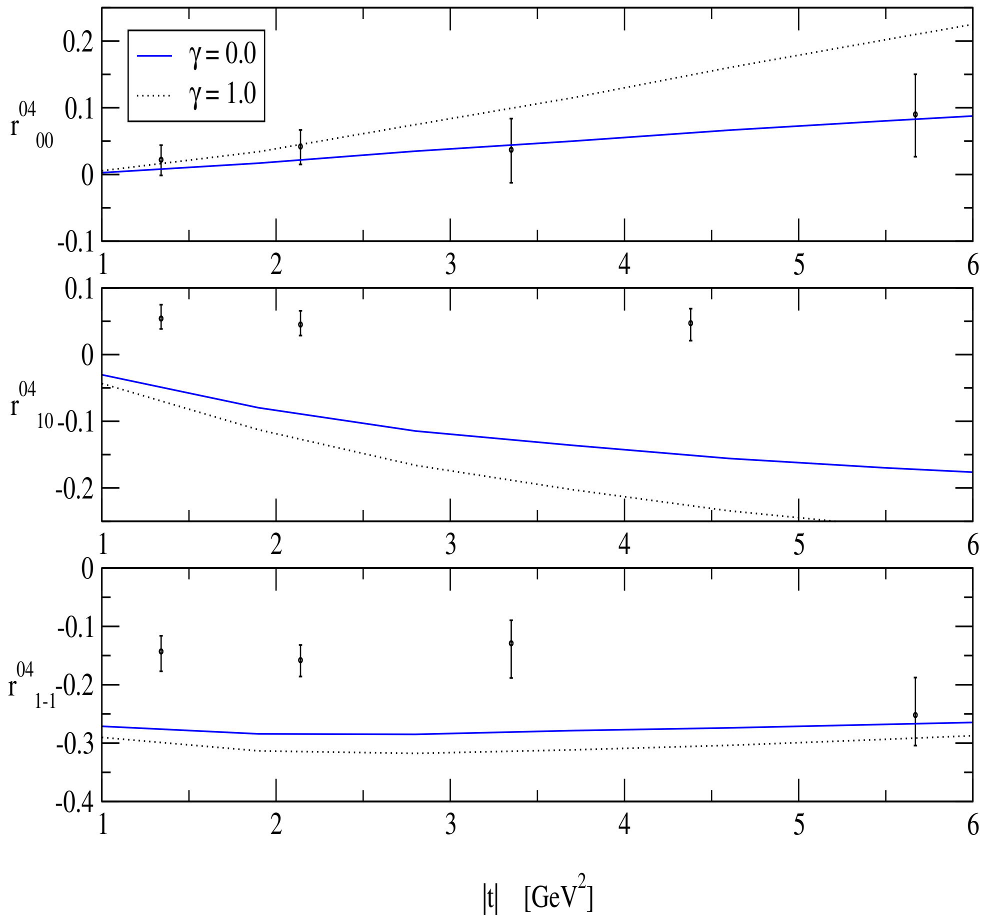

Figure 5.13: The sensitivity to varying γ: r-matrix elements for parameter values, $(\alpha_s^{BFKL}, m) = (0.2, m_\rho/2)$.

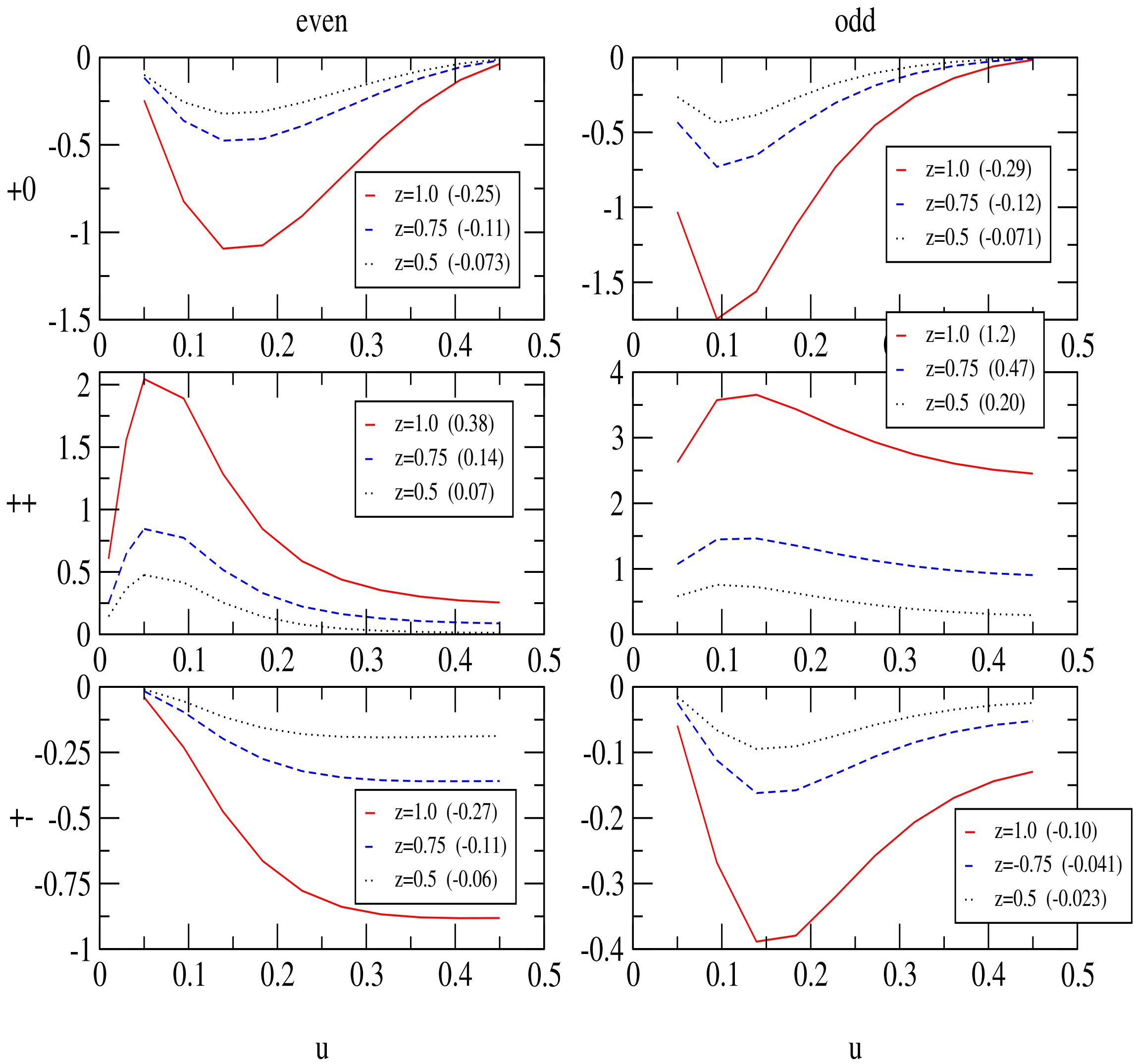

Figure 5.14: The sensitivity to varying z: the six helicity amplitudes differential in u. The y-axis is $\frac{1}{C_\rho}\frac{d\mathcal{M}^{odd/even}_{+i}}{du}$, where $C_\rho = i\hat{s}\alpha_s^{IF^2}(N^2 - 1/N^2)eQ_\rho f_\rho$ and $(m, |\mathbf{q}|) = (m_\rho/2, \sqrt{10}\,\mathrm{GeV})$.

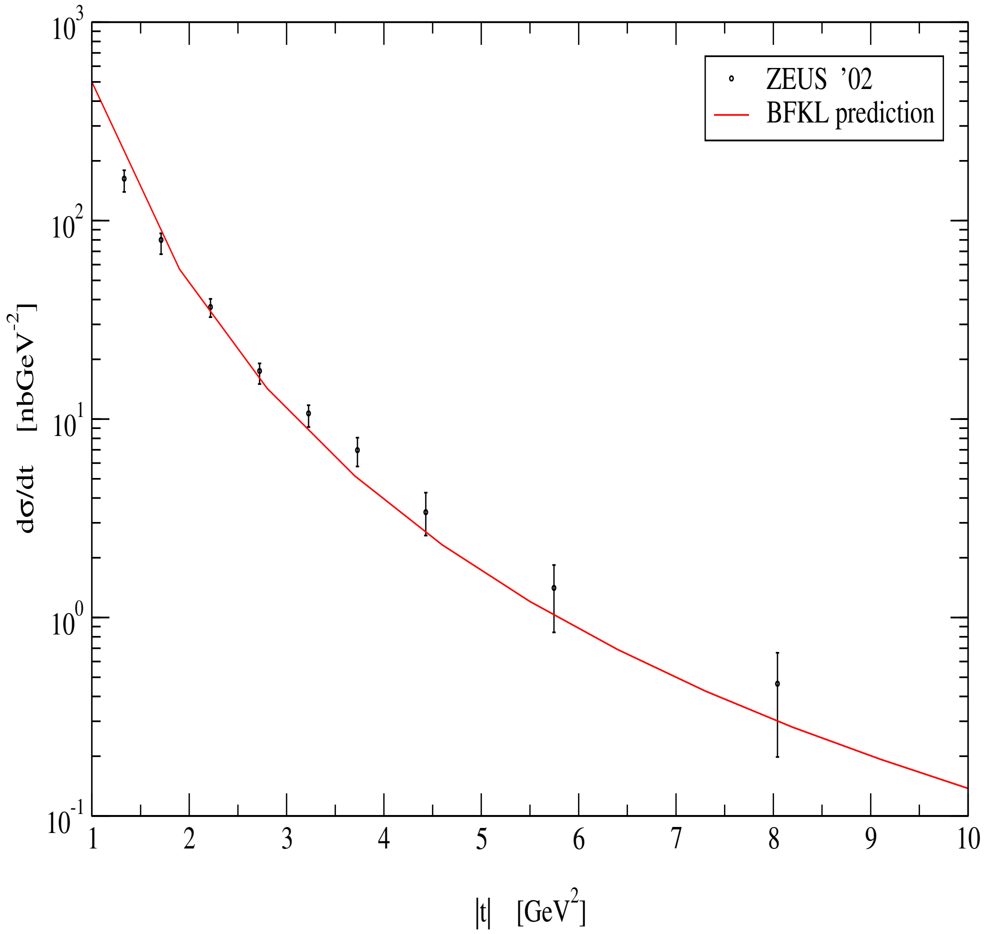

Figure 5.15: An improved fit: $d\sigma/dt$ for parameter values, $(\alpha_s^{IF}, \alpha_s^{BFKL}, \Lambda^2, m) = (0.17, 0.25, m_\rho^2 - t, m_\rho/2)$

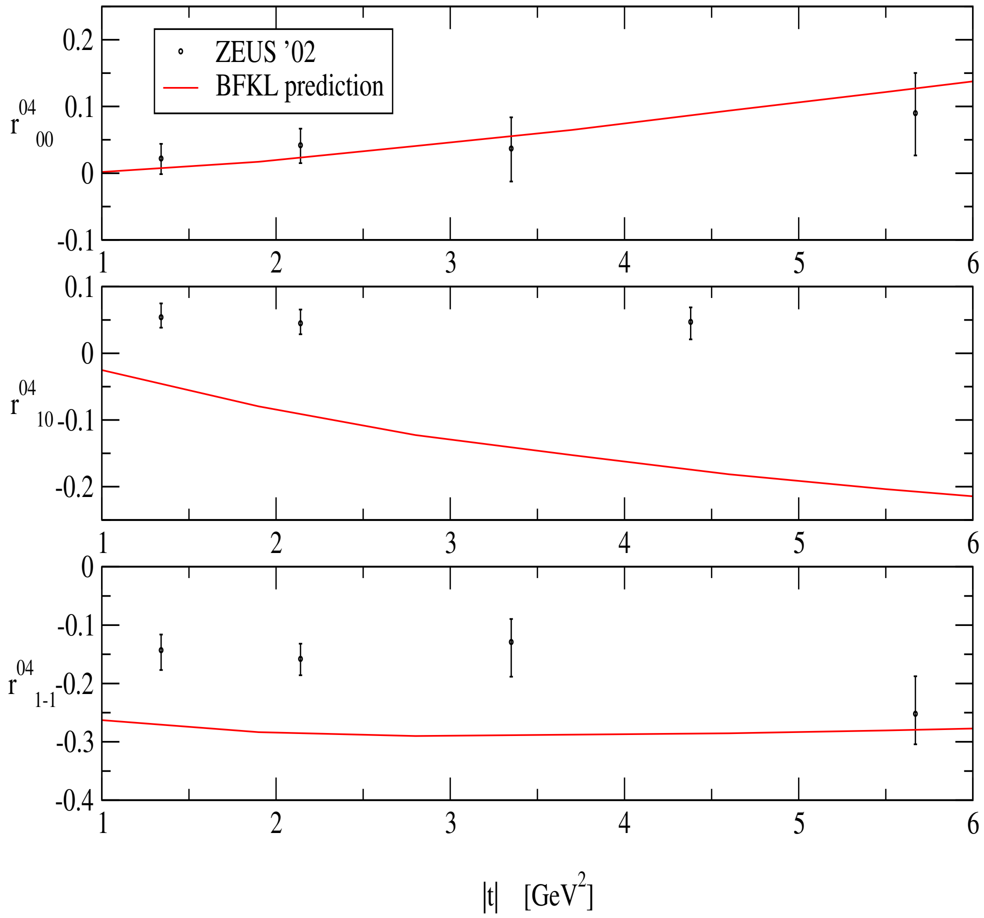

Figure 5.16: An improved fit: r-matrix elements for parameter values, $(\alpha_s^{BFKL}, \Lambda^2, m) = (0.25, m_\rho^2 - t, m_\rho/2)$.

Sensitivity to 'quark' mass

The sensitivity of our BFKL predictions to the quark mass parameter has not so far been explored. We do so now. As we do not have a strong theoretical justification for our exact choice of value, the constituent mass, it is of particular interest. Figure 5.17 shows differential cross-section predictions. The central curve is that of a previous fit, where $(\alpha_s^{IF},\, \alpha_s^{BFKL},\, \Lambda^2,\, m) = (0.17,\, 0.2,\, m_\rho^2,\, m_\rho/2)$. The other two curves were generated by doubling and halving the constituent quark mass. Bearing in mind the fact that we have varied the mass parameter considerably, we see that the cross-section has a fairly robust prediction, its shape being fairly insensitive to changes in m.

Figure 5.18 shows the r-matrix element predictions at varying the quark mass. They are all highly sensitive to this parameter, in shape and in normalisation. Why are they so sensitive to the quark mass value? Figure 5.19 helps to explain why. This figure shows the six helicity amplitudes, differential in u, for the mass values $m = m_\rho/4$, $m_\rho/2$ and m_ρ. We point out that it is not in fact the value of m that is significant, it is the value of $m/|\mathbf{q}|$, and in these plots we fixed $|\mathbf{q}| = \sqrt{10}\, GeV$. Notice that as we increase the scale $m/|\mathbf{q}|$, the peaks of the distributions become concentrated increasingly toward $u = 1/2$. This is what we expect, after all we claimed that the δ-function distribution should be a reasonable approximation as m becomes very large. However, the effect is quite dramatic. Halving the constituent mass strongly enhances the contributions close to the end-points. The effect is particularly marked for the longitudinal helicity amplitudes, since they are forced to zero at exactly $u = 1/2$. Raising the quark mass is therefore a mechanism for suppressing the longitudinal components with respect to the transverse. This kind of effect has actually been seen before. Our calculation is for $\gamma p \to \rho X \to \pi\pi X$. In the DIS process $\gamma e \to \gamma\gamma^* e \to e f \bar{f}$, where f is a fermion, the structure function F_A^γ exhibits similar behaviour. It is zero at 'u' of one-half and has large contributions close to the end-points that become suppressed as we increase the fermion mass [53].

Returning to our process, it is interesting to note that for a large enough m, the $\mathcal{M}_{+0}$ amplitude not only is small but also changes sign. Then, the prediction of r_{10}^{04} flips sign to that of the data. Figure 5.18 shows this begins to occur for m as low as

m_ρ, in the low $|t|$ region. The evidence of this can also be seen even at large t, in figure 5.19, where the values of $\mathcal{M}_{+0}$ differential in u, become positive for small u. So, increasing m would be a possible mechanism for improving our fits, however, we find it difficult to justify a mass parameter far away from the constituent mass. But what is the fact that increasing m improves the fit to data telling us?

Increasing the mass has the effect of suppressing large dipole configurations. The McDonald Bessel function, $K_i(m|\mathbf{r}|)$, present in the $\mathbf{r}$ space representation of the photon wavefunction has a large argument expansion of exponential form, involving the factor $e^{-m|\mathbf{r}|}$. Figure 5.19 shows the effect of this through the fact that larger masses suppress the end-point contributions more strongly. End-point contributions in u correspond to large dipole sizes. The data can be interpreted as suggesting that large dipole sizes should be more heavily suppressed than our calculations predict. Increasing the quark mass models the necessary large $|\mathbf{r}|$ suppression. The δ-function distribution amplitude that we used in the collinear approximation was another method of doing this, by forcing $u = 1/2$. It in fact suppressed large dipoles rather too well, as it left the longitudinal component zero. We have demonstrated in this work that our helicity amplitudes have no end-point divergences, but the underlying philosophy of our model of this process, is that small dipoles should dominate. What could provide the mechanism for a genuine perturbative suppression of large dipole sizes? A possibility is, perhaps, Sudakov factors [54]. The application of the Sudakov mechanism of suppression of large dipoles to this process would be another project in itself. We leave this as an interesting possibility. We fix m to $m_\rho/2$ again, and move on.

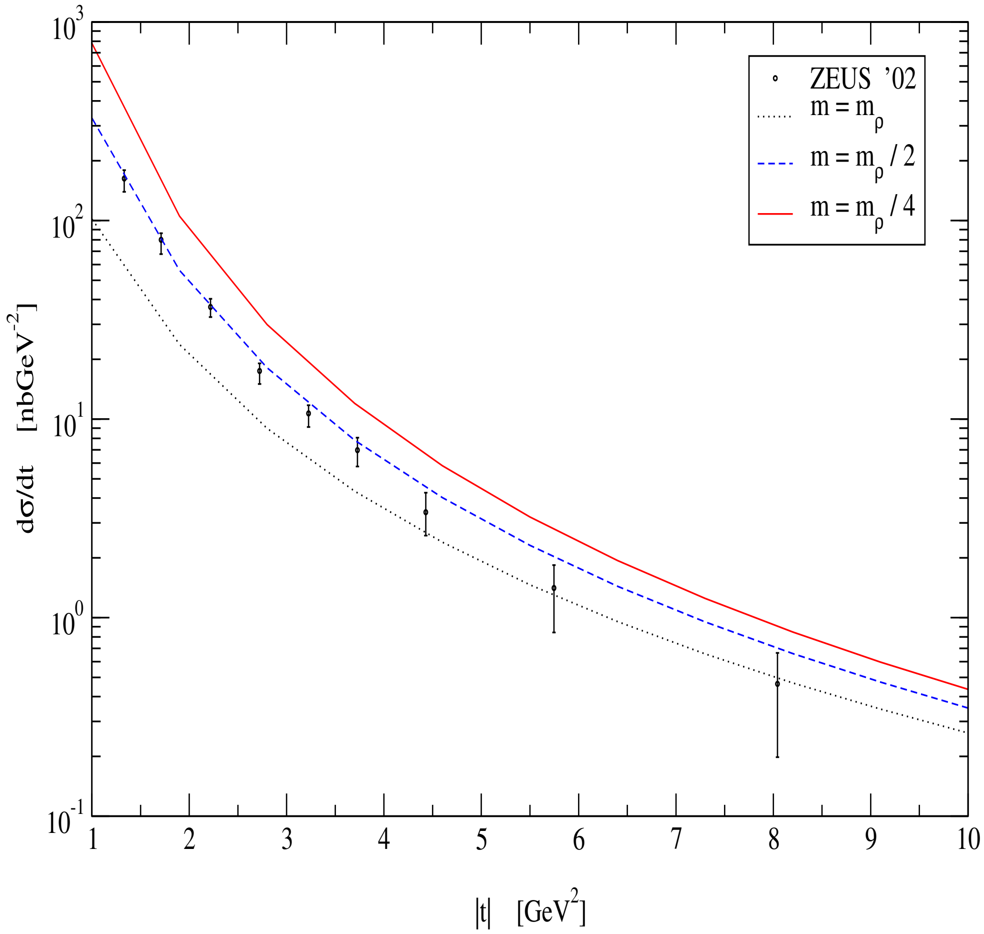

Figure 5.17: The sensitivity to varying m: $d\sigma/dt$ for parameter values, $(\alpha_s^{IF},\, \alpha_s^{BFKL}, \Lambda^2) = (0.17,\, 0.2,\, m_\rho^2)$.

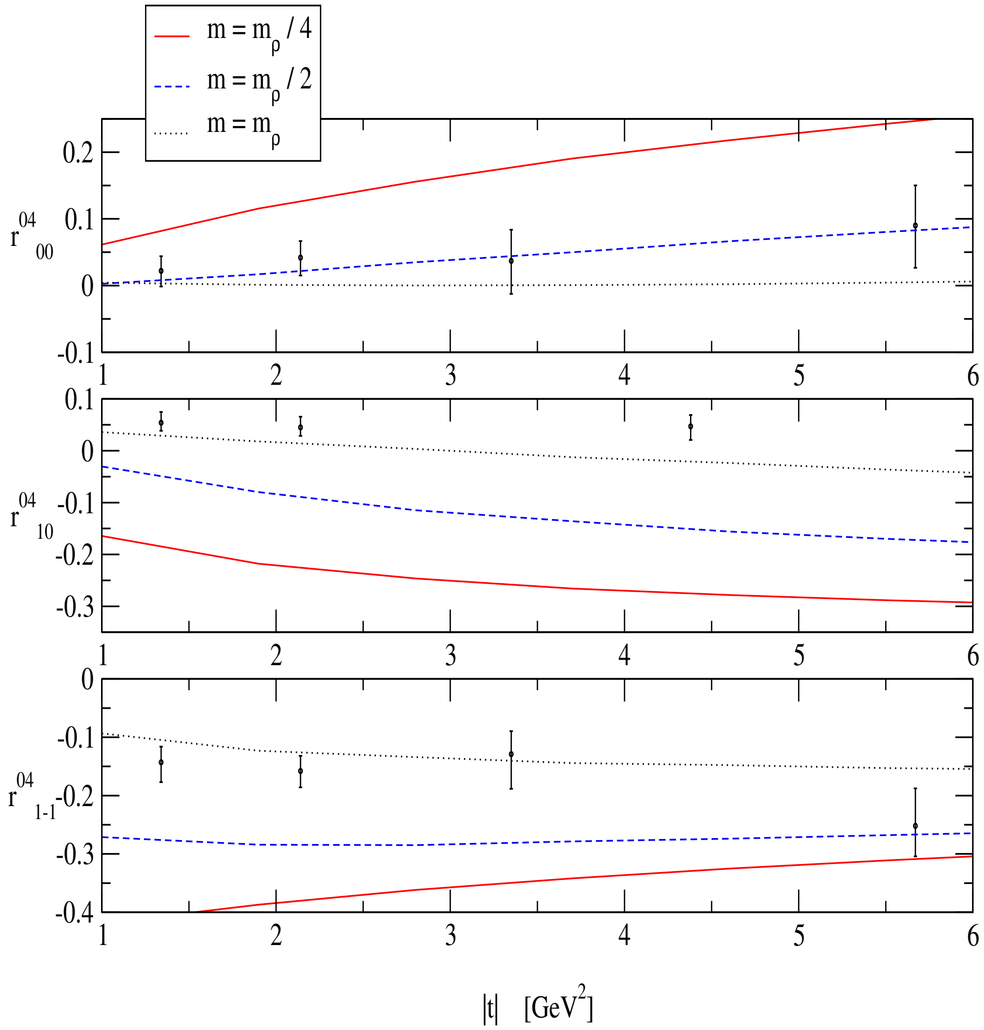

Figure 5.18: The sensitivity to varying m: r-matrix elements for parameter values, $(\alpha_s^{BFKL}, \Lambda^2) = (0.2,\, m_\rho^2)$.

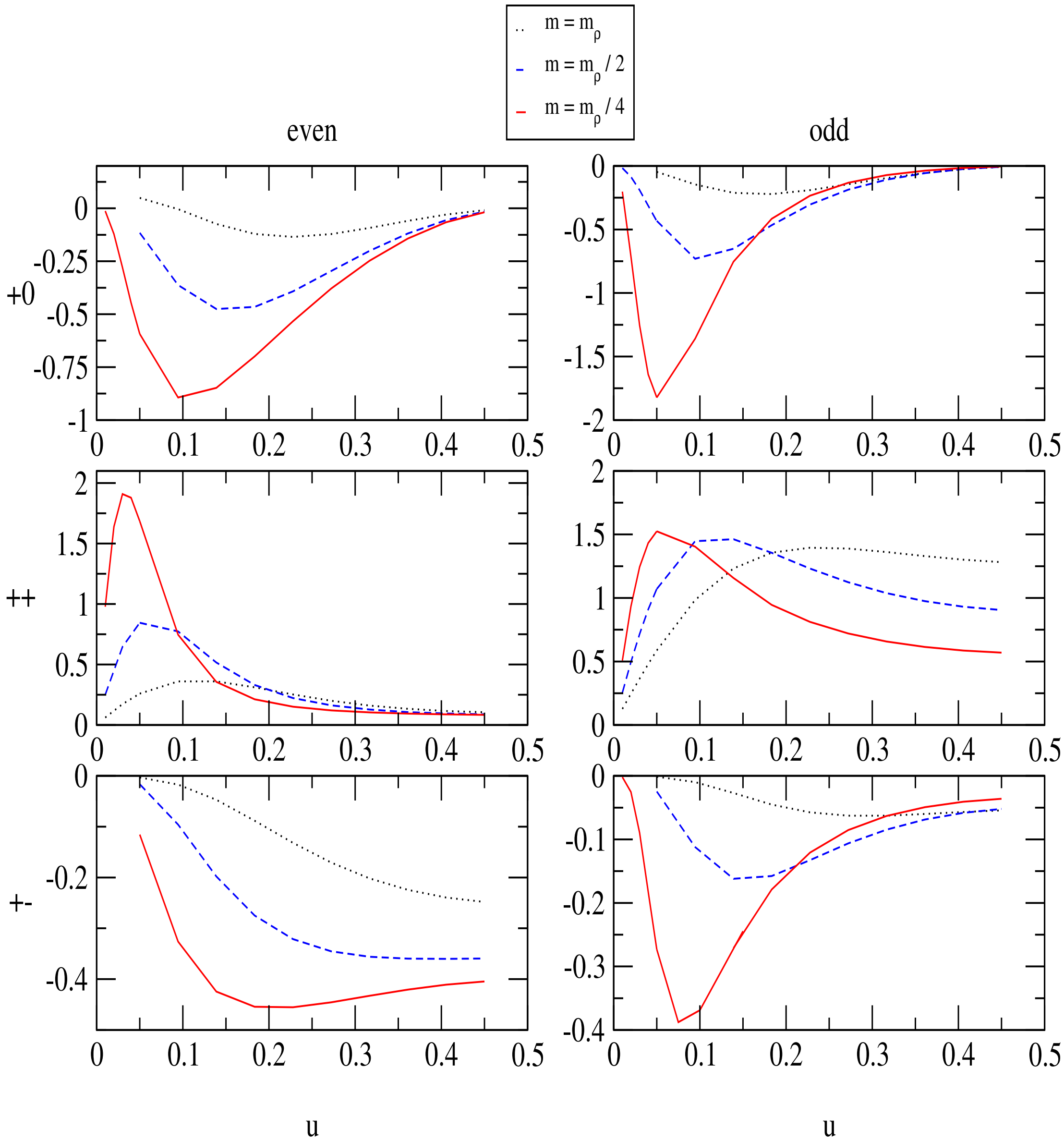

Figure 5.19: The sensitivity to varying m: the six helicity amplitudes differential in u. The y-axis is $\frac{1}{C_\rho}\frac{d\mathcal{M}^{odd/even}_{+i}}{du}$, where $C_\rho = i\hat{s}\alpha_s^{IF^2}(N^2-1/N^2)eQ_\rho f_\rho$ and $(z,\,|\mathbf{q}|) = (0.75,\,\sqrt{10}\,\mathrm{GeV})$.

5.4.5 Sensitivity to distribution amplitudes

The continuing failure to predict the correct sign for r^{04}_{10}, and the general sensitivity of the helicity amplitudes to contributions away from $u = 1/2$, motivates relaxing another approximation. Now we replace the asymptotic distribution amplitudes with those calculated exactly (up-to the third term in an expansion) by Ball and Braun and Ball, Braun, Koike and Tanaka (BBKT) [32, 33]. We then make use of our full results for the helicity amplitudes, ((4.69), (4.70), (4.71), (4.72), (4.73), (4.74)).

All helicity amplitudes with BBKT distribution amplitudes

$$\mathcal{M}^{even}_{+0} = \frac{isC_V f_V}{4\sqrt{2}|q|} \int_0^1 du\ (1-2u)\phi_{\parallel}(u)$$
$$\sum_{n=-\infty}^{n=+\infty} \int_{-\infty}^{\infty} d\nu \frac{\nu^2+n^2}{[\nu^2+(n-1/2)^2][\nu^2+(n+1/2)^2]} \frac{\exp[\chi_{2n}(\nu)z]}{\sin(i\pi\nu)}\, I_{0-1}(\nu, 2n, q, u; 1), \tag{5.28}$$

$$\mathcal{M}^{even}_{++} = \frac{sC_V f_V M_V}{8|q|} \int_0^1 du \left(\frac{g_{\perp}^{(a)}(u)}{4} - (1-2u)\int_0^u dv(\phi_{\parallel}(v) - g_{\perp}^{(v)}(v))\right)$$
$$\times \sum_{n=-\infty}^{n=+\infty} \int_{-\infty}^{\infty} d\nu \frac{\nu^2+n^2}{[\nu^2+(n-1/2)^2][\nu^2+(n+1/2)^2]} \frac{\exp[\chi_{2n}(\nu)z]}{\sin(i\pi\nu)}\, I_{00}(\nu, 2n, q, u; 1), \tag{5.29}$$

$$\mathcal{M}^{even}_{+-} = \frac{sC_V f_V M_V}{8|q|} \int_0^1 du \left(\frac{g_{\perp}^{(a)}(u)}{4} + (1-2u)\int_0^u dv(\phi_{\parallel}(v) - g_{\perp}^{(v)}(v))\right)$$
$$\times \sum_{n=-\infty}^{n=+\infty} \int_{-\infty}^{\infty} d\nu \frac{\nu^2+n^2}{[\nu^2+(n-1/2)^2][\nu^2+(n+1/2)^2]} \frac{\exp[\chi_{2n}(\nu)z]}{\sin(i\pi\nu)}\, I_{1-1}(\nu, 2n, q, u; 1). \tag{5.30}$$

$$\mathcal{M}^{odd}_{+0} = \frac{isC_V f_V^T M_V}{4\sqrt{2}|q|} \int_0^1 du \int_0^u dv(h_{\parallel}^{(t)}(v) - \phi_{\perp}(v))$$
$$\times \sum_{n=-\infty}^{n=+\infty} \int_{-\infty}^{\infty} d\nu \frac{\nu^2+n^2}{[\nu^2+(n-1/2)^2][\nu^2+(n+1/2)^2]} \frac{\exp[\chi_{2n}(\nu)z]}{\sin(i\pi\nu)}\, I_{\frac{1}{2}-\frac{1}{2}}(\nu, 2n, q, u; 0), \tag{5.31}$$

$$\mathcal{M}_{++}^{odd} = \frac{sC_V f_V^T}{4|q|} \int_0^1 du\, \phi_\perp(u)$$
$$\times \sum_{n=-\infty}^{n=+\infty} \int_{-\infty}^{\infty} d\nu \frac{\nu^2+n^2}{[\nu^2+(n-1/2)^2][\nu^2+(n+1/2)^2]} \frac{\exp[\chi_{2n}(\nu)z]}{\sin(i\pi\nu)} I_{-\frac{1}{2}-\frac{1}{2}}(\nu,2n,q,u;0), \tag{5.32}$$

$$\mathcal{M}_{+-}^{odd} = \frac{sC_V f_V^T M_V^2}{8|q|} \int_0^1 du \int_0^u dv \int_0^v d\eta \left(h_\parallel^{(t)}(\eta) - \frac{1}{2}\phi_\perp(\eta) - \frac{1}{2}h_3(\eta) \right)$$
$$\times \sum_{n=-\infty}^{n=+\infty} \int_{-\infty}^{\infty} d\nu \frac{\nu^2+n^2}{[\nu^2+(n-1/2)^2][\nu^2+(n+1/2)^2]} \frac{\exp[\chi_{2n}(\nu)z]}{\sin(i\pi\nu)} I_{\frac{3}{2}-\frac{1}{2}}(\nu,2n,q,u;0). \tag{5.33}$$

The specific forms of the distribution amplitudes we use are presented in Appendix D. We remind the reader that we do not 'play' with any of the parameters of the distribution amplitudes, we simply use their theoretical values. These values are not in all cases known precisely and we note that, potentially, varying some of them may have notable effects. It is not, however, a particular fit of optimum quality we are interested in, rather only in observing the general sensitivity of our observables to the effect of relaxing the approximation of asymptotic distribution amplitudes. We observe before proceeding that we might expect the more accurate distribution amplitudes to worsen the fit to data, since typically they enhance the contributions from configurations where the quark and anti-quark have asymmetric momentum configuration *i.e.* away from $u = 1/2$.

Figure 5.20 shows the differential cross-section in the two distribution amplitude prescriptions. The more accurate distribution amplitudes prove to make no qualitative difference. Note that the logarithmic scale masks the appreciable quantitative difference, however. The more accurate distribution amplitudes predict a cross-section that has a marked departure from the asymptotic for $|t|$ greater than a few GeV^2.

Figure 5.21, for the r matrix elements, shows that the effects largely cancel in these ratios.

Figure 5.22 shows the six helicity amplitudes, differential in u, at fixed rapidity $z = 0.75$. Referring back to the amplitudes $\mathcal{M}_{++}^{even}$ and $\mathcal{M}_{+-}^{even}$, given by (5.29) and

(5.30), we see that the difference between their u dependence is a relative switch in sign between two pieces (one corresponding to the vector component of the Fierz decomposition and the other to the pseudovector). The plots in 5.22 demonstrate a cancellation in the effects of the non-asymptotic distribution amplitudes for $\mathcal{M}^{even}_{++}$, but an amplification for $\mathcal{M}^{even}_{+-}$. The effects of the different distribution amplitudes on the u distributions of the amplitudes are most significant for $\mathcal{M}^{even}_{+-}$ and $\mathcal{M}^{odd}_{++}$. However, even then there is a significant cancellation in their integrated values.

We again stress, even in this more accurate approximation, the inability of our BFKL results to fit r^{04}_{10}. Leading log BFKL seems insufficient to describe the complete set of observables relating to the ρ meson.

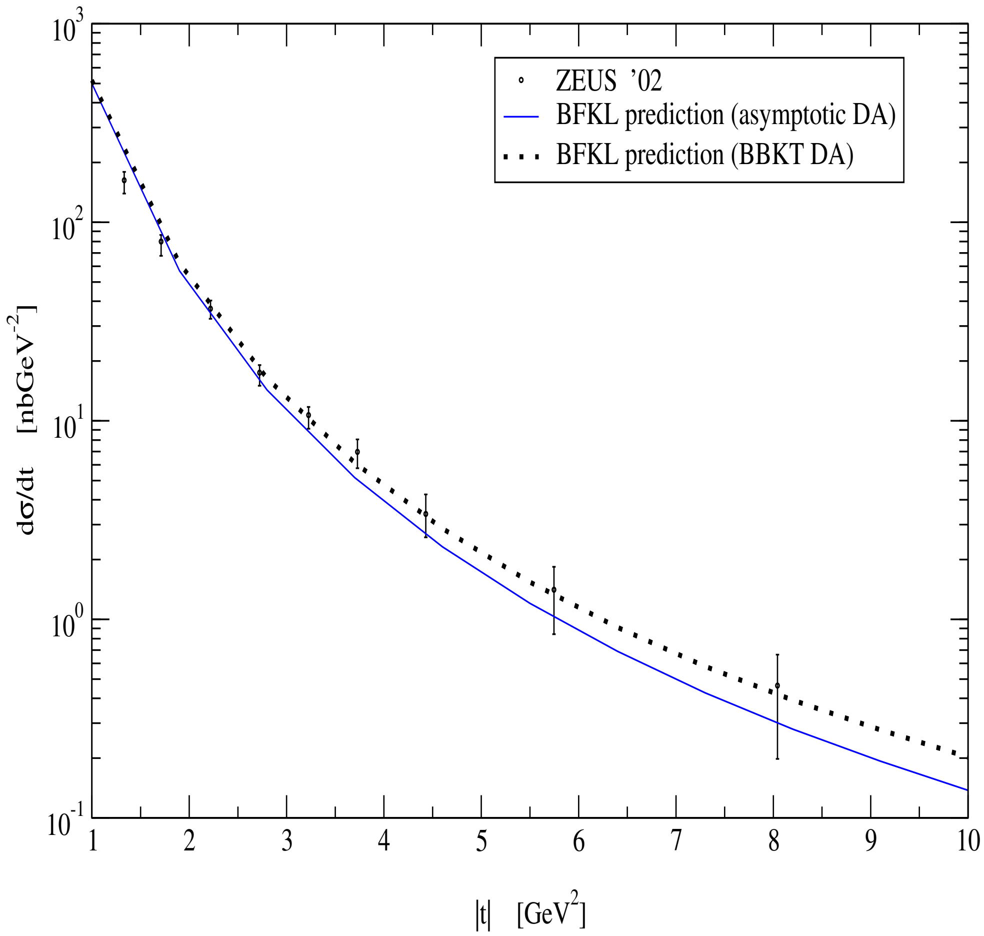

Figure 5.20: The effect BBKT DA: $d\sigma/dt$ for parameter values, (α_s^{IF}, α_s^{BFKL}, Λ^2, m) = (0.17, 0.25, $m_\rho^2 - t$, $m_\rho/2$)

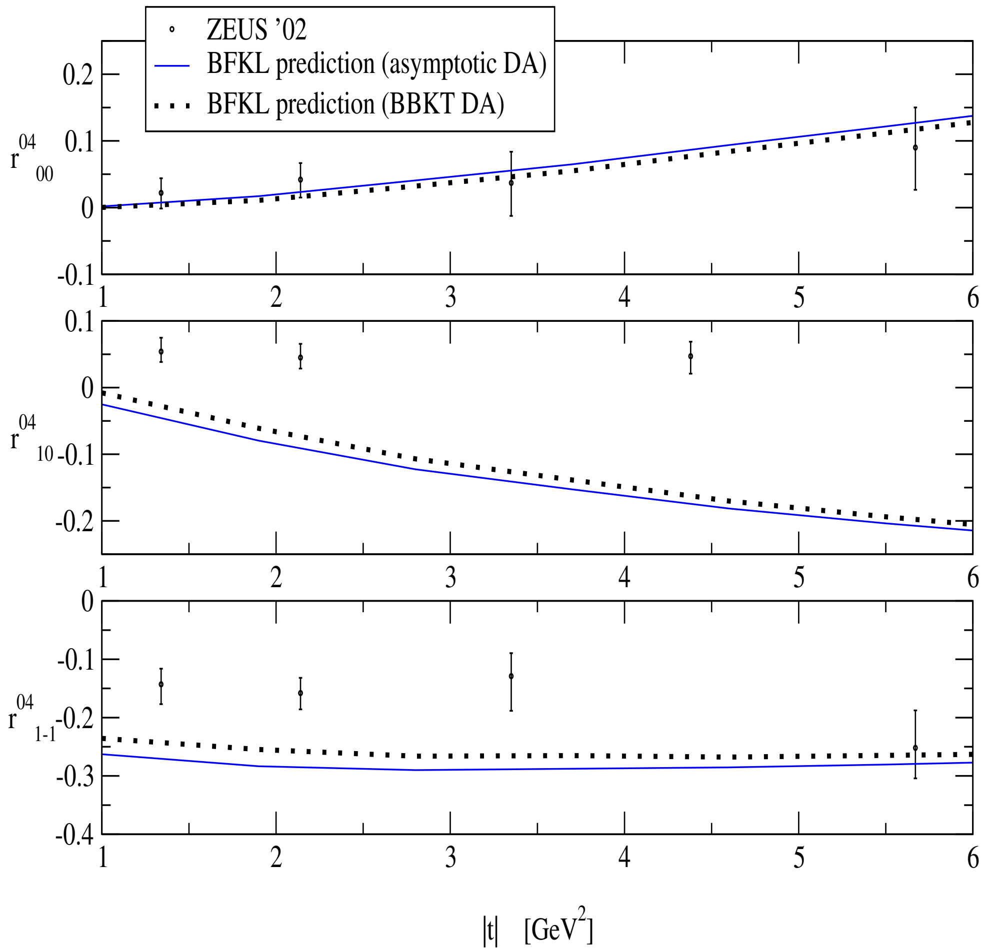

Figure 5.21: The effect of BBKT DA: r-matrix elements for parameter values, $(\alpha_s^{BFKL},\, \Lambda^2,\, m) = (0.25,\, m_\rho^2 - t,\, m_\rho/2)$

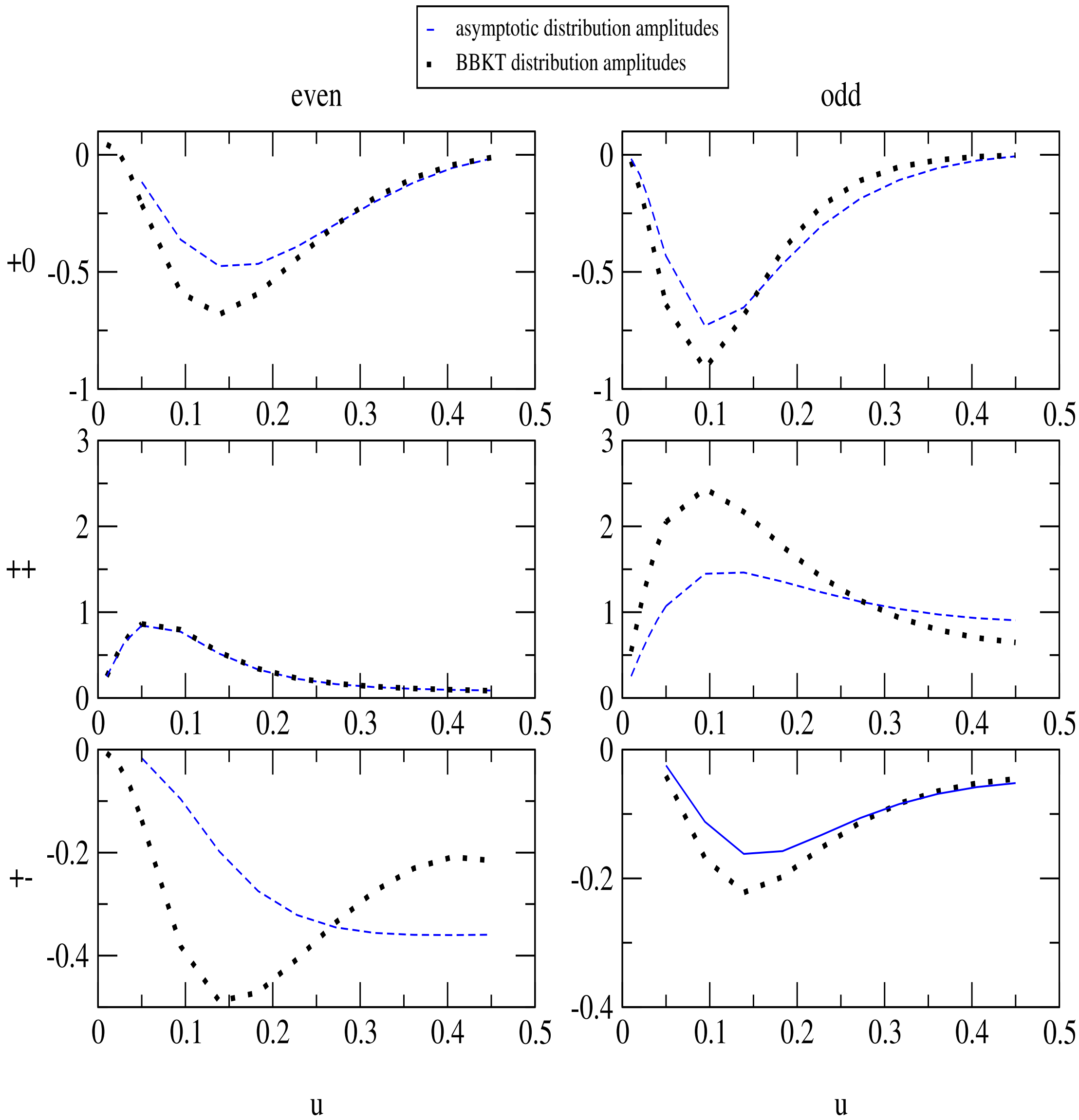

Figure 5.22: The effect of BBKT DA: the six helicity amplitudes differential in u. The y-axis is $\frac{1}{C_\rho}\frac{d\mathcal{M}^{odd/even}_{+i}}{du}$, where $C_\rho = i\hat{s}\alpha_s^{IF^2}(N^2 - 1/N^2)eQ_\rho f_\rho$ and $(z,\, m,\, |\mathbf{q}|) = (0.75,\, m_\rho/2,\, \sqrt{10}\,\mathrm{GeV})$.

5.5 Phenomenology for the ρ, ϕ and J/ψ

We now turn our attention to the ϕ and J/ψ, reverting to the use of the asymptotic distribution amplitudes, since we wish to treat the three mesons on the same footing. We do not know the non-asymptotic distributions for the J/ψ. In addition, the BBKT distributions for the ϕ, excepting mass corrections, are much closer to those of the asymptotic distributions than in the case of the ρ (see Appendix D and the particular distribution parameters for the ρ and ϕ).

To what extent do the observations, made for the ρ in the preceding sections, hold for the other mesons? The calculation for a general meson, V, with asymptotic distribution amplitude, requires only the substitution $(f_\rho/f_\rho^T,\, Q_\rho,\, m_\rho) \rightarrow (f_V/f_V^T,\, Q_V,\, m_V)$. The values for the meson couplings (f_V) and electromagnetic coupling (Q_V) are constants of proportionality. m_V appears in the BFKL log and the γV impact factor (through the quark mass $m = m_V/2$), and is qualitatively the most significant parameter. The mass of the ϕ is similar to that of the ρ, while the mass of the J/ψ is significantly larger. We might therefore expect the predictions for the ϕ to be, qualitatively, very similar to the ρ, and those for the J/ψ to be, perhaps, very different. This is in fact what we see.

Figure 5.23 and 5.24 reproduce our 'improved fit' prediction for the ρ, where we played off the effects or adjusting α_s^{BFKL} and Λ^2 to our advantage. We also show the two-gluon exchange predictions. Two-gluon exchange with a fixed strong coupling predicts a differential cross-section far too flat in $|t|$. Running the coupling solves this problem and provides a good fit to the cross-section. However, looking at the two-gluon predictions for the r-matrix elements (which are independent of how we treat α_s^{IF}), we see that the values for the r_{00}^{04} far exceed those constrained by the data. This means that the longitudinal ($(+0)$) component dominates for two-gluon exchange. This is in line with our observation that the longitudinal fraction increases as we lower the z rapidity (recall that the BFKL solution tends to two-gluon exchange in the limit $z \rightarrow 0$). Thus, even though we succeeded in getting the two-gluon curve to 'go through the points' for the cross-section, it is generated by fundamentally wrong dynamics. We do note the improvement with respect to working within the collinear, leading twist approximation, with δ-function distribution amplitudes. In that prescription, two-gluon exchange was compared to cross-section data in [23]. The dip to zero manifest at $|t| = m_V^2$ (see figure 3.2) is not seen in data and was an artificial prediction arising from the crudity of the treatment of the meson distribution amplitudes.

Figure 5.25-5.26 and 5.27-5.28 present the predictions for the ϕ and J/ψ mesons. The ϕ predictions are similar to those for the ρ. We again see the two-gluon exchange cross-section requiring a running strong coupling to fit the data, and the r-matrix elements telling us this is an artificial result. The BFKL predictions are again correctly dominated by the transverse contributions, but again fail to predict the correct sign for r_{10}^{04} in the case of the ϕ. However, for the J/ψ, the BFKL predictions are (fairly) compatible with all the observables. The large quark mass drives the longitudinal amplitudes small enough to agree with the r_{10}^{04} data. We note that although the two-gluon r-matrix predictions for the J/ψ are in marginal agreement with the data, we have to doubt the validity of the underlying dynamics, given the comments above.

We stress here that the BFKL predictions for the ϕ and J/ψ are not fitted. We have only fitted the ρ. The BFKL predictions (1) in figures 5.25 and 5.27 were obtained by simply making the appropriate change in meson constants and masses. In BFKL prediction (2) we altered the values of the meson tensor coupling. These are not well constrained by theoretical calculations. We did not treat this as a truly free parameter, however. The results of [23] for leading twist and conformal spin in the heavy meson approximation, can be interpreted as suggesting the ratios of the tensor coupling to the vector coupling should take on the same value for each meson. That assumption was implicit in their calculation, and they succeeded in obtaining the correct relative normalisations. Following this observation, in prediction (2) we set

$$f_V^T = \frac{f_\rho^T}{f_\rho} f_V, \tag{5.34}$$

where we still made use of the value calculated by Ball, Braun, Koike and Tanaka, for f_ρ^T [33]. Fixing f_V^T in this way greatly improves the fit to data[11].

Comparing two-gluon exchange and BFKL predictions, we see that the BFKL

[11] Note that if we allowed ourselves slightly more freedom with the values of f_V^T, the quality of the fits to the cross-sections could be improved even further.

calculation is a definite step forward. The t dependence is improved and the longitudinal cross-section fraction is reduced. The success of the unfitted predictions for the ϕ and J/ψ is a noteworthy result. This agrees with the results of [23] in cruder approximations, and indeed, through the dominance of the $\mathcal{M}_{++}^{odd}$ amplitude, we explain the success of these results. However, the inability of BFKL to agree with the data for r_{10}^{04} suggests that while the longitudinal contribution is brought down by BFKL effects, it is still not under enough control to accurately describe all the observables measured at ZEUS and H1.

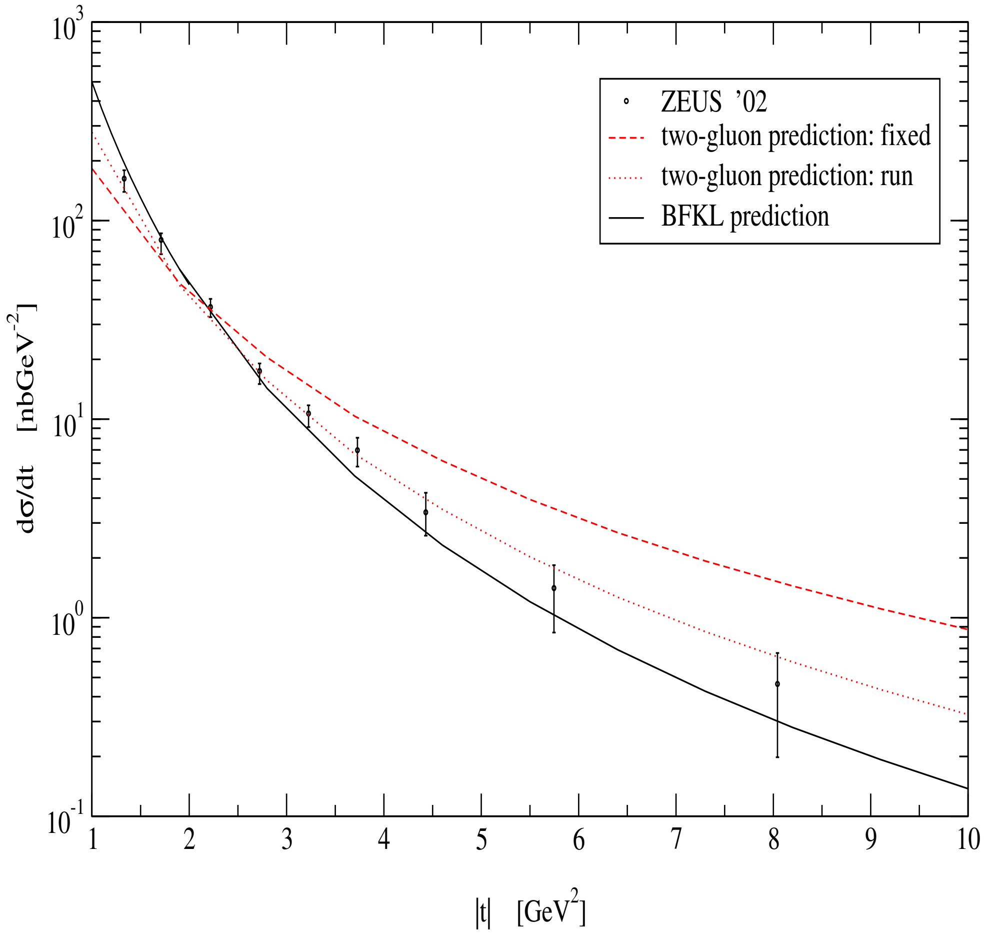

Figure 5.23: ρ photoproduction: $d\sigma/dt$. The fixed two-gluon curve was calculated with the parameter values $(\alpha_s^{IF},\, f_\rho,\, f_\rho^T,\, m) = (0.27,\, 0.216\,\text{GeV},\ 0.160\,\text{GeV},\, m_\rho/2)$. The run two-gluon curve was calculated with the parameter values $(\alpha_s^{IF}(1\,\text{GeV}),\, f_\rho,\, f_\rho^T,\, m)$ $=(0.30,\, 0.216\,\text{GeV},\, 0.160\,\text{GeV},\, m_\rho/2)$. The BFKL calculated for the parameter values $(\alpha_s^{IF},\, \alpha_s^{BFKL},\, \Lambda^2,\, f_\rho,\, f_\rho^T,\, m) = (0.17,\, 0.25,\, m_\rho^2 - t,\, 0.216\,\text{GeV},\ 0.160\,\text{GeV},\, m_\rho/2)$.

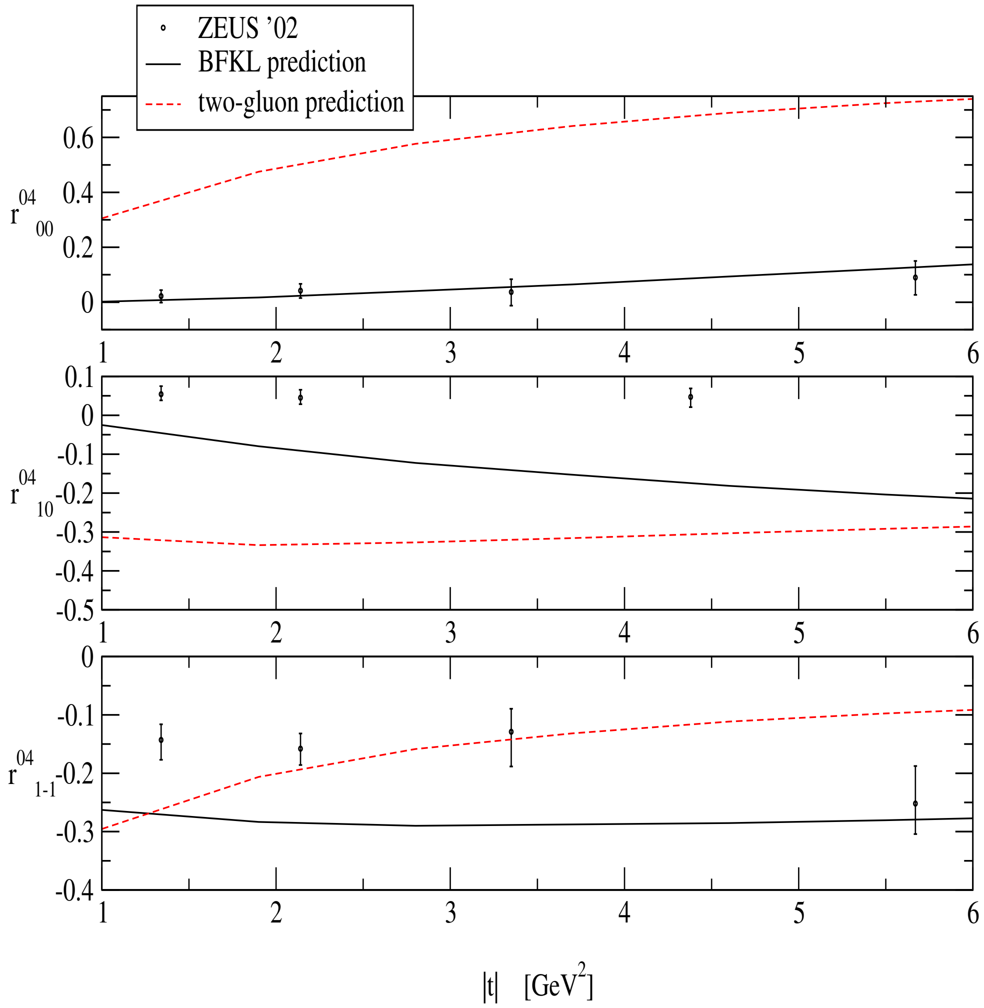

Figure 5.24: ρ photoproduction: r-matrix elements. The two-gluon curve was calculated with the parameter values $(f_\rho,\, f_\rho^T,\, m) = (0.216\,\text{GeV},\, 0.160\,\text{GeV},\, m_\rho/2)$. The BFKL curve was calculated for the parameter values $(\alpha_s^{BFKL},\, \Lambda^2,\, f_\rho,\, f_\rho^T,\, m) = (0.25,\, m_\rho^2 - t,\, 0.216\,\text{GeV},\ 0.160\,\text{GeV},\, m_\rho/2)$.

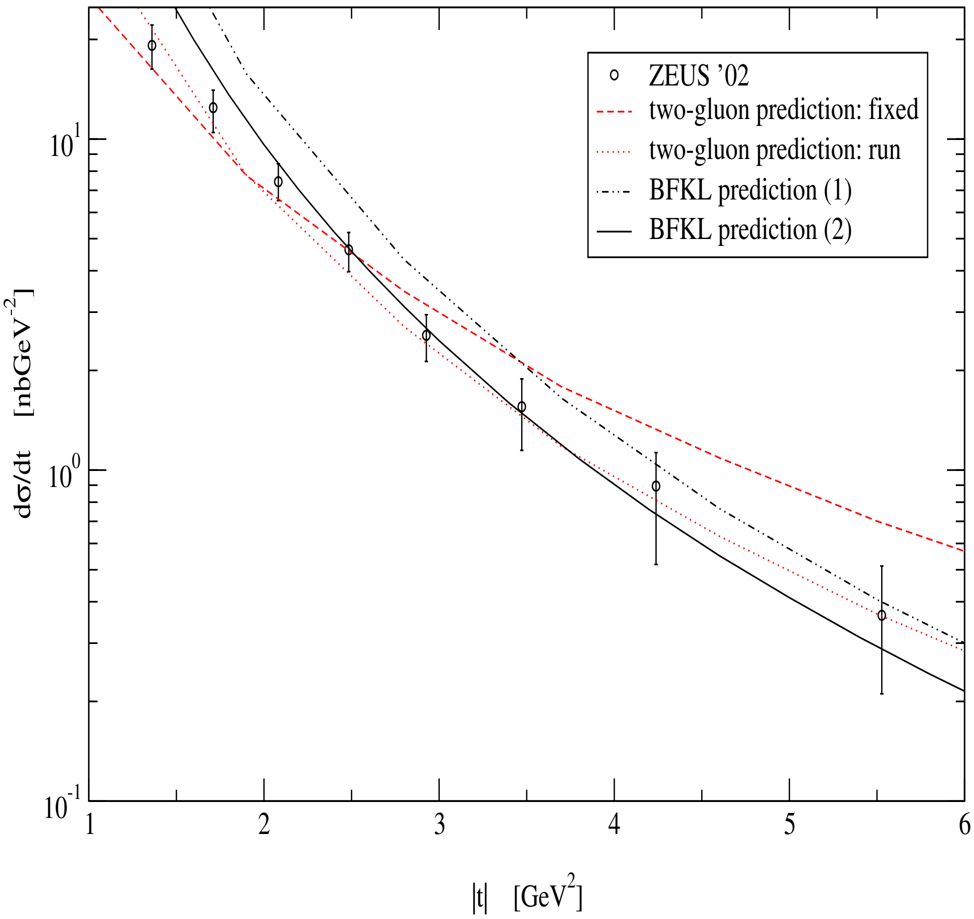

Figure 5.25: ϕ photoproduction: $d\sigma/dt$ for parameter values. The fixed two-gluon curve was calculated with the parameter values $(\alpha_s^{IF}, f_\phi, f_\phi^T, m) = (0.25, 0.231\,\mathrm{GeV}, 0.215\,\mathrm{GeV}, m_\phi/2)$. The run two-gluon curve was calculated with the parameter values $(\alpha_s^{IF}(1\,\mathrm{GeV}), f_\phi, f_\phi^T, m) = (0.28, 0.231\,\mathrm{GeV}, 0.215\,\mathrm{GeV}, m_\phi/2)$. BFKL prediction (1) is for the parameter values $(\alpha_s^{IF}, \alpha_s^{BFKL}, \Lambda^2, f_\phi, f_\phi^T, m) = (0.17, 0.25, m_\phi^2 - t, 0.231\,\mathrm{GeV}, 0.215\,\mathrm{GeV}, m_\phi/2)$. BFKL prediction (2) is for the parameter values $(\alpha_s^{IF}, \alpha_s^{BFKL}, \Lambda^2, f_\phi, f_\phi^T, m) = (0.17, 0.25, m_\phi^2 - t, 0.231\,\mathrm{GeV}, 0.171\,\mathrm{GeV}, m_\phi/2)$.

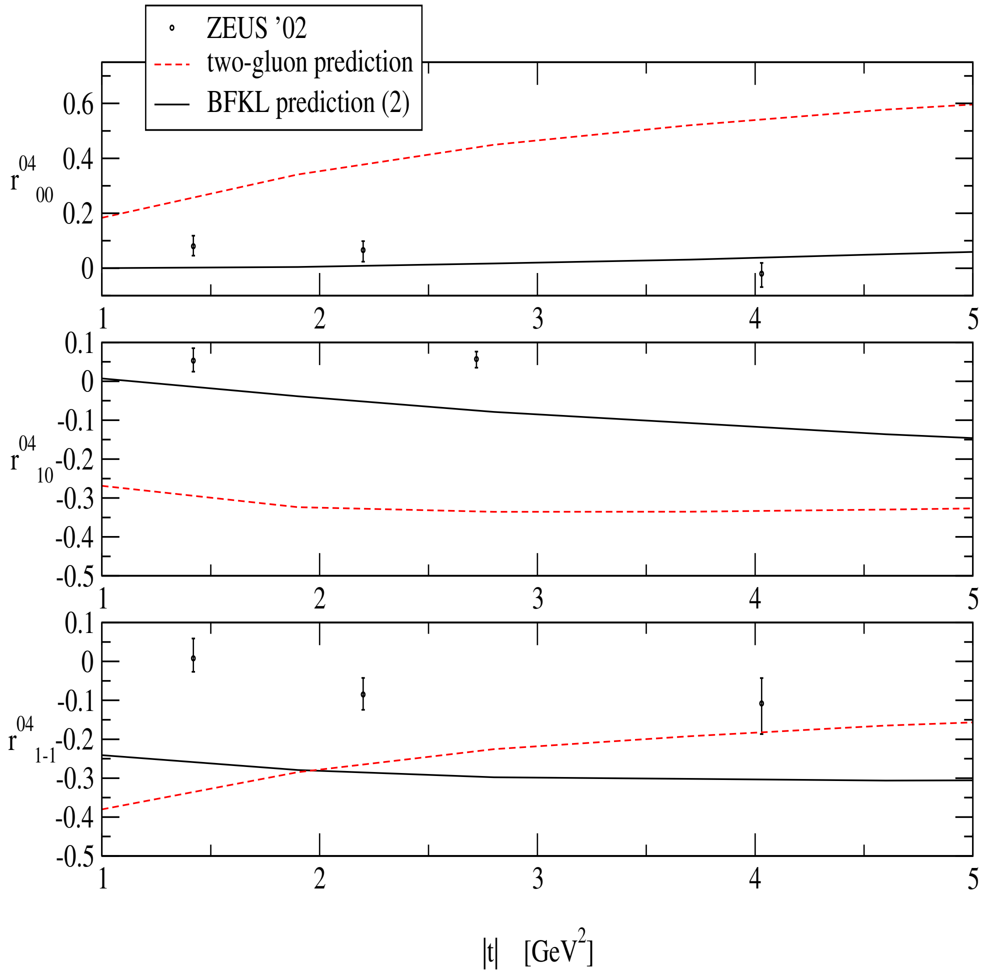

Figure 5.26: ϕ photoproduction: r-matrix element. The fixed two-gluon curve was calculated with the parameter values $(f_\phi,\ f_\phi^T,\ m) = (0.231\,\mathrm{GeV},\ 0.215\,\mathrm{GeV},\ m_\phi/2)$. The BFKL prediction ((2)) is for the parameter values $(\alpha_s^{BFKL},\ \Lambda^2,\ f_\phi,\ f_\phi^T,\ m) = (0.25,\ m_\phi^2 - t,\ 0.231\,\mathrm{GeV},\ 0.171\,\mathrm{GeV},\ m_\phi/2)$.

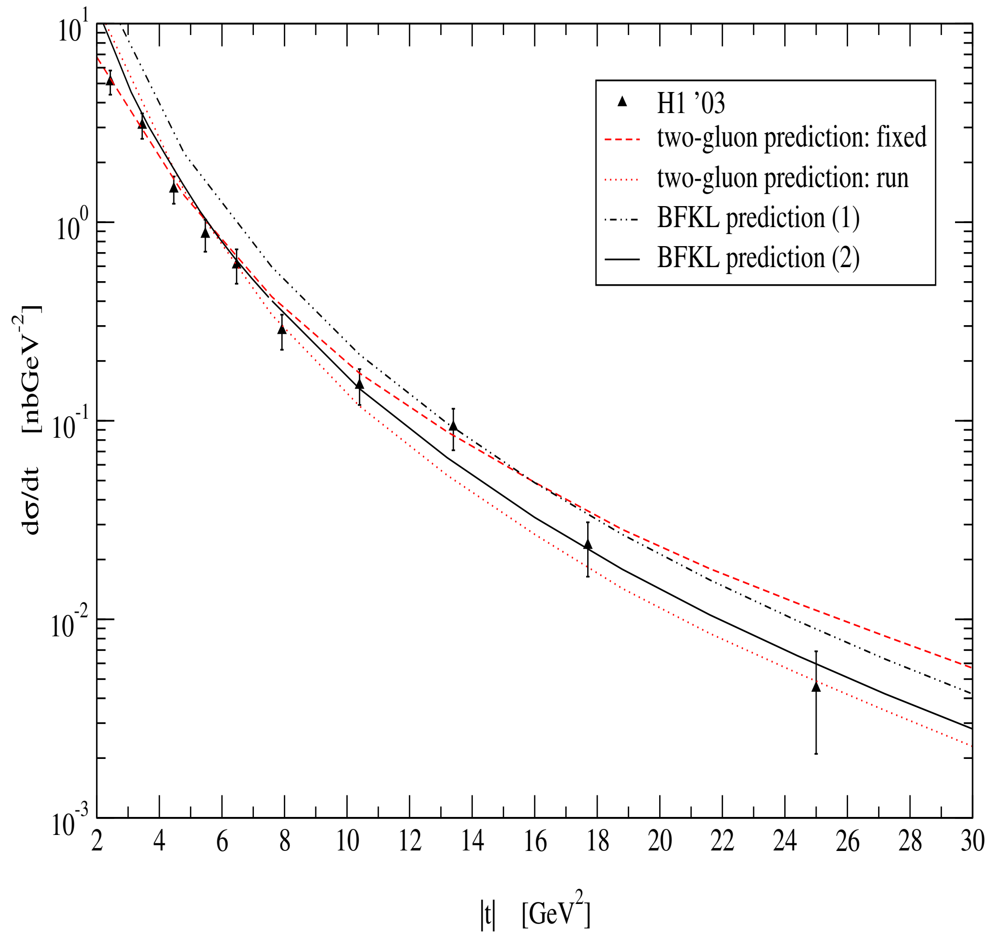

Figure 5.27: J/ψ photoproduction: $d\sigma/dt$. The fixed two-gluon curve was calculated with the parameter values $(\alpha_s^{IF}, f_{J/\psi}, f_{J/\psi}^T, m) = (0.23, 0.405\,\text{GeV}, 0.405\,\text{GeV}, m_{J/\psi}/2)$. The run two-gluon curve was calculated with the parameter values $(\alpha_s^{IF}(1\,\text{GeV})\ \ f_{J/\psi}, f_{J/\psi}^T, m) = (0.29, 0.405\,\text{GeV},\ \ 0.405\,\text{GeV}, m_{J/\psi}/2)$. BFKL prediction (1) is for the parameter values $(\alpha_s^{IF}, \alpha_s^{BFKL}, \Lambda^2, f_{J/\psi}, f_{J/\psi}^T, m) = (0.17, 0.25, m_{J/\psi}^2 - t, 0.405\,\text{GeV}, 0.405\,\text{GeV}, m_{J/\psi}/2)$. BFKL prediction (2) is for the parameter values $(\alpha_s^{IF}, \alpha_s^{BFKL}, \Lambda^2, f_{J/\psi}, f_{J/\psi}^T, m) = (0.17, 0.25, m_{J/\psi}^2 - t, 0.405\,\text{GeV}, 0.300\,\text{GeV}, m_{J/\psi}/2)$.

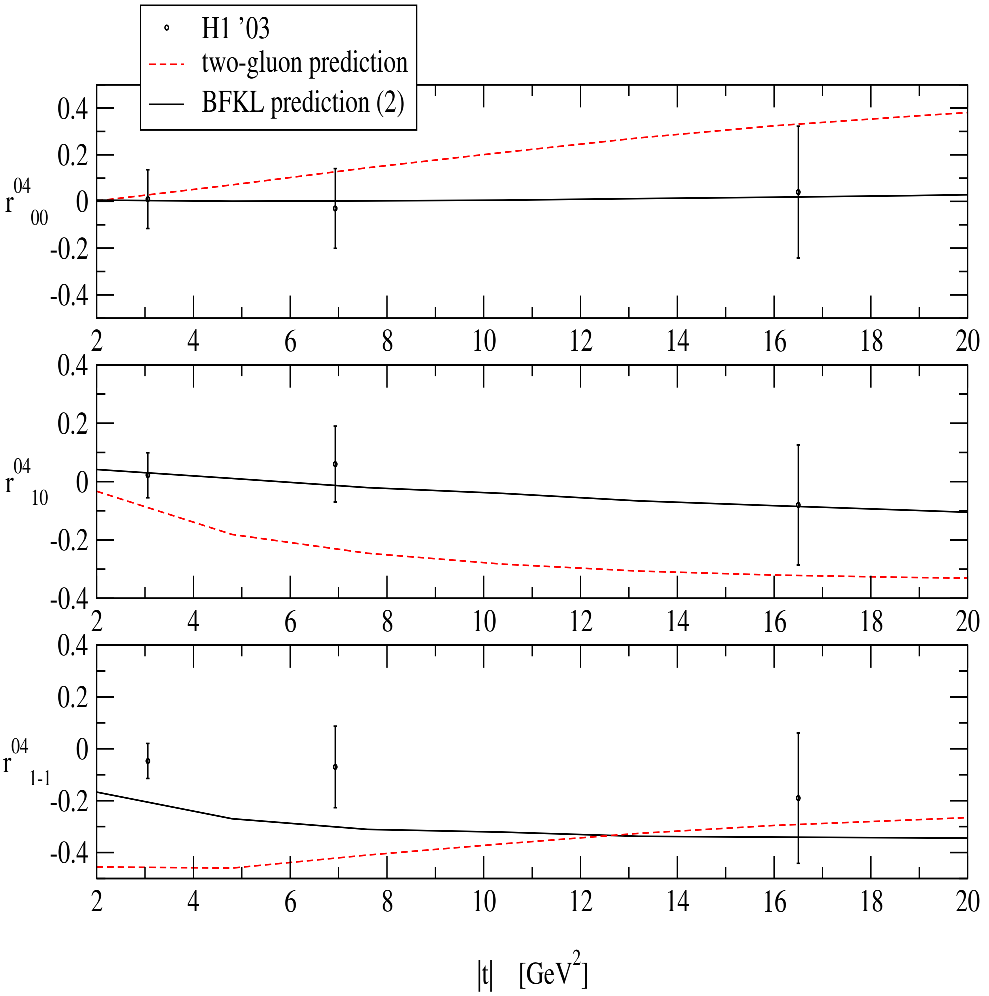

Figure 5.28: J/ψ photoproduction: r-matrix elements. The two-gluon curve was calculated with the parameter values $(f_{J/\psi},\ f^T_{J/\psi},\ m) = (0.405\,\text{GeV},\ 0.405\,\text{GeV},\ m_{J/\psi}/2)$. The BFKL prediction ((2)) is for the parameter values $(\alpha_s^{BFKL},\ \Lambda^2,\ f_{J/\psi},\ f^T_{J/\psi},\ m) = (0.25,\ m^2_{J/\psi} - t,\ 0.405\,\text{GeV},\ 0.300\,\text{GeV},\ m_{J/\psi}/2)$.

5.6 Summary

We compared our theoretical prediction for $d\sigma/dt$ and the three r-matrix elements to the data of ZEUS and H1, in various levels of approximation. The only meson we found complete agreement for, in any scheme, was the J/ψ. We nevertheless could, generally, obtain good fits to the r^{04}_{00} observable. Fits to the cross-sections favoured running the BFKL scale in a natural way: $\Lambda^2 = m_V^2 - t$. The theoretical predictions for r^{04}_{10} were the main obstacles to obtaining satisfactory fits for the ρ and ϕ. We found the natural predictions of both two-gluon and BFKL pomeron exchange to be the wrong sign. The predictions of the observables proved insensitive to higher twist terms, suggesting that these corrections are unlikely to provide a solution. We also found that using the distribution amplitudes of BBKT had little effect on the quality of fits compared to the asymptotic ones. The inability of theoretical predictions to fit r^{04}_{10}, and the general sensitivity of the r-matrix elements to the quark mass parameter, m, therefore seem to locate the problem at the level of the hard subprocess. The data hint that we may require a greater suppression of larger dipoles than we predict and we tentatively suggest that this may be provided by Sudakov suppression of emissions off the quark lines.

We noted that the $\mathcal{M}^{odd}_{++}$ contribution dominated and demonstrated that this corresponded to the amplitude used in the BFKL calculation of [23] (which was, in addition, conducted in a δ-function approximation). We were able to get excellent agreement for the ϕ and J/ψ differential cross-sections *using the same parameters* that fitted the ρ. On the whole the evidence suggests that leading log BFKL predictions work well for the transverse amplitudes but, despite suppressing the longitudinal component relative to Born level, it fails to have enough control over this contribution.

Does the leading logarithm BFKL pomeron work? Yes and no. It fails when confronted with all the available data, but has success, even in crude approximations, when we consider only $d\sigma/dt$. Our results also show that the BFKL pomeron is clearly a positive step forward from two-gluon exchange in the attempt to accurately describe the r-matrix elements.

Chapter 6

Conclusion

The aim of this thesis was to contribute to the understanding of the strong force through the investigation of the diffractive photoproduction of vector mesons. Chapters 1 to 3 provided a synthesis of previous work in the field. In Chapter 1 we introduced fundamental concepts and results that allowed us to calculate the $\gamma \to V$ impact factor, to leading log accuracy, in Chapter 2. These results for the six helicity amplitudes had been presented before [25]. Using our results we were able to demonstrate that the leading twist contributions (collinear quarks) were $\mathcal{M}^{even}_{\gamma(+)V(0)}$ and $\mathcal{M}^{odd}_{\gamma(+)V(+)}$, where *even* and *odd* refer to quark and anti-quark chiralities. We showed that these reduced to the Born level results of [17] (who obtained their results outside the light-cone formalism) in Chapter 3. In that chapter we also reobtained the BFKL results of [19, 20, 23] in the heavy meson approximation. In Chapter 4 we presented entirely new results for the generalisation of the results of [25] from Born level to leading log BFKL level, outside of the light-quark limit. In Chapter 5 we compared to the observables measured by the ZEUS and H1 collaborations at HERA, for ρ, ϕ and J/ψ photoproduction. These observables were the total differential cross-section, $d\sigma/dt$, and the three r-matrix elements relating to the angular decay distribution of the vector meson two-body decay products.

We demonstrated that the massive quark BFKL predictions were a marked improvement on Born level, the latter predicting a far too large longitudinal component.

We did not explore whether the full BFKL machinery was required to make this improvement. What would the prediction of the exchange of two-gluons plus one rung be? Is the resummation of some terms in the BFKL equation enough (see the resummation corresponding to gluon reggeisation outlined in Appendix E)? Whether we require the full BFKL result or not, it is clear that the full BFKL result is not enough to accurately describe all the observables. In particular we predicted the wrong sign and magnitude for r^{04}_{10}, in the case of the ρ and the ϕ. We presented arguments suggesting that this discrepency was unlikely to be solved by an appeal to higher twist or more accurate meson distribution amplitudes.

Could next-to-leading logarithms provide the solution to fitting the HERA data for the three r-matrix elements? To calculate these would be a formidable task. We would be required to calculate the next-to-leading order impact factors, the-next-to-leading order BFKL pomeron as well as consider the various next-to-leading terms we have thrown away in the light-cone hadronic matrix elements, in the vector meson polarisation vectors and in kinematic variables. Alternatively, perhaps there is some other vital missing ingredient that is an impediment to comprehensively understanding the data? The sensitivity of the helicity amplitudes, especially the longitudinal, to the suppression of end-point contributions, hints that the solution may be in a further suppression of large dipole sizes, through for example, Sudakov suppression. The process of vector meson photoproduction at high momentum exchanges certainly promises to remain a rich field for theoretical and experimental work[1].

[1]The new results presented in Chapter 5 of this thesis have recently been published (hep-ph/0311017).

Appendix A

The polarisation vectors of a vector meson

The polarisation vectors of a vector meson, $e^{[\alpha]}$, must obey the conditions:

$$e^{[0]} \cdot e^{[0]*} = 1, \tag{A.1}$$

$$e^{[0]} \cdot e^{[i]*} = 0 \tag{A.2}$$

and

$$e^{[i]} \cdot e^{[j]*} = -\delta_{ij} \tag{A.3}$$

where $i, j = 1, 2 \,\mathrm{or}\, 3$. Let us work in the frame where the directions $i = 1, 2$ are transverse to the momentum of the the meson, p. We can then write

$$e^{[1]} = -\frac{1}{\sqrt{2}}(0, 1, i, 0), \tag{A.4}$$

$$e^{[2]} = \frac{1}{\sqrt{2}}(0, 1, -i, 0) \tag{A.5}$$

and

$$e^{[0]} = \frac{p}{m_V}. \tag{A.6}$$

The high energy centre-of mass frame

Consider the centre-of-mass frame for two-to-two scattering, at high energies. We may write the meson momentum

$$p = p_1 + \frac{m_V^2}{s} p_2 \tag{A.7}$$

where we define

$$p_1 = (\frac{\sqrt{s}}{2}, 0, 0, -\frac{\sqrt{s}}{2}) \tag{A.8}$$

and

$$p_2 = (\frac{\sqrt{s}}{2}, 0, 0, \frac{\sqrt{s}}{2}). \tag{A.9}$$

The longitudinal vector is constrained by the other three. We can construct it using the totally antisymmetric tensor. We find

$$e^{[3]\mu} = N \epsilon^{\mu\nu\sigma\rho} e_\nu^{[1]} e_\sigma^{[2]} p_\rho = i\frac{N}{2}\sqrt{s}(1 - m_V^2/s, 0, 0, 1 + m_V^2/s). \tag{A.10}$$

We can eliminate N by noting that

$$e^{[3]} \cdot e^{[3]*} = -m_V^2 |N|^2 = -1. \tag{A.11}$$

This gives

$$\begin{aligned} e^{[3]\mu} &= e^{i\phi} \frac{\sqrt{s}}{2m_V}(1 - m_V^2/s, 0, 0, 1 + m_V^2/s) \\ &= e^{i\phi} \frac{1}{m_V}\left(p_1 - \frac{m_V^2}{s} p_2\right), \end{aligned} \tag{A.12}$$

where ϕ is some unprescribed phase factor. It is straightforward to confirm that

$$e^{[3]} \cdot e^{[0]*} = 0 \quad \text{and} \quad e^{[3]} \cdot e^{[3]*} = -1. \tag{A.13}$$

When these two polarisation vectors are not contracted together, to leading logs, we have

$$e^{[3]} = e^{i\phi}\, e^{[0]} = e^{i\phi} \frac{p}{m_V}. \tag{A.14}$$

The meson rest frame

In the meson rest frame we write the meson 4-momentum

$$p = (m_V, 0, 0, 0) \tag{A.15}$$

and

$$e^{[0]} = (1, 0, 0, 0). \tag{A.16}$$

The polarisations

$$e^{[\pm]} = \mp\frac{1}{\sqrt{2}}(0, 1, \pm 1, 0) \tag{A.17}$$

in conjunction with this yield

$$e^{[3]} = e^{i\phi}(0, 0, 0, 1), \tag{A.18}$$

with ϕ again an unprescribed phase factor, and where the orthogonality and normalisation conditions can be seen to be fulfilled by inspection.

A general frame

The two polarisation vectors found in the two different frames above are examples of the general result that for

$$e^{[0]} = \frac{1}{m_V}(p^0, 0, 0, |\vec{p}|), \tag{A.19}$$

we find

$$e^{[0]} = \frac{e^{i\phi}}{m_V}(|\vec{p}|, 0, 0, p^0). \tag{A.20}$$

Our choice of phase, which proves to correspond with that implicitly assumed in experiment, is $\phi = 0$. This gives us the three independent vector meson polarisations: one longitudinal ((0)) and two transverse ((±)). We have

$$e^{(0)} = \frac{1}{m_V}(|\vec{p}|, 0, 0, p^0) \tag{A.21}$$

and

$$e^{(\pm)} = \mp\frac{1}{\sqrt{2}}(0, 1, \pm 1, 0). \tag{A.22}$$

Appendix B

The electronic decay width of a meson

We wish to calculate the lowest order contribution to the decay $V \to e^+e^-$. The amplitude for this decay is given by the diagram below.

Using the techniques of Chapter 2, section 2.1, we can write the $V \to e^+e^-$ transition,

$$\langle e^+e^-|T|V(p,\lambda)\rangle = \int d^4r \frac{d^4l}{(2\pi)^4} e^{i\frac{r}{2}(2l-p')}$$
$$\times\langle 0|\bar{\psi}_\alpha(-r/2)\psi_\beta(r/2)|V(p,\lambda)\rangle(2\pi)^4\delta^{(4)}(p-p')\mathcal{A}^{q\bar{q}\to e^+e^-}_{\alpha\beta}(l,p-l). \quad \text{(B.1)}$$

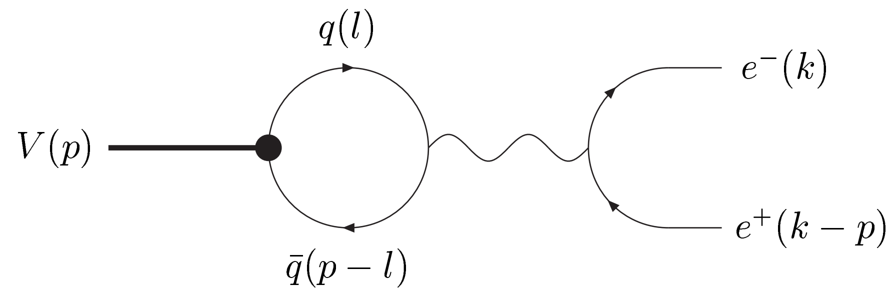

Figure B.1: The lowest order contribution to the decay $V \to e^+e^-$.

From the definition of the scattering amplitude in (2.1) we therefore arrive at

$$\begin{aligned}\mathcal{M}(V \to e^+e^-) &= \int d^4r \frac{d^4l}{(2\pi)^4} e^{i\frac{r}{2}(2l-p)} \\ &\times \langle 0|\bar{\psi}_\alpha(-r/2)\psi_\beta(r/2)|V(p,\lambda)\rangle \mathcal{A}_{\alpha\beta}^{q\bar{q}\to e^+e^-}(l,p-l) \\ &= \int d^4r \frac{d^4l}{(2\pi)^4} e^{i\frac{r}{2}(2l-p)} \psi_{\alpha\beta}^{(\lambda)*}(r/2,-r/2)\mathcal{A}_{\alpha\beta}^{q\bar{q}\to e^+e^-}(l,p-l), \end{aligned} \tag{B.2}$$

where we define,

$$\psi_{\alpha\beta}^{(\lambda)*}(r/2,-r/2) = \langle 0|\bar{\psi}_\alpha(-r/2)\psi_\beta(r/2)|V(p,\lambda)\rangle. \tag{B.3}$$

The quark and anti-quark must annihilate to a photon to produce two leptons. The lowest order contribution to this is pure QED and can be written,

$$i\mathcal{A}_{\alpha\beta}^{q\bar{q}\to e^+e^-} = (-ieQ_V\gamma_{\alpha\beta\,\mu})\frac{-ig^{\mu\nu}}{p^2}\bar{u}_s(k)(-ie\gamma_\nu)v_{s'}(p-k). \tag{B.4}$$

This amplitude has no dependence on l, rendering the l and r integrations trivial. Therefore

$$\mathcal{M}(V \to e^+e^-) = \psi_{\alpha\beta}^{(\lambda)*}(0,0)\mathcal{A}_{\alpha\beta}^{q\bar{q}\to e^+e^-} \tag{B.5}$$

To proceed, we will disentangle the spinor indices using the Fierz transformation. This gives us,

$$\mathcal{M}(V \to e^+e^-) = \frac{1}{4}(\Gamma^t_{\alpha'\beta'}\psi^\lambda_{\alpha'\beta'}(0,0))(\Gamma_{\beta\alpha,\,t}\mathcal{A}_{\alpha\beta}^{q\bar{q}\to e^+e^-}(p)). \tag{B.6}$$

Now, from (2.147) we know,

$$\gamma^\mu_{\alpha\beta}\psi_{\alpha\beta}^{(\lambda)*}(0,0) = f_V m_V e^{(\lambda)\,\mu}. \tag{B.7}$$

This is the only Fierz component that contributes since all others give zero when the trace is taken with the hard subamplitude. That is,

$$\Gamma_{\beta\alpha,\,t}\mathcal{A}_{\alpha\beta}^{q\bar{q}\to e^+e^-}(p) = e^2 Q_V \frac{\bar{u}_s(k)\gamma_\nu v_{s'}(p-k)}{p^2} Tr[\gamma_\mu\gamma^\nu], \tag{B.8}$$

giving us the full amplitude

$$\mathcal{M}(V(\lambda) \to e_s^+e_{s'}^-) = e^2 f_V Q_V m_V e^{(\lambda)\,\nu}\frac{\bar{u}_s(k)\gamma_\nu v_{s'}(p-k)}{p^2}. \tag{B.9}$$

Let us work in the rest frame of the initial state meson. Therefore,

$$\mathcal{M}(V \to e^+e^-) = \frac{e^2 f_V Q_V}{m_V} e^{(\lambda)\,\nu} \bar{u}_s(k)\gamma_\nu v_{s'}(p-k). \tag{B.10}$$

Squaring the matrix, summing over final states, and averaging over initial states we get,

$$\begin{aligned}\frac{1}{3}\sum_{s,s',\lambda} |\mathcal{M}(V \to e_s^+ e_{s'}^-)|^2 &= \frac{e^4 f_V^2 Q_V^2}{3m_V^2} \sum_\lambda e^{(\lambda)\,\nu} e^{(\lambda)\,\mu\,*}\, Tr[(\not{k} + m_e)\gamma_\nu(\not{p} - \not{k} - m_e)\gamma_\mu] \\ &= \frac{4e^4 f_V^2 Q_V^2}{3m_V^2} \sum_\lambda e^{(\lambda)\,\nu} e^{(\lambda)\,\mu\,*} \left(k_\nu(p-k)_\mu + k_\mu(p-k)_\nu - g_{\mu\nu}(k\cdot(p-k) + m_e^2)\right).\end{aligned} \tag{B.11}$$

Using the Ward identity we can make the replacement,

$$\sum_\lambda e^{(\lambda)\,\nu} e^{(\lambda)\,\mu\,*} \to -g^{\mu\nu}. \tag{B.12}$$

Thus

$$\begin{aligned}\frac{1}{3}\sum_{s,s',\lambda} |\mathcal{M}(V(\lambda) \to e_s^+ e_{s'}^-)|^2 &= -\frac{4e^4 f_V^2 Q_V^2}{3m_V^2}\left(2k\cdot(p-k) - 4(k\cdot(p-k) + m_e^2)\right) \\ &= \frac{4e^4 f_V^2 Q_V^2}{3m_V^2}\left(2k\cdot(p-k) + 4m_e^2\right) \\ &= \frac{4e^4 f_V^2 Q_V^2}{3m_V^2}\left(m_V^2 + 2m_e^2\right)\end{aligned} \tag{B.13}$$

where we have used the fact that

$$k\cdot p = m_V^2/2 \tag{B.14}$$

in the meson rest frame and that

$$k^2 = m_e^2. \tag{B.15}$$

Using this result we can find the electronic decay width of the meson. We use

$$\Gamma(V \to e^+e^-) = \frac{1}{2m_V}\int d(P.S.^2)\frac{1}{3}\sum_{\lambda,s,s'} |\mathcal{M}(V(\lambda) \to e_s^+ e_{s'}^-))|^2, \tag{B.16}$$

and assuming isotropy we find

$$
\begin{aligned}
&\Gamma(V \to e^+e^-) = \frac{1}{16\pi}\frac{2|k|}{m_V^2}\frac{1}{3}\sum_{\lambda,s,s'} |\mathcal{M}(V(\lambda) \to e_s^+ e_{s'}^-))|^2 \\
&= \frac{1}{16\pi m_V}\left(1 - \frac{4m_e^2}{m_V^2}\right)^{1/2} \frac{1}{3}\sum_{\lambda,s,s'} |\mathcal{M}(V(\lambda) \to e_s^+ e_{s'}^-))|^2 \\
&= \frac{4\pi\alpha^2 f_V^2 Q_V^2}{3m_V}\left(1 + \frac{2m_e^2}{m_V^2}\right)\left(1 - \frac{4m_e^2}{m_V^2}\right)^{1/2} \\
&\simeq \frac{4\pi\alpha^2 f_V^2 Q_V^2}{3m_V}.
\end{aligned}
\tag{B.17}
$$

This result corresponds with that of [55]. It allows us to determine the vector coupling of the meson from its decay to an electron and positron.

Appendix C

The angular distribution of the $\mu^+\mu^-$ decay from a vector meson produced by diffractive photoproduction

Angular dependence

In the main body of the thesis, we calculated the helicity amplitudes for the process $\gamma(+)q \to V(\lambda)q$, which we denoted $\mathcal{M}_{+\lambda}$. The transverse momentum exchanged in the hard subprocess is denoted $\mathbf{q}$. The vector mesons are not measured directly in experiment. Their two body decays are measured, from which the momentum state, but not the polarisation state, of the vectors mesons can be reconstructed. This leaves us the possibility of quantum interference effects between the vector meson production helicity amplitudes. Consider the case of muonic decay. We may write the angular dependence of the two body decay products

$$W(\theta_h,\phi_h) \propto \sum_{s,s',\lambda,\lambda'} \langle \mu^+(s)\mu^-(s')|V(\lambda)\rangle \, \langle V(\lambda)|\gamma(+)\rangle \, \langle \gamma(+)|V(\lambda')\rangle \, \langle V(\lambda')|\mu^+(s)\mu^-(s')\rangle, \tag{C.1}$$

where we define θ_h and ϕ_h are the angles of the positive decay product, with the direction of the vector meson defining the z-axis. We have factorised out the hard scatter from the quark line for simplicity - it makes no difference. We can therefore write

$$W(\theta_h, \phi_h) \propto \sum_{s,s',\lambda,\lambda'} \mathcal{M}_{V(\lambda)\to\mu^+(s)\mu^-(s')} \mathcal{M}^*_{V(\lambda')\to\mu^+(s)\mu^-(s')} \mathcal{M}_{+\lambda} \mathcal{M}^*_{+\lambda'}. \tag{C.2}$$

The calculation of $\mathcal{M}_{+\lambda}$ was what chapters 1 to 4 of this thesis was about. But, also in fact, we calculated $\mathcal{M}_{V(\lambda)\to\mu^+(s)\mu^-(s')}$ in Appendix B. The result (B.10) gives us

$$\mathcal{M}_{V(\lambda)\to\mu^+(s)\mu^-(s')} = \frac{e^2 f_V Q_V}{m_V} e^{(\lambda)\,\nu} \bar{u}_{s'}(l-p)\gamma_\nu v_s(l). \tag{C.3}$$

To unlock the angular dependence from this we need to make use of some Dirac algebra results.

Angular decomposition of the vector coupling

We define the vector coupling current

$$j_\mu = \bar{u}(\Lambda', l')\gamma_\mu v(\Lambda, l), \tag{C.4}$$

where we denote the *helicities* of the muon (anti-muon), $\Lambda' = \pm 1$ ($\Lambda = \pm 1$). The results of [56] allow us to write in the massless muon limit

$$j_\mu = -m_V\, \eta^\Lambda_\mu(l)\, \delta_{\Lambda,-\Lambda'}. \tag{C.5}$$

where working in the meson rest-frame

$$\begin{aligned} l + l' &= (m_V, 0, 0, 0), \\ l &= (m_V/2, |\vec{l}\,| \sin\theta_h \cos\phi_h, |\vec{l}\,| \sin\theta_h \sin\phi_h, |\vec{l}\,| \cos\phi_h), \\ l' &= (m_V/2, -\vec{l}\,), \end{aligned} \tag{C.6}$$

and $\eta_i(l) \cdot l = 0$, $\eta_i^2 = -1$ with $\eta_1 \cdot \eta_2 = 0$. The authors of [56] also provide[1]

$$\begin{aligned} \eta^\Lambda_\mu(l) &= \eta_1(l) - i\Lambda\, \eta_2(l) \\ \eta_1 &= (0, -\cos\theta_h \cos\phi_h, \cos\theta_h \sin\phi_h, -\sin\theta_h) \\ \eta_2 &= (0, \sin\phi_h, \cos\phi_h, 0). \end{aligned} \tag{C.7}$$

[1] We have taken angles with respect to the positive particle, unlike the convention in [56]. Our η vectors therefore relate to theirs by $\theta_h \to \pi - \theta_h$ and $\phi_h \to -\phi_h$.

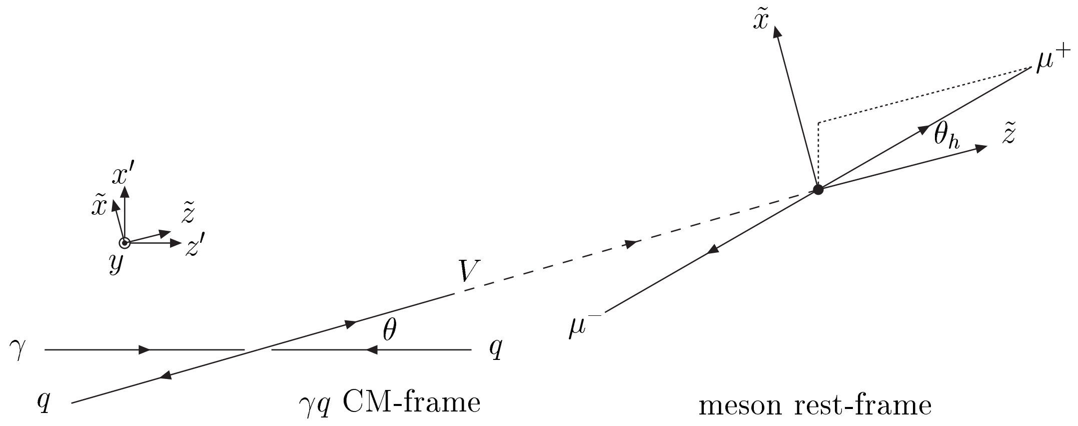

Figure C.1: The coordinate systems defined by the initial (γq) and final (Vq) states. For the calculation of the helicity amplitudes we work in the γq CM frame. The meson 3-momentum defines the $\tilde{z}$-axis. Helicity amplitudes are Lorentz invariant. For the decay of the vector meson we work in the vector meson rest-frame. Note that the muon pair decay vectors will not in general lie in the $x-z$ plane.

Using these results we find

$$\begin{aligned}(e^{(0)\mu} j_\mu)_\Lambda &= -m_V \delta_{\Lambda,-\Lambda'} \sin\theta_h \\ (e^{(\pm)\mu} j_\mu)_\Lambda &= -m_V \delta_{\Lambda,-\Lambda'} \frac{1}{\sqrt{2}} (\mp \cos\theta_h + \Lambda) e^{\mp i\phi_h}.\end{aligned} \tag{C.8}$$

Summing over helicities

From the results of the previous subsections we know therefore that

$$W(\theta_h, \phi_h) \propto \sum_{\Lambda,\lambda,\lambda'} (e^\lambda_\mu j^\mu)_\Lambda (e^{\lambda' *}_\mu j^\mu)_\Lambda \,\mathcal{M}_{+\lambda} \mathcal{M}^*_{+\lambda'}. \tag{C.9}$$

We now need to perform the sum over the anti-muon and vector meson helicities.

In experiment, the momentum exchange in the hard subprocess is defined to be in the (positive) x-direction [47], as illustrated in figure C.1. It is useful for us to work in this coordinate system. Note that the definition of the transverse polarisation vectors

(A.22), have an imaginary y component. This choice of polarisation vector gives the $(+0)$ and $(+-)$ helicity amplitudes a real component as well as an imaginary one, if $\mathbf{q}$ takes on a non-zero y-component (see (2.193), (2.195), (2.196), (2.198)). Choosing $\mathbf{q}$ in the x-direction renders all the vector meson helicity amplitudes purely imaginary and we can use the relation

$$\mathcal{M}_{+\lambda}\mathcal{M}^*_{+\lambda'} = \mathcal{M}_{+\lambda'}\mathcal{M}^*_{+\lambda}. \tag{C.10}$$

Performing the summations we arrive at:

$$\begin{aligned}
&W(\theta_h,\phi_h) \propto \\
&+(1+\cos^2\theta_h)\,|\mathcal{M}_{+-}|^2 + \frac{1}{\sqrt{2}}\sin 2\theta_h\, e^{i\phi_h}\,\mathcal{M}_{+-}\mathcal{M}^*_{+0} \\
&+(1-\cos^2\theta_h)\,e^{2i\phi_h}\,\mathcal{M}_{+-}\mathcal{M}^*_{++} + \frac{1}{\sqrt{2}}\sin 2\theta_h\, e^{-i\phi_h}\,\mathcal{M}_{+0}\mathcal{M}^*_{+-} \\
&2\sin^2\theta_h\,|\mathcal{M}_{+0}|^2 - \frac{1}{\sqrt{2}}\sin 2\theta_h\, e^{i\phi_h}\,\mathcal{M}_{+0}\mathcal{M}^*_{++} \\
&+(1-\cos^2\theta_h)\,e^{-2i\phi_h}\mathcal{M}_{++}\mathcal{M}^*_{+-} - \frac{1}{\sqrt{2}}\sin 2\theta_h\, e^{-i\phi_h}\,\mathcal{M}_{++}\mathcal{M}^*_{+0} \\
&\qquad +(1+\cos^2\theta_h)\,|\mathcal{M}_{++}|^2.
\end{aligned} \tag{C.11}$$

Dividing through by $\sum_\lambda |\mathcal{M}_{+\lambda}|^2$, using relation (C.10) and a little manipulation, we find

$$\begin{aligned}
&W(\theta_h,\phi_h) \propto \left[1+\left(\frac{|\mathcal{M}_{+0}|^2}{\sum_\lambda |\mathcal{M}_{+\lambda}|^2}\right)\right] - \left[3\left(\frac{|\mathcal{M}_{+0}|^2}{\sum_\lambda |\mathcal{M}_{+\lambda}|^2}\right) - 1\right]\cos^2\theta_h \\
&+2\sqrt{2}\,\left(\frac{1}{2}\frac{\mathcal{M}_{++}\mathcal{M}^*_{+0} - \mathcal{M}_{+-}\mathcal{M}^*_{+0}}{\sum_\lambda |\mathcal{M}_{+\lambda}|^2}\right)\,\sin 2\theta_h\,\cos\phi_h \\
&+2\sin^2\theta_h\,\cos 2\phi_h\,\left(\frac{\mathcal{M}_{++}\mathcal{M}^*_{+-}}{\sum_\lambda |\mathcal{M}_{+\lambda}|^2}\right).
\end{aligned} \tag{C.12}$$

This angular distribution is at the parton level, when we convolute the products of amplitudes with the parton distribution functions (denoting the convolution $\langle ... \rangle$) we get[2]

$$
\begin{aligned}
W(\theta_h,\phi_h) &\propto \frac{1}{2}\left[1+\left(\frac{\langle|\mathcal{M}_{+0}|^2\rangle}{\sum_\lambda\langle|\mathcal{M}_{+\lambda}|^2\rangle}\right)\right]-\frac{1}{2}\left[3\left(\frac{\langle|\mathcal{M}_{+0}|^2\rangle}{\sum_\lambda\langle|\mathcal{M}_{+\lambda}|^2\rangle}\right)-1\right]\cos^2\theta_h \\
&+\sqrt{2}\left(\frac{1}{2}\frac{\langle\mathcal{M}_{++}\mathcal{M}^*_{+0}\rangle-\langle\mathcal{M}_{+-}\mathcal{M}^*_{+0}\rangle}{\sum_\lambda\langle|\mathcal{M}_{+\lambda}\rangle|^2}\right)\sin 2\theta_h\,\cos\phi_h \\
&+\sin^2\theta_h\,\cos 2\phi_h\left(\frac{\langle\mathcal{M}_{++}\mathcal{M}^*_{+-}\rangle}{\sum_\lambda\langle|\mathcal{M}_{+\lambda}|^2\rangle}\right) \\
&=\left[\frac{1}{2}(1+r^{04}_{00})-\frac{1}{2}(3r^{04}_{00}-1)\cos^2\theta_h\right. \\
&\left.+\sqrt{2}\mathrm{Re}[r^{04}_{00}]\,\sin 2\theta_h\,\cos\phi_h+r^{04}_{1-1}\,\sin^2\theta_h\,\cos 2\phi_h\right],
\end{aligned}
\tag{C.13}
$$

where we have used the definitions (5.10-5.12) in conjunction with the assumption that all the helicity amplitudes are imaginary (which is true in our calculation). Our result agrees with the result (5.9) quoted for decays to fermions. We have arrived at the angular distribution for $\gamma p \to VX \to \mu^+\mu^- X$. Notice that if we had chosen the momentum exchange in the hard subprocess to be in the $-x$ direction, then the sign of the term proportional r^{04}_{10} would flip sign. Our convention for our coordinate system is the same as used at HERA, however, and our angular distribution agrees with their result. The sign that we have obtained for the r^{04}_{10} term is also dependent on the phase of the longitudinal polarisation vector in (A.21). The fact that we have derived the same angular distribution as the ZEUS and H1 groups quote tells us that we agree with their implicit choice of phase.

[2]Note, for when comparing to (5.10-5.12), that our choice of coordinate system gives $\mathcal{M}_{++}=\mathcal{M}_{--}$, $\mathcal{M}_{+-}=\mathcal{M}_{-+}$ and $\mathcal{M}_{+0}=-\mathcal{M}_{-0}$.

Appendix D

Vector meson distribution amplitudes

Distribution amplitudes arise in non-perturbative wavefunctions when they are expressed in terms of their light-cone expansion. They relate to the momentum fraction distributions of partons of a particular Fock state within a meson. The amplitudes are categorised according to their suppression in momentum, or 'twist'. The distribution amplitudes that are relevant to this thesis are up to and including twist-4 and are classified in table (D.1). Ball, Braun, Koike and Tanaka presented results for the parameterisation of the complete set of distribution amplitudes up to twist-3 for the ρ and ϕ (and K) [33]. Ball and Braun then presented the twist-4 results for the ρ in a later paper [32]. We summarise their relevant results in this appendix. Their results are exact up to the third term in an expansion. Note that their distribution amplitudes are not only in fact a function of the light-cone momentum fraction, u,

twist	2 $O(1)$	3 $O(1/q)$	4 $O(1/q^2)$
$\parallel$	$\phi_\parallel$	$h_\parallel^{(t)}$, $h_\parallel^{(s)}$	
$\perp$	$\phi_\perp$	$g_\perp^{(v)}$, $g_\perp^{(a)}$	h_3

Table D.1: Classification of distribution amplitudes up to twist-4.

	$a_1^\parallel$	$a_2^\parallel$	ζ_3	ω_3^A	ω_3^V	ζ_4	ω_4^A
ρ	0	0.18 ± 0.10	0.032 ± 0.010	-2.1 ± 1.0	3.8 ± 1.8	0.15 ± 0.10	0.8 ± 0.8
ϕ	0	0 ± 0.10	0.032 ± 0.010	-2.1 ± 1.0	3.8 ± 1.8	unavailable	unavailable

Table D.2: Chiral even parameters: $\mu^2 = 1\,\mathrm{GeV}^2$.

	$a_1^\perp$	$a_2^\perp$	ζ_3	ω_3^T	ζ_4^T	$\tilde{\zeta}_4^T$
ρ	0	0.20 ± 0.10	0.032 ± 0.010	7.0 ± 7.0	0.1 ± 0.05	-0.10 ± 0.05
ϕ	0	0 ± 0.10	0.032 ± 0.010	7.0 ± 7.0	unavailable	unavailable

Table D.3: Chiral odd parameters: $\mu^2 = 1\,\mathrm{GeV}^2$.

but also a renormalisation scale, μ^2. This is significant because the parameters in the expansion of the distribution amplitudes are dependent on μ^2. The values of the expansion parameters were presented at $\mu^2 = 1\,\mathrm{GeV}^2$. Strictly, they should be evaluated at the large momentum exchange, q. Since, however, they run slowly with the scale (as a logarithm to a fractional power) we neglect to do so. In the $q \to \infty$ limit the parameters vanish. We refer to this as the asymptotic limit, and the distribution amplitudes in this limit as the asymptotic distribution amplitudes. The distributions then correspond to only the first term in an expansion.

Tables (D.2, D.3) hold the values of all the relevant parameters, at the scale $\mu^2 = 1\,\mathrm{GeV}^2$.

The ϕ values are included for comparison, although we only use those of the ρ in the text. Note that the twist-4 parameters were unavailable for the ϕ. We also note that quark mass corrections, that we do not present in the following distribution amplitudes, will be significant for the ϕ.

D.1 Twist-2 distribution amplitudes

Even

There is one chiral even, twist-2 amplitude. This can be written

$$\phi_{||}(u) = 6u\bar{u}\left(1 + 3a_1^{||}\xi + a_2^{||}\frac{3}{2}(5\xi^2 - 1)\right). \tag{D.1}$$

The asymptotic distribution is therefore,

$$\phi_{||}^{asy}(u) = 6u\bar{u}. \tag{D.2}$$

Odd

There is one chiral odd, twist-2 amplitude. This can be written

$$\phi_{\perp}(u) = 6u\bar{u}\left(1 + 3a_1^{\perp}\xi + a_2^{\perp}\frac{3}{2}(5\xi^2 - 1)\right). \tag{D.3}$$

The asymptotic distribution is therefore,

$$\phi_{\perp}^{asy}(u) = 6u\bar{u}. \tag{D.4}$$

D.2 Twist-3 distribution amplitudes

Even

There are two even, twist-3 distributions. They can be written

$$g_{\perp}^{(a)}(u) = 6u\bar{u}\left[1 + \left\{\frac{1}{4}a_2^{||} + \frac{5}{3}\zeta_3\left(1 - \frac{3}{16}\omega_3^A + \frac{9}{16}\omega_3^V\right)\right\}(5\xi^2 - 1)\right] \tag{D.5}$$

and

$$\begin{aligned} g_{\perp}^{(v)}(u) &= \frac{3}{4}(1+\xi^2) + (\frac{3}{7}a_2^{||} + 5\zeta_3)(3\xi^2 - 1) \\ &+ \left[\frac{9}{112}a_2^{||} + \frac{15}{64}\zeta_3(3\omega_3^V - \omega_3^A)\right](3 - 30\xi^2 + 35\xi^4) \end{aligned} \tag{D.6}$$

where the subscript of '3' refers to three-particle corrections and we neglect mass corrections. In the asymptotic limit,

$$g_{\perp}^{(a)\,asy}(u) = 6u\bar{u}. \tag{D.7}$$

and

$$g_{\perp}^{(v)\,asy}(u) = \frac{3}{4}\,(1+\xi^2). \tag{D.8}$$

Odd

There are two odd twist-3 distributions. They can be written

$$h_{\parallel}^{(s)}(u) = 6u\bar{u}\left[1+\left(\frac{1}{4}a_2^{\perp}+\frac{5}{8}\zeta_3\omega_3^T\right)(5\xi^2-1)\right] \tag{D.9}$$

and

$$h_{\parallel}^{(t)}(u) = 3\xi^2+\frac{3}{2}\,a_2^{\perp}\,\xi^2(5\xi^2-3)+\frac{15}{16}\,\zeta_3\,\omega_3^T(3-30\xi^2+35\xi^4). \tag{D.10}$$

In the asymptotic limit,

$$h_{\parallel}^{(s)\,asy}(u) = 6u\bar{u} \tag{D.11}$$

and

$$h_{\parallel}^{(t)\,asy}(u) = 3\xi^2. \tag{D.12}$$

D.3 Twist-4 distribution amplitudes

Odd

There is one (relevant) odd twist-4 distribution;

$$\begin{aligned} h_3(u) = 1 &+ \left(-1+\frac{3}{7}a_2^{\perp}-10(\zeta_4^T+\tilde{\zeta}_4^T)\right)C_2^{1/2}(\xi) \\ &+ \left(-\frac{3}{7}a_2^{\perp}-\frac{15}{8}\zeta_3\omega_3^T\right)C_4^{1/2}(\xi). \end{aligned} \tag{D.13}$$

where $C_n^{\lambda}(\xi)$ are the Gegenbauer polynomials. In the asymptotic limit,

$$h_3^{asy} = 1 - C_2^{1/2}(\xi) = \frac{3}{2}(1-\xi^2). \tag{D.14}$$

D.4 Distribution amplitude schemes

We have previously obtained six helicity amplitudes (4.69-4.74). We now denote their individual dependence on the distribution amplitudes in terms of new functions, Φ:

$$(+0)\,\text{even}: \qquad \phi_{\|}(u) \equiv \Phi^{even}_{+0}(u) \tag{D.15}$$

$$(++)\,\text{even}: \qquad \left(\frac{g_{\perp}^{(a)}(u)}{4} - (1-2u)\int_0^u dv\,(\phi_{\|}(v) - g_{\perp}^{(v)}(v))\right) \equiv \Phi^{even}_{++}(u) \tag{D.16}$$

$$(+-)\,\text{even}: \qquad \left(\frac{g_{\perp}^{(a)}(u)}{4} + (1-2u)\int_0^u dv\,(\phi_{\|}(v) - g_{\perp}^{(v)}(v))\right) \equiv \Phi^{even}_{+-}(u) \tag{D.17}$$

$$(+0)\,\text{odd}: \qquad \Phi^{odd}_{+0}(u) \equiv \int_0^u dv\,\left(h_{\|}^{(t)}(v) - \phi_{\perp}(v)\right) \equiv \Phi^{odd}_{+0}(u) \tag{D.18}$$

$$(++)\,\text{odd}: \qquad \phi_{\perp}(u) \equiv \Phi^{odd}_{++}(u) \tag{D.19}$$

$$(+-)\,\text{odd}: \qquad \int_0^u dv \int_0^v d\eta\left(h_{\|}^{(t)}(\eta) - \frac{1}{2}\phi_{\perp}(\eta) - \frac{1}{2}h_3(\eta)\right) \equiv \Phi^{odd}_{+-}(u). \tag{D.20}$$

We now present the explicit formulae for these in four different prescriptions.

D.4.1 Prescription 1: leading twist (collinear) approximation with δ-function distributions

We keep only the twist-2 contributions and equate the corresponding distribution amplitudes to a δ-function that enforces the quark and anti-quark share the meson momentum equally. Then

$$\Phi^{even}_{+0}(u) = \delta\left(u - \frac{1}{2}\right) \tag{D.21}$$

$$\Phi^{even}_{++}(u) = 0 \tag{D.22}$$

$$\Phi^{even}_{+-}(u) = 0 \tag{D.23}$$

$$\Phi^{odd}_{+0}(u) = 0 \tag{D.24}$$

$$\Phi^{odd}_{++}(u) = \delta\left(u - \frac{1}{2}\right) \tag{D.25}$$

$$\Phi^{odd}_{+-}(u) = 0. \tag{D.26}$$

D.4.2 Prescription 2: leading twist (collinear) approximation with asymptotic distribution amplitudes

We keep only the twist-2 contributions and equate the corresponding distribution amplitudes to their asymptotic forms. Then

$$\Phi_{+0}^{even}(u) = 6u\bar{u} \tag{D.27}$$

$$\Phi_{++}^{even}(u) = 0 \tag{D.28}$$

$$\Phi_{+-}^{even}(u) = 0 \tag{D.29}$$

$$\Phi_{+0}^{odd}(u) = 0 \tag{D.30}$$

$$\Phi_{++}^{odd}(u) = 6u\bar{u} \tag{D.31}$$

$$\Phi_{+-}^{odd}(u) = 0. \tag{D.32}$$

D.4.3 Prescription 3: higher twist approximation with asymptotic distribution amplitudes

We keep all the twist terms we have calculated and equate the corresponding distribution amplitudes to the asymptotic forms. After integration, then

$$\Phi_{+0}^{even}(u) = 6u\bar{u} \tag{D.33}$$

$$\Phi_{++}^{even}(u) = 3u\bar{u}(u^2 + \bar{u}^2) \tag{D.34}$$

$$\Phi_{+-}^{even}(u) = 6u^2\bar{u}^2 \tag{D.35}$$

$$\Phi_{+0}^{odd}(u) = 3(1-2u)u\bar{u} \tag{D.36}$$

$$\Phi_{+-}^{odd}(u) = \frac{3}{2}u^2\bar{u}^2 \tag{D.37}$$

D.4.4 Prescription 4: higher twist approximation with BBKT distribution amplitudes

We keep all the twist terms we have calculated and equate the corresponding distribution amplitudes to the BBKT forms listed in this appendix. Then, For the full results we just again have:

$$\Phi_{+0}^{even}(u) \equiv \phi_{\|}(u) \tag{D.38}$$

$$\Phi_{++}^{even}(u) \equiv \left(\frac{g_{\perp}^{(a)}(u)}{4} - (1-2u)\int_0^u dv\,(\phi_{\|}(v) - g_{\perp}^{(v)}(v))\right) \tag{D.39}$$

$$\Phi_{+-}^{even}(u) \equiv \left(\frac{g_{\perp}^{(a)}(u)}{4} + (1-2u)\int_0^u dv\,(\phi_{\|}(v) - g_{\perp}^{(v)}(v))\right) \tag{D.40}$$

$$\Phi_{+0}^{odd}(u) \equiv \int_0^u dv\,\left(h_{\|}^{(t)}(v) - \phi_{\perp}(v)\right) \tag{D.41}$$

$$\Phi_{++}^{odd}(u) \equiv \phi_{\perp}(u) \tag{D.42}$$

$$\Phi_{+-}^{odd}(u) \equiv \int_0^u dv\int_0^v d\eta\left(h_{\|}^{(t)}(\eta) - \frac{1}{2}\phi_{\perp}(\eta) - \frac{1}{2}h_3(\eta)\right). \tag{D.43}$$

We neglect to explicitly quote the trivial, but bulky, integrated forms for the sake of brevity.

Appendix E

The (++) even amplitude: a study of the end-point contributions

E.1 The light-quark limit

The importance of contributions at, and close to, end-points is a matter of debate (see for example ([57])). The authors of [25] worked at the Born level in the light-quark limit and obtained the results that all the helicity amplitudes, excepting the (++) even, were convergent at the end-points. We showed numerical results in Chapter 4 that demonstrated that the BFKL prediction for the (++) amplitude remained finite even in the light-quark limit (see 4.3). We shall investigate how this divergence in (++) at the Born level arises and how higher orders bring it under control. The authors of [25] worked with the asymptotic distribution amplitudes; we shall also do so (see appendix D for the asymptotic formulae). The end-point behaviour is independent of this approximation.

The light-quark limit corresponds to putting the mass of the quarks that form the meson to zero. This leads to the replacements

$$mK_1(m|r|) \to 1/|r| \quad \text{and} \quad K_0(m|r|) \to -m\ln(m|r|) \sim 0, \tag{E.1}$$

where we have assumed that $m|r| \to 0$ *i.e.* that we get no significant contributions from asymptotically large $|r|$.

E.2 Born level

We can apply the light quark approximation to the Born level (two-gluon) amplitudes previously derived. Consequently our chiral odd amplitudes vanish and we are left with

$$\mathcal{M}_{+0}^{even\,2g} = isC_V \int \frac{d^2\mathbf{k}}{\mathbf{k}^2(\mathbf{k}-\mathbf{q})^2} \frac{d^2r\,du}{4\pi} \frac{1}{r^*} f^d \frac{f_V}{\sqrt{2}} (1-2u)\,6u\bar{u} \tag{E.2}$$

$$\mathcal{M}_{++}^{even\,2g} = \frac{sC_V}{2} \int \frac{d^2\mathbf{k}}{\mathbf{k}^2(\mathbf{k}-\mathbf{q})^2} \frac{d^2r\,du}{4\pi}\; f^d f_V M_V\, 3u\bar{u}(u^2+\bar{u}^2) \tag{E.3}$$

and

$$\mathcal{M}_{+-}^{even\,2g} = sC_V \int \frac{d^2\mathbf{k}}{\mathbf{k}^2(\mathbf{k}-\mathbf{q})^2} \frac{d^2r\,du}{4\pi}\; \frac{r}{2r^*} f^d f_V M_V\, 6u^2\bar{u}^2, \tag{E.4}$$

where we have explicitly put in the asymptotic distributions listed in Appendix D. $\mathcal{M}_{+0}^{even\,2g}$ and $\mathcal{M}_{+-}^{even\,2g}$ prove to be convergent over the full u range [25]. Let us investigate what happens with $\mathcal{M}_{++}^{even\,2g}$. The integration proves trivial due to the form of f^d (see equation (4.12)). That is[1],

$$\int d^2\mathbf{r} f^d = (2\pi)^2 \left(\delta^{(2)}(u\mathbf{q}) - \delta^{(2)}(u\mathbf{q}-\mathbf{k}) - \delta^{(2)}(\bar{u}\mathbf{q}-\mathbf{k}) - \delta^{(2)}(\bar{u}\mathbf{q})\right) \tag{E.5}$$

and therefore,

$$\begin{aligned} M_{++}^{even\,2g} &= \frac{sC_V}{2} \int \frac{d^2\mathbf{k}}{\mathbf{k}^2(\mathbf{k}-\mathbf{q})^2} \frac{du}{4\pi}\; f_V M_V \\ &\times (2\pi)^2 \left(\delta^{(2)}(u\mathbf{q}) - \delta^{(2)}(u\mathbf{q}-\mathbf{k}) - \delta^{(2)}(\bar{u}\mathbf{q}-\mathbf{k}) - \delta^{(2)}(\bar{u}\mathbf{q})\right) 3u\bar{u}(u^2+\bar{u}^2) \\ &= -\frac{\pi}{|\mathbf{q}|^4} sC_V f_V M_V \int_{u_{min}}^{1-u_{min}} \frac{du}{u\bar{u}} 3(u^2+\bar{u}^2), \end{aligned} \tag{E.6}$$

where we have introduced a cut-off in u, u_{min}. Integrating, we arrive at

$$\mathcal{M}_{++}^{even\,2g} = -sC_V f_V M_V \frac{6\pi}{|q|^4} \left(\ln\left(\frac{1-u_{min}}{u_{min}}\right) - 1 + 2u_{min} \right). \tag{E.7}$$

[1] Again we see the contributions from different diagrams appearing as a sum of δ-functions. The δ-functions independent of $\mathbf{k}$ are again due to diagrams where the pomeron couple to just one parton and again these give zero contributions.

The upshot is that

$$\mathcal{M}_{++}^{2g\,even}(u_{min} \to 0) \to sC_V f_V M_V \frac{6\pi}{|q|^4} \ln(u_{min}) \,. \tag{E.8}$$

A clear divergence.

E.3 Resummation of the BFKL Equation

The full all order BFKL solution has proven in the past to improve infra-red finiteness of scattering amplitudes; see for example [39] for the case of $qq \to qq$ scattering. At finite order in α_s this scattering amplitude diverges. Even in cases where a process is infra-red finite, the Born level result can be observed to weight the contributions from momentum configurations which are unphysical *i.e.* where all the momentum is short-circuited down one gluon. The authors of [19] demonstrated how this problem can be resolved without recourse to the full BFKL result, but rather by a fixed order resummation of BFKL equation. We follow the kernel of their argument here.

High energy factorisation is valid to all orders in z (equivalently α_s). The leading s amplitude for any QCD process can be written in the form,

$$\mathcal{M}(z, \mathbf{q}) = is \sum_{n=0}^{\infty} \int \frac{d^2\mathbf{k}}{(2\pi)^2} \frac{\phi_m^A(\mathbf{k})\phi_{n-m}^B(\mathbf{k})}{\mathbf{k}^2\hat{\mathbf{k}}^2} \frac{z^n}{n!}, \tag{E.9}$$

where we have used the notation $\hat{\mathbf{k}} = \mathbf{k} - \mathbf{q}$. The Born level calculation corresponds to the first term of the sum *i.e.* $n = m = 0$. ϕ_0 is the Born level impact factor and ϕ_n is the nth order impact factor, n orders above Born level. The BFKL equation tells us how to get from an nth order impact factor to a $(n + 1)$th one. By a process of iteration, in principle, we can arrive at any arbitrary order simply from the Born level impact factor. Note that the above formula allows us to choose to put all the higher orders in one impact factor, or a combination of both. The BFKL equation is given by,

$$\phi_i(\mathbf{k}_i, z_i) = \frac{1}{\pi}\int_0^{z_i} dz' \int \frac{d^2\mathbf{k}_{i-1}}{(\mathbf{k}_i - \mathbf{k}_{i-1})^2} \times$$
$$\left(\phi_{i-1}(\mathbf{k}_{i-1}, z_{i-1})\left[\frac{\hat{\mathbf{k}}_i^2}{\hat{\mathbf{k}}_{i-1}^2} + \frac{\mathbf{k}_i^2}{\mathbf{k}_{i-1}^2} - \mathbf{q}^2\frac{(\mathbf{k}_i - \mathbf{k}_{i-1})^2}{\hat{\mathbf{k}}_{i-1}^2\mathbf{k}_{i-1}^2}\right]\right.$$
$$\left.-\phi_{i-1}(\mathbf{k}_i, z_{i-1})\left[\frac{\mathbf{k}_i^2}{\mathbf{k}_{i-1}^2 + (\mathbf{k}_i - \mathbf{k}_{i-1})^2} + \frac{\hat{\mathbf{k}}_i^2}{\hat{\mathbf{k}}_{i-1}^2 + (\mathbf{k}_i - \mathbf{k}_{i-1})^2}\right]\right) \tag{E.10}$$

where

$$z = \frac{3\alpha_s}{2\pi}\ln\left(\frac{\hat{s}}{\Lambda^2}\right) \tag{E.11}$$

We will now resum this equation. Let us write this equation for the sum of impact factors,

$$\phi(\mathbf{k}, z) = \sum_{i=0}^{\infty}\phi_i(\mathbf{k}, z). \tag{E.12}$$

We get,

$$\phi(\mathbf{k}, z) = \phi_0(\mathbf{k}) + \frac{1}{\pi}\int_0^{z} dz' \int \frac{d^2\mathbf{k}'}{(\mathbf{k} - \mathbf{k}')^2} \times$$
$$\left(\phi(\mathbf{k}', z')\left[\frac{\hat{\mathbf{k}}^2}{\hat{\mathbf{k}}'^2} + \frac{\mathbf{k}^2}{\mathbf{k}'^2} - \mathbf{q}^2\frac{(\mathbf{k} - \mathbf{k}')^2}{\hat{\mathbf{k}}'^2\mathbf{k}'^2}\right]\right.$$
$$\left.-\phi(\mathbf{k}, z')\left[\frac{\mathbf{k}^2}{\mathbf{k}'^2 + (\mathbf{k} - \mathbf{k}')^2} + \frac{\hat{\mathbf{k}}^2}{\hat{\mathbf{k}}'^2 + (\mathbf{k} - \mathbf{k}')^2}\right]\right). \tag{E.13}$$

Splitting the terms in the last square bracket up using partial fractions we get,

$$\phi(\mathbf{k}, z) = \phi_0(\mathbf{k}) + \frac{1}{\pi}\int_0^{z} dz' \int \frac{d^2\mathbf{k}'}{(\mathbf{k} - \mathbf{k}')^2}\phi(\mathbf{k}', z')\left[\frac{\hat{\mathbf{k}}^2}{\hat{\mathbf{k}}'^2} + \frac{\mathbf{k}^2}{\mathbf{k}'^2} - \mathbf{q}^2\frac{(\mathbf{k} - \mathbf{k}')^2}{\hat{\mathbf{k}}'^2\mathbf{k}'^2}\right]$$
$$+\int_0^{z} dz'\frac{\phi(\mathbf{k}, z')}{\pi}\int d^2\mathbf{k}'\left[\frac{\mathbf{k}^2/\mathbf{k}'^2}{\mathbf{k}'^2 + (\mathbf{k} - \mathbf{k}')^2} - \frac{\mathbf{k}^2/\mathbf{k}'^2}{(\mathbf{k} - \mathbf{k}')^2}\right.$$
$$\left.+\frac{\hat{\mathbf{k}}^2/\hat{\mathbf{k}}'^2}{\hat{\mathbf{k}}'^2 + (\mathbf{k} - \mathbf{k}')^2} - \frac{\hat{\mathbf{k}}^2/\hat{\mathbf{k}}'^2}{(\mathbf{k} - \mathbf{k}')^2}\right]. \tag{E.14}$$

We can rearrange this to give,

$$\phi(\mathbf{k}, z) = \phi_0(\mathbf{k}) + \frac{1}{\pi}\int_0^{z} dz' \int \frac{d^2\mathbf{k}'}{(\mathbf{k} - \mathbf{k}')^2}\Big(\phi(\mathbf{k}', z') - \phi(\mathbf{k}, z')\Big)$$
$$\times\left[\frac{\hat{\mathbf{k}}^2}{\hat{\mathbf{k}}'^2} + \frac{\mathbf{k}^2}{\mathbf{k}'^2} - \mathbf{q}^2\frac{(\mathbf{k} - \mathbf{k}')^2}{\hat{\mathbf{k}}'^2\mathbf{k}'^2}\right]$$
$$+\int_0^{z} dz'\frac{\phi(\mathbf{k}, z')}{\pi}\int d^2\mathbf{k}'\left[\frac{\mathbf{k}^2/\mathbf{k}'^2}{\mathbf{k}'^2 + (\mathbf{k} - \mathbf{k}')^2} + \frac{\hat{\mathbf{k}}^2/\hat{\mathbf{k}}'^2}{\hat{\mathbf{k}}'^2 + (\mathbf{k} - \mathbf{k}')^2} - \frac{\mathbf{q}^2}{\mathbf{k}'^2\hat{\mathbf{k}}'^2}\right]. \tag{E.15}$$

The purpose of this rearrangement is to split the integral into two parts, each part being separately convergent over the complete range of the integration, the second of which can be evaluated exactly. The $\phi(\mathbf{k}', z') - \phi(\mathbf{k}, z')$ term in the first part guarantees convergence when $\mathbf{k}' = \mathbf{k}$. Evaluating the second term is involved but we find

$$\begin{aligned}\phi(\mathbf{k}, z) = \phi_0(\mathbf{k}) + \frac{1}{\pi}\int_0^z dz' \int \frac{d^2\mathbf{k}'}{(\mathbf{k}-\mathbf{k}')^2}\Big(\phi(\mathbf{k}', z') - \phi(\mathbf{k}, z')\Big) \\ \times\left[\frac{\hat{\mathbf{k}}^2}{\hat{\mathbf{k}}'^2} + \frac{\mathbf{k}^2}{\mathbf{k}'^2} - \mathbf{q}^2\frac{(\mathbf{k}-\mathbf{k}')^2}{\hat{\mathbf{k}}'^2\mathbf{k}'^2}\right] \\ + \int_0^z dz' \phi(\mathbf{k}, z') \ln\left(\frac{\mathbf{k}^2\hat{\mathbf{k}}^2}{\mathbf{q}^4}\right).\end{aligned} \tag{E.16}$$

Differentiating this result with respect to z we get,

$$\begin{aligned}\frac{d\phi(\mathbf{k}, z)}{dz} = \frac{1}{\pi}\int \frac{d^2\mathbf{k}'}{(\mathbf{k}-\mathbf{k}')^2}\Big(\phi(\mathbf{k}', z) - \phi(\mathbf{k}, z)\Big)\left[\frac{\hat{\mathbf{k}}^2}{\hat{\mathbf{k}}'^2} + \frac{\mathbf{k}^2}{\mathbf{k}'^2} - \mathbf{q}^2\frac{(\mathbf{k}-\mathbf{k}')^2}{\hat{\mathbf{k}}'^2\mathbf{k}'^2}\right] \\ +\phi(\mathbf{k}, z') \ln\left(\frac{\mathbf{k}^2\hat{\mathbf{k}}^2}{\mathbf{q}^4}\right).\end{aligned} \tag{E.17}$$

From this result we can see that we can write $\phi(\mathbf{k}, z)$ in the form,

$$\phi(\mathbf{k}, z) = \psi(\mathbf{k}, z) \exp\left[z \ln\left(\mathbf{k}^2\hat{\mathbf{k}}^2/\mathbf{q}^4\right)\right], \tag{E.18}$$

and write the equation in the new form,

$$\begin{aligned}\frac{d\psi(\mathbf{k}, z)}{dz} = \frac{1}{\pi}\int \frac{d^2\mathbf{k}'}{(\mathbf{k}-\mathbf{k}')^2}\left[\left(\frac{\mathbf{k}'^2\hat{\mathbf{k}}'^2}{\mathbf{k}^2\hat{\mathbf{k}}^2}\right)^z \psi(\mathbf{k}', z) - \psi(\mathbf{k}, z)\right] \\ \times\left[\frac{\hat{\mathbf{k}}^2}{\hat{\mathbf{k}}'^2} + \frac{\mathbf{k}^2}{\mathbf{k}'^2} - \mathbf{q}^2\frac{(\mathbf{k}-\mathbf{k}')^2}{\hat{\mathbf{k}}'^2\mathbf{k}'^2}\right].\end{aligned} \tag{E.19}$$

Looking at the powers in the equation we see that it is convergent for $z < 0.5$. From the properties of the original power series in ϕ_i we know we will be able to define a power series in ψ_n,

$$\psi(\mathbf{k}, z) = \sum_{n=0}^{\infty} \psi_n(\mathbf{k})\frac{z^n}{n!}. \tag{E.20}$$

Therefore,

$$\phi(\mathbf{k}, z) = \exp\left[z \ln\left(\mathbf{k}^2\hat{\mathbf{k}}^2/\mathbf{q}^4\right)\right] \sum_{n=0}^{\infty} \psi_n(\mathbf{k})\frac{z^n}{n!} \tag{E.21}$$

We can then write the scattering amplitude,

$$\begin{aligned}\mathcal{M}(z,\mathbf{q}) &= is\sum_{n=0}^{\infty}\int\frac{d^2\mathbf{k}}{(2\pi)^2}\frac{\phi_m^A(\mathbf{k})\phi_{n-m}^B(\mathbf{k})}{\mathbf{k}^2\hat{\mathbf{k}}^2}\frac{z^n}{n!}\\
&= is\int\frac{d^2\mathbf{k}}{(2\pi)^2}\frac{\phi_0^A(\mathbf{k})\sum_{n=0}^{\infty}\phi_n^B(\mathbf{k})}{\mathbf{k}^2\hat{\mathbf{k}}^2}\frac{z^n}{n!}\\
&= is\int\frac{d^2\mathbf{k}}{(2\pi)^2}\frac{\phi_0^A(\mathbf{k})\phi^B(\mathbf{k})}{\mathbf{k}^2\hat{\mathbf{k}}^2}\frac{z^n}{n!}\\
&= is\int\frac{d^2\mathbf{k}}{(2\pi)^2}e^{z\ln\left(\mathbf{k}^2\hat{\mathbf{k}}^2/\mathbf{q}^2\right)}\frac{\phi_0^A(\mathbf{k})\sum_{n=0}^{\infty}\psi_n^B(\mathbf{k})}{\mathbf{k}^2\hat{\mathbf{k}}^2}\frac{z^n}{n!}\\
&= is\int\frac{d^2\mathbf{k}}{(2\pi)^2}\frac{\phi_0^A(\mathbf{k})\sum_{n=0}^{\infty}\psi_n^B(\mathbf{k})}{\mathbf{k}^2\hat{\mathbf{k}}^2}\left(\frac{\mathbf{k}^2\hat{\mathbf{k}}^2}{\mathbf{q}^4}\right)^z\frac{z^n}{n!}.\end{aligned}\tag{E.22}$$

The $\mathbf{k}^2\hat{\mathbf{k}}^2$ denominator introduces possible divergences at $\mathbf{k}=0$, $\mathbf{q}$. The result of this resummation is that we see higher orders decreasing the infra-red sensitivity, through the z variable. The resummed 'Born level' result is in fact finite. If we know the first n unsummed iterations we know the first n resummed iterations; equating powers of z gives us,

$$\begin{aligned}&\psi_n(\mathbf{k}) = \phi_n(\mathbf{k}) - \phi_{n-1}\ln\left(\mathbf{k}^2\hat{\mathbf{k}}^2/\mathbf{q}^4\right)\frac{n!}{(n-1)!} + \ldots\\
&+\phi_{n-m}(\mathbf{k})\ln^m\left(\mathbf{k}^2\hat{\mathbf{k}}^2/\mathbf{q}^4\right)\frac{(-1)^m n!}{(n-m)!m!} + \ldots\end{aligned}\tag{E.23}$$

Note that $\psi_0=\phi_0$. The resummed Born level amplitude is then,

$$\mathcal{M}^{2gR}(z,\mathbf{q}) = is\int\frac{d^2\mathbf{k}}{(2\pi)^2}\frac{\phi_0^A(\mathbf{k})\phi_0^B(\mathbf{k})}{\mathbf{k}^2\hat{\mathbf{k}}^2}\left(\frac{\mathbf{k}^2\hat{\mathbf{k}}^2}{\mathbf{q}^4}\right)^z\frac{z^n}{n!}.\tag{E.24}$$

E.4 Resummation: the (++) even amplitude

The results (E.22, E.23) tell us that the lowest order impact factor and resummed impact factor are equal. This allows us to go from the Born amplitude to the resummed one by the simple substitution,

$$\frac{1}{\mathbf{k}^2(\mathbf{k}-\mathbf{q})^2}\to\frac{1}{\mathbf{k}^2(\mathbf{k}-\mathbf{q})^2}\left(\frac{\mathbf{k}^2(\mathbf{k}-\mathbf{q})^2}{\mathbf{q}^4}\right)^z.\tag{E.25}$$

The substitution above clearly suppresses small gluon momenta. Therefore

$$\mathcal{M}_{++}^{even\,2gR} = \frac{sC_V}{2q^{4z}}\int\frac{d^2\mathbf{k}}{\mathbf{k}^{2-2z}(\mathbf{k}-\mathbf{q})^{2-2z}}\frac{d^2r\;du}{4\pi}\;f^d f_V M_V\,3u\bar{u}(u^2+\bar{u}^2).\tag{E.26}$$

Again we integrate f^d to get δ-functions and we obtain,

$$\mathcal{M}_{++}^{even\,2gR} = -\frac{\pi}{|\mathbf{q}|^4} sC_V f_V M_V \int_{u_{min}}^{1-u_{min}} \frac{du}{u^{2-2z}\bar{u}^{2-2z}} 3u\bar{u}(u^2+\bar{u}^2). \tag{E.27}$$

Using the definition of the incomplete beta function we arrive at

$$\begin{aligned}\mathcal{M}_{++}^{even\,2gR} &= -\frac{6\pi}{|\mathbf{q}|^4} sC_V f_V M_V \\ &\times \Big[B(1-u_{min}, 2z, 1+2z) - B(1-u_{min}, 1+2z, 1+2z)\Big]_{u_{min}}^{1-u_{min}}.\end{aligned} \tag{E.28}$$

We can safely put $u_{min} \to 0$ for $z > 0$ and using the definition of the complete beta-function we get,

$$\begin{aligned}\mathcal{M}_{++}^{even\,2gR} &= -\frac{6\pi}{|\mathbf{q}|^4} sC_V f_V M_V \; \left(B(2z, 1+2z) - B(1+2z, 1+2z)\right) \\ &= -\frac{6\pi}{|\mathbf{q}|^4} sC_V f_V M_V \,\frac{\Gamma(2z)\Gamma(2+2z)}{\Gamma(2+4z)}.\end{aligned} \tag{E.29}$$

The last line follows from the gamma function representation of the complete beta function and a little gamma function manipulation. We recover the divergence in the limit $z \to 0$;

$$\mathcal{M}_{++}^{even\,2gR}(z \to 0) \to -\frac{3\pi}{|\mathbf{q}|^4} sC_V f_V M_V \frac{1}{z}. \tag{E.30}$$

We observe that this is equal to that derived for $qq \to qq$ scattering amplitude in [39], excepting a factor of $-3C_V f_V M_V/2q^2$. The clear result, however, is that the resummed (++) even amplitude remains finite even in the light-quark limit for non-zero rapidity. We have demonstrated analytically that higher orders accomplish this. BFKL contains the contributions we resummed so it is not surprising that figure 4.3 demonstrated the finite result in the light-quark limit.

E.5 The BFKL calculation in the small u limit.

Equation (4.69) and the definition of the asymptotic distributions in Appendix D give us the result that for LL BFKL,

$$\mathcal{M}_{++}^{even} = \frac{sC_V f_V M_V}{8|q|} \int_0^1 du\, 3\, u\bar{u}\, (u^2+\bar{u}^2)$$
$$\times \sum_{n=-\infty}^{n=+\infty} \int_{-\infty}^{\infty} d\nu \frac{\nu^2+n^2}{[\nu^2+(n-1/2)^2][\nu^2+(n+1/2)^2]} \frac{\exp[\chi_{2n}(\nu)z]}{\sin(i\pi\nu)} I_{00}(\nu, 2n, q, u; 1) \tag{E.31}$$

where

$$I_{\alpha\beta}(\nu,n,q,u;a) = \frac{m}{2}\int_{C'-i\infty}^{C'+i\infty} \frac{d\zeta}{2\pi i}\Gamma(a/2-\zeta)\Gamma(-a/2-\zeta)\,\tau_q^\zeta\, (i\,\mathrm{sign}\,(1-2u))^{\alpha-\beta+n}$$
$$\times \left(\frac{4}{|q|}\right)^4 [\sin\pi(\alpha+\mu+\zeta)\;\; B(\alpha,\mu,q^*,u,\zeta)\, B(\beta,\widetilde{\mu},q,u^*,\zeta)$$
$$-(-1)^n \sin\pi(\alpha-\mu+\zeta)\, B(\alpha,-\mu,q^*,u,\zeta)\, B(\beta,-\widetilde{\mu},q,u^*,\zeta)\,] \tag{E.32}$$

and

$$B(\alpha,\mu,q^*,u,\zeta) = (-4u\bar{u})^{-(\mu+2+\alpha+\zeta)/2}\left(\frac{4}{q^*}\right)^\alpha 2^{-\mu}\,\frac{\Gamma(\mu+2+\alpha+\zeta)}{\Gamma(\mu+1)}$$
$${}_2F_1\left(\frac{\mu+2+\alpha+\zeta}{2}\,,\,\frac{\mu-1-\alpha-\zeta}{2}\,;\,\mu+1\,;\,\frac{1}{4u\bar{u}}\right), \tag{E.33}$$

with $\tau_q = 4m^2/|q|^2$.

The even amplitudes have $a=1$ so the integrand in $I_{\alpha\beta}(\nu,n,q,u;1)$ has a pole at $\zeta=-1/2$, where $-1<C'<-1/1$. If we shift the contour to the right we pick up pole contributions from $\mathrm{Re}\,\zeta \geq -1/2$. In the limit $m\to 0$ we might expect the leading pole to be that at $\zeta=-1/2$, the residue of which is independent of m, the other poles contributions vanishing in the limit. The integrand is complicated, however, expressed how it is in terms of blocks of hypergeometric functions. It is difficult to see clearly the analytic behaviour in ζ. For example the true expansion parameter may not be $4m^2/q^2$, rather something like $4m^2/u^2q^2$, where it is not clear whether the 'leading pole' actually is leading in the simultaneous limit $m\to 0$ and $u\to 0$. We shall see if some manipulation of the formula can be enlightening. Using the following hypergeometric identity 9.132:2 from [5], that

$$\begin{aligned} {}_2F_1(a,b;c;z) = \quad & \frac{\Gamma(c)\Gamma(b-a)}{\Gamma(b)\Gamma(c-a)}(-z)^{-a}\,{}_2F_1(a,a+1-c;a+1-b;1/z) \\ & + \frac{\Gamma(c)\Gamma(a-b)}{\Gamma(a)\Gamma(c-b)}(-z)^{-b}\,{}_2F_1(b,b+1-c;b+1-a;1/z), \end{aligned} \tag{E.34}$$

we can re-write,

$$\begin{aligned} & B(\alpha,\mu,q^*,u,\zeta) = (-4u\bar{u})^{-(\mu+2+\alpha+\zeta)/2}\left(\frac{4}{q^*}\right)^{\alpha} 2^{-\mu}\,\Gamma(\mu+2+\alpha+\zeta) \\ & \times\left[\frac{\Gamma(-3/2-\alpha-\zeta)}{\Gamma\left(\frac{\mu-1-\alpha-\zeta}{2}\right)\Gamma\left(\frac{\mu-\alpha-\zeta}{2}\right)}\left(-\frac{1}{4u\bar{u}}\right)^{-\frac{\mu+2+\alpha+\zeta}{2}}\right. \\ & \times{}_2F_1\left(\frac{\mu+2+\alpha+\zeta}{2},\frac{2+\alpha+\zeta-\mu}{2},5/2+\alpha+\zeta,4u\bar{u}\right) \\ & +\frac{\Gamma(3/2+\alpha+\zeta)}{\Gamma\left(\frac{\mu+2+\alpha+\zeta}{2}\right)\Gamma\left(\frac{\mu+3+\alpha+\zeta}{2}\right)}\left(-\frac{1}{4u\bar{u}}\right)^{-\frac{\mu-1-\alpha-\zeta}{2}} \\ & \left.\times{}_2F_1\left(\frac{\mu-1-\alpha-\zeta}{2},-\frac{1+\alpha+\zeta+\mu}{2},-1/2-\alpha-\zeta,4u\bar{u}\right)\right]. \end{aligned} \tag{E.35}$$

The advantage of this expression is that the hypergeometrics now have well defined power series expansions for $0 < u < 1$. We can simplify this expression further using the gamma function identity,

$$\frac{1}{\Gamma(z)\Gamma(z+1/2)} = \frac{2^{2z-1}}{\sqrt{\pi}}\frac{1}{\Gamma(2z)}. \tag{E.36}$$

We find,

$$\begin{aligned} B(\alpha,\mu,q^*,u,\zeta) = & \left(\frac{2}{q^*}\right)^{\alpha}\frac{1}{\sqrt{\pi}}2^{-2-\zeta} \\ \times & \left[C(\mu,\alpha,|u|,\zeta) + (-u\bar{u})^{-3/2-\alpha-\zeta}D(\mu,\alpha,|u|,\zeta),\right] \end{aligned} \tag{E.37}$$

where we define

$$\begin{aligned} C(\mu,\alpha,|u|,\zeta) = & \frac{\Gamma(\mu+2+\alpha+\zeta)\Gamma(-3/2-\alpha-\zeta)}{\Gamma(\mu-1-\alpha-\zeta)} \\ \times & {}_2F_1\left(\frac{\mu+2+\alpha+\zeta}{2},\frac{2+\alpha+\zeta-\mu}{2},5/2+\alpha+\zeta,4u\bar{u}\right) \end{aligned} \tag{E.38}$$

and

$$\begin{aligned} D(\mu,\alpha,|u|,\zeta) = & \,\Gamma(3/2+\alpha+\zeta) \\ \times & {}_2F_1\left(\frac{\mu-1-\alpha-\zeta}{2},-\frac{1+\alpha+\zeta+\mu}{2},-1/2-\alpha-\zeta,4u\bar{u}\right). \end{aligned} \tag{E.39}$$

Note that both the C and D functions are single-valued in u, but that the B function explicitly breaks single-valuedness. This is not a problem, since it is only the combination of blocks that must be single-valued. The blocks occur in the combination

$$\begin{aligned}
&\sin\pi(\alpha+\mu+\zeta)\, B(\alpha,\mu,q^*,u\zeta)B(\beta,\tilde{\mu},q,u^*,\zeta)\\
&\qquad\qquad -(-1)^n\sin\pi(\alpha-\mu+\zeta)\, B(\alpha,-\mu,q^*,u\zeta)B(\beta,-\tilde{\mu},q,u^*,\zeta)\\
&=\sin\pi((\alpha+\mu+\zeta))\left(\frac{2}{q^*}\right)^{\alpha}\left(\frac{2}{q}\right)^{\beta}\frac{1}{\pi}2^{-4-2\zeta}\\
&\times\Big[C(\mu,\alpha,|u|,\zeta)C(\tilde{\mu},\beta,|u|,\zeta)\\
&\qquad +C(\mu,\alpha,|u|,\zeta)D(\tilde{\mu},\beta,|u|,\zeta)\,(u\bar{u})^{-3/2-\beta-\zeta}e^{\pm\pi(3/2+\beta+\zeta)}\\
&\qquad +D(\mu,\alpha,|u|,\zeta)C(\tilde{\mu},\beta,|u|,\zeta)\,(u\bar{u})^{-3/2-\alpha-\zeta}e^{\mp\pi(3/2+\alpha+\zeta)}\\
&\qquad\qquad +D(\mu,\alpha,|u|,\zeta)D(\tilde{\mu},\beta,|u|,\zeta)\,(u\bar{u})^{-3-\alpha-\beta-2\zeta}(-1)^{\alpha-\beta}\Big]\\
&-(-1)^n\sin\pi(\alpha-\mu+\zeta)\left(\frac{2}{q^*}\right)^{\alpha}\left(\frac{2}{q}\right)^{\beta}\frac{1}{\pi}2^{-4-2\zeta}\left[\mu,\,\tilde{\mu}\to-\mu,\,-\tilde{\mu}\right].
\end{aligned}\tag{E.40}$$

This expression is complicated but in fact simplifies. Note that in the square bracket there are two multi-valued pieces corresponding to the cross multiplication of C's and D's. The sum of the two multi-valued pieces are not single-valued together in general; they have different u-dependences. In fact each multi-valued piece cancels exactly with another piece from the other square bracket[2]. We can throw away the cross multiplied terms. We obtain the result,

$$\begin{aligned}
I_{\alpha\beta}(\nu,n,q,u;a)&=\frac{m}{2\pi}\left(\frac{2}{q}\right)^{2+\beta}\left(\frac{2}{q^*}\right)^{2+\alpha}(\mathrm{i}\,\mathrm{sgn}\,(1-2u))^{\alpha-\beta+n}\\
&\times\int_{C'-i\infty}^{C'+i\infty}\frac{d\zeta}{2\pi i}\Gamma(a/2-\zeta)\Gamma(-a/2-\zeta)\,(m^2/|q|^2)^{\zeta}\\
\times\Big[\sin\pi(\alpha+\mu+\zeta)\,&G(\alpha,\beta,\mu,\widetilde{\mu},|u|,\zeta)\\
&-(-1)^n\sin\pi(\alpha-\mu+\zeta)\,G(\alpha,\beta,-\mu,-\widetilde{\mu},|u|,\zeta)\Big]
\end{aligned}\tag{E.41}$$

[2]This has been verified numerically.

where we introduce the notation,

$$G(\alpha,\beta,\mu,\widetilde{\mu},|u|,\zeta) = C(\mu,\alpha,|u|,\zeta)C(\tilde{\mu},\beta,|u|,\zeta)$$
$$+(-1)^{\alpha-\beta}\,(u\bar{u})^{-3-\alpha-\beta-2\zeta}\,D(\mu,\alpha,|u|,\zeta)D(\tilde{\mu},\beta,|u|,\zeta). \qquad \text{(E.42)}$$

We are now in a better position to examine the behaviour of the (++) even amplitude as $u \to 0$.

Note that the full (++) even amplitude is proportional to the integral over u of I_{00} multiplied by the u-dependence arising from the distribution amplitudes. At the endpoints, using results (4.75, E.42) we get the behaviour,

$$\frac{d\mathcal{M}^{even}_{++}(u\to 0)}{du} \propto 3u\bar{u}(u^2+\bar{u}^2)\,u^{-3-2\zeta} \to 3u^{-2-2\zeta}. \qquad \text{(E.43)}$$

The leading pole approximation would put $\zeta \to -0.5$, leaving the integrated amplitude logarithmically divergent as in the Born level case. However, earlier we showed that resumming leads to a finite result for non-zero rapidity. We now seek to show that the leading pole divergence, for non-zero rapidity, is an artifact indicating the break down of assumptions made rather than genuine asymptotic behaviour.

The G-function (E.42) simplifies greatly at the end-points. In the limit $u \to 0$ the dominant u-dependence allows us to write

$$G(\alpha,\beta,\mu,\widetilde{\mu},|u|\to 0,\zeta) \to (-1)^{\alpha-\beta}\,u^{-3-\alpha-\beta-2\zeta}\,\Gamma(3/2+\alpha+\zeta)\Gamma(3/2+\beta+\zeta), \qquad \text{(E.44)}$$

where we have put the hypergeometrics to unity in this limit. This simplification leads to

$$I^{u\to 0}_{\alpha\beta}(\nu,n,q,u;a) = \frac{m}{\pi}\left(\frac{2}{q}\right)^{2+\beta}\left(\frac{2}{q^*}\right)^{2+\alpha}(-1)^{\alpha-\beta}\,(\mathrm{i}\,\mathrm{sgn}\,(1-2u))^{\alpha-\beta+n}\,\frac{\sin\pi\mu}{u^{3+\alpha+\beta}}$$
$$\times\int_{C'-i\infty}^{C'+i\infty}\frac{d\zeta}{2\pi i}\Gamma(a/2-\zeta)\Gamma(-a/2-\zeta)\Gamma(3/2+\alpha+\zeta)\Gamma(3/2+\beta+\zeta)$$
$$\times\sin\pi(\alpha+1/2+\zeta)\,(m^2/|q|^2)^{\zeta}$$
$$= -m\left(\frac{2}{q}\right)^{2+\beta}\left(\frac{2}{q^*}\right)^{2+\alpha}(-1)^{\alpha-\beta}\,(\mathrm{i}\,\mathrm{sgn}\,(1-2u))^{\alpha-\beta+n}\,\frac{\sin\pi\mu}{u^{3+\alpha+\beta}}$$
$$\times G^{21}_{22}\left(\frac{m^2}{u^2|q|^2}\Big|^{-1/2-\beta,\,-1/2-\alpha}_{a/2,\,-a/2}\right), \qquad \text{(E.45)}$$

where we have used the integral definition of the Meijer G-function (see for example 9.301 of [5]). For $(a, \alpha, \beta) = (1, 0, 0)$ we find that this simplifies;

$$G_{22}^{21}\left(\frac{m^2}{u^2|q|^2}\Big|_{1/2,\,-1/2}^{-1/2,\,-1/2}\right) = G_{11}^{11}\left(\frac{m^2}{u^2|q|^2}\Big|_{1/2}^{-1/2}\right) = \frac{\frac{m}{u|q|}}{\left(1+\frac{m^2}{u^2|q|^2}\right)^2}. \tag{E.46}$$

We can therefore write down the (++) even amplitude in the $u \to 0$ limit as

$$\frac{dM_{++}^{even}(u \to 0)}{du} \to \frac{3C_V f_V M_V m^2}{8|q|^2}\left(\frac{2}{|q|}\right)^4 \frac{1}{u^3}\frac{1}{\left(1+\frac{m^2}{u^2|q|^2}\right)^2}$$
$$\times \sum_{n=-\infty}^{n=+\infty}\int_{-\infty}^{\infty} d\nu \frac{\nu^2+n^2}{[\nu^2+(n-1/2)^2][\nu^2+(n+1/2)^2]} e^{\chi_{2n}(\nu)z}. \tag{E.47}$$

Note that the u-dependence has completely factorised from the n and ν dependences. In fact the result, up to a factor, is that of $qq \to qq$ scattering found in [39]. We observed this earlier when performing the resummed calculation. From inspection of (E.47), for any particular conformal spin, we can see that it vanishes as $u \to 0$ for finite $m/|q|$ and also for $m/|q| \to 0$ and non-zero u. We know, however, that we must recover the Born level divergence as $z \to 0$. In fact we do achieve this; the sum over conformal spins is infinite for zero z. The fact that conformal spin has decoupled from u in our formula seems to imply that for zero z we face a divergence regardless of $m \to 0$. In fact this is not so. For sufficiently large n the assumption we made in putting the hypergeometric functions to zero breaks down. We should have a cut off in n relating to the inverse of u_{min}.

E.6 The single-parton coupling correspondence

As noted in section 3.2.2, the Mueller-Tang subtraction (3.29) gives an identical result to the original BFKL eigenfunction (3.25) for a colourless particle. This is manifest, for example, through the fact that the δ-function pieces in expression (4.35) cancel when combined with the subtracted eigenfunction piece. This is because the properties of coloured impact factors ensure cancellation between the diagrams where the pomeron couples to one and both partons in the dipole. We also noted that the diagrams with one parton coupling could not contribute when combined with the original BFKL eigenfunction. Therefore the calculation that followed on from equation (4.35) was equivalent to simply taking the diagrams where the pomeron couples to both partons and combining it with just the original BFKL eigenfunction. In section 3.2.2 we observed that in the limit $u \to 0$, which corresponds to large transverse separations in the dipole, this result should correspond to that of just taking the diagrams where the pomeron couples to a single parton and combining that with the Mueller-Tang subtraction (3.29). That is for a colourless impact factor, ϕ:

$$E^{MT}_{n,\nu} \otimes \phi_{1p} = E_{n,\nu} \otimes \phi_{2p}|_{u\to 0}. \tag{E.48}$$

This means that we should be able to derive formula (E.47) from this other route. We now proceed to do so.

We already have the machinery set up to do this calculation from chapter 4. We need to make the substitution

$$(e^{i\frac{\xi}{2}q\cdot\rho} + e^{-i\frac{\xi}{2}q\cdot\rho}) \to -d^2r\, \delta^{(2)}(\rho)\, (e^{iuq\cdot r} + e^{-i\bar{u}q\cdot r}) \tag{E.49}$$

in equation (4.37) and then combine that with the Mueller-Tang subtracted eigenfunction piece. We find that

$$\begin{aligned}\phi^{\gamma(+)V(+)\,1p}_{even}(\rho_1-\rho_2) &= me_q\frac{g^2\delta_{ab}}{2N}\frac{f_V}{2}m_V\, K_1(m|r|)|r| \\ &\times\int\frac{d^2r du}{4\pi}(e^{iuq\cdot r}+e^{-i\bar{u}q\cdot r})\delta^{(2)}(\rho_1-\rho_2)\, 3u\bar{u}(u^2+\bar{u})^2,\end{aligned} \tag{E.50}$$

where we have explicitly put in the (asymptotic) distribution amplitudes. Apart from the single-parton coupling condition imposed by the δ-function, we have no dependence on ρ_1 or ρ_2 in the vector meson impact factor. This is the same result as the qq impact factor. In fact a little work shows that we can write,

$$\begin{aligned}I^{\gamma(+)V(+)\,E\,1p}_{n,\nu} &= I^{qq}_{n,\nu}mee_q\frac{f_V}{2}m_V\int du\, 3u\bar{u}(u^2+\bar{u}^2) \\ &\times\int\frac{d^2r}{4\pi}|r|K_1(m|r|)(e^{iuq\cdot r}+e^{-i\bar{u}q\cdot r}).\end{aligned} \tag{E.51}$$

Using 6.576:6 and 8.411:1 from [5] we get

$$\int\frac{d^2r}{4\pi}\,K_1(m|r|)(e^{iuq\cdot r}+e^{-i\bar{u}q\cdot r}) = \left(\frac{m^2}{(m^2+u^2|q|^2)^2}+\frac{m^2}{(m^2+\bar{u}^2|q|^2)^2}\right). \tag{E.52}$$

Then using our result (4.31) we find that

$$|I^{qq}_{n,\nu}|^2 = \alpha_s^2 \frac{N^2-1}{N^2}\frac{(4\pi)^4}{4|q|^4}. \tag{E.53}$$

Combining all this we obtain the result,

$$\begin{aligned} \frac{dM^{even}_{++1p}}{du} &= \frac{3C_V f_V M_V m^2}{8|q|^2}\left(\frac{2}{|q|}\right)^4 \frac{1}{u^3}\frac{1}{\left(1+\frac{m^2}{u^2|q|^2}\right)^2} \\ &\times \sum_{n=-\infty}^{n=+\infty}\int_{-\infty}^{\infty} d\nu \frac{\nu^2+n^2}{[\nu^2+(n-1/2)^2][\nu^2+(n+1/2)^2]} e^{\chi_{2n}(\nu)z}. \end{aligned} \tag{E.54}$$

This is identical to (E.47).

E.7 Conclusions

- the two gluon exchange (++) even amplitude diverges as $\ln u_{min}$ as $u_{min} \to 0$ for $m = 0$
- the resummed (++) even amplitude converges as $u_{min} \to 0$ and $m \to 0$ for non-zero z, but diverges as $1/z$, as $z \to 0$ (the two-gluon limit).
- the BFKL (++) even amplitude converges as $u_{min} \to 0$ and $m \to 0$, when z is non-zero.
- for the complete (or resummed) leading log calculation we can only get a divergence with the following simultaneous limits $(u_{min}, m, z) \to 0$ and any one can provide a cut-off.

We have non-zero rapidity in our BFKL calculations, which include the essential higher order diagrams; we don't have to worry about divergences in the amplitudes, even in the light-quark limit.

References

[1] J.R. Forshaw and D.A. Ross, "QCD and the Pomeron", Cambridge University Press (1997).

[2] R.J. Eden, P.V. Landshoff, D.I. Olive and J.C. Polkinghorne, "The Analytic S-matrix", Cambridge University Press (1966).

[3] A. Donnachie, G. Dosch, P.V. Landshoff and O. Nachtmann, "Pomeron Physics and QCD", Cambridge University Press (2002).

[4] J.A.Vermaseren, "Axodraw", Comput. Phys. Commun.**83** (1994) 45.

[5] I.S. Gradshteyn and I.M. Ryzhik, "Tables of Integrals, Series and Products" 6th edition, Academic Press (2000).

[6] G.F.P. Chew and S.C. Frautschi, Phys. Rev. Lett. **7** (1961) 394; G.F.P. Chew and S.C. Frautschi, Phys. Rev. Lett. **8** (1962) 41.

[7] K. Hagiwara et al., Phys. Rev. **D66** (2002) 010001.

[8] A. Donnachie and P.V. Landshoff, Phys. Lett. **B296** (1992) 227.

[9] I.Y. Pomeranchuk, Sov. Phys. **3** (1956) 306.

[10] L.B. Okun and I.Y. Pomeranchuk, Sov. Phys. **JETP3** (1956) 307.

[11] M.E. Peskin and D.V. Schroeder, "An introduction to Quantum Field Theory", Perseus Books Publishing (1995).

[12] H. Cheng and T.T. Wu, Phys. Rev. **182** (1969) 1852. H. Cheng and T.T. Wu, Phys. Rev. **182** (1969) 1868. H. Cheng and T.T. Wu, Phys. Rev. **182** (1969) 1873. H. Cheng and T.T. Wu, Phys. Rev. **182** (1969) 1899.

[13] Y.Y. Balitsky and L.N. Lipatov, Sov. J. Nucl. Phys. **28** (1978) 822; E.A. Kuraev, L.N. Lipatov, V.S. Fadin, Phys. Lett **B60** (1975) 50; Sov. Phys. JETP **44** (1976) 443; Sov. Phys. JETP **45** (1977) 199.

[14] L.N. Lipatov, Sov. Phys. JRTP **63** (1986) 904.

[15] L.N. Lipatov, "Perturbative QCD", edited by A.H. Mueller, World Scientific (1989) 441.

[16] L.V. Gribov, E.M. Levin and M.G. Ryskin,"Semihard Processes in QCD", Phys. Rep. **100** (1983).

[17] I.F.Ginzburg, S.L.Panfil and V.G.Serbo, Nuc.Phys **B284** (1987) 685.

[18] I.F.Ginzburg, S.L.Panfil and V.G.Serbo, Nuc.Phys **B296** (1988) 569.

[19] J.R.Forshaw and M.G.Ryskin, Zeit.Phys. **C68** (1995) 137.

[20] J.Bartels, J.R.Forshaw, H.Lotter and M.Wustoff, Phys.Lett **B375** (1996) 301.

[21] S. Chekanov *et al.*, Eur.Phys.J. **C26** (2003) 389.

[22] A. Aktas, Phys. Lett. **B568** (2003) 205.

[23] J.R. Forshaw and G. Poludniowski, Eur. phys. J. **C26** (2003) 411.

[24] R. Enberg, L. Motyka and G. Poludniowski, Eur. Phys. J. **C26** (2002) 219.

[25] D.Y. Ivanov, R. Kirschner, A. Schäfer and L. Szymanowski, Phys. Lett. 478 (2000) 101 [eratum-*ibid.* bf B498 (2001) 295].

[26] J.A.Crittenden, published proceedings of DPF 2000: The Meeting of the Division of Particles and Fields of the American Physical Society, Columbus, Ohio, August 2000.

[27] K.Klimek on behalf of the ZEUS Collaboration presented at: Photon2000, August 2000, Ambleside, England.

[28] A.Kowal on behalf of the ZEUS Collaboration presented at: DIS2001, April 2001, Cracow, Poland.

[29] D.P. Brown, published proceedings of Moriond 2003: Conference on QCD and High Energy Interactions.

[30] M. Seymour, "Introduction to QCD", Lecture Notes (2000).

[31] P. Ball and V.M. Braun, Phys.Rev. **D54** (1996) 2182.

[32] P. Ball, V.M. Braun, Y. Koike and K. Tanaka, Nucl.Phys. **B529** (1998) 323

[33] P. Ball and V.M. Braun, Nucl.Phys. **B543** (1999) 201.

[34] "Dispersion Relations", edited by G.R. Screaton, Scottish Universities' Summer School, Oliver and Boyd (1960).

[35] R.J. Eden, "High Energy Collisions Elementary Particles", Cambridge University Press (1976).

[36] V.L. Chernyak and A.R. Zhitnitsky, Phys. Rep. **112** (1984) 173.

[37] A.H. Mueller and W.K. Tang, Phys. Lett. **B284** (1992) 123.

[38] J. Bartels, J.R. Forshaw, H.Lotter, L.N. Lipatov, M.G. Ryskin and M, Wüstoff, Phys. Lett. **B348** (1995) 589.

[39] L.Motyka, A.D. Martin and M.G. Ryskin, Phys. Lett. **B524** (2002) 107.

[40] J.R. Forshaw and P.J. Sutton, Eur. Phys. J. **C1** (1998) 285.

[41] H. Navelet and R. Peschanski, Nucl. Phys. **B507** (1997) 353.

[42] N.G. Evanson, “Diffractive photon production”, Ph.D. thesis, The University of Manchester.

[43] N.N. Lebedev, “Special Functions and their Applications”, Dover Publications (1972).

[44] “Higher Transcendental Functions”, edited by A.Erdelyi, Magraw-Hill Book Co. (1953).

[45] R. Enberg, L. Motyka and G. Poludniowski, Acta Phys. Polon. **B33** (2002) 3511.

[46] R. Enberg, J.R. Forshaw, G. Poludniowski and L. Motyka, JHEP 09(2003)008.

[47] J.A. Crittenden, “Exclusive Production of Neutral Vector Mesons at the Electron-proton Collider HERA”, Springer Tracts in Modern Physics v.140, Springer-Verlag (1997).

[48] K. Schilling, P. Seyboth, G.E. Wolf, Nucl. Phys. **B15** (1970) 397 [Erratum-ibid. **B18** (1970) 332.

[49] K. Schilling and G.E. Wolf, Nucl.Phys. **B61** (1973) 381.

[50] S.J. Brodsky, V.S. Fadin, V.T. Kim, L.N. Lipatov and G.B. Pivovarov, JETP Lett.70 (1999) 155.

[51] B.E. Cox, J.R. Forshaw and L. Lönnblad, JHEP 9910:023.

[52] R.K. Ellis, W.J. Stirling and B.R. Webber, “QCD and Collider Physcics” (chapter 2), Cambridge Monographs on Particle Physics, Cambidge University Press (1996).

[53] R. Nisius (CERN) and M.H. Seymour, Phys. Lett. **B452** (1999) 409.

[54] J. Botts and G. Sterman, Nuc. Phys. **B325** (1989) 62.

[55] B.L. Ioffe, V.A. Khoze, L.N. Lipatov, "Hard Processes Volume 1: Phenomenology Quark-Parton Model" (chapter 5), Elsevier Science Publishers (1984).

[56] R. Vega and J. Wudka, Phys. Rev. **D53** (1996) 5286 [Erratum-ibid. **D56** (1997) 6037.

[57] P. Hoyer, J.T. Lenaghan, K. Tuominen and C. Vogt, hep-ph/0210124.